MRS-J
The Materials Research Society of Japan

第9回年次総会・学術シンポジウム

講演要旨集

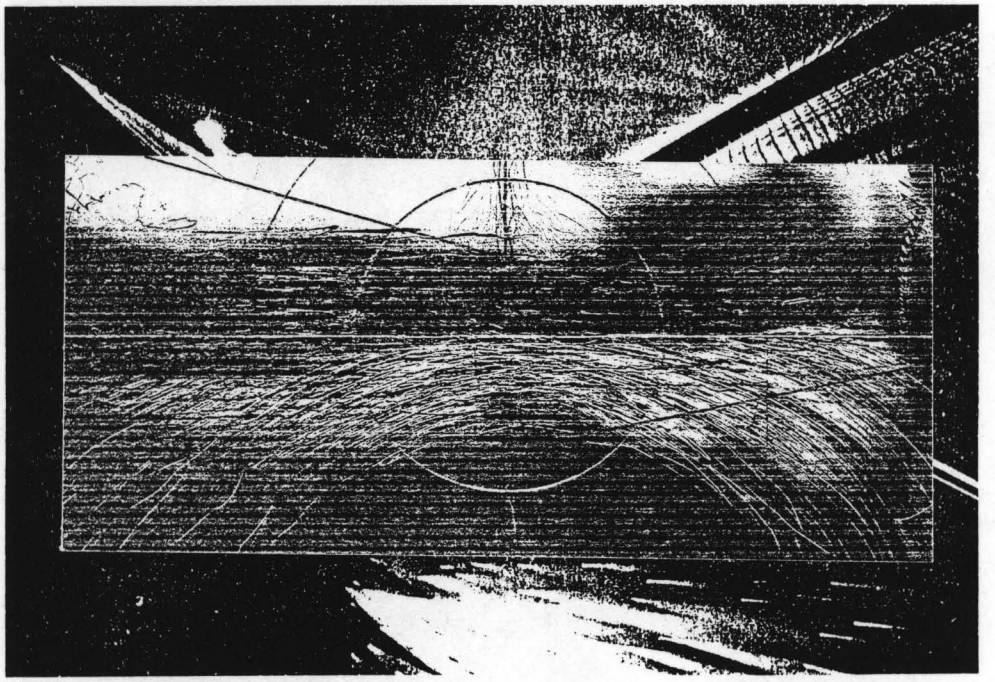

1997.12.11-12 川崎市 KSP

The Materials Research Society of Japan

第９回年次総会・学術シンポジウム

講演要旨集

日本ＭＲＳ
The Materials Research Society of Japan

事務局　　川崎市高津区坂戸３－２－１　西３０４
株式会社ケイエスピー内
TEL 044-819-2001　FAX 044-819-2009

＝正　誤　表＝

P．3	誤	P 1-15 D　※大野弘幸
	正	P 1-15 S　※大野弘幸
P．27	誤	16：00-16：45　懇親会
	正	18：00-19：30　懇親会
P．30	誤	P 2-23 D　※阪本清志
	正	P 2-23 D　※坂本清志

日本ＭＲＳ第９回年次総会・学術シンポジウム

日時　１９９７年１２月１１日（木）、１２日（金）
場所　かながわサイエンスパーク　西棟７Ｆ　会議室
（川崎市高津区坂戸 3-2-1）

第１シンポジウム　701 号室
第２シンポジウム　708 号室
第３シンポジウム　701 号室
ポスターセッション　709 号室

スケジュール

１２月１１日（木）

12：00 - 12：30　年次総会
13：00 - 17：30　第一シンポジウム　講演・ポスター
テーマ　高分子ナノ組織体
チェア　西出宏之（早大）
第二シンポジウム　講演・ポスター
テーマ　分子系超構造
チェア　荒木孝二（東大）
18：00 - 19：30　懇親会

１２月１２日（金）

10：00 - 17：05　第三シンポジウム　講演・ポスター

第１シンポジウム　　「高分子ナノ組織体」Nano-polymer　Architechyure

チェア　西出宏之（早大）

鎖長、組成、シーケンスなどが精密に制御された高分子の合成が進んでいる。これら高分子間の特異な相互作用を基礎として、ナノサイズの組織体を構築し、新しい機能発現に繋げる試みがある。この立場から機能材料の開発を目指す下記の依頼講演と、一般から募集するポスターセッションで討論と意見交換を行う。

１２月１１日（木）　＜＊招待講演＞

13：00-13：45　＊1　「液晶分子ナノ組織化と機能化」加藤隆史（東大院・工）

13：45-14：30　＊2　「金属錯体を含むデンドリマーナノ組織体」
木村　睦（信州大・繊維）

14：30-16：00　ポスターセッション

16：00-16：45　＊3　「分子間溶融塩形成を利用した新しいイオン伝導性
高分子の設計」大野弘幸（東農工大・工）

16：45-17：30　＊4　「ポリラジカルのナノ構造と磁性発現」
西出宏之（早大・理工）

18：00-19：30　懇親会

ポスターセッション・プログラム

於　７０９号会議室

＜B：学士課程　M：修士課程　D：博士課程　S：一般＞

=番号=　= 著者 ※印:発表者 =　= タイトル =

P1-1M.　※小笠原益美、加藤隆史（東大院・工）　「二重水素結合による超分子液晶の構築」

P1-2M. ※福地崇史、森野慎也、中川　勝、関　隆広、市村國宏（東工大・資源研）
「Urea を親水基とする新規アゾベンゼン誘導体の単分子膜」

P1-3M. ※生方　俊、森野慎也、中川　勝、関　隆広、市村國宏（東工大・資源研）
「LB 法によるコマンドサーフェス界面領域のモデル化と分光学的評価」

P1-4M. ※細野千明、長谷川正木（桐蔭横浜大・工）
金原　数、阿出川豊、西郷和彦（東大院・工）
「混晶／分子錯体の光重合により得られる高度に組織化された高分子ナノコンポジット」

P1-5M. ※沓名貴昭、加藤隆史（東大院・工）
英　謙二（信州大・繊維）
「分子ナノ組織化による液晶のゲル化と電場応答」

P1-6M. ※平塚香織、英　謙二、木村　睦、白井汪芳（信州大・繊維）
「アミノ酸誘導体によって作製したゲルの電解特性」

P1-7M. ※田中礼央、英　謙二、木村　睦、白井汪芳（信州大・繊維）
「双頭型アミノ酸誘導体のオイルゲル化剤 」

P1-8M. ※河上　敦、英　謙二、木村　睦、白井汪芳（信州大・繊維）
「シクロヘキサン誘導体によるオルガノゲル」

P1-9D. ※粕谷マリア、畑中研一（東工大・生命理工）
「分子多糖、オリゴ糖の合成」

P1-10M. ※里見倫明、田中敬二、高原淳、梶山千里（九大院・工）
「温度依存走査型粘弾性顕微鏡（TDSVM）による高分子固体膜表面の分子鎖熱運動解析」

P1-11M. ※渡辺和人、細野千明、相良智和、斎藤　潔、長谷川正木（桐蔭横浜大・工）
「新規ジスチリルピラジン誘導体のトポケミカル光反応挙動」

P1-12M. ※塚原幸弘、西出宏之、土田英俊（早大・理工）「キャリア膜での酸素ホッピング透過」

P1-13D. ※山崎裕一、吉川研一（名古屋大院）「鉄イオンの酸化還元反応を利用したDNA高次構造制御」

P1-14M. ※雨宮隆浩、鈴木拓生、加藤隆史（東大院・工）「バイオミネラリゼーションプロセスによる高分子／無機複合体の形成」

P1-15D. ※大野弘幸、川原夏江（東農工大・工）「イオン伝導性ポリエーテルオリゴマー内でのレドックス活性タンパク質の熱安定化」

P1-16M. ※宮坂　誠、西出宏之、土田英俊（早大・理工）「星型ラジカルポリマーの合成とスピン整列」

P1-17M. ※水野克俊、木村睦、英謙二、白井汪芳（信州大・繊維）「ターピリジンリガンドを含むデンドリマーの合成と電気化学的特性」

P1-18M. ※前田忠俊、西出宏之、土田英俊（早大・理工）「ポリ（2-オキシフェニル-1、4-フェニレンエチニレン）の合成と磁気的性質」

P1-19M. ※夫　勇進、高橋正洋、西出宏之、土田英俊（早大・理工）「オリゴ（4-オキシフェニル-1、2-フェニレンエチニレン）環状体の合成と

Nano-Organization and Functionalization of Liquid Crystals

Takashi Kato

Department of Chemistry and Biotechnology, Graduate School of Engineering, The University of Tokyo, Bunkyo-ku, Tokyo 113

The processes of self-assembly and self-organization of various molecules using specific molecular interactions lead to the formation of new functional molecular systems where various molecules cooperate. For liquid crystals, we have been preparing supramolecular mesomorphic materials from independent and different molecules. The supramolecular liquid crystals are a homogeneous system where molecular complexes built through intermolecular hydrogen bonds form one phase. Recently, we have developed a novel type of nano-ornganized composite materials, liquid crystal gels. We report here two anisotropic systems: (1) supramolecular liquid crystals (homogeneous materials); (2) liquid crystal gels (heterogeneous materials).

Polyamides based on 2,6-bis(acylamino)pyridine moieties form supramolecular mesogenic structures by complexation with low molecular weight compounds. Such supramolecular polyamides exhibit significantly thermally stable mesophases.

The association of low molecular compounds such as *trans*-1,2-bis(amino)cyclohexane derivatives results in the successful gelation of liquid crystals. These anisotropic gels consist of H-bonded aggregates and normal liquid crystals such as cyanobiphenyls. Two gel states derived from isotropic and nematic states, which are thermally reversible, are observed for these gels.

Dendritic Nano-organized Systems Containing Metal Complexes

Mutsumi Kimura

Department of Functional Polymer Science, Faculty of Textile Science and Technology, Shinshu University, Ueda 386, Japan

email: mkimura@giptc.shinshu-u.ac.jp

The synthesis of dendrimers have recently attracted much interest. Dendrimers are well-defined globular structure with uniform molecular weight. The functional dendrimers have been prepared by the introduction of functional compounds such as metal complexes, fullerenes and biomaterials to the exterior surface and the interior cores of dendrimers. The highly branched dendrimers provided a unique environment for these functional compounds, which resulted in a variety of new and modified properties. Constructing a dendrimer around a phthalocyanine core could control the aggregation of complex in aqueous media and modify its photoreactivity. We report here on the synthesis of the first dendric Zn^{II} phthalocyanine using cascade polymer methodology. The environment of photoactive Zn phthalocyanine can be controlled through the encapsulation in dendrimers.

The polyether-amide dendrimer containing a Zn^{II} phthalocyanine derivative was prepared by the method of Newkome et al. The UV-visible spectrum shows the inner environment of Zn phthalocyanine located in the interior core of the dendrimers. The spectra of **1** and **3** showed a sharp peak at 678.0nm (logε=5.47) bearing a shoulder at 621.0nm in $CHCl_3$, and were not influenced by the number of the generations. In aqueous media, the UV-visible spectra of **2** and **4** were much different based on the number of generations. Dendrimer **4** showed the Q band at 687.0nm which is typical of a nonaggregated Zn phthalocyanine. However, a sharp peak was not observed in the case of **2**. These spectra of **2** and **4** were little affected by the increasing of pH value from 7.1 to 10.5. This broad peak at 622.0nm, which is attributed to the aggregation of Zn phthalocyanine, indicates that the complexes interacted through a hydrophobic interaction in aqueous media. With increasing of dendrimer generation, the shielding effect of the dendrimer is enhanced by increasing the size of the molecular cage.

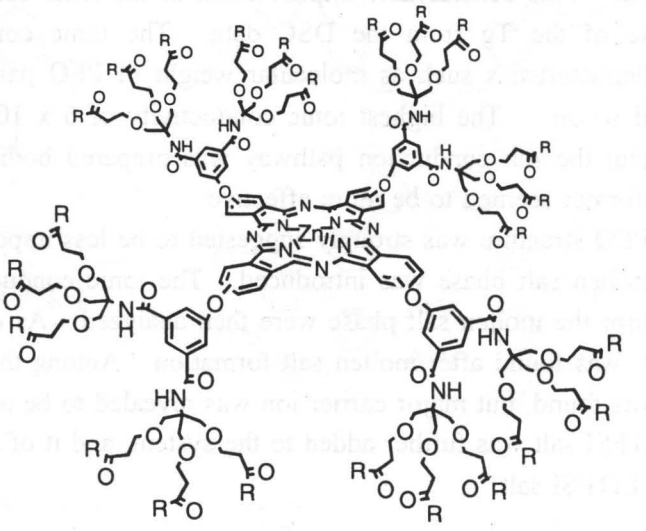

1: -OEt
2: -OLi
3: -NH($CH_2OCH_2CH_2COOEt$)$_3$
4: -NH($CH_2OCH_2CH_2COOLi$)$_3$

Ref) M. Kimura, K. Nakada, Y, Yamaguchi, K. Hanabusa, and H. Shirai, *Chem. Commun.*, **1997**, 1215.

Design of Novel Ion Conductive Polymers through the Intermolecular Molten Salt Formation

Hiroyuki Ohno
Department of Biotechnology, Tokyo University of Agriculture and Technology,
Koganei, Tokyo 184-8588, Japan

Introduction:

The ion conductive polymers are quite important materials for the design of novel ionics devices, such as film battery. Poly(ethylene oxide) (PEO) has been used for a long time as basic materials for that purpose. However, the upper limit of the ionic conductivity in PEO matrix is estimated to be in the order of 10^{-3} S/cm even in the liquid state. Accordingly, new type of ion conductive polymers is being desired to drastically improve the ionic conductivity. In the present paper, I would like to introduce the new type polymers which have ability to form molten salt phase in the polymer matrix. Their ionic conductivity before and after the molten salt formation is reported.

Experimental:

PEO having alkyl imidazolium groups or alkyl sulfonamide salt groups on one or both ends (PEO/salt hybrids) were prepared according to our previously published paper.[1] Vinyl polymers having alkyl imidazolium groups or alkyl sulfonamide salt groups on the side chains were also prepared.[2] The structure of these polymers was confirmed by proton NMR measurements.

Ionic conductivity was measured with Solartron 1260 (Schlumberger) with custom made temperature sweep unit. Impedance data were analyzed to calculate the ionic conductivity at every temperature. The glass transition temperature (Tg) was determined by DSC measurement (SEIKO).

Results and Discussion:

The ionic conductivity of the PEO/salt hybrid was improved 10^4 - 10^5 after molten salt formation at the chain end. This considerable improvement of the ionic conductivity was comprehended to be due to the decrease of the Tg from the DSC data. The ionic conductivity was affected by the following structural characteristics such as molecular weight of PEO part, charged end group species, counter ion species, and so on. The highest ionic conductivity of 6×10^{-5} S/cm was found at 50 ℃. These data suggested that the ion conduction pathway was prepared both in the molten salt phase and PEO chain phase, and former seemed to be more effective.

The PEO structure was strongly suggested to be less important to provide fast ion conductive matrix when the molten salt phase was introduced. The ionic conductivity for the vinyl type polymers having ability to form the molten salt phase were then analyzed. As expected, considerable improvement of the conductivity was found after molten salt formation. Among these, the highest ionic conductivity of 2×10^{-3} S/cm was found, but major carrier ion was revealed to be an anion. To improve the lithium transport number, LiTFSI salt was further added to the system, and it of about 0.6 was obtained after the equimolar addition of LiTFSI salt.

References:

1. H. Ohno, Y.Nakai, and K. Ito, *Chem. Lett.*, (1998) in press.
2. K. Ito, M. Omori, and H. Ohno, *11th Int'l Conf. Solid State Ionics,* p143 (1997)

Radical Polymers: Their Nano-Structure and Ferromagnetic Spin-Alignment

Hiroyuki Nishide

Dept Polymer Chemistry, Waseda University, Tokyo 169

There is much interest in preparation of magnetically responsive, purely organic-derived polymers. The goal of these works is to synthesize π-conjugated polymers bearing radical groups and to explore the possibility of ferromagneticallty coupled- or high-spin alignment between unpaired electrons of the pendant radicals. For π-conjugated and alternant, but non-Kekule-type organic polymers bearing multi radicals, the spin quantum number (S) at the ground state is cleary related to the macromolecular structure or molecular connectivity of the radical centers on the conjugated backbone (Fig.1). First, recent progress in synthesizing of these radical polymers(**1**, **2**) is mini-reviewed.

We focused on π-conjugated linear polymers bearing pendant radical groups, which are also π-conjugated with the polymer backbone and have substantial chemical stability. Typical examples are poly(phenylenevinylene)-based radicals(**3**, **4**): **3** with a spin concentration of 0.67 displayed S=5/2, indicating a ferromagnetic alignment of five spins on the average. A spin defect was not fatal for a partial but strong ferromagnetic spin alignment between the pendant unpaired electrons through the π-conjugated poly(phenylenevinylene) backbone. The design and synthesis of extended star-shaped, hyper-branched, and ladder polyradical frameworks employing π-conjugated backbones are described as a promising route towards the development of ferromagnetic polymers.

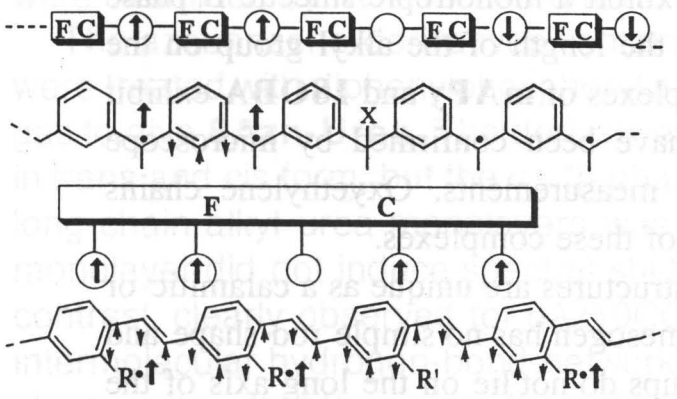

Fig. 1

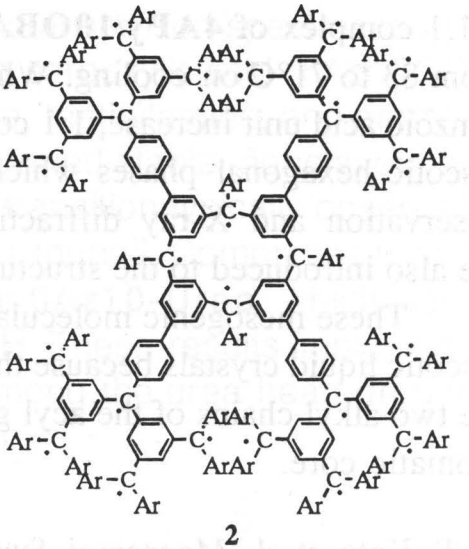

2

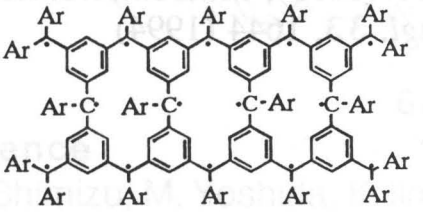

1

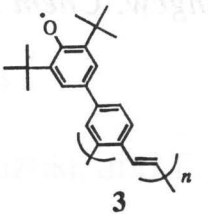

3

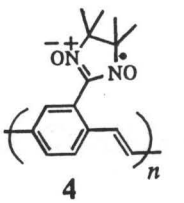

4

Self-Assembly of Supramolecular Liquid Crystals through the Formation of Double Hydrogen Bonds

Masumi Ogasawara and Takashi Kato
Department of Chemistry and Biotechnology, Graduate School of Engineering, The University of Tokyo, Hongo, Bunkyo-ku, Tokyo 113, Japan

A wide variety of H-bonded liquid crystalline complexes have been prepared through the formation of a single hydrogen bond between pyridines and carboxylic acids.[1] Aminopyridines and their related compounds that have both hydrogen donating and accepting moieties are key components for crystal engineering and host-guest chemistry in the solid-state and solution states. Our intention is to employ 2,6-bis(acylamino)pyridines for liquid crystalline materials.

As H-bonding components, 2,6-bis(acylamino)pyridines **mAPy**(m=3~8) were selected and designed to complex with 4-(alkoxy)benzoic acids **nOBA**(n=10, 12, 18). Molecular recognition processes between these two components result in the formation of doubly hydrogen-bonded mesogenic complexes. These 1:1 complexes of **mAPy** and **nOBA**(n=10, 12,) exhibit a monotropic smectic B phase, which are not observed for each of the single components. For example, a 1:1 complex of **4APy/10OBA** exhibit a monotropic smectic B phase from 83 to 71°C on cooling. When the length of the alkyl group on the benzoic acid unit increase, 1:1 complexes of **mAPy** and **18OBA** exhibit discotic hexagonal phases which have been confirmed by microscope observation and X-ray diffraction measurements. Oxyethylene chains are also introduced to the structure of these complexes.

These mesogenic molecular structures are unique as a calamitic or discotic liquid crystals because the mesogen has no simple rod shape and the two alkyl chains of the acyl groups do not lie on the long axis of the aromatic core.

1) T. Kato et al. *Macromol Symp.*, **98**, 311 (1995); *Macromolecules.*, **22**, 3818 (1989); *Angew. Chem Int. Ed. Engl.* **33**, 1644 (1994)

Monolayer properties of azobenzene derivatives containing hydrophilic urea group

Takashi Fukuchi, Shin'ya Morino, Masaru Nakagawa,
Takahiro Seki, and Kunihiro Ichimura
Research Laboratory of Resources Utilization, Tokyo Institute of Technology
4259 Nagatsuta-cho, Midori-ku, Yokohama 226, JAPAN

It is well known that amphiphiles including urea group as a hydrophilic group are formed the monolayer at the air-water interface with the highly strong intermolecular hydrogen-bonding (Fig. 1)[1]. On the other hand, it has been a lot of reports about monolayer and Langmuir-Blodgett films in the azobenzene-containing amphiphiles. We have synthesized the azobenzene derivatives containing ureas as the head group (**6Azn-Urea**). The molecular orientation and photoisomerization behavior at the air-water interface were examined by π-A measurements and absorption spectroscopy.

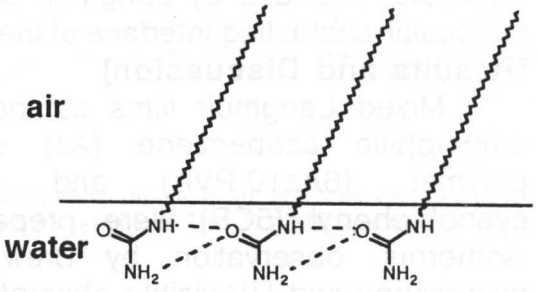

Fig. 1 Supposed hydrogen-bonding mode in alkyl urea monolayers

The azobenzene derivatives containing carboxylic acid (6AznCOOH) were treated with diphenylphosphoryl azide, triethylamine, and ammonia gas to give **6Azn-Urea**. The derivatives formed stable monolayers both in trans and cis form, but the $\alpha \rightleftarrows \beta$ phase transition typically observed in long-chain alkyl urea monolayers was not found[1]. Compression of the monolayer did not induce spectral shift for **6Az10-Urea**, which was, in contrast, clearly observed for 6Az10COOH. These results imply that an intermolecular hydrogen-bond network among the urea head groups is stronger than that for carboxylic acid group.

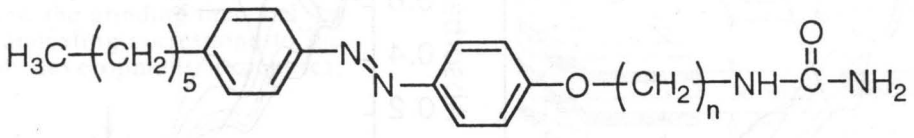

6Azn-Urea

Reference

1). M. Shimizu, M. Yoshida, K. Iimura, N. Suzuki, and T. Kato, *Colloids and Surfaces A*, **102**, 69 (1995) *etc.*

Modeling the Intrface Region of Command Surface by LB Method and Specroscopic Evaluations

T. Ubukata, S. Morino, N. Nakagawa, T. Seki, and K. Ichimura

Research Laboratory of Resources Utilization, Tokyo Institute of Technology

[Introduction]

Monolayers having photocromic functional group on the solid substrate can induce alignment changes of nematic liquid crystal (LC) by photoirradiation. In this regards such layers can be referred to as command surfaces. We constituted a research approach for modeling the hetero-molecular interface by Langmuir-Blodgett (LB) technique to understand the molecular contacting interface of the command layer / LC.

[Results and Discussion]

Mixed Langmuir films composed of an amphiphilic azobenzene (Az) side chain polymer (6Az10-PVA) and 4'-pentyl-4-cyanobiphenyl (5CB) were prepared. π-A isotherms, observation by Brewster angle microscopy and UV-visible absorption spectra revealed that two compounds in these films were mixed molecularly homogeneously, and Az side chain of 6Az10-PVA and 5CB molecules were highly oriented perpendicularly to the air-water interface.

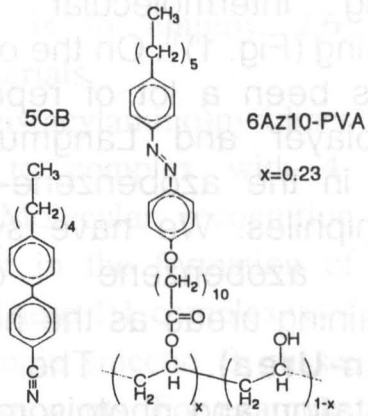

Photoresponsive properties of mixed LB films were investigated by UV-visible absorption spectroscopy. UV light (365nm) illumination induced large absorption enhancement particularly in the band of 5CB molecule around 280nm (Fig.1a). The enhancement of absorption band at 280 nm was clearly consorted with that of the n-π* band of Az unit (440 nm), indicating that the orientational change of 5CB with respect to the surface plane was induced by the photoisomerization of the Az side chain. The reverse process could also be performed by visible light irradiation (Fig.1b). Orientational evaluation of each component of molecules was also performed using FT-IR spectroscopy.

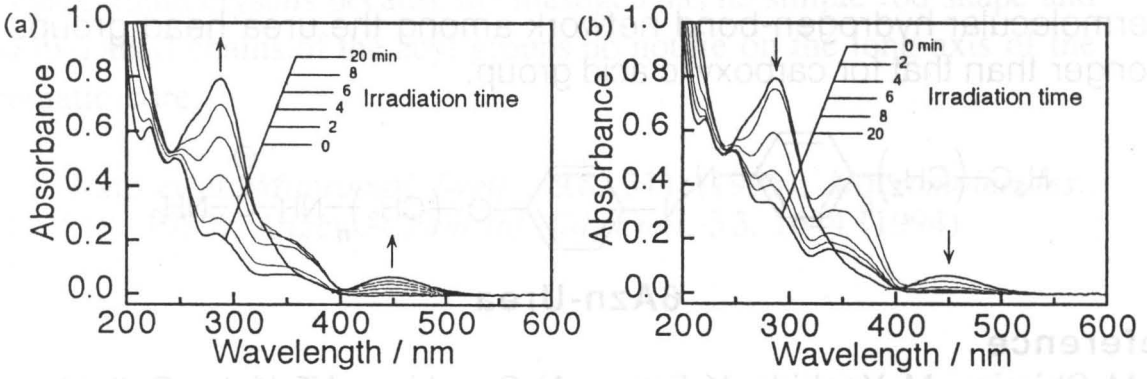

Fig.1 UV-visible absorption spectra of the 6Az10-PVA / 5CB (1:1) mixed LB films (39 layers). Spectral change on exposure (a) to UV (365nm) and (b) to visible (436nm) light.

PERFECTLY ORDERED POLYMER NANO-COMPOSITE BY PHOTOPOLYMERIZATION OF MIXED CRYSTAL / MOLECULAR COMPLEX

Chiaki Hosono, Masaki Hasegawa, Kazushi Kinbara†, Yutaka Adegawa†, and Kazuhiko Saigo†
Department of Materials Science and Technology, Faculty of Engineering, Toin University of Yokohama, Kurogane-cho, Aoba-ku, Yokohama 225, Japan, †Department of Chemistry and Biotechnology, Faculty of Engineering, The University of Tokyo, Hongo, Bunkyo-ku, Tokyo 113, Japan

Introduction

We have prepared a large number of highly crystalline linear polymers by topochemical [2+2] photopolymerization of various types of diolefin crystals.[1] The polymerization proceeds with retaining the space group of starting crystal and gives highly ordered polymer crystal only with few structural defects.

Here, we like to report first preparation of highly ordered polymer crystal nano-composite by topochemical [2+2] photopolymerization of the mixed crystals and the molecular complexes comprising two kinds of conjugated diolefins.

Results and Discussion

By recrystallization of the mixture of two organic compounds the mixed crystal is often obtained if their crystal structures are isomorphous to each other.

In present study, we found that several pairs of diolefin compounds formed photoreactive mixed crystal or molecular complex, e.g., the mixed crystal (**1c**) consisting of ethyl and *S*-ethyl 4-[2-(2-pyrazyl)ethenyl]-cinnamates (**1a** and **1b**).

For example, on photoirradiation, the mixed crystal (**1c**) gives highly crystalline linear high copolymer with a random sequence of two compounds.[2]

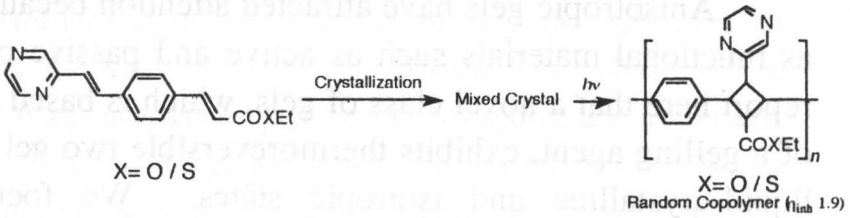

Furthermore, the mixture of 2,5-DSP and **1a** forms photoreactive molecular complex having a molar ratio of 1:2, although the crystal structures of each of the pure compounds are not isomorphous to each other. On photoirradiation, the molecular complex affords a crystalline linear high polymer. The ^{1}H NMR spectrum of the polymer coincides perfectly with that of a 1:2 mixture of poly-2,5-DSP and poly-**1a**, indicating that the photoproduct is not a copolymer but a mixture of poly-2,5-DSP and poly-**1a** with the molar ratio 1:2.[3]

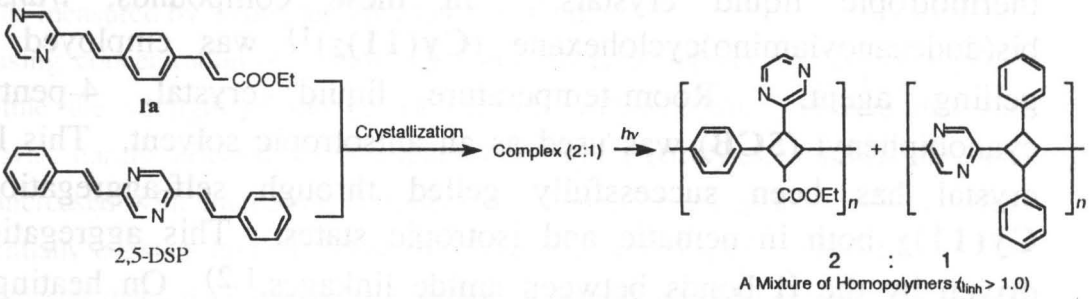

X-ray crystallographic analysis of the molecular complex reasonably explains its topochemical behavior and the structure of resulting photoproduct thus obtained, as is shown in Fig.1.

All the results lead to the conclusion that polymer nano-composite having an alternating monolayer of poly-2,5-DSP and bilayer of poly-**1a** was prepared through the topochemical [2+2] photopolymerization, as is shown schematically in Fig. 2.

The mixed crystals and molecular complexes mentioned above are obtained not only by recrystallization from the solution but, surprisingly, also by simple grinding the mixture of two diolefin crystals, followed by thermal annealing at the ordinary temperature.

We propose that the observed process of crystal formation is kinetically analogous to the photographic processes; the grinding time and the subsequent thermal annealing correspond to the exposure time and development processes, respectively.[4]

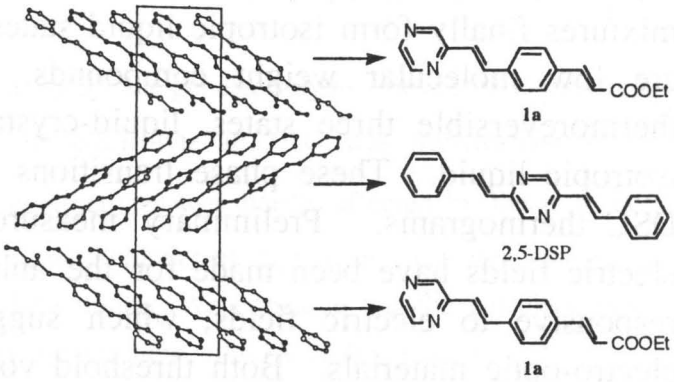

Fig. 1 Crystal structure of the molecular complex of 2,5-DSP and **1a**.

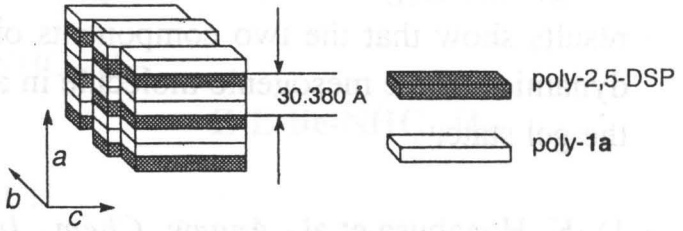

Fig.2 Schematic representation of the polymer nano-composite, poly-2,5-DSP•poly-**1a**.

References

1 For recent review, see; M. Hasegawa, *Advances in Physical Organic Chemistry*, **30**, 117 (1996).
2 Y. Maekawa, S. Kato, K. Saigo, and M. Hasegawa, *Macromolecules*, **24**, 5752 (1991).
3 M. Hasegawa, K. Kinbara, Y. Adegawa, and K. Saigo, *J. Am. Chem. Soc.*, **115**, 3820 (1993).
4 K. Kinbara, Y. Adegawa, K. Saigo, and M. Hasegawa, *Bull. Chem. Soc. Jpn.*, **66**, 1204 (1993).

Liquid-Crystalline Self-Organized Gels and Their Electro-Optic Effects

Takaaki Kutsuna, Takashi Kato, and Kenji Hanabusa†
Department of Chemistry and Biotechnology, Graduate School of Engineering, The University of Tokyo, Bunkyo-ku, Tokyo 113, Japan
†Department of Functional Polymer Science, Faculty of Textile Science and Technology, Shinshu University, Ueda, Nagano 386, Japan

Anisotropic gels have attracted attention because of great potential as functional materials such as active and passive optical devices. We report here that a novel class of gels, which is based on self-organization of a gelling agent, exhibits thermoreversible two gel states derived from liquid-crystalline and isotropic states. We focused on *trans*-1,2-bis(acylamino)cyclohexane derivative for the gelling agent of thermotropic liquid crystals. In these compounds, *trans*-1,2-bis(dodecanoylamino)cyclohexane (**Cy(11)$_2$**)[1] was employed as a gelling agent. Room-temperature liquid crystal, 4-pentyl-4'-cyanobiphenyl (**5CB**) was used as an anisotropic solvent. This liquid crystal has been successfully gelled through self-aggregation of **Cy(11)$_2$** both in nematic and isotropic states. This aggregation is driven by the H bonds between amide linkages.[1,2] On heating, the mixtures finally form isotropic liquid states because all of components are low molecular weight compounds. The mixtures show the thermoreversible three states, liquid-crystalline gel, normal gel, and isotropic liquid. These phase transitions are clearly observed in the DSC thermograms. Preliminary measurements of the response to electric fields have been made for the anisotropic gel. The gels are responsive to electric fields, which suggests applicability for new electro-optic materials. Both threshold voltage and response times of the gel are larger than those only for the component of **5CB**. These results show that the two components of the gel are interacting and the dynamics of the mesogenic molecule in anisotropic state are restricted in the gel state.

1) K. Hanabusa et al., *Angew. Chem., Int. Ed. Engl.* **1996**, *35*, 1949.
2) T. Kato et al., *Angew. Chem., Int. Ed. Engl.* **1997**, *36*, 1617; *Chem. Lett.*, **1997**, 1143.

Characterization of gel electrolyte from amino acid derivative

Kaori Hiratsuka, Kenji Hanabusa, Mutsumi Kimura, Hirofusa Shirai

Faculty of Textile Science and Technology, Shinshu University

3-15-1 Tokida, Ueda-shi, Nagano 386, Japan

Tel: 0268-21-5487 Fax: 0268-24-7248 e-mail: hanaken@giptc.shinshu-u.ac.jp

Octadecylamide of N-benzyloxycarbonyl-L-isoleucine (Z-L-Ile-$NHC_{18}H_{37}$) is an excellent gelator which can form gels with a wide variety of organic solvents. The gelation mechanism of Z-L-Ile-$NHC_{18}H_{37}$ can be explained as follows: the macromolecule-like aggregates are formed from numerous gelator molecules through intermolecular interactions such as hydrogen bonding and van der Waals interaction, then they are juxtaposed and interlocked, and finally immobilize solvents. To apply the gelator to new solid electrolyte materials, we prepared gel electrolytes of organic solvents containing electrolytes such as $LiClO_4$, $LiCF_3SO_3$, $LiBF_4$, and Bu_4NClO_4 by using Z-L-Ile-$NHC_{18}H_{37}$. Ion conductivity of the gel electrolytes was measured by a complex impedance method.

With increasing concentration of gelator, ion conductivity of the gel electrolytes slightly decreased, while the strength of the gel electrolytes increased. This indicated that ion conductivity was hardly affected by strength of the gel electrolytes. Further, the ion conductivity increased with increasing concentration of electrolytes up to 0.3M, but then remained essentially constant up to 1.5M before decreasing at the higher concentration. This observation indicates that ion aggregates or ion pairs are formed in the gel matrix at the higher concentration of electrolyte.

Temperature dependence of ion conductivity for the gel electrolytes obeyed Arrhenius type over the range 20-90°C. Although the gel electrolyte at 20°C was transformed to the homogeneous solution at 90°C, the ion conductivity was hardly affected by the transition from gel to homogeneous solution. Namely, the behavior of supporting electrolytes in the gel matrix was essentially similar to that in the solution. We conclude that the gel electrolytes from Z-L-Ile-$NHC_{18}H_{37}$ can be sufficiently used as new solid electrolyte materials.

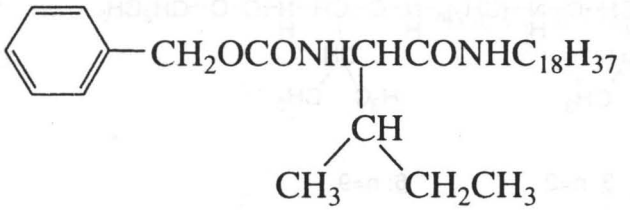

Z-L-Ile-$NHC_{18}H_{37}$

Organogel-forming agents of bipolar amino acid derivatives

Reo Tanaka, Kenji Hanabusa, Mutsumi Kimura, and Hirofusa Shirai

Department of Functional Polymer Science, Faculty of Textile Science & Technology,

Shinshu University, Ueda 386

Tel: 0268-21-5487 Fax: 0268-24-7248 e-mail: hanaken@giptc.shinshu-u.ac.jp

Organogel of synthetic polymers and aqueous gels of biopolymers have received considerable attention, while the study of the gelation of organic solvents by low molecular weight gelators has only been carried out on a limited number of compounds and is still in its infancy. Bolaamphiphiles of amino acid derivatives were synthesized, and the effects of the length of the alkylene segment and the N-terminal protecting group on gelation ability for various organic liquids were examined. Bolaamphiphiles of amino acid derivatives could cause gelation of a wide variety of organic liquids. The bolaform amide **3** is of special interest to us because it contain neither an aromatic moiety nor a long methylene segment. The boraform amide **3**, which is expected to be a smoothly-biodegradable gelator, may have a wide range of possible applications, e.g., environmentally as a gelator of spilled toxic solvents and cooking oils, or medically as a drug-delivery material. The FT-IR spectrum of the transparent benzene gel of **1** was characterized by bands attributed to intermolecular hydrogen bonding, whereas the isotropic solution of **1** in chloroform indicated of non-hydrogen bonding stretching vibrations. The FT-IR spectra suggested that hydrogen bonding plays an important role in gelation. Transmission electron micrographs, scanning electron micrographs, and dark-field optical micrographs of gel exhibited that the networks were build up by numerous fibers. It is assumed that the numerous fibers are in contact with each other and then form three-dimensional network, and finally immobilize the fluid component on a macro-scopic scale.

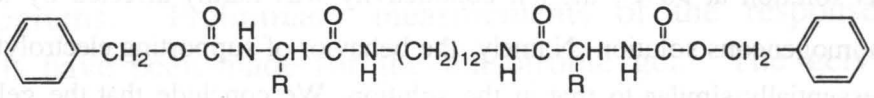

1: R = -CH(CH$_3$)$_2$ (L-Val) **2**: R = -CH(CH$_3$)CH$_2$CH$_3$ (L-Ile)

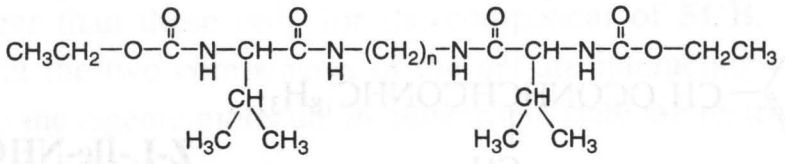

3: n=2 **6**: n=9

4: n=7 **7**: n=10

5: n=8 **8**: n=12

Organogels from cyclohexane derivatives

Atsushi Kawakami, Kenji Hanabusa, Mutsumi Kimura and Hirofusa Shirai

Faculty of Textile Science and Technology, Shinshu University

3-15-1 Tokida Ueda-shi, Nagano 386 Japan

Tel: 0268-21-5487 Fax: 0268-24-7248 e-mail: hanaken@giptc.shinshu-u.ac.jp

Some dilute binary solutions of low-molecular weight compounds can form thermally-reversible physical gel in appropriate organic liquids. In general, such organogel-forming compounds self-associate spontaneously to harden organic liquids on cooling of appropriate isotropic solution. The main driving forces for gelation by low-molecular weight compounds are non-covalent bonds, i.e., hydrogen bond, electrostatic interaction, van der Waals interaction, $\pi-\pi$ interaction, and hydrophobic interaction.

We report here on gelation behavior of trialkyl *cis*-1,3,5-cyclohexanetricarboxamides as new organogel-forming agents. The addition of small amount of trialkyl-*cis*-1,3,5-cyclohexanetricarboxamides was able to cause thermally-reversible physical gelation in organic liquids. The gelling ability and gel mechanisms were investigated by gelation tests, FT-IR spectroscopy, DSC, and TEM. TEM images of loose gel and gel-like fluid show different types of aggregates. One is three dimentional network aggregate for gel, and the other is rod-like aggregate for gel-like fluid. It is thought that the transformation of isotropic solution to crystal, gel, or viscoelastic fluid on cooling process depends on the structure of alkyl group and the type of solvent. When favorable hydrophilic-hydrophobic balance of trialkyl *cis*-1,3,5-cyclohexane-tricarboxamides against solvent is performed, gel or highly viscoelastic gel-like fluid is formed.

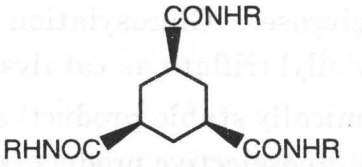

1; R = CH_3

2; R = $CH_2(CH_2)_4CH_3$

3; R = $CH_2(CH_2)_6CH_3$

4; R = $CH_2(CH_2)_8CH_3$

5; R = $CH_2(CH_2)_{10}CH_3$

6; R = $CH_2(CH_2)_{16}CH_3$

7; R = $CH_2CH_2CH(CH_3)CH_2CH_2CH_2CH(CH_3)_2$

8; R = $\begin{matrix} CH \\ | \\ CH_2CH_2CH_2CH_2CH_2CH_3 \end{matrix}\begin{matrix} CH_2CH_2CH_2CH_2CH_2CH_2CH_2CH_3 \\ \end{matrix}$

Synthesis of Branched Polysaccharide and Oligosaccharide

Kasuya, M.C., Hatanaka, K.
Department of Biomolecular Engineering
Tokyo Institute of Technology
4259 Nagatsuta-cho, Midori-ku, Yokohama 226, Japan

Many kinds of carbohydrate chains show biological activity due to the branching units. However, the chemical synthesis of branched polysaccharides requires careful consideration in controlling the branching position, the kind of branching unit and the length of branching. In this research, the chemical synthesis of a branched polysaccharide, with potential hypoglycaemic activity, is being investigated using cationic ring-opening polymerization of a disaccharide derivative.

The disaccharide monomer (1,6-anhydro-3-*O*-benzyl-4-*O*-(2,3,4,6-tetra-*O*-benzyl-α-D-glucopyranosyl)-2-deoxy-β-D-*arabino*-hexopyranose with the glucopyranosyl branching unit at C-4 position was prepared via glucosylation of the 1,6:2,3-dianhydro glucose derivative using the trichloroacetimidate of tetrabenzyl glucose. Glucosylation carried out in dichloromethane with *tert*-butyldimethylsilyl triflate as catalyst proceeded with high α-anomeric selectivity (thermodynamically stable product) at room temperature. On the other hand, at -30°C, the β-stereoselective product (kinetically stable) was produced.

Ring-opening polymerization of the 1,6-anhydrodisaccharide monomer was carried out under high vacuum in dichloromethane with phosphorous pentafluoride as initiator. The polymerization gave a mixture of a cyclic oligomer and an α- (1→6) - linked "comb-shaped" polysaccharide (DPn ~ 14) having an α-glucopyranosyl branching unit per each sugar residue in the backbone chain.

Copolymerization of the 1,6-anhydrodisaccharide monomer with a monosasaccharide monomer (1,6-anhydro-3,4-di-*O*-benzyl-2-deoxy-β-D-*arabino*-hexopyranose) under high vacuum with phosphorous pentafluoride as initiator was also carried out.

ANALYSIS OF THERMAL MOLECULAR MOTION AT SURFACE OF POLYMERIC SOLIDS BASED ON TEMPERATURE DEPENDENT SCANNING FORCE MICROSCOPY

Noriaki Satomi, Keiji Tanaka, Atsushi Takahara, and Tisato Kajiyama

Department of Materials Physics and Chemistry, Graduate School of Engineering, Kyushu University

Lateral force between solid surface and sliding cantilever tip can be evaluated by detecting the torsion of the sliding cantilever on nanometer scale. Since the frictional behavior of polymeric solids is closely related to their dynamic viscoelastic properties, it is possible to investigate surface molecular motion of the polymeric solids by using lateral force microscope(LFM). The temperature dependence of lateral force for the polystyrenes (PSs) thin films was investigated in order to reveal thermal molecular motion at the surface of PS. LFM measurements of PS with molecular weight, Mn of 140k at various temperatures revealed that the scanning rate dependence of lateral force was appeared only in a temperature range from 343 K to 383 K. In a temperature range from 363 K to 383 K, the peak on the scanning rate-lateral force curve was observed. In the case of PS with Mn of 4.9k, the magnitude of lateral force depended on the scanning rate in a temperature range from 263 K to 303 K, and the peak was observed in a temperature one from 283 K to 293 K. These results indicate that the surfaces of the monodisperse PSs films are in a glass-rubber transition state at a lower temperature range compared with the bulk glass transition temperature, Tg.

A master curve was obtained by horizontal and vertical shifts of the scanning rate dependences of lateral force at various temperatures. Reference temperatures were 293 K for Mn of 4.9k and 363 K for Mn of 140k, respectively. It was revealed that the time-temperature superposition principle, which is characteristic to amorphous bulk polymeric materials at around Tg, could be also applied to the surface αa-relaxation process corresponding to the surface glass transition behavior. The relationship between horizontal shift factor, a_T and reciprocal measuring absolute temperature followed the Arrehenius type equation. Then, the magnitude of activation energy for the surface αa- relaxation process (surface micro-Brownian motion) was calculated from the slope of the a_T vs. 1/T plot, 190 - 220 kJ·mol^{-1}. This magnitude is fairly lower than that for the bulk one, 360 kJ·mol^{-1}. At the air-polymer interface, an excess free volume is induced by the surface localization of the chain end groups and also, the degree of freedom of polymeric segments contacting with the air might be greater than that in the bulk state. Then, it can be predicted from the magnitude of the activation energy that the energy barrier for the surface αa-relaxation process might be lower in comparison with those for the bulk one.

TOPOCHEMICAL PHOTOREACTION BEHAVIOR OF NEW 2,5-DISTYRYLPYRAZINE DERIVATIVES

K.Watanabe, C. Hosono, K. Saito and M. Hasegawa
Department of Materials Science and Technology, Faculty of Engineering,
Toin University of Yokohama
1614 Kurogane-cho, Aoba-ku, Yokohama, Kanagawa 225 Japan.

Introduction

Topochemical [2+2] photopolymerization was first reported on the reaction of 2,5-distyrylpyrazine (DSP) crystal. Since then, a great number of highly crystalline linear polymers have been prepared from diolefinic compound crystals by repeating step-by-step growth mechanism of [2+2] photocyclodimerization. Among these crystals, unsymmetric diolefin compounds are particularly interesting since their behavior and photoproducts are so "kaleidoscopic".[1]

In this study, we report the photoreaction of several kinds of unsymmetrically substituted diolefin crystals having DSP skeleton. Structure and properties of the resulting polymers were investigated by conventional spectroscopic measurements. Furthermore, mixed crystals consisting of two types of DSP derivatives, were prepared and their topochemical behavior was also investigated.

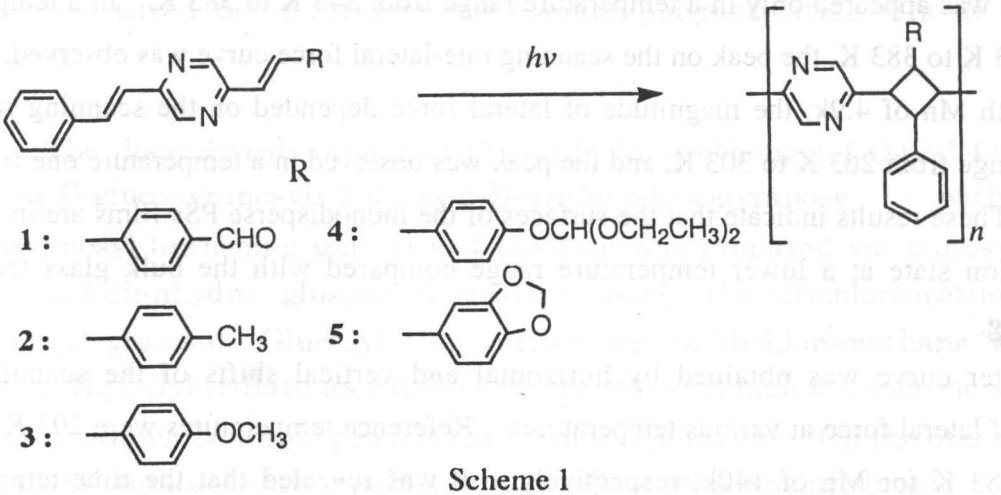

Scheme 1

Results and Discussion

Several DSP derivatives were newly synthesized, and their photoreactivity was investigated in the crystalline state. Monomer crystals (**1-5**) showed an extremely high photoreactivity and gave highly crystalline linear high-molecular-weight polymers ($[\eta]$=0.98-5.2) having cyclobutane rings in the main chain in nearly quantitative yields.

By IR, DSC/TG and X-ray diffraction studies the photoreactions were proved to be typical of the crystal-to-crystal transformation through the [2+2] photocyclodimerization. The polymer crystals as-polymerized, were stable on further photoirradiation in the air whereas amorphous polymers regenerated, readily degraded under similar condition. During the photoirradiation pyrazine moiety in the amorphous polymer gradually decreased and nitrile group newly appeared, indicating the photo-oxidative degradation of pyrazine ring to give the nitrile derivatives, as was the case of poly-2,5-DSP.

Photoreactive mixed crystal was obtained by recrystallization, e.g. from the mixture of equimolar **1** and **2**. On photoirradiation, the crystal gave high molecular weight of highly crystalline linear copolymer ($[\eta]$=5.6).

Reference

1 M. Hasegawa, *Adv. Phys. Org. Chem.*, **30**, 117 (1995).

Oxygen Hopping in a Fixed Carrier Membrane

Yukihiro Tsukahara, Hiroyuki Nishide, Eishun Tsuchida
Dept Polymer Chemistry, Waseda University, Tokyo 169

Polyvinylidenchloride is a typical gas barrier polymer. *meso*-Tetrakis(α, α, α, α-*o*-pivalamidophenyl)porphyrinatocobalt(II) (CoP) was combined, in this paper, with poly(vinylidenchloride-co-vinylimidazole) (CIm) (Scheme 1), to yield a red-colored and glassy but still tough membrane. Oxygen was selectively bound with the CoP fixed in the membrane. Oxygen-binding affinity and absorption amount were 0.1cmHg^{-1} and 2.0 cm^3/cm^3(polymer), respectively.

Gas permeation through the CoP-CIm membrane was carefully measured by three methods, low-vacuum/pressure measurment, electrochemical measurment, and gaschromatography, because of low gas permeability of the membrane: The data almost coincided each other. Examples of oxygen permeability coefficient (P_{O2}) for the membrane were shown in Figure. P_{O2} steeply increased at low upstream oxygen pressure and also increased with the CoP concentration in the membrane. The CoP fixed in the membrane facilitates the oxygen transport through a carrier-mediated pathway or acts as both a chemical absorption site and a carrier for oxygen, and increases the transport rate of oxygen relative to that of nitrogen. The effect of the CoP complex fixed in the polymer membrane on the facilitated transport oxygen was analyzed.

$$CoP + O_2 \rightleftharpoons CoP\text{-}O_2$$

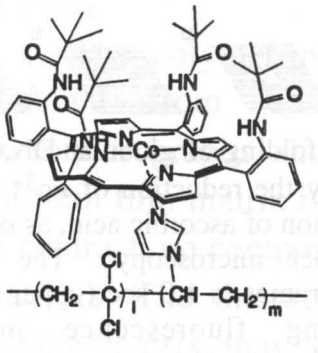

Scheme 1 CoP-CIm

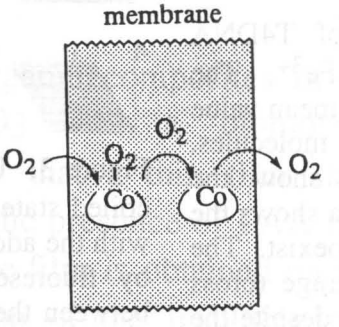

Scheme 2

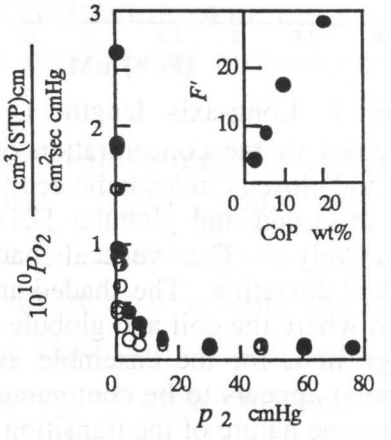

Fig. Effect of upstream oxygen pressure (p_2) on oxygen permeability coefficient (P_{O2}) for the CoP-CIm membrane (●; 20wt%, ◑; 10wt%, ◐; 5wt%, ○; 2.5wt%), Inset: Facilitation factor(F')

Higher Order Structure of DNA Controlled by the Redox State of Fe^{2+}/Fe^{3+}

Yuichi Yamasaki and Kenichi Yoshikawa
Graduate School of Human Informatics, Nagoya University, Nagoya 464-01, Japan

Abstract

We performed fluorescence microscopic observation of the conformational change of individual T4DNAs (166kbp) induced by Fe^{2+}/Fe^{3+}. Individual DNAs undergo a marked discrete transition from an elongated coil into a collapsed globule with an increase in the Fe^{3+} concentration at around 1-2 μM. On the other hand, DNAs remained in the elongated coil state with the addition of Fe^{2+} up to a concentration of 30 μM. Using these experimental results we tried to control the transition of DNA by the redox reaction of Fe^{2+}/Fe^{3+}. We found that collapsed globule DNA unfolds with the reduction of Fe^{3+}. The morphology of DNA that had been collapsed with Fe^{3+} was also studied by electron microscopy, and showed a quasi-spherical structure that presumably was the result of an intermediate collapsed state with a flexible rod-like structure. The results have been analyzed theoretically in terms of the double minima in the free energy profile of a single DNA molecule, indicating that the change in the translational entropy of the counter ions is the main reason why high-valency ions are more effective in inducing the collapse.

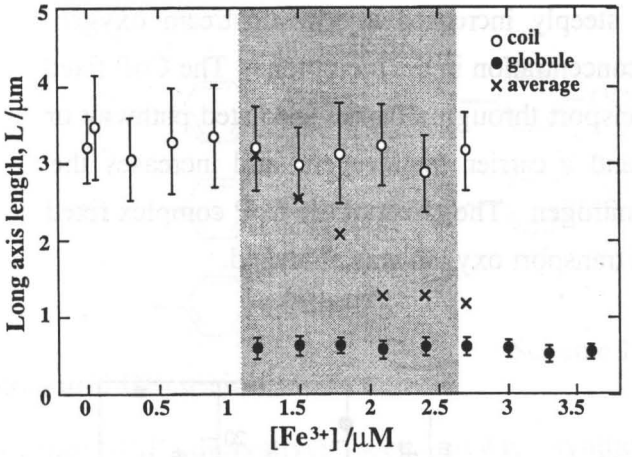

Figure 1. Long-axis length, L, of T4DNA molecules vs the concentration of Fe^{3+}. The open and closed circles indicate the mean value of L in coiled and globular DNA molecules, respectively. The vertical bars show the standard deviation. The shaded area shows the region where the coil and globule coexist. The change in L for the ensemble average (cross symbols) appears to be continuous, despite the all-or-none nature of the transition in individual DNAs.

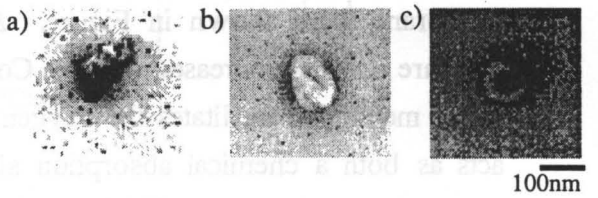

Figure 2. Transmission electron micrograph of globular T4DNA. a), b) were formed with Fe^{3+}, and c) was formed with $Co(NH_3)_6^{3+}$.

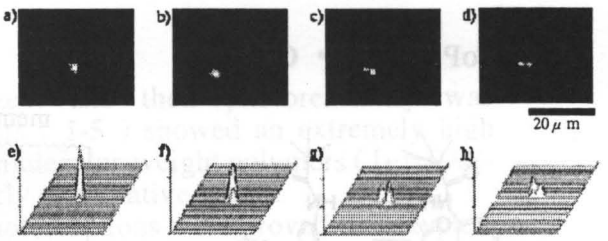

Figure 3. Unfolding of globular DNA into a coiled state by the reduction of Fe^{3+} to Fe^{2+} with the addition of ascorbic acid, as observed by fluorescence microscopy. The interval between the frames is 1.0 sec (upper panels). Corresponding fluorescence intensity distributions (bottoms).

References
1) Y.Yamasaki and K.Yoshikawa, *J.Am.Chem.Soc.*,**119**, 10573-10578 (1997).
2) M.Takahashi, A.R.Khokhlov, V.V.Vasilevskaya and K.Yoshikawa, *J.Phys.Chem.*, **B101**, 9396-9401(1997).

Polymer/Inorganic Composites Formed by a Biomineralization Process

Takahiro Amamiya, Takuo Suzuki, and Takashi Kato
Department of Chemistry and Biotechnology, Graduate School of Engineering, The University of Tokyo, Hongo, Bunkyo-ku, Tokyo 113, Japan

Biological minerals associate organic macromolecules containing functional groups such as carboxylic acid moieties. The study on biomineralization has shown that macromolecules control the crystallization processes of the minerals as soluble and insoluble matrices and the formation of the polymer/inorganic composite structures. Calcium carbonate ($CaCO_3$) is important inorganic, geological and bioinorganic materials. Our intention is to develop a new strategy for the controlled synthesis of polymer/inorganic composites with organized structures. We report here: (1) the effect of soluble matrix of biomolecules on the crystallization of $CaCO_3$; (2) the preparation of thin composite films consisting of $CaCO_3$ and macromolecules.

The crystallization of $CaCO_3$ in aqueous solution without insoluble matrix has been done in the presence of a soluble matrix of poly(glutamic acid)(PGA) or poly(acrylic acid)(PAA). These matrices affect the polymorphs of $CaCO_3$. Calcite has been obtained without these soluble matrices. The crystallization was inhibited in the presence of PAA. The spherical crystals are formed with PGA. X-ray diffraction patterns show that both vaterite and calcite are obtained in the presence of biomolecules of PGA.

The polymer/inorganic composites in thin film states have been obtained from $CaCO_3$ and a biomolecule. SEM and optical photomicrographs show that a thin film state of calcite grows on a chitosan film matrix in the presence of PAA or PGA as a soluble matrix. In contrast, no composite film is obtained on the chitosan without soluble matrices. The interaction of the insoluble matrix of chitosan and the soluble matrix may play an important role for the formation of thin composite films.

Thermal Stabilization of Redox-active Proteins in Ion Conductive Polymers

Natsue Y. Kawahara and Hiroyuki Ohno
Department of Biotechnology
Tokyo University of Agriculture & Technology
Koganei, Tokyo 184-8588, JAPAN

Introduction

Poly(ethylene oxide) (PEO) has been used as ion conductive polymers, and it satisfies the requirement as a solvent for the electrochemical reactions. The use of PEO as a polymer solvent for various molecules may support new interesting properties of redox active molecules. We have been studying the redox reaction of PEO-modified heme proteins in PEO oligomers. The thermal stability of PEO-modified hemoglobin (PEO-Hb)[1] and myoglobin (PEO-Mb)[2] was extremely improved by the use of PEO as a solvent, and these PEO-modified heme proteins showed redox activity from -10 to 120°C when PEO was used as a solvent. In this study, some factors for the thermal stabilization of PEO-Mb in PEO oligomers were discussed.

Experimental

Myoglobin from horse skeletal muscle (SIGMA) was used as a heme protein for all experiments. PEO-Mb was synthesized according to the conventional method as reported previously[3]. PEO with average molecular weight of 750 was used for PEO modification of heme proteins in this study. The degree of PEO modification on one Mb was determined by the titration of amino groups. The PEO-Mb having 13 PEO chains was used. PEO-Mb was dissolved in PEO_{200} containing 0.5M KCl, and the thermal stability and redox activity of PEO-Mb in PEO with average molecular weight of 200 (PEO_{200}) were investigated with visible spectroscopy (Shimadzu, UV-2200A) and cyclic voltammetry (Fuso Seisakusho, HECS 326PC) at various temperatures. Effect of water content on the thermal stability of PEO-Mb in PEO_{200} was also analyzed. Water content was determined with Karl-Fischer moisture titrator (Kyoto electronics, MKS-210).

Results and Discussion

Effect of water content on the stability of PEO-Mb at 80°C was investigated in PEO_{200} through the visible spectral change. The absorbance at Soret band of oxidized PEO-Mb in PEO_{200} decreased gradually with time at 80°C when water content was 14.0wt% and more. Even after removal of water in PEO_{200} after heating, reduced absorbance was not recovered. The thermal stability of PEO-Mb in PEO_{200} was also analyzed with cyclic voltammetry. The typical redox peaks of PEO-Mb were obtained in PEO_{200} regardless water content. However, the peak current decreased in PEO_{200} at 80°C when water content was 18.0wt% and more (Fig.1). These suggest that the irreversible thermal denaturation of PEO-Mb was attributable to the added water molecules. PEO-Mb in PEO oligomers should be stabilized at high temperatures by the use of PEO_{200}.

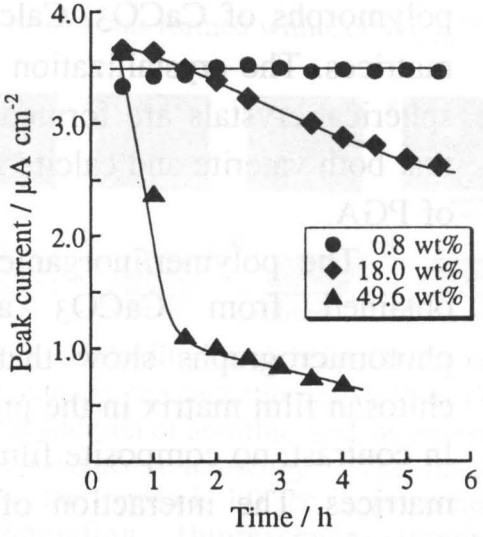

Fig.1 Effect of water content on the peak current of PEO-Mb in PEO_{200} at 80°C. Sweep rate : 33 mV/s, W.E. : ITO

References

1. N.Y. Kawahara and H. Ohno, Bioconjugate Chem., **8**, 643 (1997).
2. N. Y. Kawahara and H. Ohno, Solid State Ionics, in contribution.
3. H. Ohno and T. Tsukuda, J. Electroanal. Chem., **341**, 137 (1992).

Synthesis of and Spin Alignment in Star-Shaped Radical Polymers

Makoto Miyasaka, Hiroyuki Nishide, Eishun Tsuchida
Dept Polymer Chemistry, Waseda University, Tokyo 169

We recently synthesized poly(1,2-phenylenevinylene) bearing di-*tert*-butylphenoxyl and have for the first time reported a through-conjugated backbone bond and long-range ferromagnetic exchange interaction between the pendant unpaired electrons. In order to improve spin quantum number S by following a two-dimensional strategy, we extended it to star-shaped homologues **1** and **2**.

The star-shaped poly(1,2-phenylenevinylene)s with a 4-substituted pendant phenoxyl were synthesized by polymerizing a 2-bromo-4-(acetoxyphenyl)styrene derivative in the presence of 1,3,5-triiodobenzene or 1,3,5-tris(3',5'-diiodophenyl)benzene as the core *via* Heck reaction using a palladium catalyst. The iodide of the cores was initially reacted with the monomer, and heating the reaction mixture allowed the polymerization. Head-to-tail linkage of the branch chains and completely reacted core structures were confirmed with NMR *etc*. The hydroxy precursor compounds were quantitatively converted to the phenolate anion in the presence of alkaline and chemically oxidized to yield the corresponding radicals. The polyradical **1** even with a spin concentration of 0.6 spin/unit revealed an average S value of 6/2, indicating an heptet ground state. The 1,3,5-benzene core acted as an effective magnetic coupler, and an intramacromolecular ferromagnetic exchanging interaction was realized through the star-shaped π-conjugated backbone. The polyradical **2** was also described.

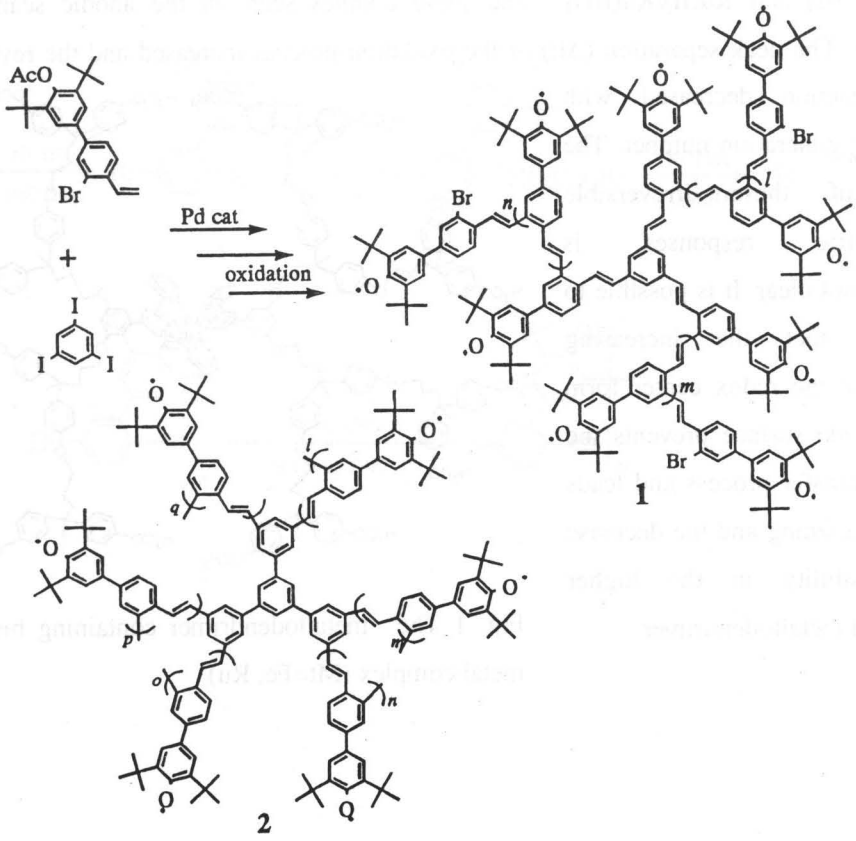

Metallodendrimers containing Bis(terpyridine) Iron(II) and Ruthenium(II) Complexes

Katsutoshi Mizuno, Mutsumi Kimura, Kenji Hanabusa, and Hirofusa Shirai

Department of Functional Polymer Science, Faculty of Textile Science and Technology, Shinshu University, Ueda 386 (JAPAN)

Tel: 0268-21-5499, FAX: 0268-24-7248, E-mail: mkimura@giptc.shinshu-u.ac.jp

The incorporation of metal functionality in dendrimers has received significant attention because of the change of photophysical/photochmical, electrochemical, optical catalytic properties when metal complexes are attached to a dendric matrix. We present about the change in redox property of a series of iron(II) and ruthenium(II) complexes in which the metal ion is encapsulated between two dendric terpyridine ligands. These metallodendrimers were synthesized by the metal-mediated assembly through the formation of metal complex between two ligands possessing a well-defined hyperbranced macromolecule and one metal ion (fig. 1). New dendritic terpyridine ligand with two different numbers of generations were prepared on the basis of Frechet convergent approach. Treatment of the dendric terpyridine ligands with $FeCl_2 \cdot 4H_2O$ or $RuCl_3 \cdot 3H_2O$ generated the desired metallodendrimers. The UV spectra were consistent with complex formation: the electronic spectra of all iron and ruthenium complexes in MeCN showed exactly the same characteristic MLCT transitions in the visible region. The results of cyclic voltammetry studies of these metallodendrimers provided useful information regarding the redox properties of metal complex in the dendrimer. The bis(terpyridyl)iron and ruthenium complexes exhibited one oxidation (Fe(II)/Fe(III) and Ru(II)/Ru(III)) , and these couples seen on the anodic scan is chemically reversible. The peak separation (ΔE) of the oxidation process increased and the reversibility of the redox reaction decreased with increasing generation number. The reason of these irreversible voltammetric responses is currently not clear. It is possible to speculate that the increasing distance of the redox center form the electrode surface prevents the electron transfer process and leads to the broadening and the decrease in reversibility in the higher generation metallodendrimer.

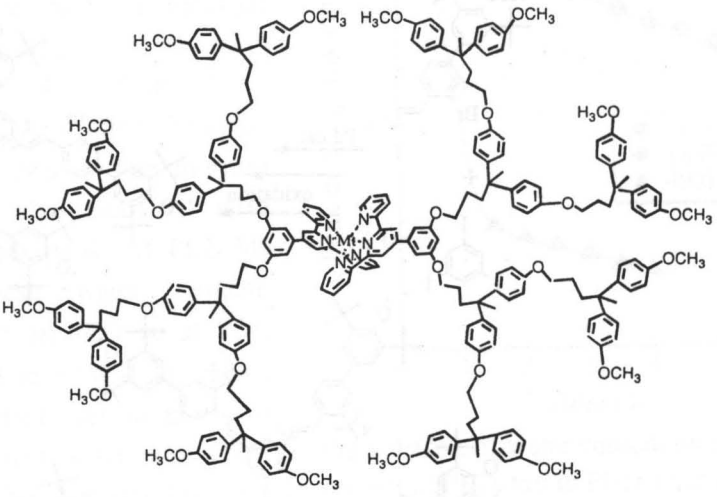

Fig. 1 The metallodendrimer containing bis(terpyridine) metal complex (Mt=Fe, Ru)

Synthesis and Magnetic Property of Poly(2-oxyphenyl-1,4-phenyleneethynylene)

Tadatoshi Maeda, Hiroyuki Nishide, Eishun Tsuchida
Dept Polymer Chemistry, Waseda University, Tokyo 169

We have been realizing a throughbond ferromagnetic interaction between the side-chain phenoxy radicals by synthesizing the polyradical with poly(phenylenevinylene) backbone. To enhance the ferromagnetic interaction, we selected poly(1,4-phenyleneethynylene) as a π-conjugated backbone because of its developed conjugation and spin polarization even after substitution on the phenylene ring.

4-Bromo-2-(3',5'-di-*tert*-butyl-4'-hydroxyphenyl)toluene was prepared by cross-coupling [3,5-di-*tert*-butyl-4-(trimethylsiloxy)phenyl]magnesiumbromide to 4-bromo-2-iodotoluene with Ni catalyst. The trimethylsiloxy group was exchanged for an acetoxy group, and the methyl group was converted to a vinyl group *via* the Wittig reaction. The monomer, 4-bromo-2-(3',5'-di-*tert*-butyl-4'-hydroxyphenyl)ethynylbenzene, was synthesized by bromination to the vinyl group, and dehydrobromination under alkaline conditions.

4-Bromo-2-(3',5'-di-*tert*-butyl-4'-hydroxyphenyl)ethynylbenzene was polymerized with a Pd-Cu catalyst.

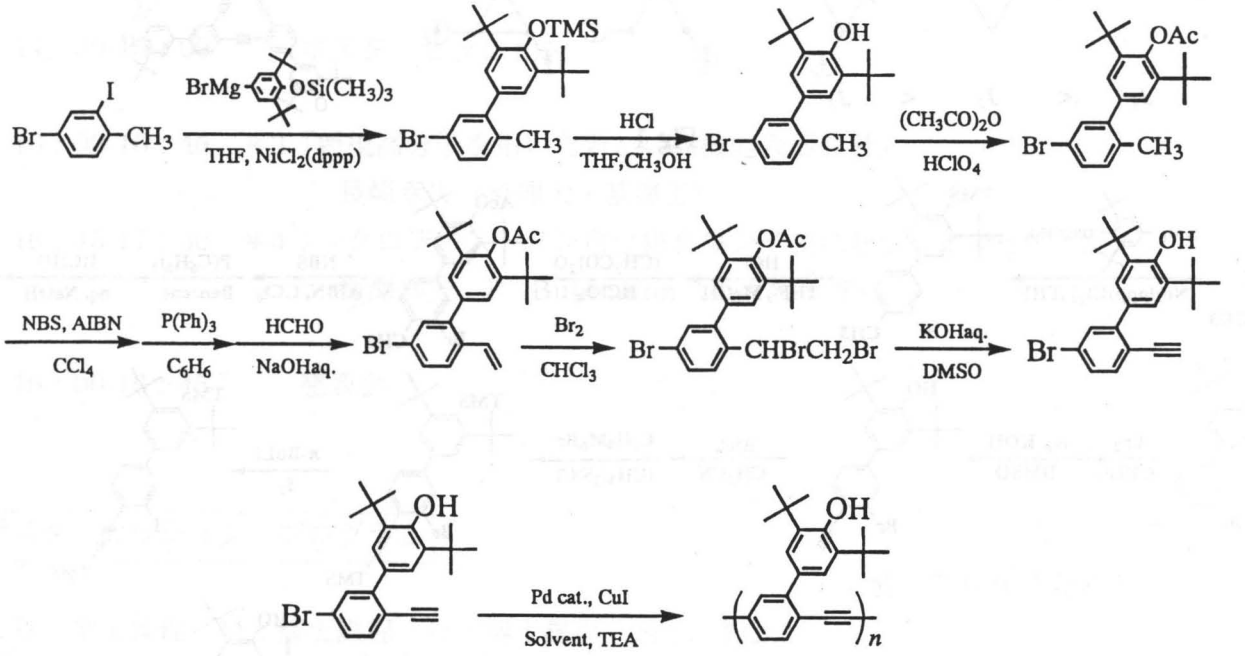

Synthesis and Magnetic Property of Cyclic Oligo(4-oxyphenyl-1,2-phenyleneethynylene)

Yong-Jin Pu, Masahiro Takahashi, Hiroyuki Nishide, Eishun Tsuchida
Dept Polymer Chemistry, Waseda University, Tokyo 169

We have reported ferromagnetic interaction between spins on phenoxyl radicals through π-conjugated poly(1,2-phenyleneethynylene) skeleton. 5,6,11,12,17,18-Hexadehydro-tribenzo [*a, e, i*]cyclododecene was selected in this paper as a model of a cyclic poly(1,2-phenyleneethynylene) coupler. It is expected a larger ferromagnetic interaction between spins because the neighboring spin sites connects with each other through two paths(Fig 1).

4-(3',5'-*Tert*-butyl-4'-hydroxyphenyl)-2-bromoethynylbenzene was synthesized by cross-coupling the hydroxyphenyl group with bromotoluene using Ni catalyst, the vinylation via Wittig reaction, and dehydrobromidation under aikaline conditions. After iodination of *o*-position of the ethynyl group and condensation to phenylethynyl copper derivative, we obtained the cyclic-trimer bearing the phenoxyl precursor by cyclization with Castro reaction. On the other hand, we also synthesized the trimer using Pd(0)-Cu(I)catalyst from the crresponding *o*-bromomonomer.

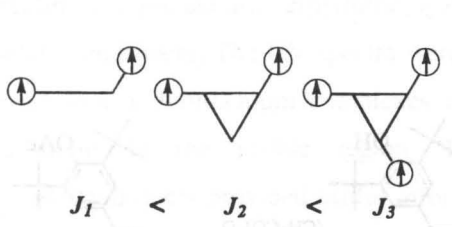

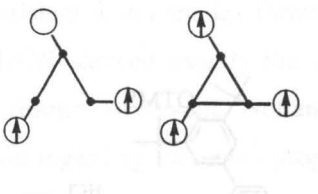

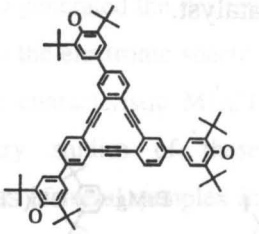

Fig 1

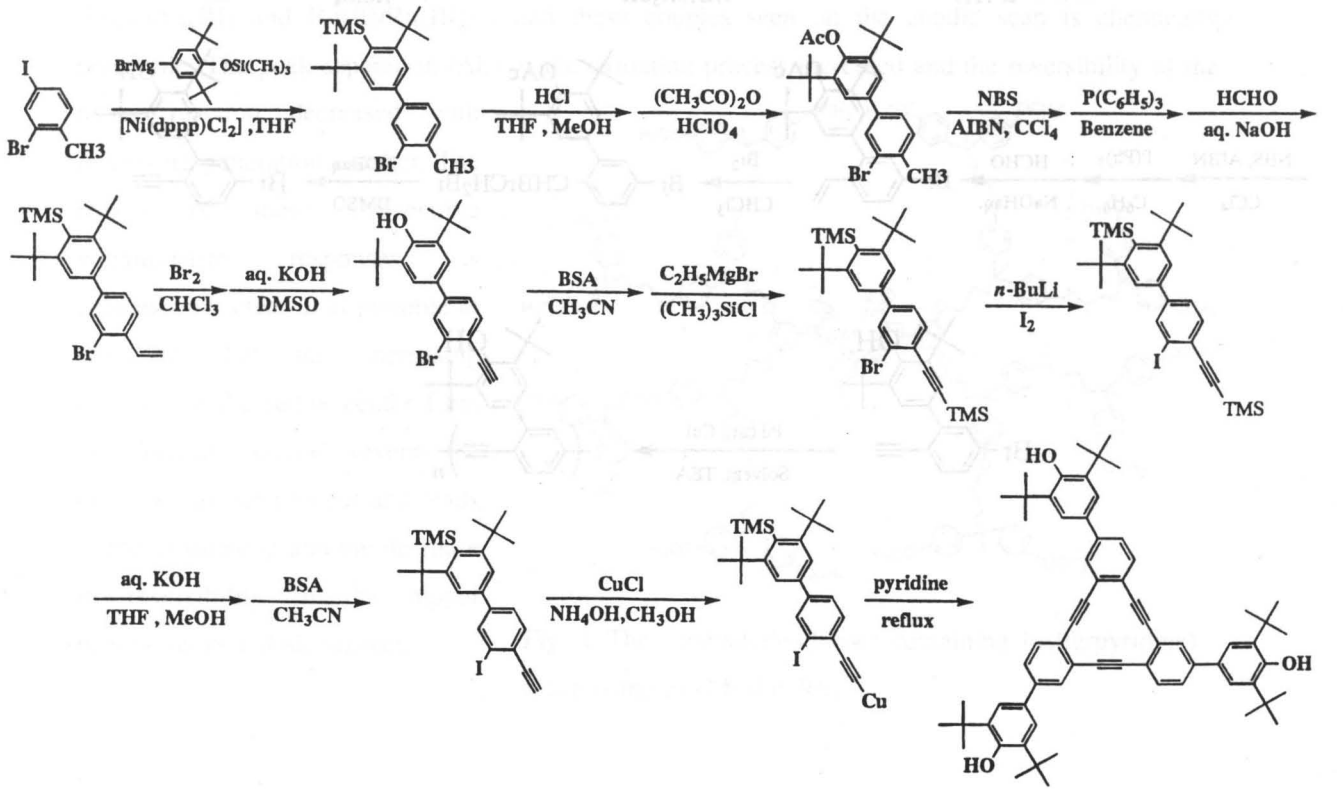

第２シンポジウム　「分子系超構造」Molecular Superstructure

チェア　荒木孝二（東大）

分子組織化過程を制御し、分子集合組織を断層的に高次化した「分子系超構造」の作製は、革新的な機能・特性をもつ材料の創成に向けたアプローチとして注目を集めている。本シンポジウムは、主に二次元超分子構造の設計と機能に焦点を当てた下記の依頼講演４件と、一般から募集する分子系超構造に関連するポスター・セッションで構成する。

１２月１１日（木）　＜＊招待講演＞

13：00-13：45　＊1「環状両親媒性分子からなる二次元組織分子膜」
市村國宏（東工大・資源研）

13：45-14：30　＊2「二次元結晶のクリスタルエンジニアリング」
奥山健二（東農工大・工）

14：30-16：00　ポスターセッション

16：00-16：45　＊3「新規高分子を用いた新しい高機能表面設計」
長崎幸夫（東理大・基礎工）

16：45-17：30　＊4「シクロデキストリン自己集合単分子膜に基づく化学センシング」
梅澤喜夫、P　Buhlmann（東大院・理）

16：00-16：45　懇親会

ポスターセッション・プログラム

於　７０９号会議室

＜B：学士課程　M：修士課程　D：博士課程　S：一般＞

=番号=　＝著者 ※印:発表者＝　＝タイトル　＝

P2-1M.　※中台弥秀、野口恵一、奥山健二（東農工大・工）　「カチオン性界面活性剤の形成する層状構造」

P2-2M. ※岡田　崇、飯島道弘、長崎幸夫、加藤政雄、片岡一則（東理大・基礎工）
「新しい素構造を目指した反応性高分子ミセルの創成」

P2-3S. ※野口恵一、中台弥彦、奥山健二（東農工大・工）
「カチオン性界面活性剤と芳香族化合物が形成する層状複合体中における分子配列様式」

P2-4M. ※佐藤康雄、長崎幸夫、加藤政雄（東理大・基礎工）
「アルコラート開始による機能性ポリメタクリレートの新規合成」

P2-5M. ※門間智之、吉川　功、高澤亮一、荒木孝二（東大・生研）
「ユニットの集積化に基づくヌクレオシド誘導体の超分子構造Ⅰ．テープ状ユニット」

P2-6B. ※荒井彩子、田中滋光、水口　仁（横国大・工）
「ピロロピロール誘導体の結晶構造と電子構造」

P2-7S. ※吉川　功、門間智之、高澤亮一、荒木孝二（東大・生研）
「ユニットの集積化に基づくヌクレオシド誘導体の超分子構造Ⅱ．環状四量体ユニット」

P2-8S. ※水口　仁（横国大・工）
「チオピロロピロールの結晶多形と固体スペクトル -光ディスクへ応用- 」

P2-9M. ※薄井一裕、加藤政雄（東理大・基礎工）
山田真治、松田宏雄（物質研）
中西八郎（東北大・反応研）
「メタクリルアミド系二次非線形光学材料の合成と評価」

P2-10S. ※近藤　満、野呂真一郎、島村真理子、浅見朗子、関　健司、北川　進（都立大・理、大阪ガス応用研）
「ガスを吸着する多孔性配位高分子の合理的設計と構築」

P2-11D. ※木村龍実、加茂公彦、加藤政雄（東理大・基礎工）
段　宣明、岡田修司、中西八郎（東北大・反応研）山田真治、福田隆史、松田宏雄（物質研）
「Chained Chromophore NLO 材料：芳香族エステルオリゴマーとその誘導体」

P2-12M. ※湯村　要、松本真哉、大谷裕之
水口　仁（横国大・工）
「色素化クラウンエーテルの結晶構造と電子スペクトル」

P2-13M. ※原田健吉、廣瀬佳男、大月　穣、荒木孝二（東大・生研）
「配位相互作用を利用したポルフィリン・イミド超分子における電子移動」

P2-14D. ※落合慶子、陸川政弘、讃井浩平、緒方直哉（上智大・理工）
「光学活性基を有するポリ（チオフェン）誘導体超薄膜の構造と特性」

P2-15D. ※趙　庚娥、島田敏宏、小間　篤（東大院・理）
「高い蒸気圧を持つ有機分子のエピタシャル成長制御」

P2-16D. ※近藤　剛、石井章弘、宗片比呂夫（東工大・工）
「配向性PDA膜の半導体基板上への堆積」

P2-17D. ※徐　暁斌、真島　豊、岩本光正（東工大・工）
「リン脂質・アゾベンゼン混合膜におけるスイッチング現象に起因した変位電流に関する研究 」

P2-18S. ※松澤洋子、関　隆広、市村國宏（東工大・資源研）
「多環状両親媒性化合物 [1]
気・水界面におけるフタロシアニン誘導体からなる　2次元分子組織膜の創製」

P2-19M. ※松本裕一、久利恭士、梶山千里（九大院・工）
「分子熱運動性の異なる脂肪酸単分子膜の分子イメージ」

P2-20D. ※藤巻正典、森野慎也、中川　勝、林ゆう子、市村國宏（東工大・資源研）
「多環状両親媒性化合物 [2]
アゾベンゼン部位を有するカリックス[4]レゾルシンアレン吸着単分子膜」

P2-21M. ※岩田典子、菊池祐嗣、梶山千里（九大院・工）
「光第二次高調波発生に基づく（高分子／液晶）界面における液晶分子の配列評価」

P2-22D. ※中村史夫、居城邦治、下村政嗣（北大・電子研）
「DNA-mimeticsの組織化」

P2-23D. ※阪本清志、小幡谷育夫、
上野昭彦、三原久和
（東工大・生命理工）
「2 α-ヘリックスペプチド-ヘム複合体の構築とヘムの配向および機能制御」

P2-24S. ※畑中研一、久能めぐみ、
大石順二 （東工大・生命理工）
「ヌクレオチドを有するポリマーと糖転移酵素との相互作用」

P2-25S. ※務台俊樹、阿部泰子、
荒木孝二（東大・生研）
「蛍光性ビピリジンホストによる
リン酸ジエステルと脂肪酸の高感度識別」

P2-26M. ※植木貴之、本澤栄一、長崎幸夫、
加藤政雄、片岡一則、鶴田禎二
（東理大・基礎工）
「環状サイラミン化合物の合成とその生理活性評価」

Two-dimensionally organized monomolecular films derived from macrocyclic amphiphiles

Kunihiro Ichimura

Research Laboratory of Resources Utilization, Tokyo Institute of Technology
4259 Nagatsuta, Mirori-ku, Yokohama 226

Surface layers incorporating photoreactive moieties on solid materials bring about a vaiety of photofunctionality including the photocontrol of wettability, liquid crystal alignment, dispersibility and so on. It has been shown that these macroscopic events are triggered by changes in molecular structures on an uppermost surface of photosensitive layers, and well-defined monolayers incorporating photoreactive units have been highly required. This has our primariy modivation to achieve studies on macrocyclic amphiphiles which are a family of compounds comprised of cyclic cores substituted with hydrophobic alkyl chains.

The crown conformer of calix[4]resorcinarenes has a cylindrical skeleton with eight hydrophilic residues tethered to the upper rim so that this type of novel compounds belongs to macrocyclic amphiphiles when hydrophobic chains are introduced at the lower rim. Calix[4] resorcinarens and their *O*-substituted derivatives were prepared to reveal the behavior of their monolayers on a water surface. These compounds are very attractive because they adsorb readily on a polar surface of silica plates to form densely packed monolayers as the result of multi-site adsorption through hydrogen bonds. This convenient technique has been applied to cover a silica surface with photofunctional monolayers using calix[4]resorcinarenes having four azobenzene units at the lower rim. Since occupied areas of calix[4]resorcinarene and its derivatives are determined by cross-sectional areas of their base, a two-dimensional free volume is ensured in their monolayers even they are densely packed, leading to efficient *E*-to-*Z* photoisomerizablity. These photoreactive monolayers induce the photocontrol of liquid crystal alignment and of dispersibility of colloidal silica in organic solvents.

An alternative class of macrocyclic amphiphiles is derived from octaalkoxymetallophthalocyanines which have a disk-shaped core with eight long-chain alkyls. The macrocyclic rings lie flat on a water surface when the length of alkyls is enough long. The flat-laid conformation is markedly stabilized by adding long-chain alkanes to give homogenous host-guest monolayers under controlled speading conditions. It is assumed that the metallophthalocyanine can be regarded as a molecular vessel consisting of the macrocyclic plane as a base and eight alkoxy chains as a side wall to incorporate guest molecules in the cavity. It has been recently found that even nematic liquid crystalline molecues are included in monolayers of the metallophthalocyanines. This provides a novel model system for an interfacial region between a substrate surface and a liquid crystalline layer.

Crystal Engineering of Layered Structures

Kenji Okuyama
Faculty of Technology, Tokyo University of Agriculture and Technology,
Koganei, Tokyo 184, Japan

Amphiphilic molecules with long hydrophobic alkyl chains, such as phospholipids in biological membranes and synthetic surfactants, can aggregate spontaneously in an aqueous solution. These aggregations can take various types of higher order organization, such as a bimolecular layer arrangement, spherical micelles and rod-shaped micelles. Here, the structural differences between these organizations depend mainly on their chemical structures and concentrations. In the solid state, however, most of amphiphilic molecules take very similar two-dimensional smectic layers. These layers stack along the normal direction to the layer surface to make a three-dimensional crystal structure. The molecular arrangement in the smectic layer depends on the chemical structure of an element amphiphile. For example, dialkyldimethylammonium salts can form a bimolecular layer with some tilt, while monoalkyl-trimethylammonium salts are packed in an interdigitating manner, which results in the thickness of the smectic layer being close to the molecular length (as shown in the figure).

Recently, it was found that monoalkyl-trimethylammonium salts can be crystallized with various aromatic compounds to form crystalline clathrate compounds. Interestingly, the formation of clathrate compounds is available not only by recrystallization from their solution, but also by mixing host and guest crystalline powders in a mortar. In this paper, I will present a diversity of layered structures of clathrate compounds, together with that of host molecules.

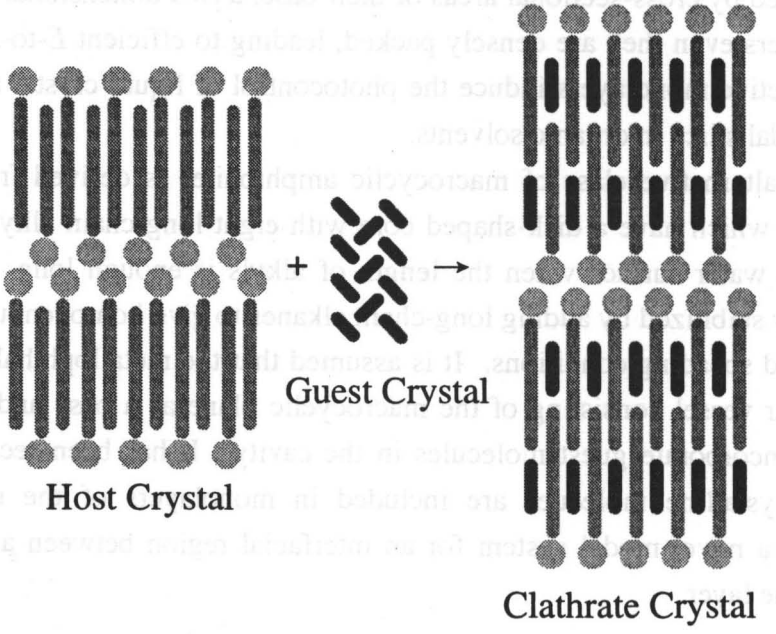

Creation of Novel Polymeric Surface with High Functionality

Yukio Nagasaki

Materials Science Department, Science University of Tokyo, Noda 278

Control of the surface properties has become progressively important in the field of biomaterials, because of the contact with biological components such as blood and organs. Surface modification is one of the ways to improve surface properties. Polymer brushes, which are densely packed on the surface attached by the end of the polymer chain, significantly varyits surface properties. For example, a PEGylated surface shows effective rejection of protein adsorption resulting in high blood compatible materials. A PEGylated surface is also utilized as a capillary for high performance capillary electrophoresis.

One of the other interests in polymer brushes on the surface is stimuli-sensitivity of the brushes. If properties of the surface such as contact angle and mobility of the brushes can be controlled by the environmental conditions, numerous applications will be possible. Okano and his coworkers prepared a temperature sensitive poly(N-isopropylacrylamide) surface and investigated a cell culture on the surface. When the surface becomes hydrophilic at low temperature, the cultured cell easily detached without Trypsin treatment.

We have been studying the synthesis of a new structured polymer using our new synthetic methods. The relation between structure and functionality of the obtained polymers has also been investigated. One of the polymers thus synthesized, poly(silamine), which has alternating repeating units of ethylene diamine and 3-silapentane in the main chain, showed unique stimuli-sensitivities. Since poly(silamine) is one of polyamine homologues, it is soluble in acidic water. The poly(silamine) aqueous solution shows phase separation not only by a pH change but also by a temperature change because of the unstable hydrations around the poly(silamine) molecules due to the hydrophilic/hydrophobic alternating structure. Protonation of an ethylenediamine unit along with the coordination of the anion to the silicon atom in the main chain varies the stiffness of the poly(silamine). For example, the glass transition temperature (Tg) of poly(silamine) attains +80 °C when the poly(silamine) is protonated by sulfuric acid. It should be noted that poly(silamine) without protonation shows a Tg of -85 °C.

Using the stimuli-sensitive heterotelechelic poly(silamine) polymer tethered chains on the glass and gold surfaces were prepared. Since poly(silamine) has a vinylsilyl group at one end and a sec-amino group at the other end, the introduction of a trimethoxysilyl group was carried out using a radical addition reaction of 3-trimethoxysilylpropanethiol to the end-double bond of poly(silamine), retaining the sec-amino group at the other end intact. The obtained polymer could be used as a surface modifier for glass to form a polymer tethered chain. Alternatingly, a radical addition reaction of thioacetic acid to the end double bond, followed by alkaline hydrolysis reaction gave poly(silamine) with thiol group at one end, retaining reactive sec-amino group at the other chain end. This heterotelechelic poly(silamine) was useful for preparation of tethered chains on the metal surface such as gold.

Surface properties of the poly(silamine) surface thus obtained can be controlled not only by the environmental pH but also by the temperature. For example, with increasing temperature at constant pH, the z-potential of the poly(silamine) surface decreased, indicating that the deprotonation of poly(silamine) on the surface was promoted by increasing temperature. The protonation of poly(silamine) on the surface was found to change not only hydrophilicity of the chain but also stiffness of the chain itself. By the protonation of the tethered chains, the stiffness of the surface became harder than that of non-protonated tethered chains surface.

sec-Amino groups at the free end of the poly(silamine) on the surface were found to be utilized for conjugation with a compound which reacts with sec-amine such as DNA and protein. The poly(silamine) surface is promising because not only the surface characteristics can be controlled by the surrounding environment but also by the conjugation with certain functional components at the free end of the polymer brushes.

Chemical Sensing Based on Self-Assembled Cyclodextrin Monolayers

Philippe Bühlmann, Hiroshi Aoki, Yoshio Umezawa
Richard Chamberlain,* Marcin Majda*

Department of Chemistry, School of Science, The University of Tokyo
**University of California at Berkeley, Berkeley, California, USA*

Analyte recognition at electrode surfaces by formation of host–guest complexes is a promising approach to chemical sensing. For this purpose, we have self-assembled channel-shaped cyclodextrin derivatives (cf. β-cyclodextrin in Fig. 1) with seven or eight thiol groups to give monolayers (SAMs) on the surface of hanging mercury drop electrodes (HMDEs). The resulting monolayers have been characterized electrochemically. The surface coverages as calculated from the charge required to reduce the Hg-SR bonds that form upon self-assembly agree with the packing density of monolayers of the same cyclodextrins at the air–water interface, as determined by surface pressure vs. mean molecular area isotherms.

The capacitances of these modified HMDEs have been investigated in the presence of various anions. If capacitances are measured at a potential at which the electrode is positively charged, that is, positive of the potential of zero charge E_{pzc}, a selectivity based on the anion size is evident for anions that do not selectively adsorb onto the Hg surface. Only negligible capacitance differences for different anions are observed at potentials negative of the E_{pzc}, where anions are repelled by electrostatic forces from the HMDE surface. Similarly, the size of cations in the aqueous solution does not influence the capacitance at potentials positive of E_{pzc}, which again can be understood by electrostatic repulsion.

These results show that small non-adsorbing anions, such as NO_3^-, can migrate into and out of the cyclodextrin cavity. Binding of guests that form inclusion complexes with cyclodextrins block the access of those anions to the surface (Fig. 2), which results in a decrease in the monolayer capacitance (Fig. 3). In case of the neutral guest adamantanol, binding to the monolayer follows a Langmuir adsorption isotherm, which allows to determine constants for binding to the cyclodextrin monolayer. Independent confirmation of these binding constants can be obtained from the observation of the position of the Hg-SR reduction peak in cyclic voltammograms because guest binding reduces the reversibility of the Hg-SR reduction.

Binding of guests to the monolayer blocks the access to the HMDE surface not only for anions but also for the electroactive marker benzoquinone, which otherwise is sufficiently small to enter the cyclodextrin cavity. This is the basis of electrochemical sensors based on intramolecular channels. A unique feature of the HMDE is that the mercury drop size can be increased after self-assembly. This opens intermolecular voids. Distinct differences in cyclic voltammograms obtained for various electroactive markers with expanded and non-expanded drops support the interpretation that benzoquinone is indeed reduced upon permeation into the intramolecular cavities of cyclodextrins.

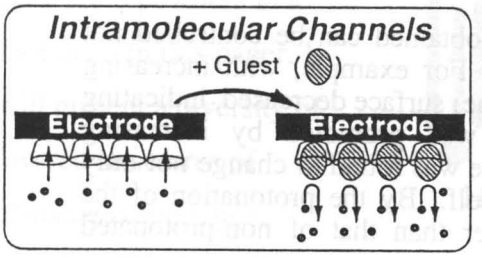

Fig. 1

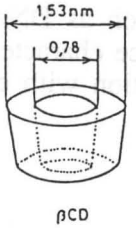

Fig. 2

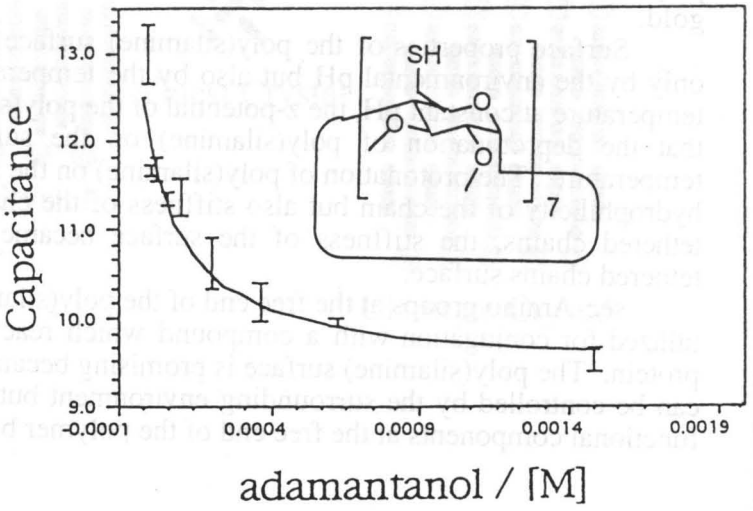

Fig. 3

Layer Structures of Cationic Surfactants

Yasuhide Nakadai, Keiichi Noguchi and Kenji Okuyama
Faculty of Technology, Tokyo University of Agriculture and Technology,Koganei, Tokyo 184, Japan.

Cationic surfactants are widely used in the chemical industry. Recently, it has been found that one of the cationic surfactants, an alkyltrimethylammonium salt has an interesting ability to form molecular complexes with various aromatics. Molecular and crystal structures of alkyltrimethylammonium salts at the atomic level give us a better understanding about complex formation with aromatics. In this study, molecular arrangements in layer structures of Decyltrimethylammonium bromide (DeTAB), Tetradecyltrimethylammonium bromide (TTAB) and Hexyltrimethylammonium chloride (CTAC) is discussed.

Crystal data : DeTAB(**1**), $C_{13}H_{30}NBr$, monoclinic $P2_1$, a=5.631(3), b=7.253(2), c=19.581(2)Å, β=97.82(2)°, Z=2, and R=0.038 for 1224 observed reflections. TTAB(**2**), $C_{17}H_{38}NBr$, monoclinic $P2_1/c$, a=5.638(6), b=7.258(4), c=47.415(5)Å, β=91.05(5)°, Z=4, and R=0.040 for 2037 observed reflections. CTAC(**3**), $C_{19}H_{42}NCl/0.5H_2O$, triclinic $P\bar{1}$, a=8.623(1), b=19.499(3), c=27.091(6)Å, α=103.01(2), β=92.47(2), γ=101.56(1)°, Z=8, and R=0.093 for 6316 observed reflections.

These surfactant molecules form a bimolecular layer in the solid state, which we can see in many packing structures of amphiphile molecules. In this layer, alkyl chains were mutually interdigitated to compensate the large cross-section of their hydrophilic head part.

Although the difference between DeTAB and TTAB is only in the alkyl chain length, they showed slightly different packing arrangement. This means that, DeTAB has one bimolecular (smectic) layer in the c-repeating unit, while TTAB has two smectic layers. We call the former the single layered type and the latter the double layered type structures. Structures of Dodecyltrimethylammonium bromide (DoTAB)[1] and Hexyltrimethylammonium bromide (CTAB)[2] can also be classified as the single, and double layered type structures, respectively. In these smectic layers, alkyl chains make a twist with one of the two directions to pack in a herring-bone manner similar to that in polyethylene crystals. In the single layered type structures (**1** and DoTAB), the direction of the twist is the same in all smectic layers. However, in the double layered type structures (**2** and CTAB), both the clockwise and the anticlockwise twist appeared alternately.

In the hydrophilic regions of the alkyltrimethylammonium bromides, cation and anion atoms are located on the planes parallel to the (001), while in the case of CTAC (**3**), these are waved-planes and water molecules are included in the hydrophilic region.

1) S.Kamitori, Y.Sumimoto, K.Vogbupnimit, K.Noguchi and K.Okuyama, *Mol. Cryst .Liq. Cryst.*, in press (1997).

2) A. R. Campanelli and L. Scaramuzza, *Acta cryst.*, **C42**, 1380-1383 (1986).

Creation of reactive polymeric micelles for a novel elemental structure

○ Takashi Okada, Michihiro Iijima, Yukio Nagasaki, Masao Kato, Kazunori Kataoka

Department of Materials Science and Technology, Science University of Tokyo
Yamazaki 2641, Noda, Japan

Introduction

A polymeric particle of nano dimension in diameter has become attractive in the field of nano-fabrication chemistry for construction of a supramolecular structure. For example,a dendrimer possesses many reactive groups on the surface. However, it is not easy to complete the consecutive reactions for the preparation of the dendrimer. If reactive groups can be introduced on the surface, the polymeric micelles can be utilized as a starting material for nano-fabrication chemistry. The objective of this study was to prepare "reactive polymeric micelle" which was prepaered by amphiphilic AB-block copolymer possessing a reactive group at the end of the hydrophilic segment end.

Experimental, results and discussion

Poly(ethylene glycol)-b-polylactide (PEG/PLA) block copolymer was synthesized by an anionic polymerization of ethylene oxide using potassium alkoxides having a protected functional group as an initiator, followed by block polymerization of lactide (Scheme 1). The obtained copolymer was confirmed as PEG/PLA block copolymer having an acetal end group quantitatively by the ^{1}H-NMR spectroscopy and the GPC analysis. For the preparation of polymeric micelle, the block copolymer was dissolved in *N,N*-Dimethylacetamide, then, the solution was dialyzed against water. The size and the shape of the obtained polymeric micelles were estimated by the DLS measurements. No angular dependency of the scaled characteristic line width was obserbed and narrow size distribution. The conversion of acetal end groups to aldehyde groups was carried out by an acid treatment using 0.01mol L^{-1} hydrochloric acid. The extent of the conversion attained more than 90% without any side reaction such as aldol condensation. No change in the micelle size and shape was obserbed before and after the conversion of the acetal end groups to aldehyde groups on the micelle (Scheme 2). A radical polymerization of the end methacryloyl group at the PLA terminus end was carried out in the core of the micelle. After the polymerization, the peaks originated from methacryloyl groups disappeared, indicating an effective polymerization of the core. Such the polymerized micelles were fairly stable as compared to the physical adsorbed micelles. An aldehyde groups on the polymeric micelle surface reacts rapidly with primary amino groups forming a Schiff's base, a chemical path which could be employed for conjugations with proteins. Further, such stable polymeric micelles with reactive groups are promising for biomedical applications such as high performance latex particles.

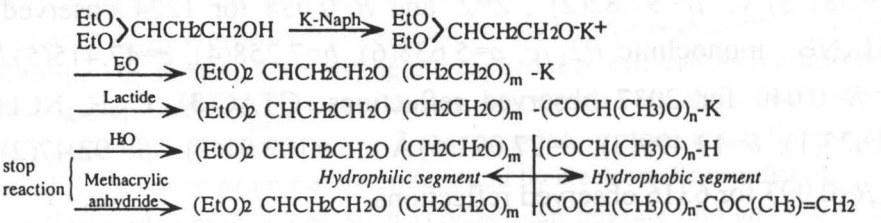

Scheme 1 Synthesis of PEO/PLA block coplymer

Scheme 2

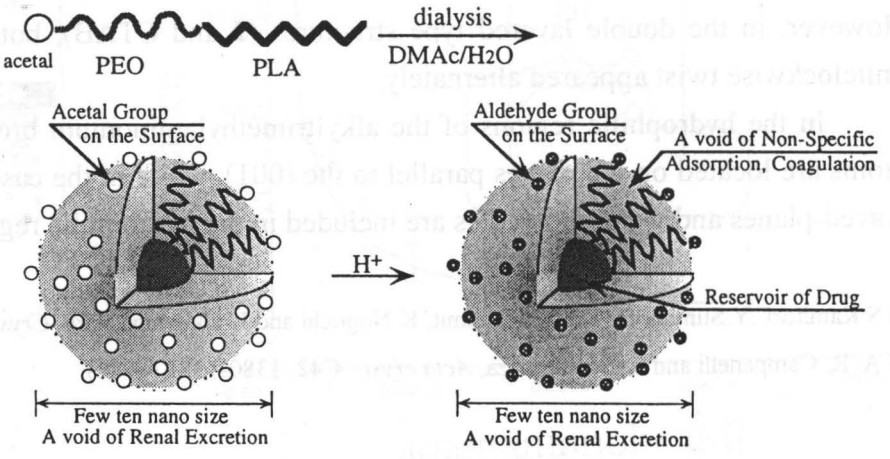

Molecular Arrangements in the Complex Crystals Composed of Cationic Surfactants and Aromatic Molecules

Keiichi Noguchi, Yasuhide Nakadai and Kenji Okuyama
Faculty of Technology, Tokyo University of Agriculture and Technology,
Koganei, Tokyo 184, Japan.

Recently, it has been found that some surfactant molecules such as ammonium salts, phosphonium salts and other onium salts have the specific ability to form complexes with aromatic molecules. Interestingly, the formation of complexes can be achieved not only by recrystallization from their solution , but also by grinding both powders of surfactants and aromatic molecules in a mortar. In order to clarify the structural details and interactions between surfactants and aromatic molecules, we have investigated the crystal structures of various complexes composed of surfactants and aromatic molecules. In the present study, molecular arrangements of the complexes between dodecyltrimethylammonium chloride (DTAC, host) and naphthalene derivatives (guest) have been discussed.

Crystal data : DTAC / 2,3-dihydroxynaphthalene(**1**), $C_{15}H_{34}NCl$ / $0.5C_{10}H_8O_2$, monoclinic $P2_1/m$, $a = 11.702(3)$, $b = 7.493(3)$, $c = 24.669(4)$ Å, $\beta = 101.66(2)^\circ$, $Z = 4$, and $R = 0.084$ for 1371 observed reflections. DTAC / 1,6-dihydroxynaphthalene(**2**), $2C_{15}H_{34}NCl$ / $C_{10}H_8O_2$, triclinic $P\bar{1}$, $a = 10.964(3)$, $b = 9.232(3)$, $c = 24.206(4)$ Å, $\alpha = 90.82(2)$, $\beta = 104.86(2)$, $\gamma = 67.18(2)^\circ$, $Z = 2$, and $R = 0.063$ for 5083 observed reflections. DTAC / 1-hydroxynaphthalene(**3**), $2C_{15}H_{34}NCl$ / $C_{10}H_8O_2$, triclinic $P\bar{1}$, $a = 11.162(1)$, $b = 9.157(3)$, $c = 23.957(3)$ Å, $\alpha = 92.01(2)$, $\beta = 105.17(1)$, $\gamma = 66.82(1)^\circ$, $Z = 2$, and $R = 0.066$ for 3559 observed reflections.

These crystal structures consist of smectic layer structures stacked along the *c*-axis. In a smectic layer, the host molecules are arranged in an antiparallel fashion and the alkyl chains of host molecules are mutually interdigitated. As observed in other complexes between monoalkyltrimethylammonium salts and aromatic molecules, the interdigitation of alkyl chains become shallow to make the space for the inclusion of the guest molecules. Since both host and guest molecules in the complex **1** are located on the crystallographic mirror plane, the zigzag planes of alkyl chains and the naphthalene rings are completely parallel. Similarly, in the case of **2** and **3**, the zigzag planes of alkyl chains and the naphthalene rings are almost parallel. Along the *c*-axis, hydrophilic and hydrophobic parts are alternately observed. The hydrophilic part is formed by ammonium groups, chloride anions and hydroxyl groups of the guest molecules. The trimethylammonium groups and chloride anions show a zigzag arrangement along the *a*-axis. Two chloride anions in an asymmetric unit of **1** are linked to the hydroxyl oxygens of the guest molecules by hydrogen bonds. In the case of **2**, one chloride anion in an asymmetric unit participates in bifurcated hydrogen bonds with the hydroxyl groups of the guest molecules, while the other chloride anion does not form a hydrogen bond. The positions of the hydroxyl groups in the naphthalene ring of the guest molecule may affect these hydrogen bond schemes and the orientation of the naphthalene ring in each complex.

A novel synthesis of functional poly(methacrylate)s through an alcoholate initiated polymerization

○ Yasuo Sato, Yukio Nagasaki, Masao Kato

Department of Materials Science and Technology, Science University of Tokyo

<Introduction> Recently, we found that potassium alcoholate can initiate the polymerization of 2-(trialkylsiloxy)ethyl methacrylate (SEMA) through the addition of alcoholate to the double bond of the monomer. The donating oxygen atom at the β -position of ester group in SEMA plays an important role in this polymerization. If methacrylate monomers with donor group at the β -position in the ester unit can also activate the alcoholate initiation, a new semi-telechelic polymethacrylate with functional donor groups in each repeating unit can be prepared.

The objective of this study was to prepare poly [2-(N,N-dimethylaminoethyl)methacrylate] macromonomaer initiated with 4-vinylbenzyl alcoholate.

<Experimental>*Synthesis of Poly AMA*: After potassium ethoxide was placed in aglass vessel, the vessel was degassed and filled with argon gas. Then THF and 2-(N,N-dimethylaminoethyl)methacrylate (AMA) were added via a syringe. After the mixture was allowed to react at 24℃, a small amount of water was added to stop the reaction

Synthesis of PAMA macromonomer: To the THF solution of 4-vinylbenzyl alcohol in a glass vessel under an argon atmosphere, potassium naphthalene was added at 0℃ to prepare potassium 4-vinylbenzyl alcoholate (PVA). After AMA was added via a syringe, the mixture was allowed to react at 24℃, then a small amount of water was added to stop the reaction.

Scheme 1

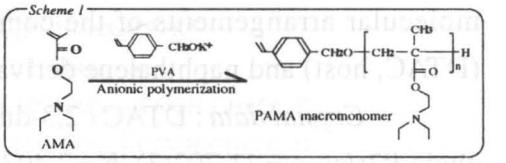

<Results and discussion> From the GPC analysis of the obtained polymer with potassium ethoxide as an initiator, no monomer was remained after 20-min reaction. The molecular weight of the obtained polymer was 7400 which was in good agreement with the caluculated value from the monomer/initiator ratio. From the ^{1}H-NMR analysis, it is confirmed that the products obtained were formed via successive addition polymerization of AMA. In this polymerization the donating nitrogen atom at the β -position of ester group in AMA plays an important role as shown in Scheme 2, viz. , this polymerization is proceeded due to the increased the nucleophilicity of the alkoxide anion by chelation of the surrounding AMA molecule.

Scheme 2

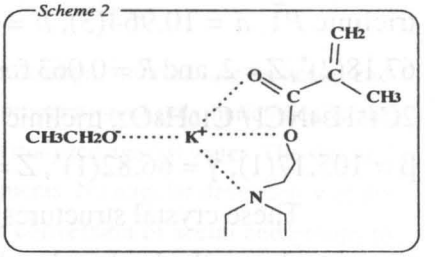

Fig.1 shows the GPC profiles of the obtained polymers initiated with PVA.With increasing reaction temperature, the molecular weight of the obtained polymer was close to the calculated date, and the value Mw/Mn of the polymer approached unity. The higher MW of the obtained polymer under the low temperature was attributable to the lower initiation rate compared to the propagation rate. From the ^{1}H-NMR analysis, the molecular weight of the polymer determined assuming one vinylbenzyl group per polymer molecule was in good agreement with that from the GPC results. This is indicating the quantitative introduction of a vinylbenzyl group at one end of the polymer.

The radical copolymerization of vinylbenzyl-terminated PolyAMA with styrene was carried out. Based on the GPC analysis, the PAMA macromonomer almost disappeared after the copolymerization. From the ^{1}H-NMR analysis, protons based on the unsaturated bond at the end of the PAMA chain completely disappeared. These results can be interpreted to proceed the coporimerization of PAMA macromonomer with styrene.

On the basis of these results, the alcoholate initiated polymerization can be applied to other methacrylate having donating functional group.

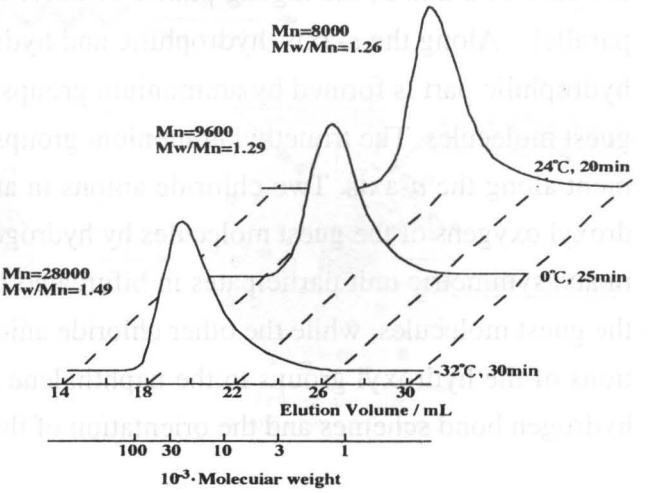

Fig.1. GPC profiles of PAMA prepared with PVA in THF

Molecular Superstructure of Nucleoside Derivatives based on the Unit Assembling Strategy I. Tape-unit

○T.Monma, I.Yoshikawa, R.Takasawa, K.Araki

Institute of Industrial Science, University of Tokyo

7-22-1 Roppongi, Minato-ku, Tokyo, 106 Japan

Design of novel molecular superstructure by more predictable way is the current topics in supramolecular chemistry. To design the superstructure of nucleoside derivatives, the molecular units formed by multiple hydrogen bonds between nucleic acid bases are assembled into higher-order structures. When guanine and/or cytosine are used as a nucleic acid base, tape-like structure, cyclic quartet, or complementary base pair unit is known to be formed by multiple hydrogen bonds.

In this study, we investigated the formation of the superstructure by assembling the tape-like hydrogen bonding units of trialkylsilylated guanosine or cytidine derivatives. Several different superstructures were obtained and effect of number or size of alkylsilyl groups and solvent used for assembling was discussed.

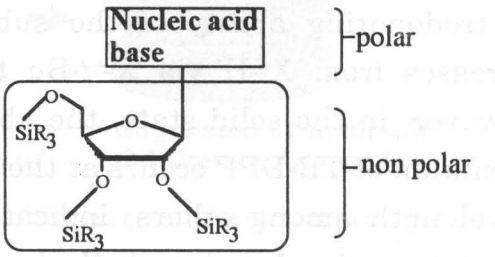

TBDMS : R = t-butyldimethylsilyl

TBDMS-dC/EtOH

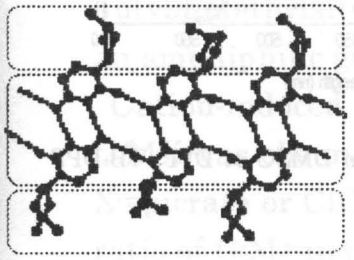

TBDMS-G/MeOH

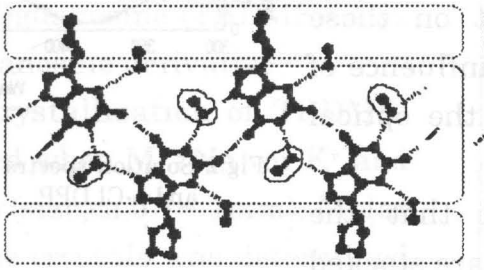

TBDMS-G/Acetone

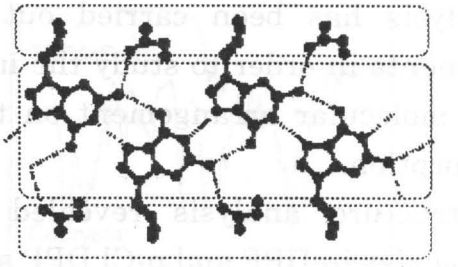

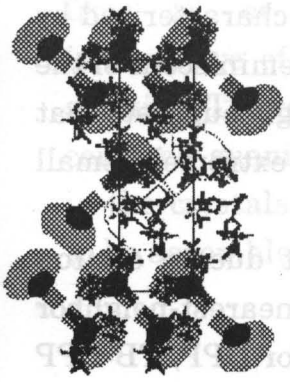

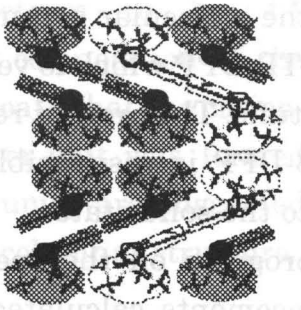

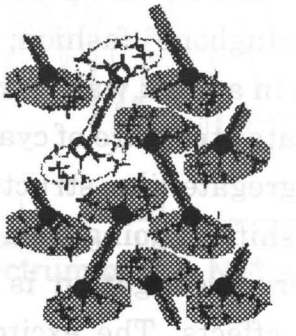

ピロロピロール誘導体の結晶構造と電子構造
Crystal structure of pyrrolopyrrole derivatives and their electronic structure

○荒井 彩子*、田中 滋光*、水口 仁**
(横浜国立大学 *教育学部 化学教室、**工学部 知能物理工学科)
○A. Arai*, S. Tanaka*, and J. Mizuguchi**
(*Department of Chemistry, Faculty of Education, **Department of Applied Physics, Faculty of Engineering, Yokohama National University)

The diketopyrrolopyrroles shown in Fig.1 are novel, red pigments based on the heterocyclic chromophore and are characterized by intermolecular hydrogen bonds between the NH group and the O atom. The absorption maximum in solution of DPP, TB-DPP and p-Cl DPP is displaced towards longer wavelengths (Fig.2) as the electrodonating ability of the substituent increases from X=H via X=*t*-Bu to X=Cl. However, in the solid state, the absorption maximum of TB-DPP occurs at the shortest wavelength among others, indicating that the intermolecular interactions play an important role. For this reason, structure analysis has been carried out on these pigments in order to study the influence of the molecular arrangement on the optical absorption.

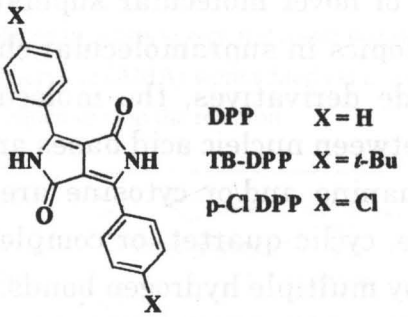

Fig.1 DPP derivatives.

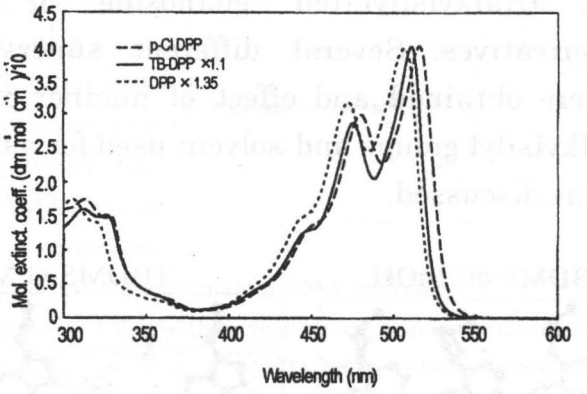

Fig.2 Solution spectra in DMSO of DPP, TB-DPP and p-Cl DPP.

Structure analysis revealed that the molecules in DPP and p-Cl DPP are stacked in a "herringbone" fashion; whereas the molecular arrangement is characterized by a "bricks in a brick wall" structure in TB-DPP which is very much reminiscent of the J-aggregate structure of cyanine dyestuffs. The present result strongly suggests that the J-aggregate-like structure of TB-DPP is responsible for the extremely small spectral shift on going from solution to the solid state.

Further investigation is now in progress on the spectral shift due to exciton coupling effects. The excitonic displacements calculated for the nearest-neighbor molecules within a sphere of about 10Å (14, 14 and 12 molecules for DPP, TB-DPP and p-Cl DPP, respectively) will also be presented at the poster.

Molecular Superstructure of Nucleoside Derivatives Based on The Unit Assembling Strategy II. Cyclic Tetramer Unit

○Yoshikawa, Isao; Monma, Tomoyuki; Takasawa, Ryoichi; Araki, Koji

Institute of Industrial Science, University of Tokyo

7-22-1 Roppongi, Minato-ku, Tokyo, 106 Japan

Amphiphilic nucleoside derivatives are expected to form three types of superstructures, *i.e.* lamellar, columnar and double helical structures, by assembling the hydrogen-bonded units. Monovalent cations are known to induce columnar structure of the guanine-rich oligonucleotides, in which hydrogen-bonded guanine cyclic tetramer is formed.

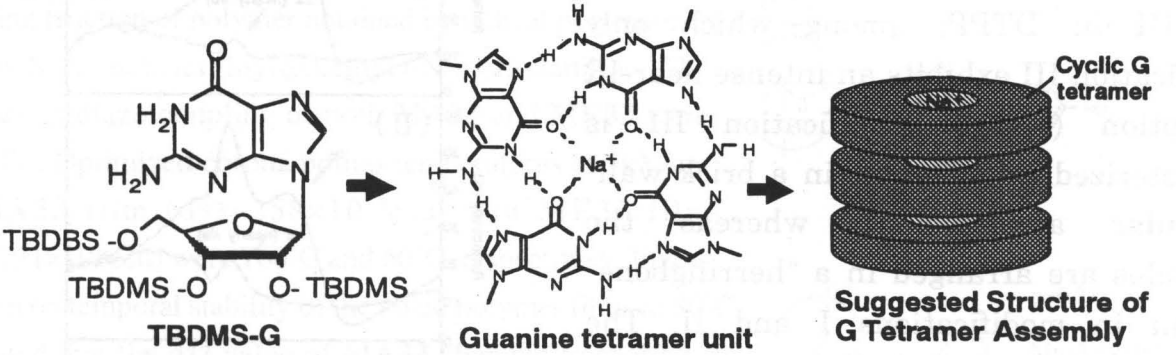

TBDMS-G **Guanine tetramer unit** **Suggested Structure of G Tetramer Assembly**

In this study, we tried to construct a columnar superstructure by assembling the guanine tetramer units. We used alkaline metal ions as a template of tetramer, and 2',3',5'-tris(t-butyldimethylsilyl)guanosine (TBDMS-G) as an amphiphilic guanosine derivative.

Cation-induced crystallization of TBDMS-G/MX was observed when M^+=Na^+ or K^+ and X^-=picrate or ClO_4^-(size,ca.0.1~ 1mm). Molar ratio of G:M^+ in the crystals was determined from IR or UV spectrum to be 4:1 irrespective of the G:M^+ composition of the solution. The results indicate that the cation-centered guanine tetramer unit was formed in the crystals, and the units are suggested to be assembled into the columnar structure.

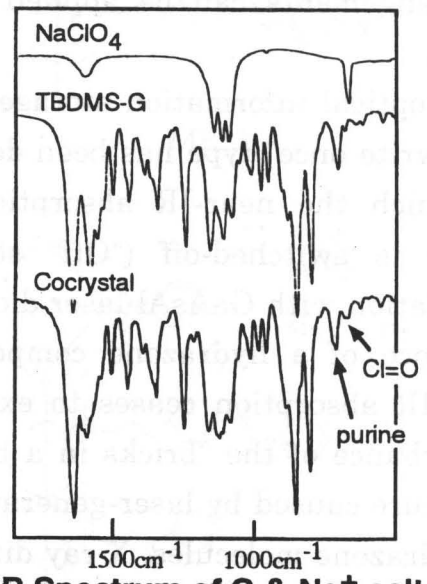

IR Spectrum of G & Na^+ salt

チオピロロピロールの結晶多形と固体スペクトル
－光ディスクへの応用－

Polymorphism and solid-state spectra of Dithioketopyrrolopyrrole
－Application to optical disks－

水口 仁
（横浜国立大学　工学部 知能物理工学科）
J. Mizuguchi
(Department of Applied Physics, Faculty of Engineering, Yokohama National University)

Dithioketopyrrolopyrrole (DTPP) shown in the inset of Fig.1 is a novel, blue pigment based on the heterocyclic chromophore. There are three crystal modifications I, II and III in DTPP, among which only modification III exhibits an intense near-IR absorption (Fig.1). Modification III is characterized by a "bricks in a brick wall" molecular arrangement; whereas the molecules are arranged in a "herringbone" fashion in modifications I and II. The appearance or disappearance of the near-IR absorption due to molecular rearrangements can be applied to optical disks.

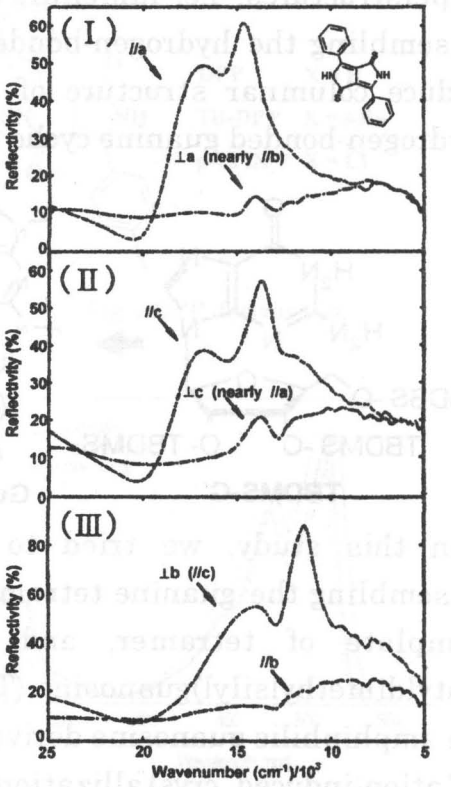

Fig.1 Polarized reflection spectra of modifications I, II and III measured on single crystals.

An optical information storage system of the "write once" type has been developed in which the near-IR absorption ("on" state) is switched-off ("Off" state) on irradiation with GaAsAl laser diodes in the presence of a hydrazone compound. The near-IR absorption ceases to exist due to disturbance of the "bricks in a brick wall" structure caused by laser-generated vapors of hydrazone molecules. X-ray diffraction analysis revealed that the present phenomenon is due to the phase change from modification quasi-III to modification II. The optical disk (structure: substrate/hydrazone/DTPP/Al) exhibits a reflectivity change about 30% to 45% on writing with a power of about 9mW at 780nm (Fig.2).

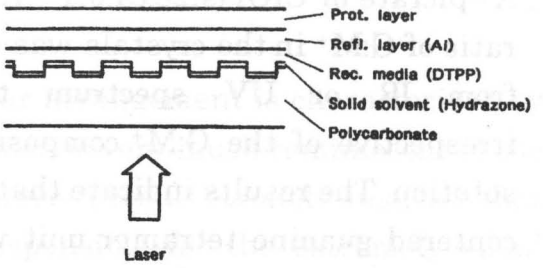

Fig.2 Structure of the optical disk of the write once type based on DTPP.

Synthesis and Properties of Methacrylamide Polymers Containing NLO-active Chromophores as SideChains

K.Usui, M.Kato[1], S.Yamada,H.Matuda[2], H.Nkanishi[3]

1):Faculty of Industrial Science and Technology,Schience University of Tokyo, 2641 Yamazaki Noda 278, JapanTEL 0471-24-1501(4363),FAX 0471-23-9362 2):National Institute of Materials and Chemical Research, 1-1-4 Higashi, Tsukuba 305, Japan 3):Institute for Chemical Reaction Science,Tohoku University, Katahira, Aoba-ku, Sendai 980, Japan

We tried to stabilize poled structure of NLO polymer with the aid of hydrogen-bonding.

NLO polymers with (**MA33**) and without (**ME33**) hydrogen-bonding were synthesized to investigate the effect of hydrogen-bonding on thermal stability of the poled structure. **MA33** was synthesized via diazo coupling reaction of polymer obtained by radical polymerization of N-(2-methacrylamidoethyl)-N-methylaniline(MAA) and **ME33** was synthesized via diazo coupling reaction of polymer obtained by radical polymerization of N-(2-methacryloyloxyethyl)-N-methylaniline. The degrees of diazo coupling of both **MA33** and **ME33** were 33mol%. Optimized corona poling temperatures at 5kV/cm of **MA33** film ($d_{33}=258\times10^{-9}$esu) and **ME33** film ($d_{33}=291\times10^{-9}$esu) were 160°C and 60°C, respectively. Investigation on temporal stability of the poled polymer films at 80°C indicated that the d_{33} value of **MA33** changed to ca.40% its initial value after 200h, after which the value unchanged for a long time, while the d_{33} value of **ME33** changed to zero after 8h. These results suggest that the hydrogen-bonding formation in polymer is apparently effective to stabilize the poled structure.

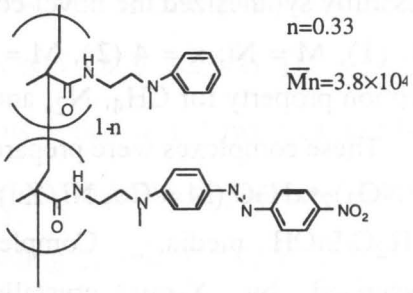

MA33

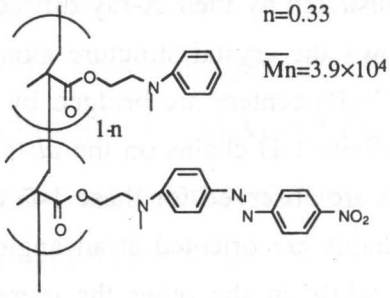

ME33

To obtain more thermal stable poled NLO polymer **MAPM** having more rigid structure than **MA33** was synthesized. Synthesis of **MAPM** was performed via diazo coupling reaction of copolymer obtained by radical copolymerization of MAA and phenyl maleimide. The d_{33} value of **MAPM** film containing 35 mol% diazo group was 291×10^{-9}esu after poling at 140°C. As expected, the d_{33} value of **MAPM** at 80°C changed to ca.70% its initial value after 200h, after which the value unchanged to a long time.

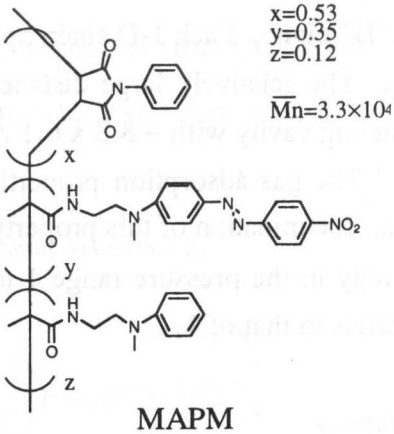

MAPM

Rational Design and Construction of Microporous Coordination Polymers with Gas Adsorption Properties

Mitsuru Kondo, Shinichiro Noro, Mariko Shimamura, Akiko Asami, Kenji Seki, and Susumu Kitagawa

Department of Chemistry, Faculty of Science, Tokyo Metropolitan University, Minami osawa, Hachioji, Tokyo 192-03, and Advanced Technology Center, Osaka Gas Co., Ltd., Chudoziminami-machi, Shimogyo-ku, Kyoto 600.

Synthesis of coordination polymers with the large channeling cavity is of great current interest due to not only the intriguing structural diversity but also their potential functionalities as the microporous solids, *e.g.* molecular adsorption, ion exchange, or heterogeneous catalysts.[1] We successfully synthesized the novel coordination polymers $\{[M_2(4,4'\text{-bpy})_3(NO_3)_4](H_2O)_x\}_n$ (M = Co; x = 4, (**1**), M = Ni; x = 4 (**2**), M = Zn; x = 2 (**3**)) with large channeling cavity, which show the gas adsorption property for CH_4, N_2, and O_2.[2]

These complexes were prepared by the reaction of $M(NO_3)_2 \cdot xH_2O$ (M = Co, Ni, Zn) with 4,4'-bpy in the H_2O/EtOH media. Complex **1** has been characterized by X-ray crystallography. The isomorphous structures of **1** - **3** have been clearly demonstrated by their X-ray diffraction patterns. Fig. 1 shows the crystal structure along the *c* axis of **1**. The Co(II) centers are bridged by 4,4'-bpy to afford the infinite 1-D chains on the *ab* plane. Two sets of arrays are observed for these 1-D chains. In the one, the chains are oriented at an angle of 54.8° to the *a* axis, while in the other the corresponding angle is -54.8°.

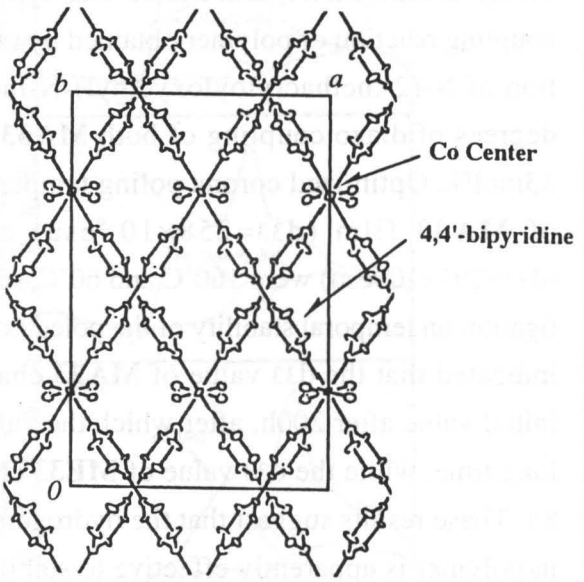

Fig. 1 The crystal structure along the *c* axis of **1**.

Two types of planes consistent with the 1-D chains in each array are represented by designation of "A "and "B" plane. Each 1-D chain on the A and B planes is sterically fixed by the 4,4'-bpy bridging as a pillar. The relatively large distance between the neighboring A and B planes (ca. 6.1 Å) gives the channeling cavity with ~ 8.8 x 6.1 Å along *a* axis, and ~ 6.1 x 6.1 Å along *b* axis.

The gas adsorption properties is one of the most attractive functionalities of the microporous solids. Examination of this property of **1** exhibits that the diffusion of the CH_4, N_2, and O_2 gases into the cavity in the pressure range 1 to 30 atom. Complexes **2** and **3** showed the similar gas adsorption properties to that of **1**.

References.

(1) C. Janiak, *Angew. Chem. Int. Ed. Engl.* **1997**, *36*, 1431-1434.

(2) M. Kondo, T. Yoshitomi, K. Seki, H. Matsuzaka, S. Kitagawa, *Angew. Chem. Int. Ed. Engl.* **1997**, *36*, 1725-1727.

Chained Chromophore NLO materials : aromatic ester oligomers and its derivatives

Tatsumi Kimura, Xuan-Ming Duan, Kimihiko Kamo, Masao Kato, Shinji Yamada, Takashi Fukuda, Hiro Matsuda, Shuji Okada and Hachiro Nakanishi

Department of Materials Science and Technology, Science University of Tokyo, Yamazaki 2641, Noda 278, Japan

We proposed "Chained Chromophores" for new types of second-order nonlinear optical (NLO) materials. As Chained Chromophores we synthesized aromatic ester oligomers consisting of 2~4 repeating units of oxy-1,4-phenylenecarbonyl group (**ArESn**, n=2~4) as well as their end-group modified oligomers with electron accepting group (**ArESn-X,** X=CF_3,CN,NO_2,DCV, n=2~3). The second-order NLO properties of poly(methyl methacrylate) (PMMA) films doped with 10wt% of **ArESn** (**ArESn/PMMA**) and 10wt% of **ArESn-X** (**ArESn-X/PMMA**), and PMMA film doped with 10wt% of *p*-nitroaniline (***p*NA/PMMA**) as control were investigated after poling treatment. UV/vis spectra of these polymer films have the cutoff wavelengths (λ_{co}) of about 300~380nm, which are much shorter than the case of *p*NA (λ_{co}=473nm) as typical strong donor-acceptor (D-A) molecule. In addition, some of the polymer films exhibited higher second-order nonlinear coefficient (d_{33}) values than ***p*NA/PMMA** (2.8×10^{-9}esu). Namely, **ArES3-CN** (d_{33}=3.1×10^{-9}esu), **ArES3-NO_2** (3.0×10^{-9}esu) and **ArES2-DCV** (4.0×10^{-9}esu) showed excellent second-order NLO activity as well as the transparency in visible region (λ_{co} = 304nm (**ArES3-CN**), 340nm (**ArES3-NO_2**) and 370nm (**ArES2-DCV**), respectively). Consequently, these compounds are believed to be promising chromophores for second-order nonlinear optics.

Moreover, we synthesized homo- and copolymer bearing **ArESn** moieties (**poly(ArESn-MA)** and **poly(ArESn-MA-co-MMA)**). These homo- and copolymer films were exhibited larger d_{33} values than **ArESn/PMMA** film because of high chromophore content.

Aromatic ester oligomers and these end-group modified oligomers

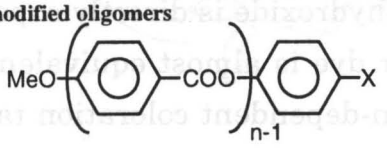

X = COOEt (ArESn)
CF_3 (ArESn-CF_3)
CN (ArESn-CN)
NO_2 (ArESn-NO_2)
$CH=C(CN)_2$ (ArESn-DCV)

Side-chain polymers bearing ArESn moieties

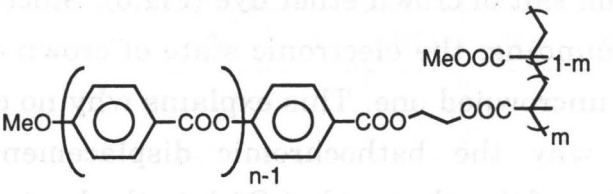

m = 1 poly(ArESn-MA)
m ≠ 1 poly(ArESn-MA-co-MMA)

色素化クラウンエーテルの結晶構造と電子スペクトル
Crystal structure of crown ether dye and its electronic spectra

○湯村 要*、松本 真哉**、大谷 裕之*、水口 仁**
(横浜国立大学 *教育学部 化学教室、**工学部 知能物理工学科)
○K. Yumura*, S. Matsumoto**, H. Otani* and J. Mizuguchi**
(*Department of Chemistry, Faculty of Education, **Department of Applied Physics, Faculty of Engineering, Yokohama National University)

The crown ether dye shown in Fig.1 is derived from 8,8-dicyanoheptafulvene together with a crown ether having a phenolic hydroxide group in its cavity. The color change on deprotonation has been spectroscopically investigated with special attention to the metal-selective coloration, using a variety of alkali metal bases. Deprotonation brought about a significant color change from red to blue (λ_{max}≈430→640nm) (Fig.2), however the coloration occurs quite irrespective of the cation species of the base added. Furthermore, the coloration is found to be very similar to that of the uncrowned compound of the same skeleton

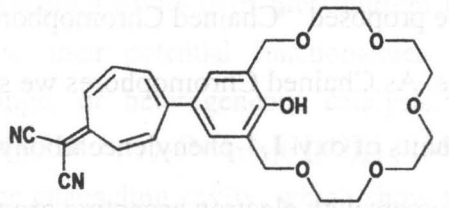

Fig.1 Conformation of the crown ether dye.

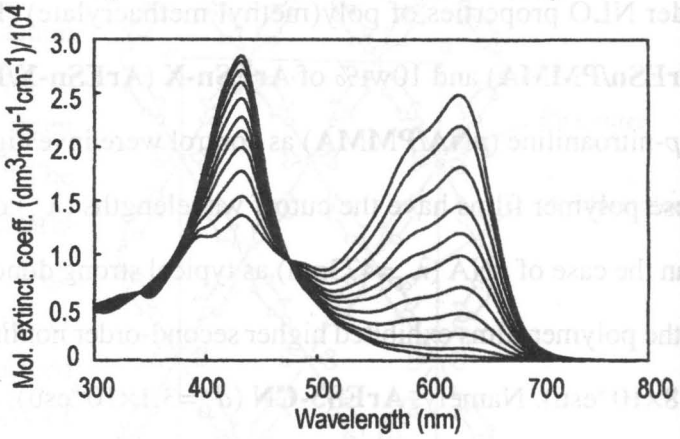

Fig.2 Spectral changes of crown ether dye in DMSO on deprotonation with KOH.

MO geometry optimization revealed that the crown ether ring is heavily deformed due to lone pair repulsion of the oxygen atoms in the cavity, making the hydroxide group directly expose to the surrounding. The present geometry is also directly borne out by X-ray structure analysis carried out on potassium salt of crown ether dye (Fig.3). Since the hydroxide is directly exposed to the surrounding, the electronic state of crown ether dye is almost equivalent to that of the uncrowned one. This explains why no cation-dependent coloration takes place and why the bathochromic displacement is mainly due to π-electron delocalization of the phenoxide ($-O^-$) into the heptafulvene chromophore.

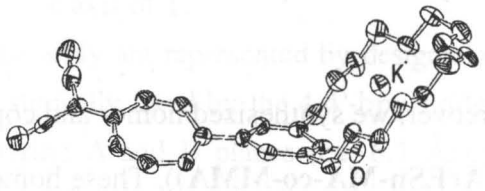

Fig.3 Structure of potassium salt of crown ether dye.

Supramolecular electron transfer in porphyrin-imide assemblies organized through coordination interaction

○Kenkichi Harada, Yoshio Hirose, Joe Otsuki, Koji Araki

Institute of Industrial Science, University of Tokyo
7-22-1 Roppongi, Minato-ku, Tokyo 106 Japan

Molecular photo/electronic devices rely on supramolecular organization of photo/redox active species and communications among them by means of electron/energy transfer. Prototypes of such devices are found in model systems for photosynthesis effecting photo-induced electron transfer (PET) reactions. While covalent linkages with rigid spacers have been proved effective to organize chromophors in a defined geometry, more recent studies are exploiting the use of non-covalent linkages which bear broader perspectives. It is known that Zn porphyrins take only one axial ligand which coordinates perpendicular to the porphyrin plane. Thus, the coordination interaction is well suited to deposit components above the porphyrin ring (J. Chem. Soc., Chem. Commun., 1989, 1765). We herein show supramolecular electron transfer in porphyrin-imide assemblies organized through coordination interaction.

We synthesized a series of imides bearing a pyridine moiety (**1-2**). Upon mixing these imide-pyridine conjugates with zinc tetraphenylporphyrin (ZnTPP), they self-assemble through the axial coordination to form an organized sensitizer-acceptor supermolecule (Fig.1). Intra-assembly PET was indicated from the quenching of fluorescence from ZnTPP. The dependence of extent of the quenching on the structure and the redox potential of imides was investigated.

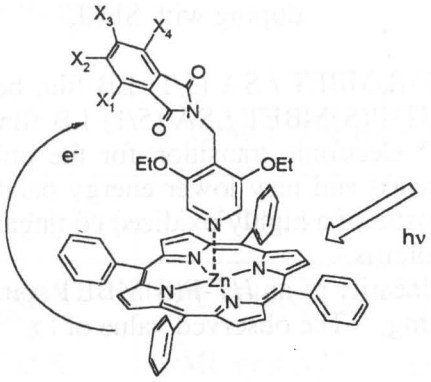

Fig. 1

	X_1	X_2	X_3	X_4
1a	H	H	H	H
1b	F	H	H	F
1c	F	F	F	F
1d	NO_2	H	H	H
1e	H	NO_2	H	H
2	H	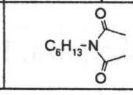		H

Structure and Properties of Poly(3-substituted thiophene) Langmuir-Blodgett Films Containing Optically Active Unit.

K. Ochiai, M. Rikukawa, K. Sanui, and N. Ogata

Sophia University, Department of Chemistry, Chiyoda-ku, Tokyo 102, JAPAN
Phone: 81-3-3238-4312 Facsimile: 81-3-3264-0867

Molecular structures and organizations play an important role in electrical and optical properties. It is an essential subject to understand the structure-property relationships of the conjugated polymers in order to create novel advanced materials. For this purpose, Langmuir-Blodgett (LB) technique is the most suitable method for investigation of these relationships, because the LB technique can control film thickness and molecular organization as a result of molecular architectures.

Recently, we have synthesized a series of regioregular poly(3-alkylthiophene)s and have investigated the self-organized structure and electrical properties of these LB films.[1) 2)] As an extension of our work, we have started to fabricate LB films of regioregular chiral poly(thiophene) derivatives in order to clear the effect of optically active unit on the electrical and optical properties.

In this study, regioregular poly(3-[2-((S)-2-methylbutoxy)ethyl]thiophene) (*HT*-P(S)MBET) was synthesized according to a modified Rieke method. The *HT*-P(S)MBET was an optically active polymer with more than 93 % of the *Head-to-Tail* linkages.

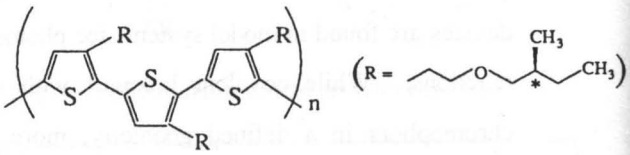

Scheme 1. Structure of *HT*-P(S)MBET.

The mixed monolayers of *HT*-P(S)MBET and stearic acid (SA) were found to be stable at the air-water interface. Multilayer thin films could be deposited onto solid substrates by the vertical lifting method.

The molecular organization and structure of the *HT*-P(S)MBET / SA LB films were investigated by using UV-Vis absorption spectra, FT-IR spectra and X-Ray diffraction measurements. It is found that the polymer chains are oriented parallel to the plane of the substrate and exhibit a tendency to orient along the dipping direction in the LB films. In addition, these LB films exhibit well-defined layer structures with 18 Å of the interlayer d-spacing calculated from the X-Ray diffraction pattern.

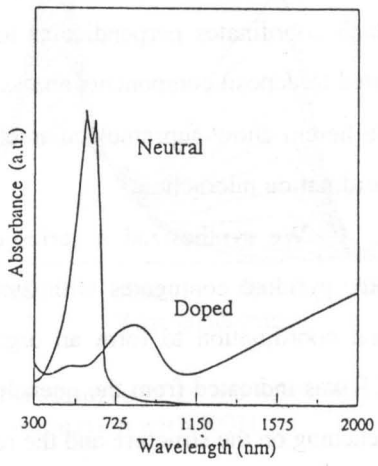

Figure 1. UV-Vis spectra of an *HT*-P(S)MBET / SA (5/1) LB film before and after doping with $SbCl_5$.

The in-plane conductivity was measured by using theVan der Pauw method in order to examine the electrical properties of these LB films. The conductivity of 10^{-4} S cm^{-1} was obtained for an *HT*-P(S)MBET / SA (5/1) LB film before doping, while the conductivity of 1.2 S cm^{-1} was achieved for an *HT*-P(S)MBET / SA (5/1) LB film doped with $SbCl_5$. After doping, the absorption bands of the π-π^* electronic transition for the poly(thiophene) conjugated backbone at about 566 and 610 nm are eliminated and new lower energy bands centered at about 820 and 2000 nm appear. These bands are characteristic of a highly oxidized conjugated backbone that is supporting localized defect states in the form of bipolarns.

Moreover, we measured the third-order optical nonlinearity of an *HT*-P(S)MBET spin-coated film around exciton resonance using degenerate four wave mixing. The observed value of $|\chi^{(3)}|$ was in the order of 10^{-10} esu.

1) M.Rikukawa, M.Nakagawa, H.Abe, K.Ishida, K.Sanui and N.Ogata, *Thin Solid Films*, 273 (1996) 240.
2) M.Rikukawa, M.Nakagawa, H.Abe, K.Sanui and N.Ogata, *Thin Solid Films*, 284-285 (1996) 636.

Epitaxial Growth Control of Organic Materials with High Vapour Pressure

K.A.Cho, T.Shimada and A. Koma

Department of Chemistry, The University of Tokyo, Bunkyo-ku 7-3-1, Tokyo 113 , Japan

Organic ultrathin films have attracted considerable attention recently because of their potential applications in optical and electronic devices. Although small aromatic organic molecules will provide a good opportunity to pursue unique physical properties, their high vapor pressure causes re-evaporation of the film in ultrahigh vacuum and has hindered the fine control of the thin film growth. It is expected that the problem will be solved by controlling the substrate temperature during the growth. Coronene is suitable for investigating the effect of the growth temperature because it has fairly high vapor pressure (~ 10^{-6} Pa at 300K) and a symmetric shape without active groups and hetero atoms. Substrates used in our experiment were cleaved surfaces of MoS_2, $MoTe_2$ and mica, and hydrogen-terminated Si(111) (H-Si). All of their surfaces have hexagonal symmetry without dangling bonds, with which coronene interacts via weak van der Waals forces. Growth of coronene was examined by reflection high energy electron diffraction (RHEED). Substrates were kept at 300K and 115K while coronene was evaporated from the Knudsen cell. As seen in Table 1, the effects of growth temperature can be classified into three categories: adsorption probability of the molecules, maximum thickness of the epitaxial films, and surface morphology of the epitaxial films (layer growth or island growth). Molecular mechanics calculation was performed to study whether we can predict the growth feature by computation. While calculated stabilization energies basically explain the tendency for forming epitaxial film (MoS_2 , $MoTe_2$ > H-Si, mica), the energy difference between H-Si and mica seems too small to account for the dissimilar experimental results. It was found that the energy difference becomes larger if we evaluate the van der Waals interaction using physical property of the substrates according to theLifshitz theory.

Table 1. The results of the experiment and calculation

substrate	MoS_2	$MoTe_2$	H-Si(111)	mica
300K	1ML epitaxy	2ML epitaxy with two domains	no growth	no growth
115K	10ML epitaxy	amorphous	1ML epitaxy	no growth
calculated stabilization energy	34.4 (kcal / mol)	35.0	23.7	21.0

Deposition of well-oriented PDA films on semiconductor substrates

T. Kondo, A. Ishii and H. Munekata

Imaging Science and Engineering Laboratory, Tokyo Institute of Technology, 4259 Nagatuda, Midori-ku, Yokohama 226, Japan

Polymer films can be very interesting electronic materials, as they have various new functions which are not available in traditional inorganic semiconductors. We believe that one of the most important points in the basic research is to develop the way to prepare crystalline-quality polymer films directly on semiconductor substrates, which would lead to the modulation of physical property of polymer films with crystal orientation and nano-scale morphology. In this paper, we describe molecular beam deposition and characterization of poly(5,7-dodecadiyne-1,12-diyl-bis-butylurethane) (PDA-4U_4) on GaAs(100) substrates.

PDA-4U_4 is a conjugated polymer which is known to exhibit photo-induced phase transition. Before the deposition of PDA-4U_4, a GaAs buffer layer was grown on a GaAs substrate at the substrate temperature of T_s = 580°C to yield a (2×4) reconstructed flat surface. This step is very crucial to obtain well-oriented PDA films. Monomer of PDA-4U_4 (DA-4U_4) was used as a source material with effusion cell temperatures of 60-80°C. During the deposition of a PDA film, the substrate was irradiated with 365-nm UV light (3 W/cm^2) to promote the photo-induced polymerization. T_s was varied between RT and 120°C. X-ray diffraction measurements showed that the *a*-plane (d~2 nm) of the monoclinic PDA crystal unit primarily align parallel to the GaAs(100) substrate surface.

Systematically studying the preparation of PDA films under various deposition conditions, we have found three different regions depending on T_s and the deposition rate R. The first region is defined by R > 0.05 Å/sec and T_s < 90°C, in which nanometer size PDA wire structures can be prepared. The second region is defined by R < 0.05 Å/sec and T_s > 90°C, in which the deposition results in the homogeneous layered structures. The third region is defined by high T_s (> 120°C) in which the sticking coefficient of a DA-4U_4 monomer is virtually zero so that no deposition takes place. The size of domains with single orientation is typically 5-10 μm square for both wire and homogeneous layered structures.

A PDA film (d~200 Å) composed of large domain size (> 100 μm square) was successfully prepared by three-step deposition process; the initial PDA-nucleation step at T_s=110°C and R < 0.05 Å/sec, the second template-layer-formation step at T_s = 95°C and R < 0.05 Å/sec, and the third epitaxial-growth step at T_s = 85°C and R > 0.05 Å/sec.

The authors gratefully acknowledge K. Takeda of Japan Synthetic Rubber Co., Ltd. for synthesizing DA-4U_4. This work is partially supported by the TORAY Science Foundation and the Grant-in-Aid for Scientific Research on the Priority Area "Molecular Superstructures-Design and Creation" from the Ministry of Education, Science, Sports and Culture.

Study on Molecular Switching in Phospholipid-azobenzene Mixed Monolayers by Maxwell displacement current

Xiaobin Xu, Yutaka Majima and Mitsumasa Iwamoto
Department of Physical Electronics, Tokyo Institute of Technology,
2-12-1 O-okayama, Meguro-ku, Tokyo 152, Japan
TEL: +81-3-5734-2191, FAX: +81-3-5734-2911, E-mail: iwamoto@pe.titech.ac.jp

Molecular cis-trans switching in mono- and multilayer systems containing azobenzene is of particular interest in physics, chemistry and electronics, because of the possible application of the switching to optical memories and information storage devices. Over the past few years, we have developed a novel technique based on Maxwell displacement current (MDC) measurement, and applied it to study the cis-trans photoisomerization in azobenzene monolayer systems. [1] In this study, we examine the molecular switching in phospholipid-azobenzene mixed monolayers by photo-isomerization by using MDC and Thermally stimulated current (TSC) measuring techniques.

The molecules used in this study were 4-octyl-4'-(5-carboxyl-pentamethyleneoxy)-azobenzene (8A5H), L-α-dioleoyl phosphatidylcholine (DOLPC) with unsaturated long alkyl chain and D-α-phosphatidylcholine dipalmitoyl with saturated long alkyl chain (DPPC). The vertical dipole moment change ($\triangle m_z$) of 8A5H molecule in the mixed LB films was induced by the cis-trans photoisomerization by alternately ultraviolet-visible light irradiation. The $\triangle m_z$ of 8A5H molecule in the DOLPC+8A5H mixed LB films increases as molar ratio of 8A5H decreases under all deposited surface pressure and decreases with increasing the deposited surface pressure. Also the $\triangle m_z$ of the 8A5H molecule in the DOLPC+8A5H mixed LB film is larger than that of the 8A5H molecule in the DPPC+8A5H mixed LB film. In contrast, the $\triangle m_z$ of the 8A5H molecule in the DPPC+8A5H mixed LB film deposited at 25 mN/m exhibited a different behavior with that of other LB films.

The charge (Q) flowing through the circuit during cis-trans photoisomerization is obtained by integrating the MDC. The temperature dependence of Q flowing across the mixed monolayer coincides well with that of Q across the pure 8A5H monolayer. The charge Q gives a maximum around 300 K and decreases as the temperature increases or decreases. Above room temperature, the cis-form 8A5H molecules change to trans-form quickly due to thermal reaction. Below room temperature, the thermal energy for photochemical reaction becomes small and prevent the photo-isomerization. In order to confirm that the cis-form 8A5H molecules change to the trans-form quickly at high temperature, we examined TSC of 8A5H LB films. We found difference between TSC of 8A5H LB film irradiated with 360 nm light and TSC of 8A5H LB film irradiated with 450 nm light. Further, 8A5H molecules changed into the cis-form by irradiation with 360 nm light return to the trans-form during TSC measurement.

Reference

1) M. Iwamoto, Y. Majima, H. Naruse, T. Noguchi and H. Fuwa: Nature 353 (1991) 645.

Macrocyclic Amphiphiles. 1. Host-guest Monolayers Derived from Octaalkoxymetallophthalocyanines at an Air/Water Interface

°Yoko Matsuzawa, Takahiro Seki and Kunihiro Ichimura

Research Laboratory of Resources Utilization, Tokyo Institute of Technology, 4259 Nagatsuta, Midori-ku, Yokohama 226, Japan

Self-assembling behavior of macrocyclic amphiphiles composed of rigid cyclic cores substituted with plural hydrophobic tails are attractive because of the controllability of orientation of the cores, leading to versatile functionality of their ultrathin films. Metallophthalocyanines (**1**) with eight long-chain alkoxyls are able to exhibit host-guest complexation with rod-shaped hydrophobic compounds at an air/water interface.[1] This is because a hydrophobic cavity is provided by the flat-laid phthalocyanine ring as a base and eight alkoxy residues as a side wall. Guest molecules are incorporated in the cavity of the macrocyclic host due to their hydrophobicity acting as a driving force. Homogeneous floating mixed monolayers consisting of **1** and long-chain normal alkanes and nematic liquid crystals are formed on a water surface under appropriate spreading conditions though no monomolecular film is obtained at all by spreading of the hydrophobic molecules in absence of **1**.

These host-guest mixed monolayers were investigated by measurements of π-A isotherms, UV-visible absorption spectra and Brewster angle microscopic observation. Furthermore, the orientation of phthalocyanine ring was elucidated by e.s.r. spectroscopy measurements of LB films of Cu complex of **1**. These results revealed that the following requirements are needed to result in monolayered host-guest complexation on a water surface. (1) Metallophthalocyanines must have long-chain alkoxy substituents to suppress self-aggregation. (2) There is an optimum mixing ratio between the macrocyclic host and guests to give stable and uniform monolayers. (3) The subphase temperature plays a critical role; this is governed by phase transition temperatures of guests.

1 : R= $C_{18}H_{37}$

1. Y. Matsuzawa, T. Seki, and K. Ichimura, *Langmuir* in press.

MOLECULAR IMAGING OF FATTY ACID MONOLAYERS IN DIFFERENT STATES OF THERMAL MOLECULAR MOTION

Hirokazu Matsumoto, Taishi Kuri, and Tisato Kajiyama
Department of Materials Physics and Chemistry, Graduate School of Engineering, Kyushu University

For the applications of the monolayer and Langmuir-Blodgett (LB) film as the molecular devices, it is indispensable to investigate the aggregation structure of the monolayer at a molecular level. The surface structured analysis of the organic materials at a molecular level has been succeeded on the basis of scanning probe microscope. In this study, the aggregation structure of the fatty acid crystalline monolayers in different states of thermal molecular motion were investigated on the basis of the high resolution atomic force microscope (AFM) observation.

Benzene solutions of montanic, ($CH_3(CH_2)_{26}COOH$) and lignoceric, ($CH_3(CH_2)_{22}COOH$) acids with the concentration of $1x10^{-3}$ $mol \cdot l^{-1}$ were spread on the pure water surface at a subphase temperature (T_{SP}) of 293 K. At this T_{SP}, the montanic acid forms the rectangular crystalline monolayer and also, the lignoceric acid monolayer shows the crystalline transition from a hexagonal system to a rectangular one with an increase of monolayer compression. The monolayers compressed to desired surface pressures were transferred onto a freshly cleaved mica by a horizontal lifting-up method for the AFM observation.

In the case of the montanic acid monolayer, many small crystalline domains in a rectangular crystal system were formed at a low surface pressure. Even though, with compressing the monolayer to a high surface pressure, these crystalline domains were gathered, the molecular arrangements in the monolayer became disordered. After compressing the monolayer at a high surface pressure, many disordered molecular arrangements and the molecular defects were observed in the monolayer. Then, it can be concluded from above results that the crystalline domains were gathered by the compression accompanying with a collapse of domains into small fragments owing to an insufficient thermal energy to induce a growth of monolayer domains.

In the case of the lignoceric acid monolayer, the crystal system of the monolayer changes from hexagonal to rectangular by the compression of the monolayer. Though at a low surface pressure, the molecules in the monolayer aligned with a hexagonal array, many molecular defects were still remained in the monolayer. After compressing the monolayer up to a high surface pressure, the molecules were in a highly ordered rectangular array as a result of a disappearance of molecular defects. Since the molecular rearrangements were induced by the crystalline transition, the crystalline transition phenomena might be useful for the structural regularization in the case of the rectangular crystalline monolayer.

On the basis of these results, we proposed the temperature-controlled multi-step creep method which was the structural regularization method of the monolayer based on the crystalline transition and the structural relaxation phenomena. By using the temperature-controlled multi-step creep method, highly ordered rectangular crystalline monolayer could be constructed. Therefore it can be concluded that the crystalline transition phenomena is quite effective for the construction of the defect-diminished rectangular crystalline monolayer.

Macrocyclic Amphiphiles [2]. Chemisorbed Monolayers of Calix[4]resorcinarenes Having Four Azobenzene Units

Masanori Fujimaki, Shin'ya Morino, Masaru Nakagawa, Yuko Hayashi, Kunihiro Ichimura (Research Laboratory of Resources Utilization, Tokyo Institute of Technology)

Calix[4]resorcinarene derivatives (AzCRA; Fig.1) with crown conformation having four azobenzene units at the lower rim and eight carboxyl groups at the upper rim are adsorbed on silica through hydrogen bonds to form densely packed chemisorbed monolayers [1]. We report here the fabrication of chemisorbed monolayers consisting of non- and cyclohexyl-substituted AzCRA to achive the photocontrol of liquid crystal (LC) alignment.

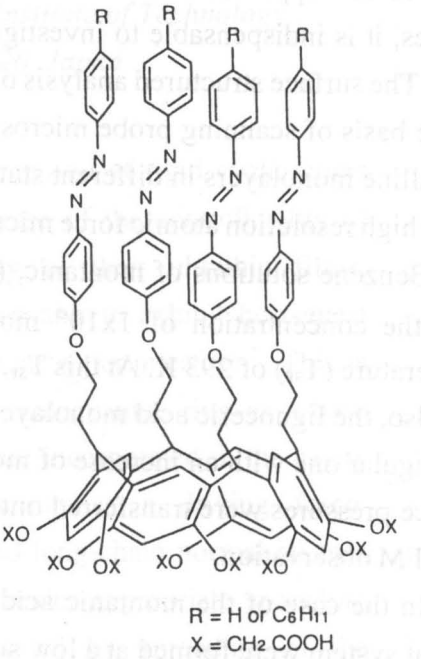

Fig.1 Chemical structure of AzCRA

AzCRA-adsorbed plates were prepared by immersing in a 2-butanone solution of AzCRA. A molecular area (1.9 nm^2) of AzCRA, determined with Langmuir plots, was almost consistent with that estimated with a CPK model (1.7 nm^2). UV spectra revealed that the azobenzene units in AzCRA monolayers exhibited no aggregation state. *E* -azobenzene units were transformed sufficientry to *Z* -isomer on UV irradiation (365nm) in monolayers. These results arise from the larger base area of AzCRA (1.7 nm^2) than the cross-sectional area of four azobenzenes (0.25×4 nm^2). Calix[4]resorcinarene derivatives provide a convenient method to give a photo-functional surface of silica plates.

LC cells were fabricated by putting a nematic LC between an AzCRA-plate and a lecithin - treated plate. LC alignment was homeotropic before photoirradiation. This suggests that LC molecules orient in parallel with azobenzene units which align perpendicularly to a surface of plates. Fig.2 shows a polarized micrograph of LC cell irradiated with polarized UV light through a photomask. Homogeneous LC alignment was induced at exposed areas, and its orientational direction is perpendicular to the polarization plane of linealy polarized light.

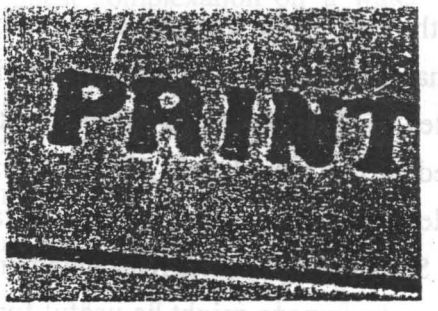

Fig.2 Polarized micrograph of LC cell

1) M.Ueda, N.Fukushima, K.Kudo, K. Ichimura, *J. Mater. Chem.*, **7**, 641 (1997)

EVALUATION OF LIQUID CRYSTAL MOLECULAR ALIGNMENT AT (POLYMER／LIQUID CRYSTAL) INTERFACE BASED ON OPTICAL SECOND HARMONIC GENERATION

Noriko Iwata, Hirotsugu Kikuchi, Tisato Kajiyama
Department of Materials Physics and Chemistry, Graduate School of Engineering, Kyushu University

Surface-induced alignment of liquid crystal (LC) molecules on properly treated substrates surface is generally used for the construction of LC devices. A polyimide-coated substrate surface is widely used to obtain unidirectional bulk alignment of LC molecular long axes along the rubbing direction. However, physical mechanisms of the surface-induced bulk alignment have not be well understood.

In this study, the molecular alignment in the LC monolayer anchored on a polymer surface was evaluated based on a Second Harmonic Generation (SHG method). When the light beam is incident on the LC cell, the second harmonic (SH) light generates from the LC monolayer at (polymer／LC) interface because of asymmetric molecular alignment at the interface. Therefore, an alignment state of LC molecules anchored on the polymer surface can be estimated from the in-plane rotational angle dependence of the SH light intensity.

8CB(4-cyano-4'-octylbiphenyl) and polyimide were used as the LC and the polymer film, respectively. The two kinds of LC cells were prepared, the homogeneous-aligned cell being induced by rubbing the polyimide surface and by flowing the LC material. As an incident light, a frequency-doubled Nd:YAG (Neodium doped:Yittrium Aluminium Garnet) laser was used. The linearly polarized beam (S-polarized or P-polarized) was incident on the LC cell mounted on a rotating stage, and polarized reflection light from the LC cell was detected through a polarizer. The preferred direction of LC molecular alignment and the order parameter of the LC monolayer were estimated by comparing the experimental results with the calculated ones.

The LC molecules at (polymer／LC) interface treated by a rubbing treatment were aligned in the direction parallel to the substrate surface and the rubbing direction. The order parameter of the LC monolayer was about 0.7. On the other hand, the LC molecules at the interface of the cell prepared by flowing the LC material effect were tilted up along the flowing direction with the tilt angle of 10 degrees with respect to the substrate surface. The order parameter of the LC monolayer was about 0.6.

It was suggested that alignment of the LC monolayer was induced by different mechanisms between the LC cells prepared by different way. The LC molecules at the interface of the cell treated by a rubbing treatment were anchored on a polymer surface stronger than those of the cell prepared by flowing the LC material effect.

Organization of DNA-mimetics at the Air-Water Interface

F. Nakamura[1], K. Ijiro[1,2] and M. Shimomura[1]

[1] *Research Institute for Electronic Science, Hokkaido University, Sapporo (JAPAN)*

[2] *PRESTO, JST, Kawaguchi (JAPAN)*

Introduction

Double-helical DNA is a supramolecular architecture composed of complementary base-pairings of adenine-thymine and cytosine-guanine with specific hydrogen bondings, and a carrier of genetic information. Recently some articles have suggested that DNA can act as a π-electron medium for the photoinduced electron transfer because of its close stacking of base-pairs. To fabricate novel materials based on unique properties of stacked base-pairs, two-dimensional DNA-mimetics[1,2] composed of nucleobase monolayers were prepared at the air waster interface.

Results and discussion

Figure 1 shows the π-A isotherms of mixed monolayers of octadecyladenine (C_{18}-Ade) and octadecylthymine (C_{18}-Thy) with various mixing ratio on pure water subphase. Each amphiphile was mixed in chloroform solution before spreading. An upper right insertion is a phase diagram of mixing molar ratio and molecular area at 5 mN/m. An equimolar mixture of C_{18}-Ade and C_{18}-Thy formed the most condensed monolayer on a pure water subphase. A FT-IR RAS spectrum of the transferred monolayer suggests the Watson-Crick type hydrogen bonds in the equimolar mixture. An *in situ* observation of fluorescence image and spectrum of the monolayer at the air-water interface indicates that an amphiphilic intercalator, octadecyl-acridine orange, can be intercalated into the equimolar monolayer, as well as DNA. These results clearly show that nucleobase monolayers prepared on water surface are the 2-D DNA-mimetics where the Watson-Crick base-pairs are densely stacked.

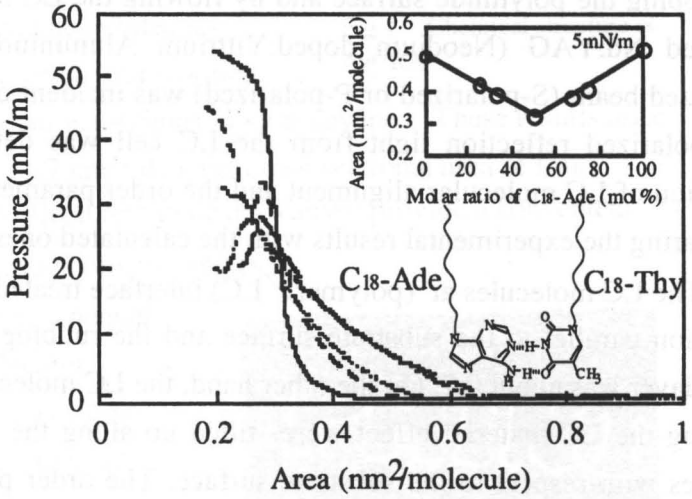

Figure 1 Π-A isotherms of C_{18}-Ade and C_{18}-Thy mixed monolayer on pure water: C_{18}-Ade and C_{18}-Thy ratio are, (—— -) 100:0; (- - - -) 75:25; (———) 50:50; (·····) 25:75;(—·—·) 0:100

1) M. Shimomura, F. Nakamura and K. Ijiro et al. *Thin Solid Films*, **284-285** (1996) 691

2) M. Shimomura, F. Nakamura and K. Ijiro et al. *J.Am.Chem.Soc.*, **119** (1997) 2341

Construction of 2α-Helix Peptide-Heme Conjugated and Regulation of Heme-Function

Seiji Sakamoto, Ikuo Obataya, Akihiko Ueno and Hisakazu Mihara

Department of Bioengineering, Faculty of Bioscience and Biotechnology, Tokyo Institute of Technology Nagatsuta, Midori-ku, Yokohama 226 (Japan)

Iron porphyrin perform diverse functions in nature as cofactors of hemeproteins. Over the years, in order to elucidate the factors which determined the specific function of hemeprotein, many studies using model porphyrin compounds and mutated proteins have been carried out. However, it is not easy to understand detailed mechanism of hemeproteins, since the natural protein contain many complicated factors. Thus, it is needed to establish the structural model system which has more native like properties than small model compounds. Along with this aspect, considerable effort has been devoted to the construction of designed polypeptide 3D structures and conjugation of porphyrin molecules by chelation or covalent linkage with peptides [1,2]. To develop a mini-hemeprotein that has minimal requirements for the function and exclude the complexities of natural counterparts, we have attempted to design and synthesize a series of 2α-helix peptides H2α(14), H2α(17), H2α(21), H2α(17)-L6, -L4, -L4sI, cH2α(17)-L4, and -L4sI, which were conjugated with Fe^{III}-mesoporphyrin (heme) through the ligation of two His residues (Fig. 1). The peptides H2α(14), (17), and (21) showed a unique heme-binding property dependimg on trifluoroethanol (TFE) contents. The conformation of H2α(14) and H2α(17) in a buffer was an random-coil and the peptides did not bind the heme. By the addition of 10-20% TFE to induce an α-helix structure, the peptides were able to bind the heme. These TFE effect revealed that the 2α-helix structure was annealed by TFE and the consequent formation of hydrophobic pocket was important for the heme binding. On the other hand, although H2α(21) took an α-helix structure in a buffer, H2α(21) also did not bind the heme due to the tight helix-helix packing. By the addition of 10% TFE to loose the helix packing, H2α(21) was able to bind the heme. These results indicated that the heme binding of the peptides was controlled by the peptide conformation. The peptides H2α(17)-L4, -L4sI, cH2α(17)-L4 and -L4sI took an α-helix structure and were able to bind the heme in water. Additionally, the CD spectra at the Soret band of the heme showed the heme was highly oriented in these peptide 3D structures. Furthermore, the *o*-methoxyphenol oxidation activities of heme in the presence of H2α(17)-L4, -L4sI, cH2α(17)-L4 and -L4sI were depressed to the level of natural electron transfer protein, cytochrome *c*. These results suggested that the heme was fixed in the peptide 3D structures as tightly as natural bis-ligated hemeproteins. In contrast, the catalytic activities of the heme bound to the peptides H2α(14), (17), and (21) in 15% TFE were accelerated. The peptides seemed to enhance the activity by isolating the heme in the peptide structure from the heme-aggregates in solution, and form the active intermediate more easily. In conclusion, the heme catalytic activity could be regulated by using a 3D structure of an artificially designed polypeptide.

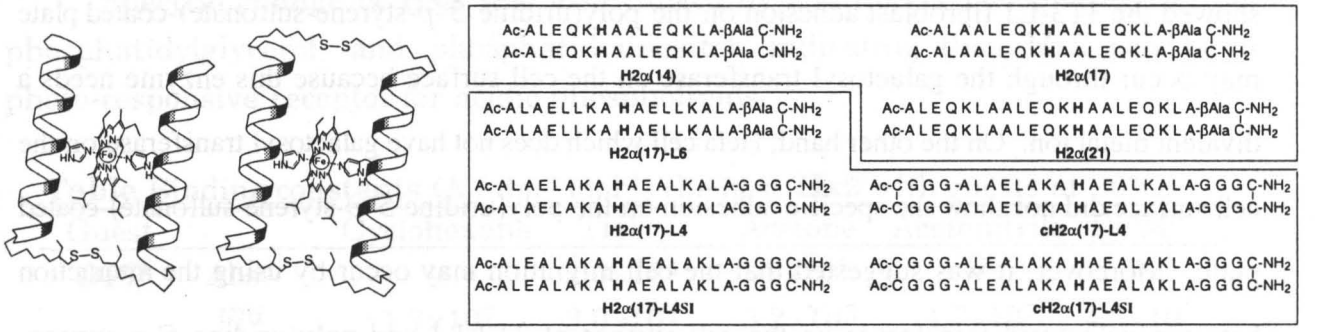

Fig. 1. Structure of designed heme-binding 2α-helix peptides.

1. S. Sakamoto, S. Sakurai, A. Ueno, H. Mihara, *J. Chem. Soc., Chem. Commun.*,1221 (1997).
2. H. Mihara, Y. Haruta, S. Sakamoto, N. Nishino, H. Aoyagi, *Chem. Lett.*, 1 (1996); H. Mihara, K. Tomizaki, T. Fujimoto, S. Sakamoto, H. Aoyagi, N. Nishino, *Chem. Lett.*, 187 (1996).

Inhibition between Nucleoside-Containing Polymer and Glycosyl Transferases

Kenichi Hatanaka, Megumi Kunou, and Junji Oishi

Department of Biomolecular Engineering, Tokyo Institute of Technology

4259 Nagatsuta-cho, Midori-ku, Yokohama 226, JAPAN

Tel: 045-924-5791 FAX: 045-924-5815 e-mail: khatanak@bio.titech.ac.jp

2',3'-Di-*O*-acetyluridine 5'-*p*-styrenesulfonate was synthesized by the reaction of 2',3'-di-*O*-acetyluridine with *p*-styrenesulfonyl chloride and polymerized. After removal of acetyl groups, the polymeric product was shown by NMR spectroscopy and gel permeation chromatography to be poly(uridine 5'-*p*-styrenesulfonate). This uridine-containing polymer was tested against the galactosyl transferase that synthesizes lactose in the presence of α-lactalbumin and trehalose 6-phosphate synthase. The polymeric compound did inhibit the both enzymes strongly.

The adsorption of poly(uridine 5'-*p*-styrenesulfonate) on the polystyrene 96-well mutiplate was confirmed by ESCA measurements. On the poly(uridine 5'-*p*-styrene-sulfonate)-coated plate, adhesion of 3T3-L1 fibroblast which has galactosyl transferase on the cell surface was increased, compared with non-coated plate. And the increase in adhesive cell number was inhibited by the addition of EDTA, indicating that the cell adhesion needs metal ions. This result showed the 3T3-L1 fibroblast adhesion on the poly(uridine 5'-*p*-styrene-sulfonate)-coated plate may occur through the galactosyl transferase on the cell surface because this enzyme needs a divalent metal ion. On the other hand, Hela cell which does not have galactosyl transferase on the cell surface did not show the specific adhesion on the poly(uridine 5'-*p*-styrene-sulfonate)-coated plate. Moreover, it was suggested that the cell migration may occur by using the interaction between galactosyl transferase on the cell surface of 3T3-L1 and poly(uridine 5'-*p*-styrene-sulfonate).

Highly Selective Recognition of Phosphoric Acid Ester against Carboxylic Acid by a Fluorescent Bipyridine Host

Toshiki Mutai, Yasuko Abe, and Koji Araki*

Institute of Industrial Science, University of Tokyo, Roppongi, Minato-ku, Tokyo, 106, Japan

Phosphoric acid esters and carboxylic acids are the major classes in hydrophobic biological substances, and show variety of important physiological activities. In this report, we studied the properties of 6,6'-bis(hexylamino)-2,2'-bipyridine (**Hx2**), that exhibited an efficient blue fluorescence, as a fluorescent host for recognition of phosphoric acid esters in various organic solutions.

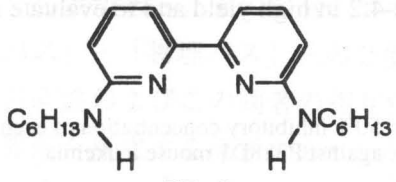

Hx2

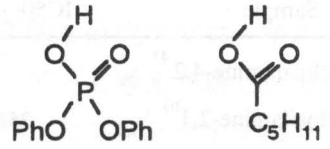

DPP

HA

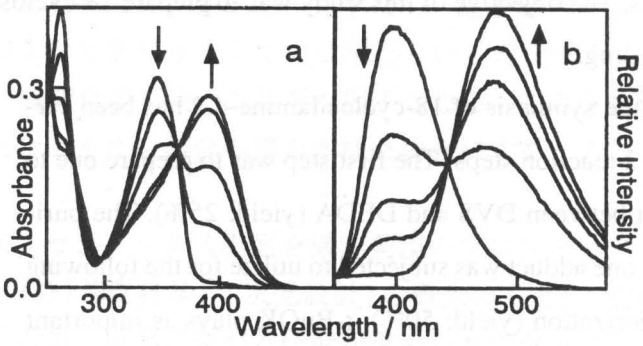

Spectral titration of Hx2 with DPP in acetonitrile. (a) Absorption and (b) fluorescence spectra.

Increasing amount of diphenyl phosphate (**DPP**) caused quantitative change in absorption spectrum of **Hx2**, showing isosbestic points around 300 and 360 nm. The blue fluorescence concomitantly diminished, and a green fluorescence appeared. On the contrary, addition of hexanoic acid (**HA**) induced only a little spectral change. Binding constants of **Hx2** with guests are collected in the Table. It was confirmed that affinity of the host **Hx2** for **DPP** was markedly high (K>10^4 dm^3 mol^{-1}), whereas that for **HA** was very low.

Spectral change of **Hx2** was also caused by addition of phosphatidylserine, phosphatidylglycerol, and phosphatidylinositol, indicating that **Hx2** can be a photo-responsive receptor for acidic phospholipids.

Table Binding constants (K / dm^3 mol^{-1}) the host **Hx2** with guests at 20°C.

Guest		Cyclohexane	THF[a]	Acetone	Acetonitrile	DCM[b]
DPP	Abs[c]	-[e]	2.0×10^4	$>1\times10^5$	-[e]	-[e]
	Fl[d]	1.7×10^7	3.0×10^4	3.2×10^5	1.7×10^7	4.5×10^7
HA	Abs[c]	6.7×10	<1×10	–	<1	
	Fl[d]	7.7×10	<1×10	–	<1	

[a] THF : Tetrahydrofuran. [b] DCM : Dichloromethane. [c] Determined from absorption change. [d] Determined from fluorescence change. [e] Too large (>10^6 dm^3 mol^{-1}) to be determined.

SYNTHESIS OF CYCLICSILAMINE COMPOUNDS AND EVALUATION OF THEIR PHYSIOLOGICAL ACTIVITY.

○Takayuki Ueki, Eiichi Honzawa, Yuki Nagasaki, Masao Kato, Kazunori Kataoka, Teiji Tsuruta, Syuji Kojima
Department of Materials Science and Technology, Science University of Tokyo, Yamazaki 2641, Noda 278, Japan

The synthesis of poly(silamine) compounds consisting of alternating organosilyl and amino groups have been carried out by anionic polyaddition reactions between dimethyldivinylsilane (DVS) and N,N'-diethylethlenediamine (DEDA) in the presence of lithium alkylamide as catalyst. Such polymers have been known to vary their characteristics such as solubility and conformation with changing surrounding conditions such as temperature and pH. In the polyaddition reactions, small amount of cyclic compounds such as 18-membered ring (18-cyclosilamine-4,2) were observed. Under the suitable conditions, 18-cyclosilamine-4,2 was prepared in good yield. Such the unique cyclic silamine compounds can be anticipated as new bioactive compounds. The objective of this study was to prepare 18-cyclosilamine-4,2 in high yield and to evaluate it as anticancer drug.

So far, the synthesis of 18-cyclosilamine-4,2 has been carried out in 2 reaction steps: The first step was to prepare one to one adduct between DVS and DEDA (yield: 25%). The purified one to one adduct was subjected to utilize for the following cyclic dimerization (yield: 50%). t-BuOK plays as important role to increase the yield of cyclization as template. However, total yields of these reaction was 12%. To improve the synthetic procedure, the direct cyclization was carried out from DVS and DEDA catalyzed by potassium amide. The yield of the cyclic compound increased even in the absence of t-BuOK under the suitable conditions to attain 21%.

Table 1 50% inhibitory concentration of each samples against P388D1 mouse leukemia

Sample	IC50(μ g/ml)
18-cyclosilamine-4,2 [a)]	1.5
9-cyclosilamine-2,1 [b)]	250
azacyclum [c)]	120
Adriamycin	0.38
5-FU [d)]	60

a) 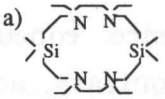 b) 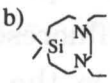 c) 

d) Fluorouracil

Antitumor effects of 18-cyclosilamine-4,2 was evaluated by in vitro examinations. As a result, It was indicated that the cytotoxicity of 18-cyclosilamine-4,2 was specifically high, from a comparison with other cyclic compounds. Actually, the IC50 (Table 1) of 18-cyclosilamine-4,2 was much higher than that of 5-FU (commercial drug) and attained the same level as Adriamycin (one of the most effective cancer drug).

From the in vivo study using leukemia P388 mice, 18-cyclosilamine-4,2 was effective when coupled with Adriamycin (Table 2) . Therefore, 18-cyclosilamine-4,2 is anticipated as one of the candidate for high performance anticancer drug.

Table 2 *In vivo* viability of Adriamycin and 18-cyclosilamine-4,2 against P388 leukemia

Sample	T/C(%) [a)]	
	Run 1	Run 2
Control	100	100
Adriamycin	123 [b)]	129 [b)]
18-cyclosilamine-4,2	105 [c)]	114 [d)]
Adriamycin + 18-cyclosilamine-4,2	127 [b) c)]	157 [b) d)]

a) $T/C\ (\%) = \dfrac{\text{median survival day of tested}}{\text{median survival day of control}} \times 100$

b) ADR (1day ; 4mg/kg ; s.c.)

c) 18-cyclosilamine-4,2 (1-7 everyday ; 50mg/kg ; i.p.)

d) 18-cyclosilamine-4,2 (odd day until 20day ; 50mg/kg ; i.p.)

第3シンポジウム　「フロンティアセラミックス」Frontier Ceramics
－Ceramic Interface as a Functional Interaction Field

現在、セラミックス材料は構造用ファインセラミックスや機能性セラミックスとして幅広い分野で利用されており、次世代に向けてますます多種多様な機能・役割が求められている。このセラミックス材料の高機能化を実現するためには、偶発的な発見を待つだけではなく、セラミックスの特徴を材料基礎科学的に明らかにして、新しい材料開発のセレンディピティーをより普遍的なものにしていく必要がある。その場合、セラミックス材料では、界面での化学反応・電子輸送－すなわち、「化学パス」・「物理パス」－の2要素、および界面に垂直あるいは平行といった化学パス・物理パスの方向性およびこの両者の相互作用が、機能発現を決める重要な因子となる。この点を踏まえ、さらに界面を構成する原子・イオンが共有結合とイオン結合の間の多様な結合様式をとることを前提とした研究アプローチをとる必要がある。

この具体的な研究アプローチの方法として、セラミックス界面を機能発現のフロンティアー機能フロンティアーと考えた新しいセラミックス材料基礎科学「二次元設計」の概念のもとに、高機能・新機能を持ったフロンティアセラミックスの設計・創製に関わる研究が進められており、今回日本ＭＲＳ学会で本シンポジウムを開催することは正に時宜にかなったものである。本シンポジウムでは、（1）界面フロンティア電子の計測・モデル化と制御、（2）界面配位構造の計測・モデル化と制御、（3）界面局所組成の計測・モデル化と制御、の三つの領域に分類した研究内容についての発表及び討論を行なう。

１２月１２日（金）＜＊招待講演＞

10：00-10：05　開会挨拶　　桑原　誠（東大・工）
　　座長　　羽田　肇（無機材研）

10：05-10：35　＊1「機能性セラミックスの材料設計」柳田博明（JFCC）

10：35-10：50　2「ZnOセラミックス中の不純物の電子状態計算」
　　大場史康，田中　功，小笠原一禎，足立裕彦（京大・工）

10：50-11：05　3「セラミックス界面の第一原理計算：SiC粒界とSiC-金属界面」
　　香山正憲、Johan Hoekstra（大阪工技研）

11：05-11：20　4「フロンティアセラミックス中の水素の拡散挙動」
　　羽田　肇、石垣隆正、森利之、田中順三（無機材研）
　　大垣　武、大橋直樹（東工大・工）

11：20-11：35　5「ZnOバリスタ単一粒界の定量的 ICTS 解析」
　　田中顕紀、向江和郎（富士電機）

11：35-11：50　6「異種セラミックス接触界面における化学反応の電気的制御」
中村吉伸（東大・工）、岡田治（大阪ガス）、柳田博明（JFCC）

11：50-14：00　**（昼食）**ポスターセッション

座長　平賀啓二郎（金材技研）

14：00-14：30　＊7「機能性フロンティアセラミックス界面・表面の構造と特性」
羽田　肇（無機材研）

14：30-14：45　8「コロイドプロセスによる微細構造物質の作製」
目　義雄、打越哲郎、鈴木　達、小澤　清、平賀啓二郎
（金材技研）

14：45-15：00　9「ICPフラッシュ蒸着法によるジルコニア薄膜の配向方位膜厚依存性とその制御」
佐伯淳、脇谷尚樹、篠崎和夫、水谷惟恭（東工大・工）

15：00-15：15　10「多結晶$BaTiO_3$ゲルの光吸収と光透過」
松田弘文、小林　健、桑原　誠（東大・工）

15：15-15：30　休憩

座長　桑原　誠（東大・工）

15：30-16：00　＊11「フロンティアセラミックスの高温力学特性」
平賀啓二郎（金材技研）

16：00-16：15　12「Ni-Zn-Cuフェライトにおける金属銅の整合析出」
西　湯二（太陽誘電）

16：15-16：30　13「溶融塩界面反応法によるマンガン酸リチウム結晶膜の調製」
湯　衛平、加納博文、大井健太（四国工技研）

16：30-17：00　＊14「フロンティアセラミックス研究開発の将来展望」
一ノ瀬　昇（早大・理工）

17：00-17：05　閉会挨拶　羽田　肇（無機材研）

ポスターセッション・プログラム

於　７０９号会議室

＜B：学士課程　M：修士課程　D：博士課程　S：一般＞

=番号=	= 著者 ※印:発表者 =	= タイトル =
P3-1B.	※篠崎裕志、須永孝一、林　卓（湘南工大・工）、佐々木昌一（元デュポン）	「$Ba(OH)_2$-$Sr(OH)_2$-$Ti(O^iPr)_4$より得られた前駆体の気相加水分解による$(Ba_xSr_{1-x})TiO_3$粒子の作製」
P3-2B.	※井上崇行、林　卓（湘南工大・工）	「ゾル・ゲル法によるPGO添加PZTセラミックスの低温焼結」
P3-3B.	※杉原　渉、須永孝一、林　卓（湘南工大・工）、佐々木昌一（元デュポン）	「金属アルコキシドを用いたZrO_2コーティング$BaTiO_3$複合粒子の合成と評価」
P3-4B.	※澤柳　悟、林　卓、高橋　宏、原　拓也、上野修司（湘南工大・工）	「非化学量論組成$Sr_{1-x}Bi_{2+y}Ta_2O_{9+\alpha}$セラミックスの強誘電特性と微構造」
P3-5B.	※高野正興、澤田　豊（東工芸大・工）	「In-Sn-O系複酸化物の合成」
P3-6B.	※杉森弘和、澤田　豊（東工芸大・工）	「In_2O_3-SnO_2系透明導電膜のスパッタ製膜と評価：Sn30及び60at％の検討」
P3-7B.	※伊藤寿英、澤田　豊（東工芸大・工）	「V_2O_5添加ITOの焼結過程」
P3-8B.	※田中伸武、木村雄二（工学院大・工）久森紀之（工学院大院・工）	「ジルコニア粒子分散アルミナセラミックス複合材料のナノスコピック構造と破壊機構の相関性」

P3-9B. ※吉田保之、天野忠昭
（湘南工大・工）
山崎潤一、後藤　孝、平井敏雄
（東北大・金材研）

「Ni-Cr および Ni-Si 系合金の N_2-H_2O-HBr 雰囲気における高温腐食」

P3-10B. ※辻村隆二、木村雄二
（工学院大・工）、
大畑宙生（工学院大院・工）

「プラズマ CVD 法により作製された TiN 薄膜の初期局部腐食過程とナノオーダー観察」

P3-11B. ※工藤幸司、玉野元士、
小早川紘一、佐藤祐
（神奈川大・工）、
山本信夫、山本夕美
（田中貴金属）

「電析による Co/Pd 多層膜の作製とその磁気特性」

P3-12B. ※荒井貴光、関根昌昭、天野忠昭
勝矢晃弘（日本発条）、
弘元修司、佐々木香
（東北大・金材研）

「微量の活性元素を添加した Fe-20Cr-10Al 繊維の高温酸化」

P3-13B. ※原　彰、天野忠昭
（湘南工大・工）、
佐々木香（東北大・金材研）

「微量の硫黄および Y を複合添加した Fe-20Cr-4Al 合金の高温酸化」

P3-14B. ※高松將倫、川島徳道、森田健一
（桐蔭横浜大・工）

「ポリアニリンを触媒とするスーパーオキシド発生装置」

P3-15B. ※佐伯修平、岸　悟史、石原久美子、
高田朋典、長谷川正木
（桐蔭横浜大・工）、
黄　謙（前田先端技術研）

「高強度・高耐水性ポリマー・石こう複合材料の開発」

P3-16B. ※石原久美子、岸　悟史、佐伯修平
高田朋典、長谷川正木
（桐蔭横浜大・工）

「高強度ポリマー・セメント複合材料中の組成物の影響」

P3-17M. ※角谷範彦、若森猛幸、山本　寛
（日大・理工）
「$In_{x-1}W_xB_a2C_uO_y$の合成」

P3-18M. ※酒井健太郎、吉村昌弘
（東工大・応セラ研）
岡田　清（東工大・工）
「アルカリ水熱処理によるSiC繊維上へのカーボンコーティング」

P3-19M. ※渡辺友亮、吉村昌弘、
Woo-Seok,Cho
（東工大・応セラ研）
「水熱電気化学法によるLi_3VO_4薄膜の合成」

P3-20M. ※釣本俊輔、韓　奎承、
吉村昌弘（東工大・応セラ研）
「水熱電気化学法による$LiNiO_2$膜のNi電極上へのその場作製」

P3-21M. ※清水禎樹、守吉佑介
（法政大・工）、
池上隆康、佐藤忠夫、石垣隆正、
小松正二郎、坂東義雄
（無機材研）
「炭素、窒化ホウ素ナノチューブの同時合成」

P3-22M. ※本田智、小早川紘一、佐藤祐一
（神奈川大・工）、
橋本一郎、牛久栄作（田中貴金属）
「電解プロセス用イリジウム被覆電極の電解法による新作製法」

P3-23M. ※関　成之、澤田　豊
（東工芸大院・工）
「酸化亜鉛の炭酸化：二酸化炭素および水蒸気雰囲気における反応過程」

P3-24M. ※江見　森、林　禎之、高島大治
飯泉清賢、久高克也
（東京工芸大・工）
「エマルジョン法による球形チタン酸バリウム微粉末の合成」

P3-25M. ※近藤康宏、鈴木久男、金子正治
（静岡大・工）、
林　卓（湘南工大・工）
「シード層を用いたゾルゲル法による$Pb(Zrx,Ti_1-x)O_3$薄膜の組成制御」

P3-26M. ※原　拓也、林　卓
（湘南工大・工）
「ゾル・ゲル法で作製した$SrBi_2Ta_2O_9$薄膜の配向性 とその誘電特性」

P3-27M. ※小村　恭、竹中　正
（東理大・理工）
「ビスマス層状構造酸化物の強誘電特性」

P3-28M. ※須永孝一、林　卓
（湘南工大・工）
佐々木昌一（元デュポン）
「疎水性溶媒における金属アルコキシドを用いたNb_2O_5-コーティング$BaTiO_3$複合粒子の合成と評価」

P3-29M. ※藤田昌樹、杉原　淳、
細谷　朗（湘南工大・工）
「反強誘電体へのカルシウム添加による電子構造とマイクロ波特性」

P3-30M. ※中島清文、小杉津代志、
金子正治（静岡大・工）、
村上健司（電子研）、
持塚多久男、深澤彰彦
（村上開明堂）
「スプレー熱分解法（SPD）による大面積酸化すず系透明導電膜の作製」

P3-31M. ※山口文親、澤田　豊
（東工芸大・工）
「酢酸塩を原料としたITO薄膜：ディップコート法による作製と評価」

P3-32M. ※根元央希、門間英毅、
高橋　聡、小林偉男
（工学院大・工）
「リン酸カルシウム電着層の表面と内部の微細組織」

P3-33M. ※前澤大輔、村上真之、
飯泉清賢、久高克也
（東京工芸大・工）、
岡田　繁（国士舘大・工）
「C_rB_2-MoB_2複合セラミックスの焼結とその性質」

P3-34M. ※前田邦宏、難波典之
（関東学院大・工）、
金子文隆（湘南工大・工）
「$PbCrO_4$-BaO系厚膜素子の感湿特性」

P3-35M. 寺田教男、伊原英雄（電総研）
※内田高明、菅沼良之、
吉山信成、山本　寛（日大・工）
「無限層構造$Sr_{1-x}CuO_2$、$(Sr_{1-y}La_y)CuO_2$膜におけるキャリアドーピングの研究」

P3-36M. ※渡辺俊樹、関屋昭彦、天野忠昭（湘南工大・工）、佐々木香（東北大・金材研）
「Fe-20Cr-4Al 合金の酸素中 1473K における硫黄の挙動」

P3-37M. ※永峰　聡、小早川紘一、佐藤祐一（神奈川大・工）
「レーザ照射による金の無電解めっき」

P3-38M. ※寒竹秀介、高谷慎一、北本仁孝、阿部正紀（東工大・工）
「垂直磁気記録媒体用 Co フェライト薄膜の磁気特性」

P3-39M. ※岩見大輔、王　重輝、中村茂夫（神奈川大・工）
「アミン塩基を有するコスモポリエステルとポリビニルアルコールのブレンドによる機能性材料の合成とその金属錯体の形成」

P3-40M. ※田部井進悟、仲川　勤、渡辺哲也（明大・理工）
「ポリ［1-（トリメチルシリル）-1-プロピン）］ブレンド膜の気体透過性と安定性」

P3-41M. ※萩原保子、仲川　勤（明大・理工）
「銀イオンを含有する高分子膜での促進輸送によるオレフィン／パラフィンの分離」

P3-42M. ※高橋周一、仲川　勤（明大・理工）
「親水性基を含むメタクリレート共重合体膜の溶存酸素透過性における重イオン照射の影響」

P3-43D. ※林　裕之、関野　徹、Y.H. Choa、新原晧一（阪大・産研）、浦部和順（龍谷大・理工）
「Li(Ti,Nb)O 系化合物の作製と微細構造」

P3-44D. ※金　晟鎔、脇谷尚樹、桜井　修、篠崎和夫、水谷惟恭（東工大・工）
「PrO_x-ZnO 系液相の粒界拡散による ZnO のバリスタ化」

P3-45D. ※椎橋博之、松田弘文、桑原　誠（東大・工）
「ゾルゲル法による$(Ba,Sr)TiO_3$結晶性モノリシックゲルの室温合成」

P3-46D. ※金　民先、島田恵理子、
伊熊泰郎（神工大・工）
「双結晶 $SrTiO_3$ における粒界溝の発達」

P3-47D. ※太田一史、門間英毅、
高橋　聡、小林偉男、大勝靖一
（工学院大・工）
「リン酸八カルシウム結晶面上でのカルボン酸およびアミノ酸の吸着」

P3-48S. ※加藤雅恒、榊原健二、
小池洋二（東北大・工）
「電子レンジによる高温超伝導材料の合成」

P3-49S. ※岸本堅剛、塚本昌義、
小柳　剛（山口大・工）
「SiGe/Si 焼結体の作製とその熱電気的特性」

P3-50S. ※平井岳根、北英紀
（いすゞセラ研）、
村尾俊裕（FCRA）
「ナノーミクロンサイズの鉄化合物を内包した Si_3N_4 の組織と特性」

P3-51S. ※小野清人、松尾良夫、
石倉　誠（富士電気化学）
「Mn-Zn フェライトの微細構造の制御」

P3-52S. ※松尾良夫、小野清人、
石倉　誠（富士電気化学）
「Mn-Zn フェライトへの三酸化モリブデン添加物の粒子径の効果」

P3-53S. ※白崎文雄、北本仁孝、
寒竹秀介、高谷慎一、
阿部正紀（東工大・工）
「メスバウアー分光法によるフェライトメッキ薄膜の評価」

機能性セラミックスの設計

（JFCC）柳田博明

1．はじめに

セラミックスの機能は異種物質間の非線形相互作用によって発現する。非線形相互作用の場として界面を設定、機能設計をおこなう。界面は3つのカテゴリーによって分類される。1）同種物質間か異種物質間か、2）機能の発生原因が界面に垂直に起こる移動現象か並行に起こるそれであるか、3）界面は閉じているか開いているか、この組合せによって8種の界面現象が考慮の対象になる。こうして界面現象をブラックボックスから解放しようとする。界面を挟んで結晶の軸関係を正確に定義しないと、たとえ同種物質間であっても異種物質間に準じて考える必要がある。酸化亜鉛バリスタ、半導性チタン酸バリウムにおけるＰＴＣ特性はこの例であろう。機能発現に有効な界面の例と特徴的な機能について論ずる。

フロンティアセラミックスプロジェクトは界面というフロンティア、界面におけるフロンティア電子、セラミックスの科学のフロンティアという3つの観点から推進されている。

2．同種物質・異種結晶方位関係・閉界面・垂直現象

酸化亜鉛バリスタの電圧ー電流特性の非線形性は、焼結体においては異種結晶方位関係・閉界面・垂直現象の統計的現象であるが、詳細に解析すると界面ごとに小個々となる特性を示す。演者の到達したイメージは、粒界の障壁は原子間距離の変化（増大）によって生ずる。原子間距離の変化（増大）は、結晶軸関係（不整合）、界面に介在する原子（例えばBi）、過剰酸素（添加したCoが2価から3価に変わること等による）によって引き起こされる。酸化亜鉛の界面における結晶軸関係についてはＣ軸方向の極性を考慮する必要がある。

半導性チタン酸バリウムにおけるＰＴＣ特性は酸化亜鉛における界面を挟んでの結晶軸関係の極性を考慮することに加え、極性が分極処理によって変化・可変であることをも考慮に入れる必要がある。高抵抗領域には酸化亜鉛と同様な議論が適用できよう。

3．異種物質間・開界面・垂直現象

P-型半導体とN-型半導体との閉界面・垂直現象は電気的には整流である。これに対し開界面では、界面付近の状況変化によってその整流作用が変化する。逆にこの変化を測定することにより、外界の状況変化をモニターすることができるセンサーになる。P-型半導体として酸化銅、N-型半導体として酸化亜鉛を用いた開界面は、室温付近では湿度センサーとして有効である。さらに電圧・電流特性を解析することにより、界面に介在する溶媒種の定性・定量分析も可能になる。

同じ組合せが260C付近ではガスセンサーとして機能する。酸化銅側に微量の炭酸ソーダを添加し、こようと析出が共存する領域で一酸化炭素に対して優れた選択性を有するものが得られた。検出機構についての提案と実用化への期待について述べる。

ZnO セラミックス中の不純物の電子状態計算

（京都大学）○大場史康・田中功・小笠原一禎・足立裕彦

Electronic structure calculation for impurities in ZnO ceramics / ○ F. Oba, I. Tanaka,K. Ogasawara, H. Adachi (Kyoto University) / In order to investigate the role of transition metal dopants on the appearance of varistor characteristics in ZnO ceramics, the electronic structure calculations for 3*d* transition metal solutes in ZnO are performed using DV-Xα cluster method. Trivalent and quadrivalent solutes are found to show larger bond overlap population with neighboring oxygens than the case of divalent solutes. Model calculations for oxygen atom adsorption on ZnO surface with and without solutes are also performed. It is found that the solute-oxygen bonding at the surface are stabilized by the oxygen adsorption when solutes are present. On the other hand, it is unstabilized when solutes are absent. This indicates solutes enhance oxygen adsorption at ZnO surface.

【緒言】ZnOセラミックスに現れるバリスター特性は，粒界に形成された界面準位を起源とする二重ショットキー障壁の降伏によって生じると考えられている．界面準位については，界面への酸素吸着によって形成されるという説が有力であるが，その時の3*d*遷移金属酸化物の役割は十分に解明されていない．本研究ではZnO中の3*d*遷移金属元素について電子状態計算を行い，その役割について考察した．

【方法】ZnOバルク中への3*d*遷移金属元素の固溶を想定したモデルクラスターの電子状態をDV-Xα法を用いて計算し，これらに特有な電子状態を調べた．この際，遷移金属元素の酸化数を２価，３価，４価と変化させ，マリケンの密度解析により化学結合状態の変化を調べた．また，遷移金属元素を含むZnO表面への酸素原子の吸着を想定したモデル計算を行い，酸素吸着による化学結合状態の変化を調べた．

【結果及び考察】バルクモデルクラスターについての計算結果の例として，図に遷移金属元素の酸化数を変化させた場合の遷移金属元素と近接の酸素間のBond overlap population（共有結合電荷）と遷移金属元素のNet charge（有効電荷）の変化を示す．これらの遷移金属元素は酸化数の増加と共に近接の酸素と強く共有結合し，遷移金属元素の有効電荷はその酸化数の変化に対して小さな変化を示すことがわかる．このため，ZnO中に固溶した遷移金属元素は，酸化されることによって安定化すると考えられる．

また，遷移金属元素を含む表面への酸素吸着のモデル計算を行うと，酸素の吸着により遷移金属元素は酸化され，表面内の遷移金属元素と近接の酸素間の共有結合はバルクの場合と同様に強くなった．一方，遷移金属元素を含まない表面について同様な計算を行った場合，酸素の吸着により表面内の結合は弱められた．このような結果から，ZnO中に固溶した遷移金属元素は，酸素吸着を促進する働きを持つと考えられる．

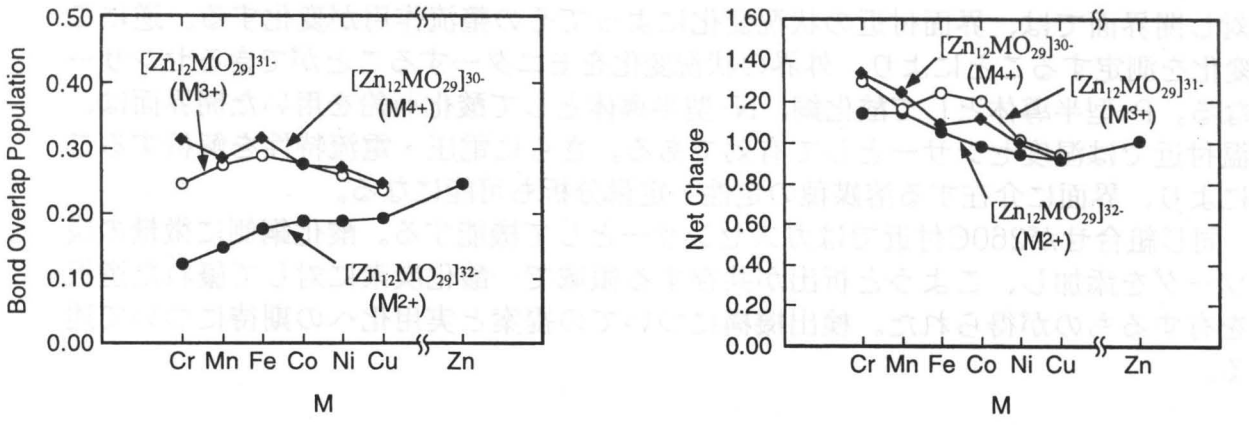

Fig. Bond overlap population between M and O and net charge of M for $[Zn_{12}MO_{29}]^{(34-x)-}$ (x=2,3,4) bulk model clusters.

セラミックス界面の第一原理計算：SiC粒界とSiC-金属界面

（工業技術院 大阪工業技術研究所）　○香山正憲・John Hoekstra

Ab Initio Calculations of Cramic Interfaces: Grain Boundaries in SiC and SiC/Metal Interfaces / OM.Kohyama and J.Hoekstra (Osaka National Research Institute) / Ab initio calculations of the Σ=9 boundary in SiC and the SiC(001)/Al interface have been performed by using the techniques of the first-principles molecular dynamics method. In the former system, it has been found that the interfacial C-C and Si-Si wrong bonds have significant effects. In the latter system, it has been shown that the C-Al and Si-Al interactions at the interface have quite different features.

1．緒言　Car-Parrinello法や共役勾配法など第一原理分子動力学法の開発により、粒界や異種物質界面など複雑構造の第一原理計算が可能になってきている。セラミックスの典型的な粒界と異種物質界面としてSiCΣ=9粒界とSiC(001)/Al界面の第一原理計算について報告する。SiC/Al界面は、電子セラミックスSiCの電極、あるいは高温材料、複合材料など、広範な分野で極めて重要である。

2．計算方法　第一原理分子動力学法を界面のスーパーセルに適用した。電子構造計算を繰り返しながら、それに基づく力に従って原子をゆっくり動かして緩和計算を行った。第一原理分子動力学法は、密度汎関数理論（局所密度近似）に基づく第一原理擬ポテンシャル法バンド計算を高速に行うテクニックである。第一に、共役勾配法等のアルゴリズム[1]により、大規模行列の対角化計算を回避して波動関数の最適化計算により効率的に基底状態の電子構造を求めること、第二に、最適化・ソフト化擬ポテンシャル[2]の使用により、平面波基底数の低減化を図ることである。平面波打ち切りエネルギーは、SiC粒界はC-Cボンドがあるのでdiamondを扱えるだけ大きくとった（60Ry）。SiC/Al界面は少し小さい値（45Ry）を用いた。Σ=9粒界は64原子スーパーセルで非極性界面、極性界面を扱った。SiC(001)/Al界面はC原子面とAlとの界面、Si原子面とAlの界面を別々に扱った。スーパーセルはSiC(001)の9原子層スラブの上下にAl5原子層を積層して真空層を挟んで繰り返す。真空層により層間が自由に緩和できる。(1X1)理想表面にAlを積層したエピ構造を扱った。

3．計算結果　①SiCのΣ=9粒界：安定原子配列を求め、原子・電子構造を詳細に分析した。非極性界面、極性界面とも、SiのΣ=9粒界の構造と同様にdangling bondを持たない五員環、七員環による再構成構造が安定である（非極性界面の粒界エネルギー1.3J/m^2）。しかし、同種原子ボンドがバルクのdiamondやSiやボンドに類似した電子密度分布やボンド長を有し、特異な局在準位をバンド端に生んでいる。次に、「第一原理引っ張り試験」を行った。セルに均等に変形を与えて各原子を緩和させる過程を繰り返し、各ボンドの様子を探った。結果の詳細は当日報告する。

②SiC(001)/Al界面：Si-terminated界面ではSi原子が四配位の構造が安定で、界面の電子密度は比較的広がっている。C-terminated界面ではC原子が三配位の構造が最安定で、C-Al間で電子移動も大きく、ボンド長や電子密度分布がC-Siのback bondに似ており、局所的に強い結合が生じている。界面エネルギー（表面との比較による利得）は、Si-terminated界面が3.74J/m^2、C-terminatedが6.42J/m^{2}である。Alバルクの(001)面間のエネルギーが2.04J/m^{2}で[3]、界面はAlより強い。MgO(001)/Al界面は1.10J/m^{2}で[3]、共有結合結晶/金属界面の方がイオン結晶/金属界面よりエネルギー利得が大きいと言える。局所状態密度(LDOS)では、Si-terminated界面ではSi-Al間がむしろAlのLDOSに近く、金属的である。C-terminated界面では、C-Siのback bond部分がバルクよりもC-Al間のLDOSに近く、配位数の違いにより電子構造がかなり変化している。LDOSからショットキー障壁高の理論値が求まる。Si-terminated界面で0.85eV、C-terminated界面は0.08eVであった。前者はSiCのSi面での実験値0.9eVに近い[4]。後者が低い理由は、界面のC-Al間の電子移動による界面dipoleのためである。最近の第一原理計算は、ショットキー障壁高が物質自体のintrinsicなものではなく、界面の局所構造に大きく依存することを示しており、それらと合致する結果である。

4．まとめ　各界面について興味深い結果が得られた。安定な原子構造を求めて構造や性質を分析する方法論は従来のモデル構造の計算の限界を突破するものである。もちろん、現実の構造はさらに複雑であるが、今後、こうした理論的アプローチを各種実験観察とも協力して進めることにより、界面設計のための多くの知見が得られることが期待できる。

1)M.Kohyama, *Modelling Simul.Mater.Sci.Eng.*4(1996)397, 2)N.Troullier and J.L. Martins, *Phys.Rev.B*43(1991)1993, 3)J.R.Smith *et al., Phys.Rev.Lett.*72(1994)4021, 4)V.M.Bermudez, *J.Appl.Phys.*63(1987)4951.

フロンティアセラミックス中の水素の拡散挙動

（無機材質研究所）　○羽田肇、石垣隆正、森利之、田中順三
（東京工業大学）　大垣　武、大橋直樹
（東北大金研）　関口隆史

Hydrogen behavior concerned with grainboundary properties in ceramics.

○H.Haneda, J.Tanaka, S.Hishita, T.OGAKI*, N.OHASHI*, **T.SEKIGUCGI
National Institute for Research in Inorganic Materials, *Tokyo Institute of Technology,
**Institute for Materials Research, Tohoku University

１．水素分析の重要性

フロンティアセラミックスとはセラミックス材料の持つ界面機能をフルに引き出すことを目指したものである。この視点から、ZnO、$SrTiO_3$等のバリスタ、あるいは$BaTiO_3$の界面機能を利用したPTCR素子がその格好の研究舞台となっている。これらの材料は酸化還元処理に敏感であることは良く知られている。例えば、ZnOは還元処理によってそのバリスタ特性が失われる。また、還元焼成された$BaTiO_3$は酸化処理を施すことで初めてPTCR特性が出現する。この処理による効果の要因は粒界の酸化・還元反応にあると考えられており、酸素イオンの出入について面から検討することが多かった。しかし、酸素の出入は一方で水素の入出にも対応するわけで、この観点からの検討も重要な要素となることが予想される。例えば、最近、バルクの性質ながら水素処理によって酸化亜鉛の発光特性が著しく変化する事が見出されてきている。

このようにそこで水素の分析等のキャラクタリゼーションが重要な課題となっているが、最も軽い（すなわち電子の少ない）元素であり、かつ日常的に存在する不純物であるため、その微量分析は難しいとされてきた。最近では徐々にこの困難は乗り越えられつつあるが、その代表的な手段の一つとして二次イオン質量分析計（SIMS）がある。ここでは、このSIMSを用いたセラミックス中水素分析を紹介すると供に、固体中の水素と関連した拡散特性について論じたい。

２．SIMSによる水素分析

セラミックスの分析対象としては酸化亜鉛とチタン酸ストロンチウム（以下ST）の単結晶を用いた。酸化亜鉛単結晶は酸化鉛を主体としたフラックスを用い育成した。また、STは市販品を用いた。酸化亜鉛の主な不純物はF, Pb, Alであったが、そのうちF, Pb 成分は表面近傍に濃縮していることがSIMSにより確認されている。当日はSTについては水素の拡散挙動、ZnOについては水素処理による酸素欠陥生成について議論したい。

SIMSはダイナミックレンジとして６桁を越えるものを持っており、ホスト元素の同位体イオンを標準とすることで、ｐｐｂのオーダーの分析も可能とされている。実際には、様々な理由でこの性能は制限されている。そのひとつが真空中のバックグラウンド元素の存在であり、水素の感度向上にはこの低減化を図ることが肝要となる。本研究では装置面、測定手法面の二点より分析限界の低減化を図ったが、このことについてダイヤモンドあるいはシリコン中の水素分析を例に説明する。

ZnO バリスタ単一粒界の定量的 ICTS 解析

(富士電機総研) ○田中顕紀・向江和郎

Quantitative ICTS analysis of single grain boundaries in ZnO Varistor / ○A. Tanaka, K. Mukae (Fuji Electric Corporate Research and Development) / Interface states at single grain boundaries in ZnO:rare-earth varistors were examined by isothermal capacitance transient spectroscopy measurements. Non-linear exponent of single grain boundaries corresponded to interface state density. By photo-ICTS and photo-capacitance measurement, several trap levels were detected in zinc oxide band gap.

1. 緒言

電圧非直線抵抗体である ZnO バリスタの粒界に存在する界面準位については、その生成機構等不明な点が多い。そこでバリスタ粒界の電子状態をより詳細に評価解析するため、従来の多結晶体による評価に代わって、単一粒界の物性を直接評価する試みがなされている。我々はこのような ZnO バリスタ単一粒界の物性測定を、微小な電極対を試料表面上に形成するという方法で行った。 ZnO バリスタ単一粒界の ICTS 測定の定量的な解析により、単一粒界の界面準位の物性と非直線性の関係を明らかにした。また定常光照射下における ICTS 測定、フォトキャパシタンス測定を行い、光励起によってフェルミレベル以下の電子状態の評価を行った。

2. 実験

ZnO に Co_3O_4 と Pr_6O_{11} または Gd_2O_3 をそれぞれ 2,0.5 at%加え、粉末固相法で合成した焼結体の表面を鏡面研磨したのち、1000℃でサーマルエッチした。この試料上に蒸着法で微小電極を形成した。電流電圧測定はカーブトレーサを用い、 ICTS 測定は高速キャパシタンス計を用い、電極間に電圧を 10 秒間印加し、その後のキャパシタンスの時間変化を測定した。光 ICTS 測定では、まず試料を暗箱の中に設置し、一定温度に保った後、試料表面に波長 300nm～1200nm の定常光を照射した状態で ICTS 測定を行った。フォトキャパシタンス測定では、同様に定常光を 20nm ステップで照射し、キャパシタンスが定常状態に達した値を測定値とした。

2. 結果と考察

単一粒界の非直線係数と界面準位密度の関係を図1に示す。界面準位密度の高い粒界ほど高い非直線性をしめすことが明らかになった。単一粒界の光 ICTS 測定の結果 1050nm (1.18eV), 700nm (1.77eV),500nm(2.48eV)の波長光照射下において、スペクトルのピークが短時間側にシフトした。これに対し 800nm (1.55eV),400nm (3.10eV) ではピークのシフトが認められなかった。フォトキャパシタンスの波長依存性の測定結果を図 2 に示す。スペクトルには 1.2eV(1033nm),1.8eV(689nm),2.5eV(496nm)に3つのピークが認められ、ICTS スペクトルのピークがシフトする波長 700nm,500nm と対応していることが明らかになった。

キャパシタンスの増加は、光励起により、電子が放出されたためで、図2のピークは先ほど述べた深さに準位が存在することを示唆している。これらの準位の由来は明かではないが、1.2eV 付近のピークは界面準位に由来するものであると推定される。その他に2つの準位については ZnO の固有欠陥か Co の準位と推定される。

謝辞 本研究は科学技術庁の平成 9 年度科学技術振興調整費による「フロンティアセラミックスの設計と創製に関する研究」の一環として行われたものである。

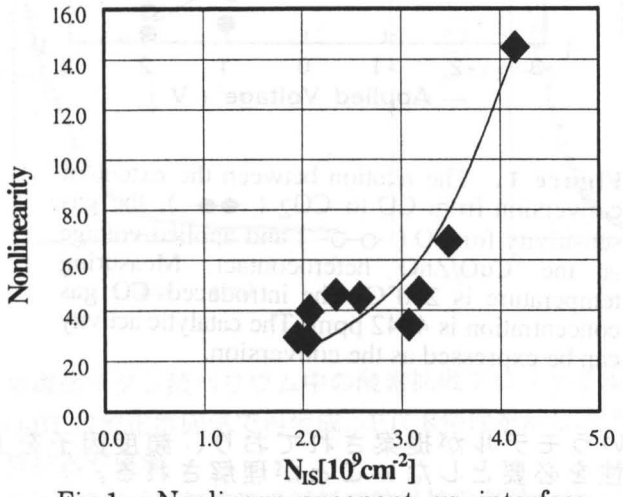

Fig.1 Nonlinear exponent vs interface state density of single junctions in ZnO-Pr-Co sample

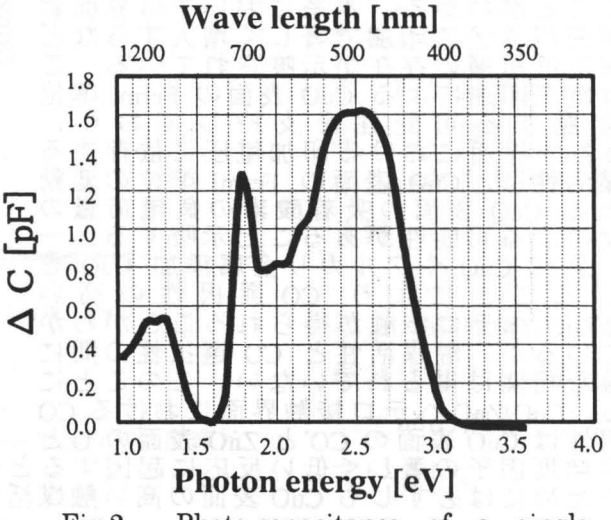

Fig.2 Photo-capacitance of a single junction in ZnO-Pr-Co sample

異種セラミックス接触界面における化学反応の電気的制御

（東大院工）中村吉伸、（大阪ガス）岡田治、（JFCC）柳田博明

Electrical Control of the Chemical Reaction over the Ceramic-ceramic Interface / ○ Y.Nakamura (The Univ. of Tokyo), O.Okada (Osaka Gas, Co., Ltd.) and H.Yanagida (JFCC) / Applied voltage dependent CO oxidation reaction is over the CuO-ZnO contact interface is observed and its working mechanisms are discussed. When the reverse bias is applied to the heterocontact, the catalytic activity for CO oxidation is enhanced. Its CO gas sensitivity is also enhanced by the reverse bias application and it is suggested that "sensitivity " is depend on the catalytic activity over CuO. The relation between the "selectivity for CO" and catalytic reaction is now being discussed.

1. 緒言 酸化第２銅（CuO）および酸化亜鉛（ZnO）の高密度焼結体を機械的に圧着して作製した CuO/ZnO ヘテロ接触は、その電気的性質が CO ガスなど還元性ガスの存在により変化するためガスセンサーとして応用が期待できる。センサー機能発現は界面における触媒反応機構に依存するが、ヘテロ接触型センサーにおいてはそのガス感度が印加電圧に著しく依存することから触媒反応機構に対する印加電圧の影響が強く示唆されていた。本研究では反応ガスの分析定量を行うことで CuO/ZnO ヘテロ接触の CO 酸化触媒能と界面に印加した電圧、電流との相関を明らかにし、CO 酸化触媒反応の機構と CO ガス感度がどのような相関にあるのかを推定した。

2. 実験 CuO/ZnO ヘテロ接触における CO ガス感度は CuO 焼結体の熱処理温度、冷却過程に著しく影響を受けるため、センサー特性の実験には様々な熱処理条件で焼結させた試料を用いた。とくに触媒反応実験に用いた CuO 焼結体は、CuO 原料粉を 850 ℃, 10 時間焼成したもので、炉内で約 10 時間かけて冷却したものである。作製した CuO 焼結体試料は表面研磨ののち、パイレックスガラス製のホルダーを用いて ZnO 焼結体（1000 ℃、4 時間焼成）とのヘテロ接触を作製し、接触部に直流定バイアスを印加した状態で乾燥空気をキャリアとして被検ガス（CO ガス）を導入し、ガスセンサー特性（CO 導入による電流値変化）および流通法による CO 酸化反応の触媒活性（CO 酸化による CO_2 発生量）の評価を行った。

3. 結果 CuO/ZnO ヘテロ接触界面における CO 酸化反応の反応生成物（発生 CO_2）は CuO の触媒活性が ZnO のそれと比べて圧倒的に大きいことからほとんど CuO 表面で発生した CO_2 であると判断できる。Figue 1 に CuO/ZnO ヘテロ接触を触媒とする CO から CO_2 への転化率と印加電圧の関係を示す。印加電圧を変えることで CO_2 発生量は変動し、逆バイアス（CuO-, ZnO+)印加により反応が促進、順バイアス印加で抑制されていることがわかった。CO ガスの導入により系の見かけの抵抗が減少し、ガスセンサーとしての動作は確認されたが、CO ガス感度が H_2 ガス感度を下回っており、CO 選択性は付与されていなかった。Figure 1 に CO ガス感度の印加電圧依存性を同時に示すが、反応活性の電圧依存性と同様の傾向を示しており、逆バイアス印加で大きなガス感度が得られた。この系においては CuO 上の CO 酸化反応の活性と CO ガス感度は正の相関にあることがわかる。本系においては界面容量が逆バイアス印加で著しく増大するなど界面高抵抗層の存在が示唆されている。これは電圧印加による CuO 表面の Fermi 準位が変動する可能性を支持しており、CuO-ZnO 界面における印加電圧に依存する触媒活性は、CuO 表面の Fermi 準位の変動による CuO 表面の吸着酸素の負電荷量の変動による可能性があること示唆する。一方、急冷 CuO やアルカリ金属添加 CuO を用いることにより CO 選択性の高い CuO/ZnO ヘテロ接触が得られることがわかっているが、触媒活性と CO 選択性の間に明確な相関は得られていない。このことに関し、CuO/ZnO ヘテロ接触界面における CO 選択性は CuO 表面の CO と ZnO 表面の O という頻度因子の著しく低い反応に起因するというモデルが提案されており、頻度因子を上げるためには必ずしも CuO 表面の高い触媒活性を必要としないことが理解される。

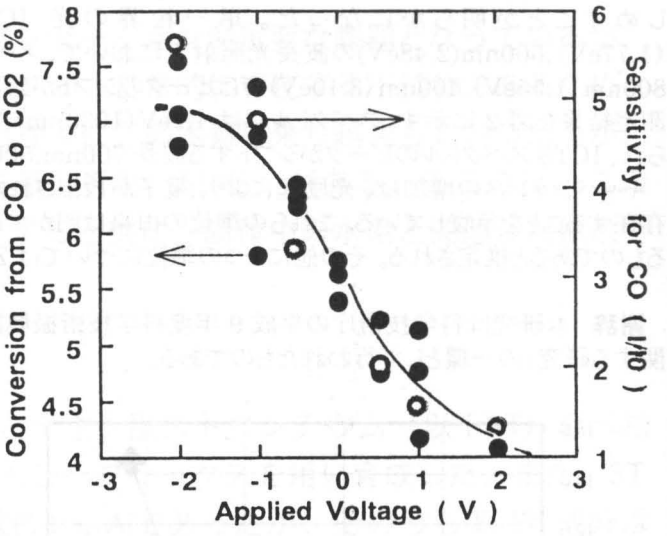

Figure 1. The relation between the extent of conversion from CO to CO_2 (●●), the gas sensitivity for CO (-o-o-) and applied voltage at the CuO/ZnO heterocontact. Measuring temperature is 270°C. The introduced CO gas concentration is 4142 ppm. The catalytic activity can be expressed as the conversion.

機能性フロンティアセラミックス界面・表面の構造と特性

（無機材質研究所）　羽田　肇

"Structure and properites at grainboundaries of " Frontier Ceramcs".

○H. Haneda

National Institute for Research in Inorganic Materials

セラミックス材料科学は、セラミックス界面や表面のさまざまな事象をあきらかにしてきた。将来、さらに精密に界面を制御していくにあたって、界面を構成している物質そのものの研究は然ることながら、界面現象の異方性や、界面が空間的に外部に開かれているか否かといったマクロ的な構造や組織についても検討していく必要がある。フロンティアセラミックス研究では、界面モデルを構築していく上で、化学・物理の両面から議論する必要があり、これらを統合していくところを目標としてきた。換言すればフロンティアセラミックス研究の立場は界面が直面している様々な問題を、構造や組成を基礎に特性との関係を明確にしていこうとするものである。

以上の様な視点に立った界面・表面の特性を研究した例として、ここではＰＴＣ特性を示すチタン酸バリウム半導体を取り上げてみたい。チタン酸バリウム半導体（以下ＢＴ）は通常還元雰囲気で焼成されることが多いが、このプロセスで止めている限りはPTCR特性を示さない。酸化雰囲気での再焼成を必要とする。これは粒界を酸化させ、粒界準位を発生させるプロセスであると考えられている。この事を、酸素拡散の立場から検討したものを、構造と特性との関係を表す例として示したい。

図にはLaを添加し半導体化したＢＴ中の酸素拡散測定例を示す。O-BTとしたものがPTCR特性を示す試料であるが、PTCR性を示さないR-BTに比して、表面より内部において、実線でしめした体積拡散係数の寄与よりもはるかに濃度が大きくなっている。これは酸素粒界拡散が優勢であることを示している。金属においては粒界拡散の違いを粒界構造のドラスティックな変化の現れであると考えている。同様の粒界準位と粒界拡散との関係は、バリスタ特性を酸化亜鉛にも観測されている。バリスタ特性は８００℃程度で失われるがこの温度域で、粒界拡散が著しく現象する。すなわち、粒界相転移的な粒界拡散の振る舞いをしている。

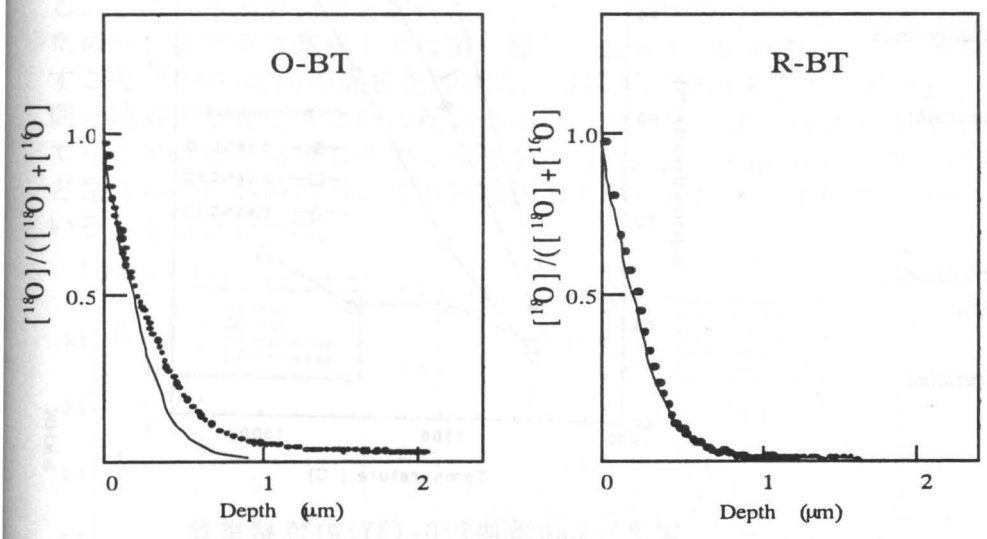

図.　半導体チタン酸バリウム中の酸素拡散プロファイル.
O-BT は酸化雰囲気で再焼成、PTCR特性を示し、テールが存在し酸素粒界拡散が優勢.
R-BT は焼結後無処理の試料で粒界拡散が見られない。

以上のように粒界構造と粒界機能と粒界拡散特性との三者関係について他の例も交え議論していきい。

コロイドプロセスによる微細構造物質の作製

（金材技研）○目　義雄、打越哲郎、鈴木　達、小澤　清、平賀啓二郎

[はじめに]：微細な結晶粒を有する物質は、飛躍的な物性の向上が期待され、種々の手法による合成が試みられている。我々は、コロイド化学的手法により微粒子の分散・凝集を制御したスラリーをプレッシャーフィルトレーションすることにより高密度で細孔分布の狭い成型体を作製し、それを低温で加熱し、微細粒焼結体を作製する研究を進めている。今回、イオン伝導体、高強度材料、超塑性材料として注目されているジルコニア系について、通常焼結法により微細構造物質を作製したので報告する。

[実験および結果]：次の２つの方法により、粒径が0.1μm以下のジルコニア系微細構造物質を作製した。

（１）加水分解法で作製したジルコニアゾルについて、図１に示す手順により、濃厚スラリーを作製し、そのままﾌﾟﾚｯｼｬｰﾌｨﾙﾄﾚｰｼｮﾝした。このとき、低温においてZrO_2の焼結を阻害するClの除去のためジルコニアゾルを陰イオン交換樹脂カラムに通す操作を入れている。さらに、CIP処理を行った後、大気中で焼結した。1100° C、６時間の焼結により、相対密度98%以上で、粒径92nmの単斜晶構造のｼﾞﾙｺﾆｱ焼結体が作製できた。

（２）市販のZrO_2(3Y)微粉末をPH=10に調整した$[NH_4OH+NH_3NO_3]$=0.1M水溶液に分散し、Cu$(NO_3)3H_2O$を添加することにより、ジルコニア粒子にCu化合物が吸着したスラリーを作製した。このスラリーを濃縮後、ﾌﾟﾚｯｼｬｰﾌｨﾙﾄﾚｰｼｮﾝし、さらにCIP成型した。図２にCuOの添加量と焼結密度-温度の関係を示す。Cuの添加による液相の生成により焼結が低温で進行することが分かる。1200° Cで２時間焼結した0.16CuO添加ZrO_2(3Y)焼結体は、粒径0.1μm以下微細構造であった。

従来のように乾燥させて粉末の状態を経由しないで、そのまま分散したスラリーを調節、ﾌﾟﾚｯｼｬｰﾌｨﾙﾄﾚｰｼｮﾝすることにより、緻密な微細構造の焼結体が得られることを示した。

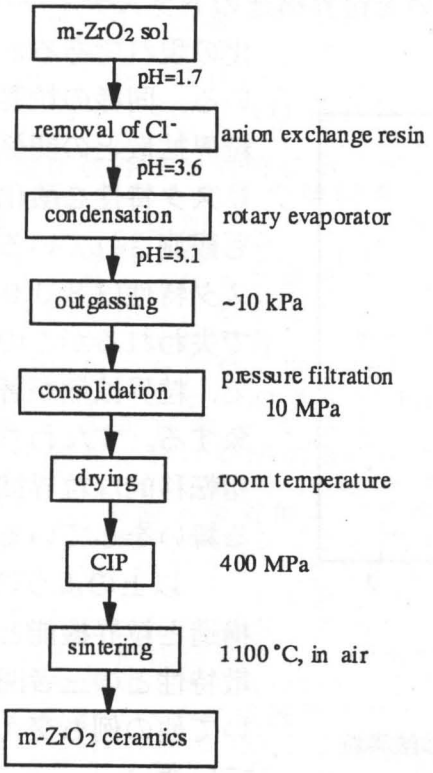

←図１　単斜晶ジルコニア焼結体の作製手順

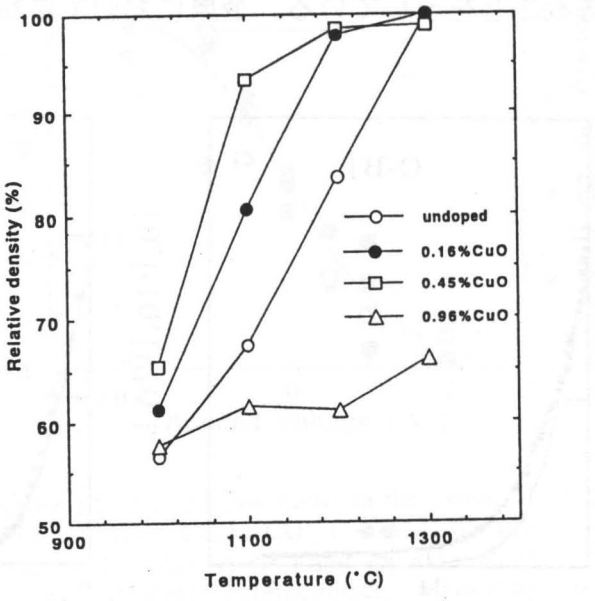

図２　CuO添加ZrO_2(3Y)の焼結挙動
（大気中２時間の加熱）

ICPフラッシュ蒸着法によるジルコニア薄膜の配向方位膜厚依存性と制御

（東工大・工）○佐伯　淳・脇谷尚樹・篠崎和夫・水谷惟恭

Dependence and control of oientational directions of zirconia thin film grown by ICP flash evaporation metod. / ○ **A.Saiki, N.Wakiya, K.Shinozaki, N.Mizutani (TIT)** / Y_2O_3–ZrO_2 (3mol%YSZ) thin films were prepared on MgO single crystal and silica glass substrates by ultrasonic spray ICP evaporation method. Thin filmes had tetragonal symmetry and (111) and (001) (100) orientations were obsreved on both substrates. Epitaxal thin films were prepared on MgO single crystal substrate. (100) orientation superior to other orientation in thiner films. Once film preparation was stoped and cooled to room temperature at the initial stage of the film preapration, initial orientational conditions were maintaind to thicker fims.

【緒言】超音波噴霧 ICP フラッシュ蒸着法は原料の選択の幅が広く、組成制御、多成分化が可能であり、また薄膜の異種材料の積層化や、組成の微構造の傾斜化にも容易に対応できるという長所がある。本研究では Y_2O_3–ZrO_2(YSZ)薄膜を合成し、基板種及び膜厚の違いによる配向性の違いを調べるとともに、積層化を行うことにより薄膜の配向方位を制御することを試みた。

【実験方法】$ZrO(NO_3)_2{\cdot}2H_2O$ と $Y(NO_3)_3{\cdot}6H_2O$ を蒸留水に溶解し、0.3mol/l の水溶液を出発原料とした。この原料を超音波噴霧器でミスト化し、Ar–O_2 熱プラズマ（4MHz、4.5kW)中に送り込み、プラズマ尾炎部に設置した石英ガラス及び劈開した MgO 単結晶基板上に蒸着させた。合成条件は全圧約 3.5 × 10⁴ Pa、プラズマ全ガス流量 18l/min、基板温度（基板裏面で測定）650 ～ 800 ℃とした。所定時間成膜後室温まで冷却し、表面を洗浄した後再び成膜する事により、積層化を行った。薄膜の相及び方位や表面組織は粉末X線回折計、ＳＥＭを用いて行った。

【結果及び考察】20 分間の成膜で約 50nm の膜厚な薄膜が得られた。XRD によりいずれの基板にも(111)及び(001)(100)配向がみられた．シリカガラス基板においては面内の配向はみられなかった．一方 MgO 基板では，(001)(100)YSZ//(001)MgO, [001][100]YSZ//[100]MgO および(111)YSZ//～(001)MgO, [$\bar{1}\bar{1}$2]YSZ//～[110]MgO のエピタキシャルな方位関係であることが分かった．成膜初期段階における(111)および(200)Ｘ線プロファイルの半価幅の変化を Fig1 に示す。成膜時間の増加とともに膜厚が増加し結晶性も良くなるため半価幅が減少したが、MgO 基板上の(200)プロファイルでは 15 分間以上の成膜で不連続な変化が現れた。またこの時に(001)配向も出現し、高角側へのシフトが観察された。膜厚の増加に伴い基板からの影響が減少して 3YPSZ 本来の格子を取ったためと考えられる。またシリカガラス基板では MgO 基板に比べて(100)配向が強くそれぞれのピークが高角側にシフトしていた。これはシリカガラスの線膨張係数が小さく冷却時に膜に引張り応力が働き、軸長の大きなｃ軸が基板に平行に配向するようにスイッチングを起こし、さらに引張り応力が残留しているためだと考えられる。このためシリカガラス基板上では第一層目の成膜を 20 分間以下で一旦終了し、再度積層を繰り返すことで(001)配向の成長を押さえた薄膜が成膜出来ることが分かった。Fig2 に１回の積層時間と積層回数を変えた時の配向性の変化を示す。第一層目の積層時間が長いと(001)配向だけでなく単斜晶が出現しやすくなる事が分かった。Fig3 は第一層目において(001)配向がほとんど見られない試料について６回積層した時の配向性の変化で、(001)配向の成長が抑制されていることが分かった。

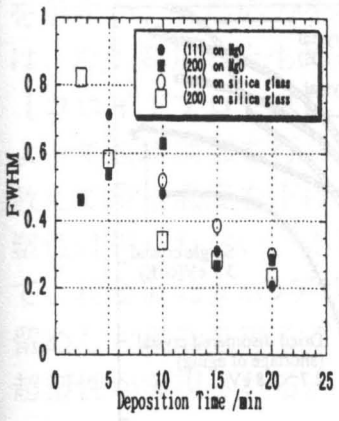

Fig.1 FWHM cheng of(111) and (200) profiles of 3YPSZ thin films.

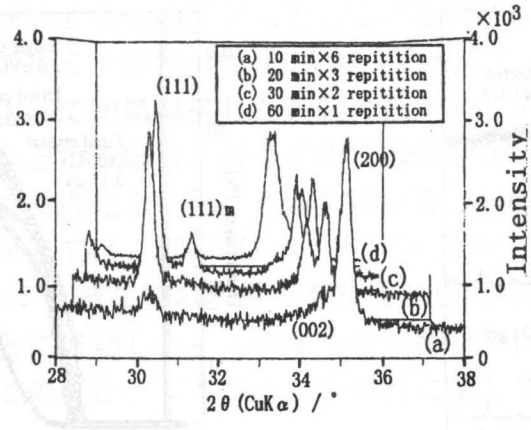

Fig.2 XRD plofiles of multilayer-stacking thin film (120 min total deposition time)

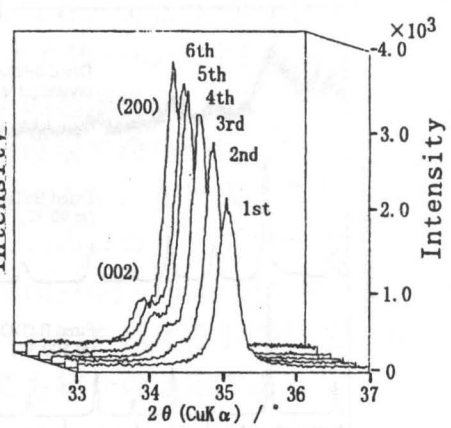

F.g.3 (002) (200) plofiles of multilayer -stacking 3YPSZ thin film.

多結晶$BaTiO_3$ゲルの光吸収と光透過

東大工 松田弘文、小林健、桑原誠

Photo absorption and light scattering in polycrystalline translucent $BaTiO_3$ gels

Dept. Mat. Sci., Univ. Tokyo, Hirofumi Matsuda, Takeshi Kobayashi, and Makoto Kuwabara

【緒言】ゾル・ゲル法で作成した結晶は、粒径10 nm程度の、通常単結晶の1次粒子が凝集して粒径100 nm程度の複雑な2次粒子を形成する、多重構造であると考えられている。微細な1次粒子は電子構造にサイズ効果を、一方複雑な2次粒子の構造は特徴的な光散乱を示し、両者の関連は興味深い。さらに$BaTiO_3$強誘電体相は2次の非線形光学効果を大きく示すことが知られており、高調波発生材料としての可能性が期待される。本研究では、高濃度ゾル・ゲル法で作成した透明$BaTiO_3$モノリシックゲル・セラミックスの微細構造と光物性との関連に注目し、光物性のサイズ効果、光散乱、透明ゲル・セラミックスの生成機構についての知見を得ることを目的としている。

【方法】等モルの$Ba(OC_2H_5)_2$、$Ti(OC_3H_7)_4$を$CH_3OH+CH_3OC_2H_4OH$混合溶媒に溶解し、濃度1.0~1.2 mol/Lの前駆体溶液を調整した。0 ℃に保持した前駆体溶液を、水蒸気により加水分解しゲル化させた。密閉容器中で50 ℃、10日程度エージングを行い熟成、結晶化させ、90 ℃窒素気流中で乾燥を行い、透明チタン酸バリウムモノリシックゲルを作成した。さらに乾燥ゲルを酸素気流中で最高600 ℃焼成した透光性ゲルを得た。X線回折(XRD)図形を測定して単相であることを確認し、また結晶化度を見積もった。透過型電子顕微鏡(TEM)観察から1次粒子の粒径を測定した。さらに励起光波長200~900 nmの範囲で、室温での光吸収スペクトルの測定を行った。定容法を用いて窒素の等温吸脱着量の相対圧依存性を測定し、乾燥ゲルの比表面積および細孔分布を見積もった。

【結果と考察】Fig. 1に透明ゲルのXRD図形を示す。これによると、十分なエージングを施した試料は高い結晶性を示す鋭いピークを持ち、$BaTiO_3$擬立方晶単相で指数付けできる。エージング時間を短くすると、ピークの幅広がりが著しく、加水分解、ポリマー化が十分に進行していない、構造の乱れの著しい微結晶を生じていることが考えられる。なお、第2高調波の検出には成功しておらず、このことからも対称中心を持つ立方晶系の結晶であると考えられる。

Fig. 2に透過率を示す。90 ℃で乾燥した結晶性の高い透明ゲルでは、十分な透明性を有していることが確認された。乾燥ゲルが50~80 %程度の透過率を示すのは、試料表面、1次粒子間の結晶粒界や、特に励起光波長に近い100 nm程度の大きさを持つ2次粒子による散乱が強いことが考えられる。実際焼成を施すことで、細孔分布は半径が増大する方向にシフトすることが確認され、透光性が失われていく定性的な原因と考えられる。次に、光学ギャップの値を見積もるため、$BaTiO_3$の基礎吸収が、バルク結晶同様価電子帯から伝導帯への間接遷移によることを考慮して見積もった光学ギャップε_0の値をFig. 2中に示した。これによると、結晶性乾燥ゲルのε_0は3.2 eVと立方晶のε_0に対して少なくとも0.2 eV増大している。これは、微結晶体では伝導バンドや価電子バンドのバンド幅が減少し、ギャップが大きくなったためと考えられる。500 ℃で焼成を行った多結晶試料では、ε_0および裾吸収が減少しており、焼成による1次粒子の成長と、加水分解反応の完了(M-O-R結合から、粒子内部ではM-O-M結合に、粒子表面ではM-O-H結合に転換)による結晶性向上の反映と考えられる。このことは、焼成によって窒素吸着比表面積が減少し、密度が上昇した事からも裏付けられる。ただし乱れた結晶からなる乾燥ゲルでは、1次粒子の成長が抑制されると考えられるにも関わらず、立方晶系単結晶に対する値を下回る最も小さなε_0を示している。この原因は、未確認であるが残留した有機酸基による吸収が支配的であるためと考えられる。

【結論】高濃度前駆体溶液を出発原料とするゾル・ゲル法を用いて、結晶性の高い透明$BaTiO_3$モノリシックゲルが作製されることを確認した。この透明$BaTiO_3$ゲルは、微結晶であるために、ギャップエネルギーにサイズ効果を示しているものの、光学的には$BaTiO_3$単結晶に近い性質を示すことが明らかとなった。

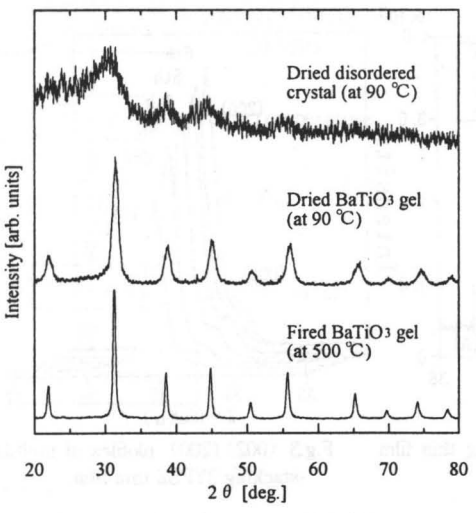

Fig.1 XRD patterns for transparent $BaTiO_3$ gels.

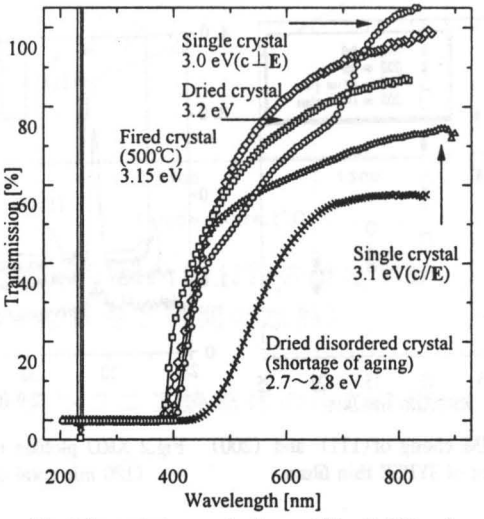

Fig. 2 Transmission spectra for crystalline $BaTiO_3$ gels

フロンティアセラミックスの高温力学特性

金属材料技術研究所　平賀啓二郎　目　義雄

[緒言] 即時破断を生じるような負荷条件を除けば、セラミックスは高温(〉融点/2)下で粒界すべりによって塑性変形する。その際には、結晶粒の間で重なりや空隙を生じないための整合過程(accomodation)が必要であり、粒内変形が困難なセラミックスでは、粒界拡散や粒界相を経路とした物質移動によってこれが進行する。ただし粒界のレッジや多重点などの応力集中部では整合過程が局所的に破綻して損傷核が形成され、これらが界面に沿って成長・合体して破壊をもたらす。したがって特性向上を図るには、変形および破壊過程と粒界の組織、組成、構造といった因子との関係を明らかにして組織制御の指針を得るとともに、そのような組織制御を実現させるためのプロセス開発を行うことが重要である。ここでは、以上の観点から高温変形破壊と微粉体プロセシングの２つのグループの連携によって行った研究について、アルミナの超塑性特性を中心に紹介する。

[損傷挙動から得られる指針] アルミナが超塑性を示さないのは、急速な動的粒成長が下式のように変形応力σを著しく上昇させ、これが損傷過程を加速するためとされる：

$$\sigma = [\dot{\varepsilon}_0 \, d^p / A \exp(\varepsilon)]^{1/n} \quad (1)$$

ここで$\dot{\varepsilon}_0$は初期ひずみ速度、dは粒径、pは粒径指数、nは応力指数、Aは拡散項を含む材料定数である。したがって従来の研究は粒成長の抑制に集中してきたが、抑制効果が弱い(MgO添加)かσの増加を招く(ZrO_2分散)ために、延性は最大でも140%に留まってきた。

本研究ではまず損傷過程の解析によって次の知見を得た。細粒セラミックスをεまで引張変形させたときの損傷体積$V_t(\varepsilon)$は、焼結後に残留する初期欠陥体積V_0、その成長による増分ΔV_0、および新たに連続発生・成長する欠陥による増分ΔV_cよりなっている：

$$V_t(\varepsilon) = V_0 + \Delta V_0 + \Delta V_c \quad (2)$$

ΔV_0はεと初期欠陥の寸法分布のみに依存し、ΔV_cはεと核発生速度の関数となってひずみ速度、変形応力、温度に強く依存する。ここでΔV_0(損傷成長)とΔV_c(損傷発生)の寄与は材料によって異なり、ジルコニアでは成長が、またアルミナでは発生がより強く寄与する。このような相違は制御に際して考慮すべき重要因子である。ここで損傷の発生速度は$\exp(-1/\sigma^2)$に依存するので、σの増加によって発生速度は極めて急峻に増大する。したがってアルミナの場合は、従来の①粒成長抑制のみでは損傷抑制には不十分であり、②変形応力の絶対値を減少させる手段が不可欠である。ZrO_2添加は①に関して最も強固な抑制効果を示すが、変形応力を増加させるので②に対しては逆効果になる。①と②を両立させるには、ZrO_2添加とともにアルミナ母相の粒径dを減少させることが唯一の手段となる。

[コロイドプロセスによって組織制御したZrO_2分散アルミナの超塑性] このような指針によって組織制御を行おうとする場合、既存手法では緻密化の段階で粒径が1μm以上に達し、敢えて焼結温度を下げて微細化しても、残留欠陥の寄与($V_0 + \Delta V_0$)が増大するために超塑性は得られない。本研究では、別報(目ら：本シンポジウム)のコロイドプロセスによって、粒径0.45μmのアルミナ結晶粒の多重点を粒径0.1μmのZrO_2粒子(10vol%)が均一にピン留めした構造を得ることに成功した。このような制御材では500%を越える引張延性を示し、超塑性が実現される。このほか、ジルコニア系材料に関しても紹介の予定である。

Ni-Zn-Cu フェライトにおける金属銅の整合析出

太陽誘電(株)総合研究所　西 湯二、　鈴木 利昌、　関口 象一、 荒井 克彦、 藤本 正之

Coherent Precipitaion of Metal Copper in Ni-Zn-Cu Ferrite ／ ○Y.Nishi, T.Suzuki ,S.Sekiguchi, K.Arai, F.Fujimoto (TaiyoYuden Co., Ltd)　Coherent Cu metal precipitates were found in Ni-Zn-Cu ferrite grains adjacent to the Σ=5 CSL grain boundary itself. The crystallographic relationship between Cu metal precipitates and spinel ferrite is <100>matrix ‖ <100>Cu. Precipitates are tetragonal platelet coherent with matrix. The Σ=5 boundary may thus not be a preferential accommodation site for coherent Cu metal precipitation in low-temperature-fired Ni-Zn-Cu ferrite.

1.*緒言*

積層チップインダクタに用いられているフェライト材料では、低温での焼結性を高めるため Cu を固溶させている。これら過剰な Cu は冷却過程で二次相として析出し、それによって生じた歪み場はデバイスの磁気特性に著しく影響を与える。我々は以前の報告で、これら析出した二次相は金属銅であり、スピネル構造をもつフェライトの格子間に、ある種の結晶学的な方位関係を持って板状に存在することを示唆した。

本報告では、積層フェライトチップインダクタで確認された特異な析出物の分析電子顕微鏡による解析結果について述べる。

2.*実験*

サブミクロンオーダーの NiO,ZnO,CuO,Fe2O3 粉末をAサイト過剰非化学量論組成である$A_{1.02}B_2O_{4+x}$（B=$Ni_{0.35}Cu_{0.25}Zn_{0.40}$，A=Fe）に調合した。これをグリーンシート化し、導体パターンを形成後、シートを重ね合わせ積層化し焼成した。これをイオンミリング装置により薄片化し TEM 試料とした。

3.*結果･考察*

Fig.1 にフェライト結晶粒子内にみられた析出物に起因すると考えられるモアレフリンジ近傍の高分解能透過電子顕微鏡(HR-TEM)像を示す。Fig. 2 は、この領域に対応する制限視野電子線回折(SAD)像である。この SAD 像中には二重回折スポット、及び高分解能像中の同じ周期をもつ複数のフリンジが存在する。また、析出物の EDS 分析の結果及び SAD 像による構造の同定から本析出物は金属銅であると推定され、フェライトと {100}ferrite ‖ {100}Cu の結晶学的方位関係をもって成長しているものと結論付けられる。

一方、Cu 析出物の多くは粒内に存在する転位周辺に形成されていたが、それら近傍にあるΣ＝５粒界上に、Cu 析出物の存在を確認することはできなかった。すなわち、この事実は金属銅析出物のアコモデーションサイトとして、Σ＝５粒界よりむしろ転位の方が優先的に機能することを示唆している。

Fig. 1　Ni-Zn-Cu フェライトの高分解能電子顕微鏡像

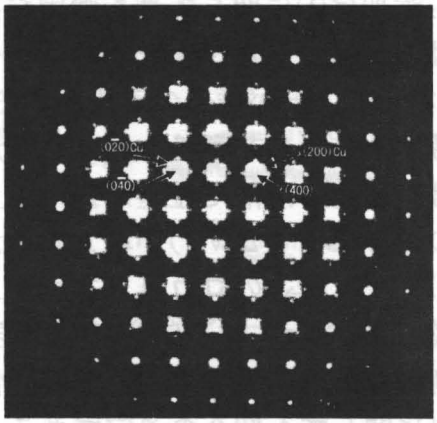

Fig.2　制限視野電子線回折像

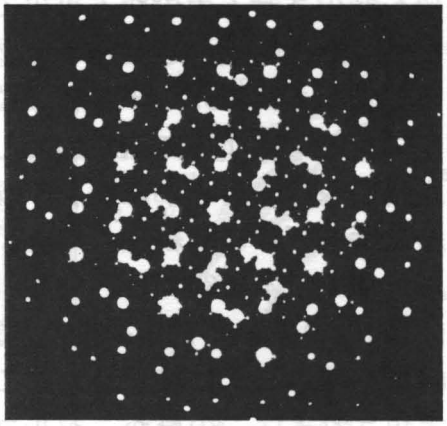

Fig.3　Σ＝５粒界の制限視野電子線回折像

Preparation of Highly Oriented Thin Films Crystal of Lithium Manganese Oxides by a LiCl Flux Evaporation

Weiping Tang, Hirofumi Kanoh, and Kenta Ooi
Shikoku National Industrial Research Institute, 2217-14, Hayashi-cho Takamatsu, 761-03

It is not easy to obtain lithium manganese oxide compounds well crystallized, monodispersed and special shaped, because manganese oxide has characteristics of both ready conversion between Mn^{III} and Mn^{IV} ions and formation of defects in the crystal structure. However, a highly crystalline thin film of lithium manganese oxide is attractive as a model compound for studying the pass and activation energy of lithium ion solid-state diffusion, and also expected to have fast lithium ion conductivity. We have first prepared well crystallized spinel-type $LiMn_2O_4$ and rock salt Li_2MnO_3 crystal thin films with a high degree of orientation using a new method of crystallization; a LiCl flux evaporation method.

A mixture of LiCl (7.2 g) and γ-MnOOH (1.0 g) was placed in a high purity alumina crucible. The crucible was set with a slope of $6\sim8^0$ in a tube furnace and heated to 700℃. The atmosphere of the tube furnace was controlled by introducing air for the Li_2MnO_3 and a mixture of nitrogen and air gas (3:1) for $LiMn_2O_4$, respectively. The LiCl flux was evaporated slowly at 700℃ and was completely evaporated by heating for 6 days. After heating, the furnace was cooled down to room temperature. Crystal thin films were formed on the layer of particles. The yield of the film-type sample was about 20% of the total amount of lithium manganese oxide.

XRD patterns were obtained by mounting crystal thin films on a glass holder (Fig.1). Only three peaks are found in the XRD patterns for $LiMn_2O_4$ and Li_2MnO_3 thin films, respectively. The peaks correspond to the (*i i i*) (*i* = 1, 2, and 3) reflections for $LiMn_2O_4$ (Fig.1A), and to (00*i*) (*i* = 2, 4, and 6) reflection for Li_2MnO_3 (Fig.1B). The (111) crystal plane for $LiMn_2O_4$ and (002) plane for Li_2MnO_3 have a high reflection density, because their peaks show the strongest intensity, respectively. The present results indicate that the LiCl evaporation method gives well crystallized $LiMn_2O_4$ and Li_2MnO_3 thin films with the high degree of orientation. Table 1 shows the properties of both the $LiMn_2O_4$ and Li_2MnO_3 crystal thin films.

The growth of crystal thin films is explained as follows. The evaporation of LiCl at 700℃ causes isothermal supersaturation of manganese dissolved in the LiCl flux. Then, the growth of lithium manganese oxide thin films proceeds at the interface between the atmosphere and the LiCl flux.

Table 1 Properties of thin films

Thin film	$LiMn_2O_4$	Li_2MnO_3
Chemical formula	$Li_{1.08}Mn_2O_{4.11}$	$Li_{2.01}MnO_{3.01}$
Orientation	(111)	(002)
Color	Black	Crimson
Size (a single crystal)	$2\sim10$ mm^2	
Thickness	$20\sim30$ μm	

Fig.1 XRD patterns.

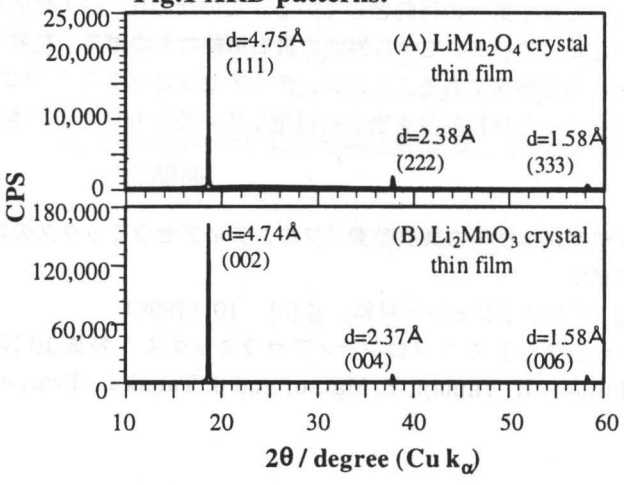

フロンティアセラミックス研究の将来展望

早稲田大学 理工学部　一ノ瀬　昇

1.　はじめに

セラミックス分野のR&Dは工業プロセスの進歩に呼応しており、これまでセラミックス材料の高度化・機能付加等に寄与してきた。またこれらの発展が、さらにその先を行くセラミックスを引き出す役割を果たしている。21世紀を迎えるに当たって、セラミックスのもつ特異でとりわけ優れた機能は、未来型テクノロジーの発展においても大いに役立つであろうという期待感は、増しこそすれ減じられてはいない。

“ フロンティアセラミックス ”はこの様な発展を目指して提案されたコンセプトの一つである。すなわちセラミック材料科学が解明すべき多くの課題の中で、ここでは特にセラミック材料の界面に着目し、界面にまつわる機能の高度化と新材料の開発を目指そうと提案された[1]。

フロンティアセラミックス研究の本プロジェクトの前半では、セラミックスの界面について、今一度、基礎的な面から界面を見直し、そこから考えられるモデル界面を構築することを目的としている。さらに後半では、確立されたモデルに基づき界面機能を制御した機能性セラミックス、とりわけエレクトロセラミックス、あるいは界面機能を高度に利用した触媒、電極材料、生体材料の開発を目指す予定となっている。ここではフロンティアセラミックス研究の事例を紹介し、その将来を展望しよう。

2.　フロンティアセラミックス研究の事例

1)　界面のモデル化研究

界面のモデル化を目指した場合、単一粒界をまず対象としようと考えることは自然であろう。この単一粒界は現実の材料でも直面しつつある課題でもある。ここに界面のモデル化を目指した“ フロンティアセラミックス ”研究のリアリティがある。本プロジェクトも多くのグループがこの方面の研究に取り組んでいる。

本プロジェクトにおける単一粒界の作成はバラエティに富んでいるが、その中の一つに単一粒子を並べた細線を作る試みが、チタン酸バリウムを対象になされている。この方法は個々の粒界の方位を制御するのには適さないが、様々な様相を呈する粒界を数多く扱うには適した方法である。この方法によりPTC効果の方位依存性が明らかになりつつある[2]。また、微小電極を用いての単一粒界の特性評価も行われている。例えば、単一粒界のICTS測定がなされているが、世界的に見ても新しい試みで、ZnO粒界におけるバリスタ特性発現機構の解明に貢献している[3]。

2)　$SrTiO_3$ バイクリスタル研究

また、単結晶同士の接合によるバイクリスタルの研究もなされている。この方法は、あらゆる方位関係に対応できる点で優れている。オーソドックスな方法で古くからなされていたが、一度、セラミックス界面機能に着目したものと限定すれば、総合的に扱ったものは意外と少ないというのが現状である。ここでは、一例に、HIP接合により得られたチタン酸ストロンチウム単一粒界の界面特性について紹介する[4]。よく知られているように、チタン酸ストロンチウムセラミックスはNbやLaのようなドナーを添加して半導体化すると共に、粒界だけ絶縁化させることで、容量性バリスタが得られる。しかしながら、バリスタ現象の発現機構についての理解はまだ十分とは言えない。構造、組成を制御できる単一モデル界面を対象とした研究を押し進めることで、現象解明に一歩近づくことができると考えている。

3.　将来展望

製品の小型化の進展に伴い、エレクトロセラミックスでは単一粒界を制御しなければならない時代となりつつある。“ フロンティアセラミックス ”プロジェクトは、このような現状に対応すべく提案された。プロジェクトでは、基礎に立ち返り、界面をモデル化する事を第一の目的としている。このために、分子軌道法、バンド理論、熱力学といった理論を基礎に、界面を理解することから始めている。モデル界面の最も単純なものは単一粒界であるが、これは、セラミックスの発展状況からみても十分リアリティのある界面である。“ フロンティアセラミックス ”プロジェクトは、実は、このような基礎的な界面研究を通して、新たな機能を持った材料開発を密かに目指しているともいえる。本プロジェクトから多くの成果を期待したい。

参考文献

1)　平成6年度科学技術振興調整費「フロンティアセラミックスの設計・創製に関する調査報告書」，平成7年3月科学技術庁研究開発局.
2)　桑原誠，インテリジェント材料，6 [3]，10（1996）.
3)　ニューセラミックス“ フロンティアセラミックス ”特集 10 No6（1997. 6）
4)　N. Ichinose, K. Yamaji, Y. Matsui and J. Tanaka,　Proc. of Electroceramics V　Vol.2,（1996）P.537.

$Ba(OH)_2$-$Sr(OH)_2$-$Ti(O^iPr)_4$より得られた前駆体の気相加水分解による$(Ba_xSr_{1-x})TiO_3$粒子の作製

（湘南工科大学）○篠崎裕志・須永孝一・林卓、（元 デュポン）佐々木昌一

Preparation of barium strontium titanate powders by vapor phase hydrolysis of precursors formed from $Ba(OH)_2$-$Sr(OH)_2$-$Ti(O^iPr)_4$./○H.Shinozaki,K.Sunaga,T.Hayashi(Shonan Institute of Technology),K.Sasaki(former DuPont)

[緒言]

$(Ba_xSr_{1-x})TiO_3$(BST)は、主にセラミックコンデンサー及びDRAM用コンデンサー材料として用いられている。本研究では、チタンアルコキシドと$Ba(OH)_2$及び$Sr(OH)_2$のメタノール溶液からの結晶性$(Ba_xSr_{1-x})TiO_3$固溶体微粒子の低温合成を目的とした。さらに、この微粒子のキャラクタリゼーション及び焼結体の作製を行い、微構造及び誘電的特性を調べた。

[実験方法]

水酸化バリウム、及び水酸化ストロンチウムをメタノールに溶解させ、それぞれの溶液の濃度を求めた後、目的の組成に対応する所定量の$Ti(O^iPr)_4$を添加し Ba-Sr-Ti 混合溶液とした。この溶液を40℃に加熱し、減圧下において溶媒除去することにより、Ba-Sr-Ti 系非晶質の前駆体を得た。この前駆体に水蒸気を含むN_2ガスを100℃で導入し加水分解を行うことにより、結晶性$(Ba_xSr_{1-x})TiO_3$微粒子を合成した。合成した粒子は FE-SEM により観察し、結晶性を XRD、熱分析を TG-DTA、比表面積をBET法によって調べた。またこの粒子を900℃、2h で仮焼した後、CIP 成型して 1250℃～1350℃で焼結した。焼結体は、相対密度と比誘電率の測定及び微構造観察により評価した。

[結果]

Ba、Sr の水酸化物と Ti アルコキシドから得られた前駆体は非晶質で、TG-DTA より約30%の重量損失が認められた。これは、含有有機基、水酸基によるものと考えられる。この前駆体は 100℃での気相加水分解により結晶化し、$(Ba_xSr_{1-x})TiO_3$ 微粒子が生成した。加水分解後、120℃で乾燥した生成粒子は高い結晶性を示していた(図 1)。この粒子の FE-SEM による粒径は 40～50nm と非常に小さく、比較的均一であり、また BET 法によって求められた比表面積は、約 40～70m^2/g であった。$(Ba_xSr_{1-x})TiO_3$ の焼結体の相対密度は焼結温度 1300℃以下では90%以上を示したが、1350℃では密度の低下が生じた。図 2 に Ba/(Ba+Sr)モル分率による格子定数、キュリー温度の変化を示した。Sr の含有量の増加に伴い格子定数、キュリー温度が直線的に低下している。120℃乾燥粒子より求めた格子定数は 900℃仮焼粒子の値より大きい値を示しているが、これは残留水酸基によるものと考えられる。

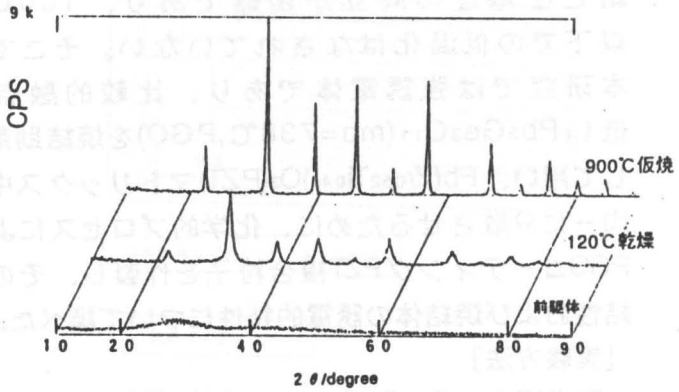

図 1　$(Ba_{0.7}Sr_{0.3})TiO_3$前駆体及び加水分解生成物(120℃乾燥、900℃仮焼)の XRD 図形

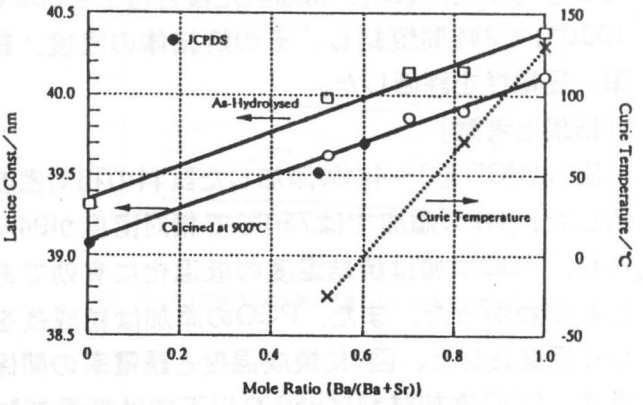

図 2　Ba/(Ba+Sr)モル分率と誘電率、キュリー温度の関係

ゾル・ゲル法による$Pb_5Ge_3O_{11}$添加PZTセラミックスの低温焼結

(湘南工科大学) ○井上 崇行、林 卓

Low temperature sintering of $Pb_5Ge_3O_{11}$ added PZT ceramics by sol-gel method

○T.Inoue、T.Hayashi (Shonan Institute of Technology)

[緒言]

現在、焼成コストの低減を目的とした低温焼結に関する、さまざまな研究がされている。一般的に低融点ガラスを加えることにより、焼結の低温化がなされている。しかし、圧電材料では低温焼結と圧電性の両立が困難であり、1000℃以下での低温化はなされていない。そこで、本研究では強誘電体であり、比較的融点が低い$Pb_5Ge_3O_{11}$(mp=738℃,PGO)を焼結助剤として用い、$Pb(Zr_{0.52}Ti_{0.48})O_3$(PZT)マトリックス中に均一に分散させるために、化学的プロセスによりPGOコーティングPZT複合粒子を作製し、その焼結性および焼結体の誘電的特性について調べた。

[実験方法]

$Pb(NO_3)_2$と$Ge(O\text{-}i\text{-}Pr)_4$をエチレングリコールに所定量溶解し、PGO前駆体溶液を作製した。この溶液にPZT(平均粒子径0.2μm)の水系サスペンジョンを加え、80℃、1時間反応させた後、限外ろ過、乾燥を行った。また、得られた複合粒子を850℃～1000℃で2時間焼結し、その焼結体の密度、誘電率、圧電性を評価した。

[結果と考察]

図1にPGOを0～4wt%添加した試料の相対密度を示した。1wt%添加では750℃で相対密度が94%であり、PGO添加は焼結温度の低温化に有効であることがわかった。また、PGOの添加は粒成長を著しく促進させた。図2に焼成温度と誘電率の関係を示す。PGO添加試料は950℃以下では無添加試料に比べ、誘電率が高いが、1000℃以上では大きく低下した。これは、温度が高いためPZTとPGOが拡散または固溶した為と考えられる。また、縦歪みは図3に示したように、誘電率と同様の傾向があり、950℃で約0.2%であった。

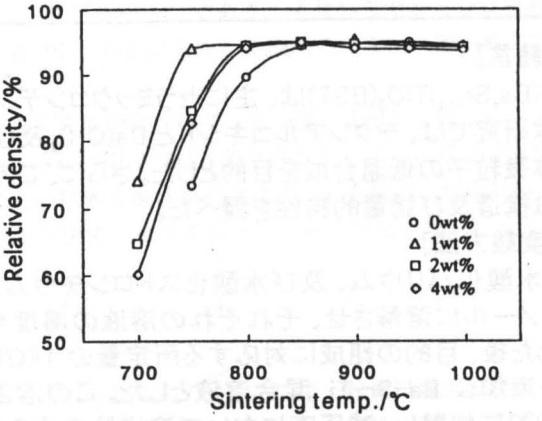

Fig.1 Sintering temperature dependence of relative density of PZT with various amounts of PGO additives.

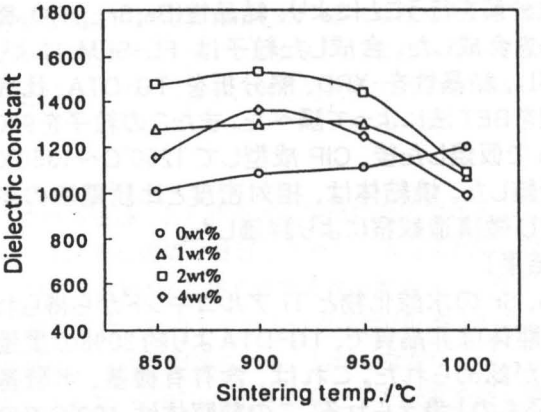

Fig.2 Sintering temperature dependence of dielectric constant of PZT with various amounts of PGO additives.

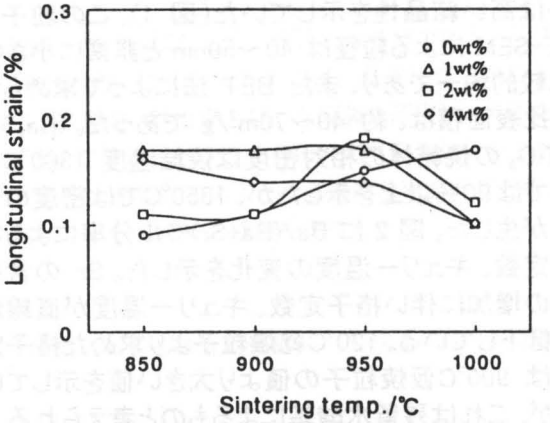

Fig.3 Sintering temperature dependence of longitudinal strain of PZT with various amounts of PGO additives.

金属アルコキシドを用いたZrO_2コーティング$BaTiO_3$複合粒子の合成と評価

（湘南工科大学）○杉原渉・須永孝一・林卓，（元デュポン）佐々木昌一

Preparation and Properties of ZrO_2-coated $BaTiO_3$ Composite Particles by Sol-Gel Method with Zr-alkoxide/○W. Sugihara, K. Sunaga, T. Hayashi (Shonan Institute of Technology), K. Sasaki (former DuPont)

【緒言】

$BaTiO_3$にNb_2O_5、CoOを添加した系において、誘電率の温度依存性平坦化が知られており、積層コンデンサー材料として期待されている。本研究では、ZrO_2を$BaTiO_3$マトリックス中に均一に分散させるために、ZrO_2コーティング$BaTiO_3$複合粒子の調製を行った。さらに複合粒子のキャラクタリゼーション及び、焼結体の作製を行い、誘電的特性を調べた。

【実験方法】

コア粒子原料として、$BaTiO_3$ {BT-05（平均粒子径500nm）（堺化学）} を用いた。その$BaTiO_3$粒子をトルエンに懸濁させ、そこに$Zr(OEt)_4$トルエン溶液を加えた後、80℃に加熱した水蒸気を含むN_2を流し加水分解させた。加水分解処理後、溶媒を除去して複合粒子を得た。その合成フローチャートを図1に示した。調製した複合粒子の比表面積をBET法により評価した。またその複合粒子を一軸成形し1250～1300℃で2時間焼結しSEM観察、XRD測定及びその誘電率温度依存性を調べた。

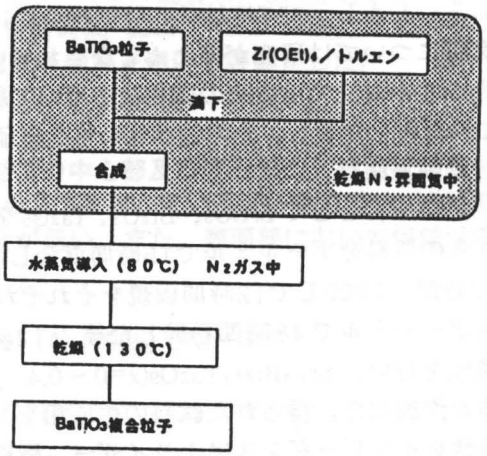

図1 複合粒子合成のフローチャート

【結果】

複合粒子の比表面積は$BaTiO_3$原料の1.86（m^2/g）に比べ1wt%では2.05、3wt%では2.52と大きくなった。複合粒子の焼結体の誘電率温度依存性を図2に示した。ZrO_2を多く添加するほど常温での誘電率は低くなる傾向を示した。ZrO_2 1wt%添加では焼結温度1250℃の試料において0～100℃付近で誘電率温度依存性平坦化が達成されており常温での誘電率は約4300と高い値を示した。また3wt%添加では焼結温度1300℃の試料において0～100℃で平坦化が同様に達成されてたが、常温での誘電率が約3300に低下した。相対密度は、1wt%試料の場合90%に対し3wt%試料では、1300℃において同様の値となった。このことはZrO_2の添加の増加が$BaTiO_3$の焼結を妨げていると考えられる。またZrO_2を添加すると焼結体中の$BaTiO_3$の粒子の粒径は無添加の場合の約2μmに比べ約0.7μmと小さくなった。これは、ZrO_2が粒界に存在し、$BaTiO_3$の粒成長を抑制したためと考えられる。

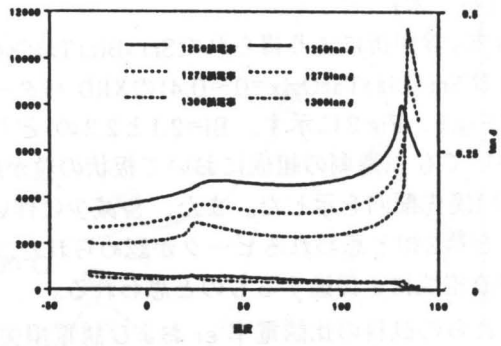

図2 1wt%の試料での各焼結温度における誘電率温度依存性

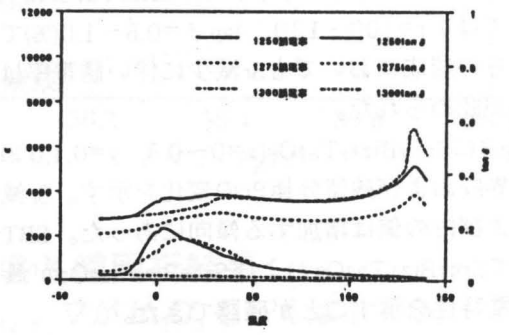

図3 3wt%での各焼結温度における誘電率温度依存性

非化学量論組成$Sr_{1-x}Bi_{2+y}Ta_2O_{9+\alpha}$セラミックスの強誘電特性と微構造

(湘南工科大学) ○澤柳　悟・高橋　宏・原　拓也・上野　修司・林　卓

Ferroelectric Properties and Microstructure of Nonstoichiometric $Sr_{1-x}Bi_{2+y}Ta_2O_{9+\alpha}$ Ceramics

○S.Sawayanagi,H.Takahashi,T.Hara,S.Ueno and T.Hayashi(Shonan Institute of Technology)

【緒　言】

$SrBi_2Ta_2O_9$(SBT) などのBi層状構造系材料は強誘電体不揮発性メモリへの応用の研究が盛んに行われている。SBT薄膜については低温化プロセスを含む強誘電特性の研究が盛んに行われており、今までに非化学量論組成$Sr_{0.8}Bi_{2.2}Ta_2O_9$薄膜において良好な強誘電特性が得られている。しかし、SBT焼結体の強誘電特性に及ぼす組成の影響については研究がほとんどなされていない。

そこで本研究では従来の固相法を用いて組成の異なるSBT焼結体を作製し、その強誘電特性を評価した。

【実験方法】

出発原料として$SrCO_3$、Bi_2O_3、Ta_2O_5を使用した。これらの原料をボールミルで15時間混合した後、900℃で12時間、1000℃で12時間仮焼をそれぞれ行った。その後ボールミルで48時間粉砕した後、1250℃で2時間本焼成を行い、$Sr_{1-x}Bi_{2+y}Ta_2O_9$(x=0～0.4, y=0.1,0.3)焼結体を作製した。得られた試料の生成相をX線回折、誘電特性をインピーダンスアナライザー、微細構造観察をSEM で行った。

【結　果】

粉末X線回折により得られた$Sr_{1-x}Bi_{2.1}Ta_2O_9$(x=0～0.4)および$Sr_{1-x}Bi_{2.3}Ta_2O_9$(x=0～0.4)のXRD パターンをそれぞれFig.1、Fig.2に示す。Bi=2.1と2.3の どちらの組成においてもBi過剰の組成において板状の粒が成長し、(00 ℓ)優先配向を示した。また、Sr減少に伴い過剰のBiを含む第2相と思われるピークが認められた。この第 2相が液相焼結を促進するものと思われる。

これらの試料の比誘電率 εr および誘電損失tan δ は$Sr_{1-x}Bi_{2.1}Ta_2O_9$ (x=0～0.4) においてεr =120～130、tan δ =0.5～1.0(%)であり、$Sr_{1-x}Bi_{2.3}Ta_2O_9$(x=0～0.4)においてはεr=100～130、tan δ =0.5～1.0(%)であった。どちらの組成においてもSr減少に伴い誘電率は向上する傾向が認められた。

Fig.3に$Sr_{1-x}Bi_{2+y}Ta_2O_9$(x=0～0.4, y=0.1,0.3)における抗電界Ecおよび残留分極Prの変化を示す。Sr減少に伴いEcおよびPrの値は増加する傾向にあった。SBT焼結体において$Sr_{0.7}Bi_{2.1}Ta_2O_9$および$Sr_{0.8}Bi_{2.3}Ta_2O_9$が最も良好な強誘電特性を示すことが確認できた。

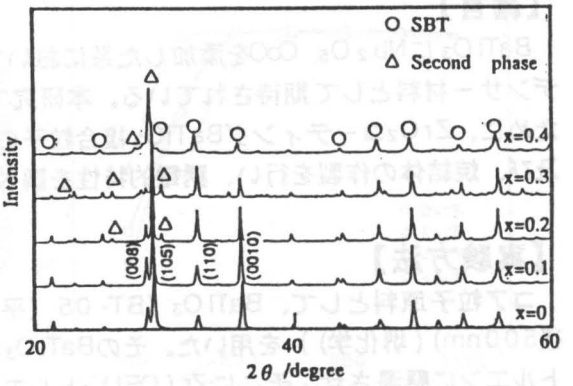

Fig.1 XRD patterns of $Sr_{1-x}Bi_{2.1}Ta_2O_9$(x=0～0.4) sintered bodies

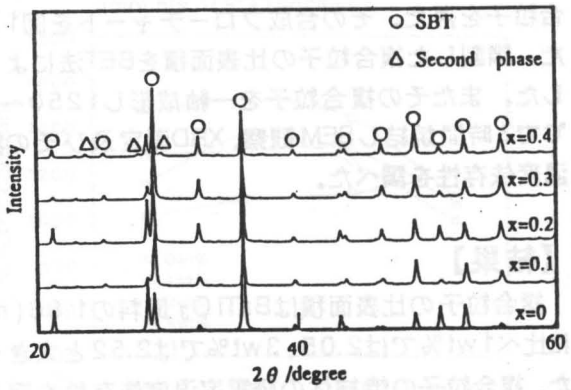

Fig.2 XRD patterns of $Sr_{1-x}Bi_{2.3}Ta_2O_9$(x=0～0.4) sintered bodies

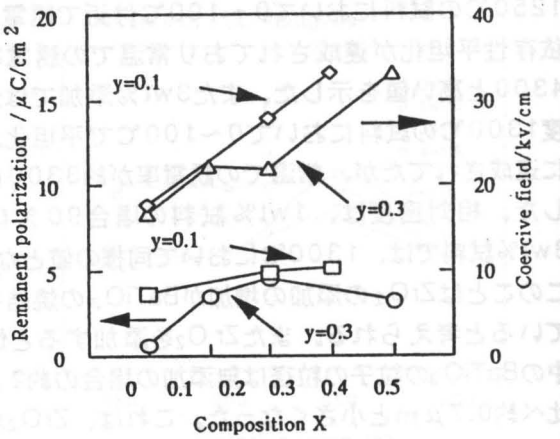

Fig.3 Effect of x values in $Sr_{1-x}Bi_{2+y}Ta_2O_9$ (y=0.1 and 0.3) ceramics on Pr and Ec

In-Sn-O 系複酸化物の合成

Synthesis of In-Sn-O double oxide

東京工芸大学工学部工業化学科　　○ 高野　正興　　澤田　豊

Department of Industrial Chemistry , Faculty of Engineering , Tokyo Institute of Polytechnics

○ Masaoki TAKANO and Yutaka SAWADA

〔背景及び目的〕

液晶ディスプレイの画素電極には、ＩＴＯ(Indium-Tin-Oxide、In_2O_3 に Sn を固溶したもの)の薄膜が使用されている。しかしながら原料の In が高価なためＩＴＯに代わる新素材が求められている。また、In-Sn-O 系複酸化物として $In_4Sn_3O_{12}$[1,2] が報告されているが、詳細は明らかではない。本研究ではこの化合物の合成及び解析を目的とした。

〔実験方法〕

In_2O_3 と SnO_2 を混合比(wt%) 50:50、55:45、60:40 及び 65:35 でボールミル混合し、約 5g をプレス成形(プレス圧 2t/cm^2、直径 16.1mm)し、焼成温度 1400～1650℃、保持時間 20hr、40hr の条件で大気中において焼成した。試料はＸＲＤ、ＳＥＭ、マイクロオージェ及び蛍光Ｘ線等を用いて評価をした。

〔実験結果〕

現在のところ $In_4Sn_3O_{12}$ 単一相の生成には成功していない。焼結体の中心部及び表面部のＸ線回折結果を図に示す。中心部は各焼成温度で In_2O_3(もしくはＩＴＯ)と $In_4Sn_3O_{12}$ が共存しているが、焼成温度 1500℃のときには、In_2O_3(もしくはＩＴＯ)に対する $In_4Sn_3O_{12}$ の相対強度が低い。また、表面部において焼成温度 1600℃のときに $In_4Sn_3O_{12}$ のピークが極端に小さくなっている。

文献１）H.Enoki　et al. , 26 (1991) 4110～4115

２）J.Lambert Bates　et al. , Am. Ceram. Soc. Bull. ,65 (4) (1986) 673～678

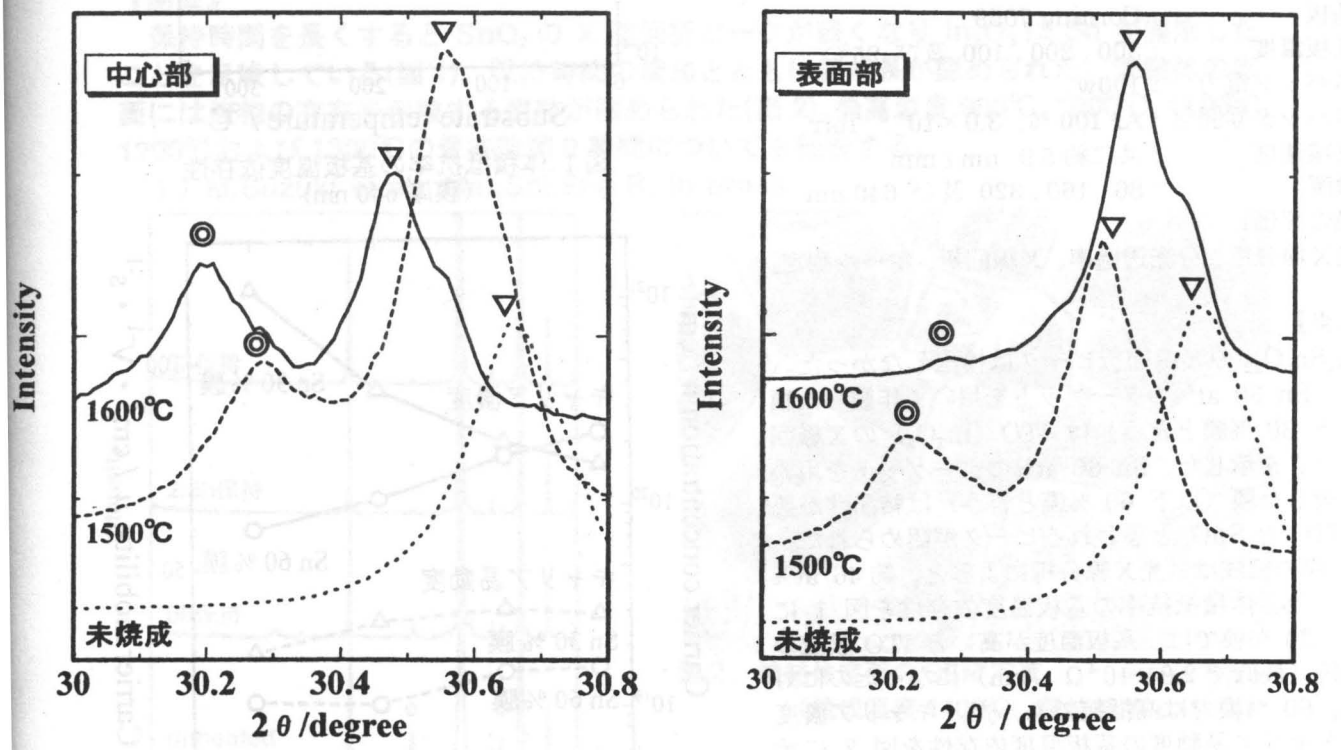

図．焼結体中心部及び表面部のＸ線回折結果

（混合比 In_2O_3:SnO_2=55:45wt% ，◎が $In_4Sn_3O_{12}$ ，▽が In_2O_3 もしくはＩＴＯ）

In_2O_3-SnO_2系透明導電膜のスパッタ製膜と評価：Sn30及び60at%の検討

Sputter-deposited In_2O_3-SnO_2 transparent conducitve films: Preparation and characterization of Sn 30 and 60 at% films

東京工芸大学工学部工業科学科　○杉森弘和　澤田豊

Department of Industrial Chemistry,Faculty of Engineering,Tokyo Institute of Polytechnics

○ Hirokazu SUGIMORI and Yutaka SAWADA

【背景と目的】

表示素子の電極材料である透明導電膜への需要増加に伴い、透明導電膜のさらなる高性能化（低抵抗）、低コスト化が望まれている。現在代表的な透明導電膜としてSnを5～10wt%程度添加した酸化インジウムの膜（Indium tin Oxide、略してITO）が挙げられる。高価なInの使用量がITO膜よりも少なく、ITO膜並みの抵抗率を示す$In_4Sn_3O_{12}$膜の存在が報告[1]されているが詳細は明らかではない。そこで本研究では、Sn添加量30及び60at%のターゲットを使用してRFマグネトロンスパッタリング法により作製した薄膜について検討した。

【実験方法】

（製膜）

ターゲット組成：

In_2O_3 : SnO_2 ＝68.2 : 31.8 及び 38.0 : 62.0 (wt%)

基板　：Corning 7059

基板温度　：300 , 200 , 100 及び 25℃

スパッタ電力　：100w

スパッタ雰囲気：Ar 100 %、3.0×10^{-3} Torr

堆積速度　：共に約59 nm / min

膜厚　：80 , 160 , 320 及び 640 nm

（膜の評価）

蛍光X線分析、分光透過率、X線回折、ホール測定。

【結果】

$In_4Sn_3O_{12}$のX線回折ピークは検出しなかった。また、Sn 30 at%のターゲットを用いて作製した膜（以下30 %膜と言う）はITO（In_2O_3）のX線回折ピークを示した。Sn 60 at%のターゲットを用いて作製した膜（以下60 %膜と言う）は結晶性が悪く、ITOとSnO_2と思われるピークが認められた。30 %膜の組成は蛍光X線分析によると、約46 at%であった。体積抵抗率の基板温度依存性を図1に示す。30 %膜では、基板温度が高いとITO膜並の低抵抗（最低で$2.9\times10^{-4}\Omega$・cm）になったのに対して、60 %膜では高抵抗であった。キャリア濃度及びキャリア易動度の基板温度依存性を図2に示す。30 %膜のキャリア濃度及びキャリア易動度は、ほとんどの場合に60 %膜のそれを上回っている。キャリア濃度は基板温度が高いと30 %膜で増加し、60 %膜では減少する。キャリア易動度は、温度依存性がわずかであった。

【文献】1)南内嗣, Sputtering E Plasma Processes, 11-1(1996)19, （社）日本工業技術振興協会

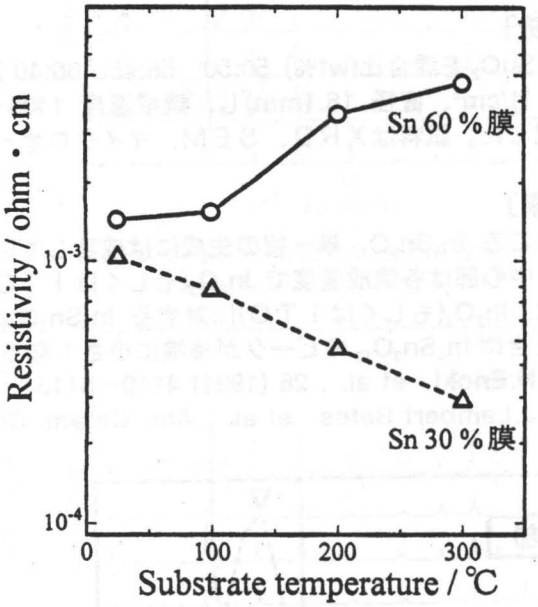

図1.体積抵抗率の基板温度依存性（膜厚 640 nm）

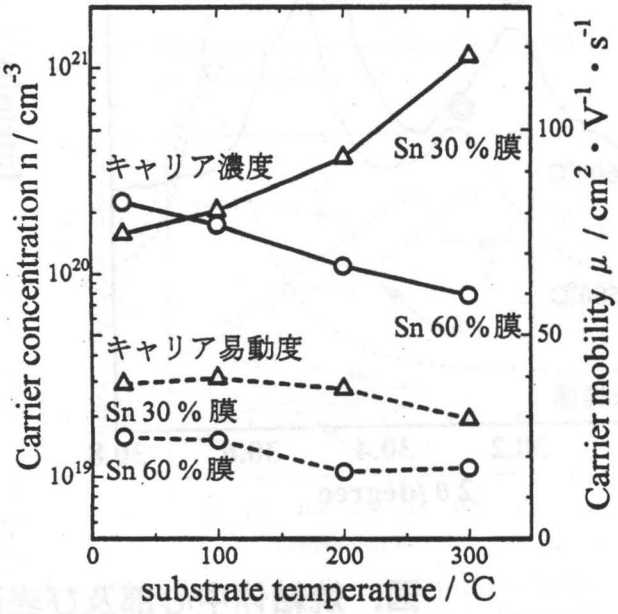

図2.キャリア濃度とキャリア易動度の基板温度依存性（膜厚 640 nm）

V_2O_5添加ITOの焼結過程

Sintering process of V_2O_5-added ITO

東京工芸大学工学部工業化学科　○伊藤　寿英　澤田　豊

Department of Industrial Chemistry,
Faculty of Engineering,
Tokyo Institute of Polytechnics

○ Toshihide ITO
and
Yutaka SAWADA

『背景と目的』

ITO（Indium-Tin-Oxide、スズを添加したIn_2O_3）は優れた透明導電膜で表示素子に使用されているが、スパッタリング法による製膜に際して高密度のターゲットが望まれている。我々は助剤としてV_2O_5を添加することにより低温で高密度の焼結体を得ることができた（1400℃で相対密度 95%以上）[1]。本研究ではその焼結過程において報告する。

『実験方法』

In_2O_3粉末とSnO_2粉末、V_2O_5をそれぞれ 94.05:4.95:1wt%の割合で混合し、約 5g、プレス圧 2t/cm^2、直径 16.1mm のサイズに成型し、大気中で焼成した。（焼成温度 1400℃、保持時間 0, 2.5, 5, 10 および 20 時間）焼成したサンプルを XRD、SEM、マイクロオージェ等を使用し評価した。

『結果』

保持時間を長くするとSnO_2の X 線回折ピークが弱くなりIn_2O_3に Sn が固溶したことを示唆している(図 1)。保持時間の増加とともに粒成長が認められた。焼結体の底面には液相の存在を示唆する痕跡が認められた(図 2)。最高温度 900℃、1000℃、1100℃、1200℃および 1300℃の保持時間 0 時間についても報告する。

1）M.Suzuki et al、Mat.Sci.Eng.B, In press

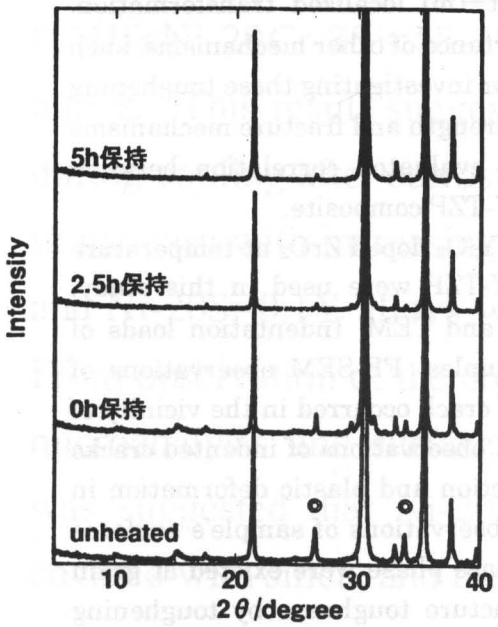

図１.焼成温度1400℃の試料のX線回折スペクトル
（◎がSnO_2、他はIn_2O_3またはITO）

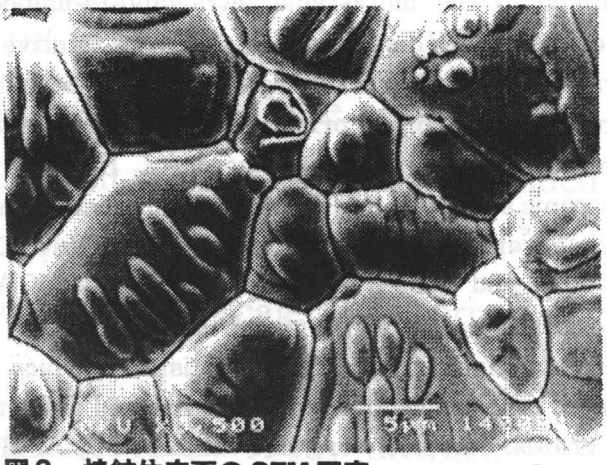

図２．焼結体底面の SEM 写真　——— 5μm
（焼成温度 1400℃、保持時間 10 時間）

Correlation between Nanoscopic Structure and Fracture Mechanism of ZrO_2 Particle Dispersed Al_2O_3

○ Nobutake TANAKA, Senior Student, Kogakuin University 1-24-2, Nishishinjuku, Tokyo, 160

Yuji KIMURA, Dept. of Environmental Chemical Eng., Kogakuin University

Noriyuki HISAMORI, Graduate Student, Kogakuin University

ABSTRACT

The addition of one ceramic to another often produced a composite with more desirable properties than the matrix ceramics. For structural applications, improved mechanical properties are the usual objective. At room temperatures, the important properties include strength, fracture toughness(K_{IC}), and hardness. These measurable properties are expected to give an indication of material's performance under applied conditions. Fiber-and whisker-reinforced ceramic composites have received much attention in the request for improved mechanical properties, however particulate composites also show attention. The addition of yttria-stabilized tetragonal ziruconia(Y-TZP) to alumina(Al_2O_3) has improved strength and toughness of alumina matrix. Y-TZP addition to Al_2O_3 may improve K_{IC} and strength by mechanism that can be divided into three-categories: those that enhance transformation toughening, those that modify the grain boundary structure, and those that involve additional energy-absorbing mechanisms due to crack deflection caused by the presence of second-phase particles.

Toughening mechanisms in Al_2O_3-Y-TZP have been widely studied and have been discussed in recent years. The principal toughening mechanism is generally accepted to be linked to the metastable tetragonal-to-monoclinic(t→m) localized transformation. However, there is disagreement about the relative importance of other mechanisms, such as crack deflection, crack bridging and microcracking. For investigating these toughening mechanisms, one of the primary study is investigating strength and fracture mechanisms in microstructure in grain size level. So this paper evaluated correlation between nanoscopic structure and fracture mechanism of Al_2O_3/Y-TZP composite.

Sample were sintered Al_2O_3 bodies with 5 and 30wt.% Y_2O_2 doped ZrO_2 at temperature of 1550℃ and 1650℃. In total, four kinds of Al_2O_3-Y-TZP were used in this study. Microstructures were compared using FE-SEM, AFM and TEM. Indentation loads of 294N were applied for 15s on polished surface of samples. FE-SEM observations of indented cracks revealed that bridging and deflection of crack occurred in the vicinity of ZrO_2 grains. Samples were also examined by AFM. AFM observations of indented cracks revealed three-dimensional crack bridging, crack deflection and plastic deformation in the vicinity of Vickers indentation. In addition, TEM observations of sample's surfaces after corrosion test revealed only limited amounts of glass phase were existed at grain boundary. As result, improvement of strength and fracture toughness by toughening mechanisms such as bridging and deflection of crack was revealed by Y-TZP addition to Al_2O_3.

High-Temperature Corrosion of Ni-Cr and Ni-Si System Alloys in a N_2-H_2O-HBr Atmosphere

Y. Yoshida, T. Amano, J. Yamazaki*, T. Goto* and T. Hirai*

Shonan Institute of Technology, 1-1-25, Tsujido-Nishikaigan, Fujisawa 251, Japan

*IMR, Tohoku University, 1-1, Katahira 2-chome, Aoba-ku, Sendai 980-77, Japan

High-temperature corrosion behavior of Ni-20Cr-3Si, Ni-20Cr-3Si-0.1(Y or Hf), Ni-20Cr-5Si, Ni-20Cr-10Si, Ni-20Cr-20Si, Ni-20Si and Ni-20Si-0.1Y alloys was studied in a N_2-H_2O-HBr(N_2:45vol%, H_2O:45vol%, HBr:10vol%) atmosphere. Mass changes of Ni-20Cr-3Si-0.1Y, Ni-20Si and Ni-20Si-0.1Y alloys showed positive values. On the other hand, Mass changes of Ni-20Cr-3Si, Ni-20Cr-3Si-0.1Hf, Ni-20Cr-5Si, Ni-20Cr-10Si and Ni-20Cr-20Si alloys showed negative values, and mass changes of these alloys increased negatively in the order of Ni-20Cr-3Si-0.1Hf<Ni-20Cr-3Si<Ni-20Cr-10Si<Ni-20Cr-5Si<Ni-20Cr-20Si alloys. This result suggested that scales on these alloys spalled during cooling after corrosion and that spalling of the scale tended to increase with increasing silicon contents of the alloys. Ni-20Si and Ni-20Si-0.1Y alloys was covered with scale after corrosion . From observation of the cross-sections of alloys by electron probe microanalysis and surface of the alloys by X-ray diffraction, it was suggested that Ni-20Cr-1Si and Ni-20Si-0.1Y alloys were covered with silica, and the both of Cr_2O_3 and silica, respectively.

Nanometric Observation of Initial Localized Corrosion Process on TiN Thin Film Fabricated by Plasma CVD method

○Ryuji TSUJIMURA, Senior Student of Kogakuin University, 2665-1, Nakano-machi, Hachioji-shi, Tokyo, Japan
Yuji KIMURA, Department of Environmental Chemical Engineering, Kogakuin University
Michio OHATA, Graduate student, Kogakuin University

ABSTRACT

Ceramics coating have been used for adding various functions to substrate surface and protecting substrate materials from severe environments. It is outstanding character of Plasma CVD method that deposition can be made on all surface including hole inside and so on. And it can be obtain relatively large thickness of coated film. As coating temperature of Plasma CVD method was relatively higher compared with other coating methods, problems of heat resistance of substrate AISI 304 are expected to occur. Therefore, substrate metal was damaged by Plasma CVD process. Because Plasma CVD coated film has inferior state of adhesion, cracking and exfoliation from thin film coating itself was expected at beginning stage by process heat damage. AFM (Atomic Force Microscope) and optical microscope observations were conducted in the depth direction. However, accurate informations concerning interface between substrate surface and thin film were not obtained on exfoliated area of thin film. Fig-1 showed AFM observation of pinhole defect at beginning stage. Some higher level regions than other surface were observed around pinhole defects. These height profile informations were supposed to be brought about by the exfoliation of film itself or entrainment impurity dust. Therefore, detailed observations of interface between substrate metal and thin film were conducted by FE-SEM (Field Emission Scanning Electron Microscope) and shown in Fig-2. Exfoliation and cracking of thin film caused degradation in film function. AFM and optical microscope data has problems of information lacks in plane direction. For this reason, FE-SEM observations were employed for getting more accurate surface and interface informations. Therefore, FE-SEM and FIB (Focused Ion Beam) methods were employed for compensating the film and interface data lacks obtain by AFM and optical microscope. And improvements in corrosion characteristic of thin film materials can be realized by obtaining detailed understandings of the initial states and degradation process of interface and film itself.

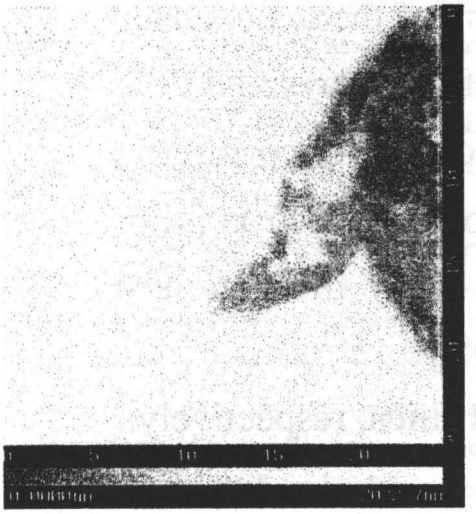

Fig-1 AFM observation of Pinhole defect at beginning stage

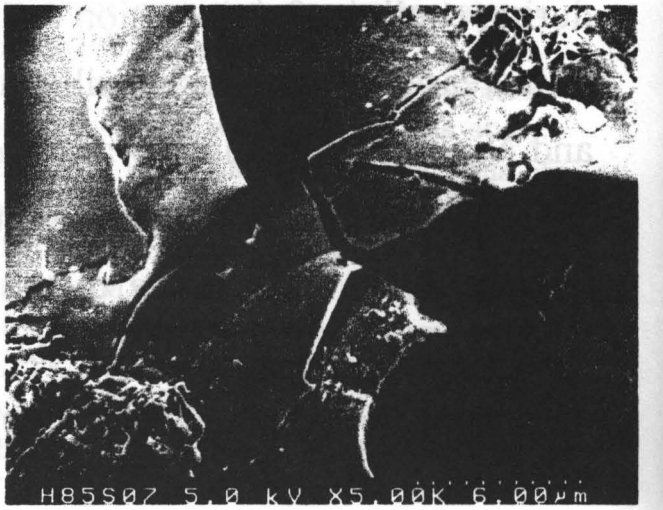

Fig-2 FE-SEM micrographs of interface between substrate and thin film

Preparation of Co/Pd Multilayers by Electroplating and Their Magnetic Properties

○Koji KUDO, Haruo TAMANO, Koichi KOBAYAKAWA, Yuichi SATO, Nobuo YAMAMOTO*, and Yumi YAMAMOTO*

Department of Applied Chemistry, Faculty of Engineering, Kanagawa University

3-27-1 Rokkakubashi, Kanagawa-ku, Yokohama 221

*Tanaka Kikinzoku Kogyo Co., 2-14, Nagatoro, Hiratsuka 254

Introduction : Co/Pt, Co/Au, and Co/Pd multilayered films exhibit a large perpendicular magnetic anisotropy. They have attracted attention as new materials for high-density magneto-optical recording media and for other applications. These mutilayered films are generally prepared by sputtering, vacuum evaporation, and the MBE method. We prepared the Co/Pd multilayered film by electroplating and observed perpendicular magnetic anisotropy in the obtained films.

Experimental : Co/Pd multilayered films were prepared on the polycrystalline copper substrate using the dual bath method. Film thickness was controlled by changing the applied current density and electroplating time. The multilayered structure and film thickness of one layer were confirmed by TEM, and Co and Pd analyses by ICP. The magnetic properties were measured using a VSM.

Results and Discussion : Fig. 1 shows an example of the cross-sectional view of the TEM image of the [Co(10 nm)/Pd(10 nm)]$_{18}$ multilayered film. Each film thickness was found to be controlled by the electricity that passed through the cathode. By changing the film thickness of Co and Pd, various types of films were prepared and their magnetic properties were measured. It is found that a perpendicular magnetic anisotropy appeared on the multilayered Co film with a thickness of less than 0.4 nm,i.e., the easy axis of magnetization of the multilayered film changed from a direction parallel to the film plane to perpendicular to the film plane as shown in Fig. 2. The coercive force and the squaranse ratio were comparable to those of the films obtained by sputtering[1].

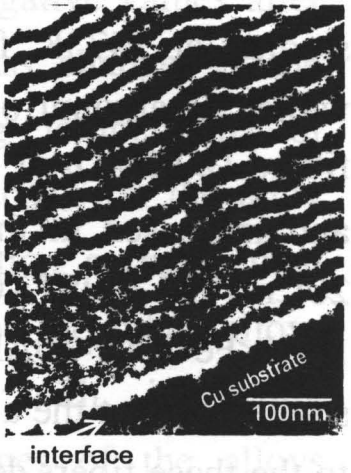

Fig.1 Cross-sectional TEM image of [Co(10nm)/Pd(10nm)]$_{18}$ multilayer.

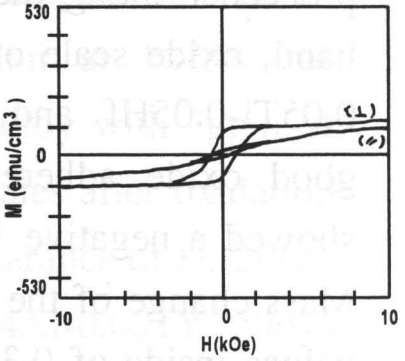

Fig2 Magnetic hysteresis loop of [Co(0.2nm)/Pd(1nm)]$_{40}$ multilayer.

Reference

1)P. F. Carcia, J. Appl. Phys., **63**, 5067 (1988).

High-Temperature Oxidation of Fe-20Cr-10Al Fibers with Amounts of Reactive Elements

T. Arai, M. Sekine, T. Amano, A. Katsuya*, S. Hiromoto* and K. Sasaki**

Shonan Institute of Technology, 1-1-25, Tsujido-Nishikaigan, Fujisawa 251, Japan
* NHK Spring Co., LTD, 3-10, Fukuura, Kanagawa-ku, Yokohama 236, Japan
** IMR, Tohoku University, 1-1, Katahi 2-chome, Aoba-ku, Sendai 980-77, Japan

High-temperature oxidation behavior of Fe-20Cr-10Al fibers and disks with small amounts of reactive elements (Y or Hf) was studied at 1473K for 18.0ks in oxygen. Mass gain (included values of amount of spalled oxide when oxide spalled) of these fibers (20-100 μ m in diameter) was values between 4 and 7%, and increased in the order of Fe-20Cr-10Al-0.05Ti-0.05Hf<Fe-20Cr-10Al-0.05Ti-0.1Y<Fe-20Cr-10Al-0.05Ti-0.1Hf<Fe-20Cr-10Al<Fe-20Cr-10Al-0.05Y<Fe-20Cr-10Al-0.05Ti. This result suggested that the addition of small amounts of reactive elements to the these fibers decreased rate of oxidation. Oxide scale on Fe-20Cr-10Al fiber spalled during cooling, and oxidation of the fiber proceeded along the grain boundary of the fiber. On the other hand, oxide scale on Fe-20Cr-10Al-0.05Ti-0.1Y, Fe-20Cr-10Al-0.05Ti-0.05Hf and Fe-20Cr-10Al-0.05Ti-0.1Hf fibers showed good oxide adherence. Mass change of Fe-20Cr-10Al disk showed a negative value because of spalling of the oxide scale. Mass change of the other disks showed positive values, and was values inside of 0.3%. Small cavities were observed into oxide scale on Fe-20Cr-10Al, Fe-20Cr-10Al-0.05Ti and Fe-20Cr-10Al-0.05Ti-0.05Y disks. However, no cavities were detected into oxide scale on the other disks.

High-Temperature Oxidation of Fe-20Cr-4Al Alloys with Small Amounts of Both of Sulfur and Yttrium

A. Hara, T. Amano and K. Sasaki*

Shonan Institute of Technology, 1-1-25, Tsujido-Nishikaigan, Fujisawa 251, Japan

*IMR, Tohoku University, 1-1, Katahira 2-chome, Aoba-ku, Sendai 980-77, Japan

High-temperature oxidation of Fe-20Cr-4Al alloys with small amounts of both of sulfur and yttrium was studied for 18.0ks in oxygen at 1273, 1373, 1473, 1573 and 1673K. Mass changes of the alloy with 7ppm of sulfur showed only negative values after oxidation of 1473, 1573 and 1673K, and mass changes of the alloy increased negatively with increasing temperature of oxidation. This result suggested that oxide scales on the alloy spalled markedly during cooling after oxidation at more than 1473K. On the other hand, mass changes of the other alloys showed positive values, and increased with increasing temperature of oxidation. The mass changes of the alloys increased in the order of Fe-20Cr-4Al-0.08Y (78ppmS)<Fe-20Cr-4Al-0.37Y (40ppmS) <Fe-20Cr-4Al-0.03Y (80ppmS)<Fe-20Cr-4Al-0.001Y (151ppmS) alloys after oxidation at 1673K for 18.0ks. Surface appearance of Fe-20Cr-4Al alloy with 7ppm of sulfur showed remarkable spalling of oxide scales after oxidation at 1373, 1473, 1573 and 1673K. Surface appearance of Fe-20Cr-4Al with 185ppm of sulfur and Fe-20Cr-4Al-0.001Y alloys showed partial spalling of oxide scales after oxidation at 1573K. On the other hand, oxide scales on the other alloys showed good oxide adherence.

Superoxide generator using polyanine catalyst

Masamichi Takamatsu , Ken-ichi Morita and Norimichi Kawashima
1614 Kurogane-cho, Aoba-ku, Yokohama 225, Japan
Materials Science and Technology Department, Toin University of Yokohama

1. Introduction

Recently, superoxide anion radical has attracted much attention in the field of biology, because superoxide is produced in biological systems[1]. Superoxide anion radical is oxygen molecule with one extra electron. It has a strong sterilizing effect and is generated even inside the human body to protect it from bacteria. The radical anion can also be generated artificially, for example, by photochemical reduction of oxygen in the presence of naturally occurring substances such as chlorophyll[2] . Apparatus based on the method of exposing titanium oxide to light is commercially available for artificially generating superoxide. The authors have already reported that the generation of superoxide by simply adding polyaniline powder to pure water[3]. This paper reports a novel method for continuous generation of superoxide.

2. Experimental

After a platinized titanium plate (30mm × 100mm) was covered with a separator film for electric cell, a carbon fiber cloth, on which polyaniline was polymerized electrochemically, was brought into contact with the both sides of the plate. The titanium plate was used as the anode and the carbon fiber cloth was used as the cathode. These composite electrodes were placed in a beaker containing 60 mℓ of physiological saline solution. In this apparatus, cathodic voltage was applied for 20min on the polyaniline deposited carbon fiber cloth while stirring the saline solution. The amount generated of superoxide was measured as the concentration of hydrogen peroxide formed by the disproportionation reaction. This amount corresponds to the accumulated amount of generated superoxide.

3. Results and discussion

As a result, the concentration of hydrogen peroxide was found to increase with increasing cathodic voltage up to -0.25V, above which it gradually decreased with further increase in cathodic voltage. This apparatus could generate superoxide as 2.5ppm of hydrogen peroxide concentration at -0.5mA of applied current and -0.25V vs SCE.

Sterilizing of Staphylococcus aureus and Pseudomonas aeruginosa was carried out in superoxide containing water treated with this apparatus. Sterilizing of S. aureus and P. aeruginosa was thus confirmed in cultivation test after 30min treatment with the superoxide genarator.

As a conclusion, the superoxide generator using polyanine catalyst could be prepared and its sterilizing effect was confirmed.

References

1. M. Nakano, K. Asada, Y. Oyanagi, Active Oxygen – Molecular Mechanism of its Production, Scavenging and Effect in Organisms, Kyoritsu Shuppan, Tokyo (1988).

2. a) L. S. Jahnke and A. W. Frenkel, Biochemical and Research Communications, 66, 144 (1975). b) G. van Ginkel and J. K. Raison, Photochemistry and Photobiology, 32, 793 (1980).

3. S. Otsuka, K. Saito, and K. Morita, Chem. Lett., 1996, 615.

DEVELOPMENT OF HIGHLY WATER-RESISTANT POLYMER-GYPSUM COMPOSITE

Shuuhei SAEKI, Satoshi KISHI, Kumiko ISHIHARA, Qian HUANG*, Tomonori TAKATA and Masaki HASEGAWA, Faculty of Engineering, Toin University of Yokohama, 1614 Kurogane-cho Aoba-ku, Yokohama, 225, Japan, *Maeta Techno Research Inc., 6-7 Kamihon-cho, Sakata. Yamagata, 998, Japan

Introduction

Gypsum has been broadly utilized for arts, crafts and some interior materials for many centuries because of its fineness on appearance with low price. However, as hardened gypsum($CaSO_4 \cdot 2H_2O$) is rather inferior to the moisture, the out-door use is extremely limited. Residual flexural strength of usual hardened gypsum after the immersion in water for a day is lower than 50 % of initial strength. Recently we have developed a new type of high strength and water-resistant phenol resin-cement composite[1,2]. In present study, for the purpose of developing water-resistant polymer-gypsum composite, we attempted to extend the method to the polymer-gypsum composite; the relationship between polymer-gypsum composition and water-resistivity of resulting composite material was investigated.

After several attempts, starting from the mixture of gypsum and one of phenolic compounds, we succeeded to prepare highly water-resistant polymer-gypsum composite.

Results and Discussion

Polymer-gypsum composite was shaped as following way. A mixture containing calcined plaster($CaSO_4 \cdot 1/2H_2O$), one of phenol derivatives, methanol, water, formalin, and one of acids, such as HCl, $C_2H_2O_4$, H_2SO_4 and CH_3COOH, was flown into the mold. The mixture was kept at room temperature for a day and then removed from the mold. The sample was cured at 70 °C for a day and subjected to tree pointed bending test before and after immersion in water.

When 1N-HCl is used as an acid, flexural strength and water resistant property of the composite was the most superior compared to those with other acids. The reason may be due to higher catalytic ability to the reaction between resorcinol and formaldehyde by hydrochloric acid than by other acids.

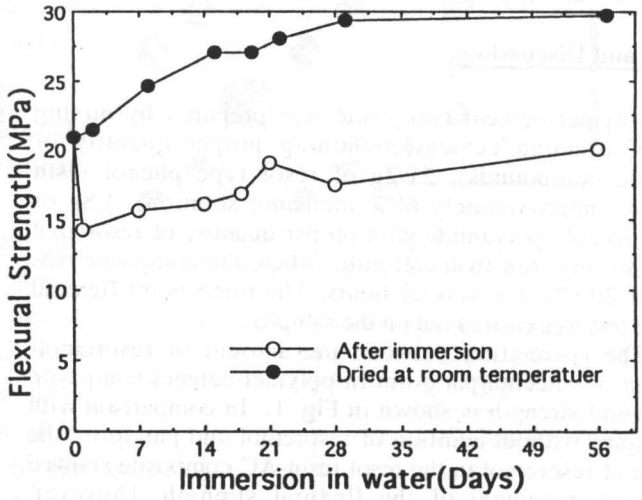

Fig.1 Flexural strength of the composite after immersion in water and then drying for a day at room temperature.

The relation between immersion period in water and flexural strength of polymer-gypsum composite is shown in Fig. 1. Residual flexural strength of the composite was about 96 % of initial strength(20.8 MPa) after immersion in water for 56 days at room temperature. Strength of the same sample increased to 140 % of the initial strength after air-dried at room temperature for a day.

The observed increase of residual flexural strength after the immersion is explained by the increase of hydrated gypsum content, accompanied with decreasing the calcined plaster, by x-ray diffraction analysis. Furthermore, x-ray diffraction pattern of the composite indicated that the calcined plaster remained in present composite more than in ordinary hardened gypsum. Then, during the immersion in water residual calcined plaster was gradually transformed into the hardened gypsum, resulting in decrease of the total volume of voids in the composite. This may be the reason why the strength was enhanced so greatly after the immersion. From the SEM photograph, it was confirmed that the gypsum was not dispersed in the resin satisfactory and that the crystal of gypsum grew larger than the crystal of ordinary hardened gypsum.

Reference

1) T. Takata, et al., JCA Proceedings of Cement and Concrete, 50, 762(1996), etc.
2) T. Takata et al., Abstract of 5th Pacific Polymer Conference (Kyongju, Korea, Oct., 1997)

INFLUENCE OF COMPOSITION ON HIGH STRENGTH POLYMER-CEMENT COMPOSITE

Kumiko ISHIHARA, Satoshi KISHI, Shuuhei SAEKI,
Tomonori TAKATA and Masaki HASEGAWA
Faculty of Engineering, Toin University of Yokohama,
1614 Kurogane-cho Aoba-ku, Yokohama 225, Japan

Introduction

Macro-defect-free(MDF) cement has been studied in several research laboratories [1] since first report by J.D.Birchall et al. in 1981[2]. The MDF cement consists of a mixture of alumina cement(AC) and aqueous polymer, such as polyvinyl alcohol with a few additives, and it shows extremely high flexural strength. It has been reported that in the MDF cement an unusual micro structure was created by chemical interactions between organic-inorganic components and greatly contributed to the high flexural strength. However, one general drawback of this material is its instability in water with swelling of polymer matrix to result in serious decrease in strength after immersion in water because of hydrophilic nature of polymeric binders used.

Rather recently, a new class of polymer cement composite with high flexural strength(>200MPa) has been developed in our group[3]. The new polymer cement composite consists of AC, thermo-setting resin precursor, such as phenol resin(resol resin), with small amounts of alcohol soluble polyamide and glycerol. Water- and heat-resistant properties of the composite is much higher than those of MDF cement.

In this paper, the effect of diphenolic compounds and paraform, on properties of resulting polymer-cement composite was studied. In addition, effect of inorganic compounds on high strength polymer-cement composite was also studied.

Results and Discussion

Polymer-cement composite was prepared by mixing 100g of alumina cement(containing proper quantity of inorganic compounds), 21.2g of resol type phenol resin precursor (approximately 60% methanol solution), 1.8g of alcohol soluble polyamide with proper quantity of resorcinol and paraform, in a twin roll mill. Then, the composite was cured at 200 °C for several hours. The three point flexural strength test was carried out on the samples.

The correlation between the amount of resorcinol/paraform or catechol/paraform in polymer-cement composite and flexural strength is shown in Fig. 1. In comparison with the samples without addition of resorcinol and paraform, the addition of resorcinol in the resol resin-AC composite showed prominent increment of the flexural strength. However, contrary to the case of resorcinol, the addition of catechol to the composite did not enhance the flexural strength. The difference may be less reactive behavior between catechol and formaldehyde than between resorcinol and formaldehyde.

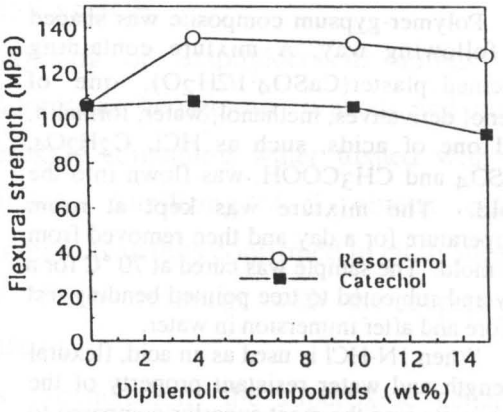

Fig.1 Correlation of flexural strength with diphenolic compounds (resorcinol and catechol) content in resol resin-almina cement composite.

Addition of inorganic compound, such as $CaCl_2$, $CaCl_2 \cdot 2H_2O$, $MgSO_4$, $CuSO_4 \cdot 1/2H_2O$, into resol resin-alumina cement composite drastically decreased the flexural strength of resulting composite and finally made difficult to produce the sheet, with increasing the amount of inorganic compound. In contrast, the addition of trivalent inorganic compound, such as $Al(OH)_3$, Al_2O_3, $In(OH)_3$, In_2O_3, into the resol resin-alumina cement composite has raised the flexural strength.

From the results, it was suggested that hydroxyl group and trivalent inorganic compounds play an important role to enhance the strength of the composite. The reason may be due to strong interaction at the interlayer between hydroxyl groups in the polymer and trivalent inorganic compounds.

References

1. J.F.Young, et al., MRS Bull. 33, 35, (1993)
2. J.D.Birchall, A.J.Howard, K.Kendall, Nature, 289, 29, 388 (1981)
3. M.Hasegawa, et al., Abstract of MRS-JAPAN Annual Symposium, 1-P5 (1993) , etc.

Synthesis of $In_{x-1}W_xBa_2CuO_y$

N. Sumitani, T. Wakamori, H. Yamamoto

College of Science and Technology, Nihon University, 7-24-1 Narashinodai, Funabashi city, Chiba 274, Japan

Introduction

Recently, Ohshima *et al.*[1] have synthesized InBa2CuOx, of which the structure similar to that of a typical homologous series of superconductors; TlBa2CuOx or HgBa2CuOx etc.[2] This compound does not, however, show superconducting properties because of its large lattice-parameters **a** and **b**.

It has been well known that a substitution of ReO3 brings a chemical stabilization and a hole-doping effect for a HgBa2Can-1CunOx superconductor.[3] Since WO3 has a rhenium(VI) oxide type of an orthorhombic structure, we expect that InBa2CuOy are chemically stabilized and lattice parameters become smaller by a substitution of WO3. In the present study, we investigated substitution effects of W atoms into a part of In sites of InBa2CuOx from a crystallographic point of view.

Experimental Procedure

W-doped In1-xWxBa2CuOy was prepared by a conventional solid-state reaction method. Powder of In2O3, WO3, BaCO3, CuO were mixed with the ratio of In:W:Ba:Cu=1-x:x:2:1 (x=0, 0.05, 0.1, 0.2, 0.3, 0.4). The mixed powder was calcined at 910℃ for 35 h in air, and pressed into pellets with a pressure of 700kgf/cm^2. They were sintered at 930℃ in O2.

Results and Discussion

Figure 1 shows a schematic structure of the (In,W)Ba2CuOx. The sample were characterized by reflected X-ray powder diffraction method and Rietveld analysis.[4]

By the refinement, lattice parameters were determined **a**=4.156, **b**=4.085, **c**=8.368Å with a space group of Pmmm, as shown in Figure 2. The value of **b** is smaller than that of the non-doped InBa2CuOy by 5 %. An occupancy and fractional coordinates were determined too. A phase transition was observed at $x \sim 0.1$ as increasing a concentration of W from a tetragonal phase to an orthorhombic one in the In1-xWxBa2CuOy system. Obtained results suggest that W atoms are effectively substituted in In sites.

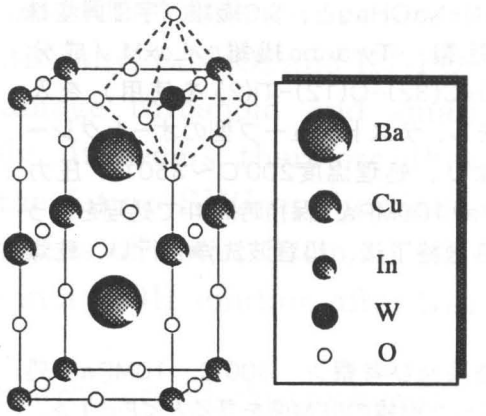

Fig. 1: Structure of the (In,W)Ba2CuOx.

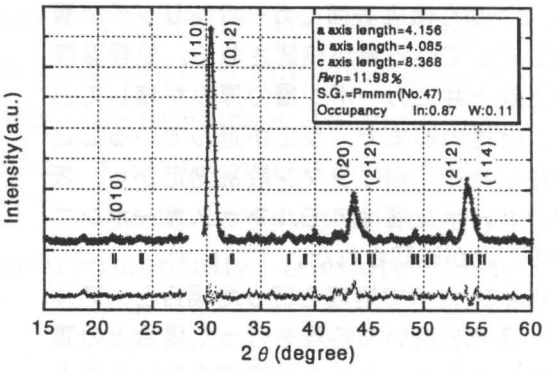

Fig. 2: Rietveld analysis of the In0.8W0.2Ba2CuOy.

Summary

We succeeded in decrease of the values of **a**, **b** and **c** by a partial substitution of W in InBa2CuOx. The sample did not show a superconductivity probably because the lattice parameters are still large. Furthermore investigations for substituted materials are needed to obtain a superconductivity.

References

[1]S. Kambe, I. Shime, S. Ohshima, K. Okuyama, Physica C, **220**(1994)119.

[2]S. N. Putilin *et al.*, Physica C212 (1993) 266; E. V. Antipov et al.: Physica C, **215**(1993)1.

[3]J. Shimoyama *et al.*, Extended Abstracts (The 55th Autumn Meeting, 1994); The Japan Society of Applied Physics ZT-13(1994).

[4]F. Izumi, J. Crystallogr. Soc. Jpn., **27**(1985)23.

アルカリ水熱処理によるSiC繊維状へのカーボンコーティング

○酒井健太郎、吉村昌弘（東京工業大学、応用セラミックス研究所）、
岡田清（東京工業大学、無機材料工学専攻）

Carbon Coating on SiC Fiber by Hydrothermal Treatment using Alkalline Solutions.

水熱条件下において、SiCからSi成分を選択的に溶解することにより、表面にカーボン膜が生成することが知られている。アルカリ水溶液を用いる事で、低温（300℃）でSiC繊維表面に均一なアモルファスカーボンの膜が生成することを、SEM、ラマン散乱測定、オージェ電子分光測定(AES)により確認した。

＜実験方法＞ SiC繊維の処理は、金パイプに6N-NaOHaqと、SiC繊維（宇部興産株式会社製 Tyranno繊維 LoxM /成分 Si(54)-C(32)-O(12)-Ti(2) を使用）を入れ封をし、テストチューブ型のオートクレーブにより、処理温度200℃～350℃、圧力10MPa/100MPa、保持時間4hで処理を行った。処理終了後、超音波洗浄を行い、乾燥した。

＜結果及び考察＞ 300℃、10MPaで処理を行った繊維のSEM像を見ると＜Fig.1＞、比較的滑らかな表面が得られた。繊維表面にSiが溶出した痕跡は見られない。AES＜Fig.2＞から繊維表面にカーボンリッチな層が生成している事が確認される。処理温度の上昇と共にカーボン層の厚みが増しており、繊維内部まで、反応が進んでいることが見られる。別にラマン散乱測定から、表面のカーボン層はアモルファスカーボンであることが確認された。

<fig.3>に水で処理を行った場合と、アルカリ溶液を用いて処理を行った場合との重量変化を示す。アルカリ溶液を用いることで、明らかに反応が低温側に移動しており、急激に反応が進んでいる。300℃のアルカリ水溶液処理で水処理時の500℃の時と同じ程度の結果が得られた事から、

$$SiC + H_2O \rightarrow SiO_2\,(Dissolve) + C + H_2\uparrow$$

上式の溶解反応がアルカリにより促進されたと考えられる。

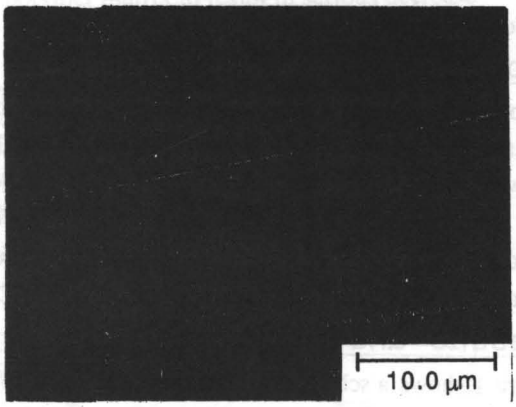

Fig.1 SEM Photograph of Tyranno Fiber ; hydrothermally treated at 300oC - 10MPa -4h in NaOHaq.

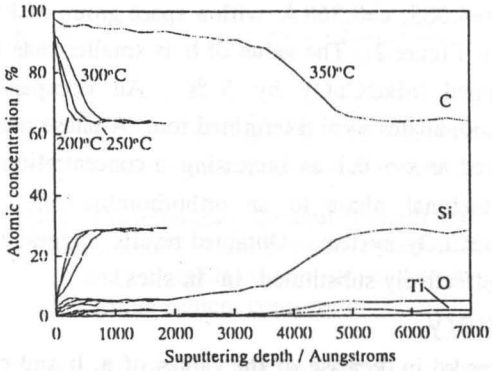

Fig.2 AES depth profile of the surface of Tyranno fiber; treated at 200°C-350°C-10MPa-4h in NaOHaq.

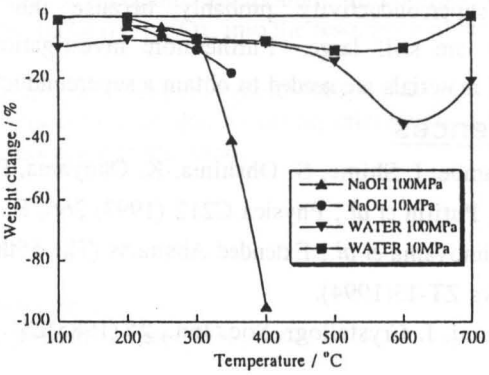

Fig.3 Weight change of Tyranno fiber; hydrothermally treated at 100°C-700°C for 4h at 10MPa/100MPa pressure in water and NaOHaq.

PREPARATION OF CRYSTALLIZED Li_3VO_4 FILMS BY HYDROTHERMAL - ELECTROCHEMICAL METHOD

Tomoaki WATANABE ,Masahiro YOSHIMURA, and Woo-Seok CHO
Center for Materials Design, Materials and Structures Laboratory,
Tokyo Institute of Technology, 4259 Nagatsuta, Midori-ku, Yokohama 226, Japan

In recent years, Li_3VO_4 has attracted much attention due to its potential application as second harmonic generation (SHG) material for green or blue lasers. The SHG conversion efficiency of the Li_3VO_4 was similar or superior to that of $LiNbO_3$ and $KTiPO_4$ which are in use as wavelength conversion materials. Additionally, $LiNbO_3$ and $KTiPO_4$ have disadvantages of weak optical damage threshold and small nonlinear optical coefficient, respectively. It seems therefore that Li_3VO_4 may replace these materials in the future SHG applications. The film consisted of well crystallized grains of about 5μm in size deposited on a vanadium metal substrate in a LiOH solution after 24h under 1mA/cm^2 current density.

In this study we have introduced the hydrothermal-electrochemical synthesis for Li_3VO_4 thin films at a low temperature (150℃). In our knowledge this is the first report dealing with preparation of Li_3VO_4 thin films. The film preparation method generally requires high temperatures (above 500℃) to crystallize as-deposited amorphous film from gas/vapor phases, or to decompose the precursor to yield an appropriate compound in "sol-gel" methods. Low temperature *in situ* fabrication of crystalline thin films might lead to improve their quality and to make the whole process environmentally friendly and economically.

水熱電気化学法による $LiNiO_2$ 膜の Ni 電極上へのその場作製

(東工大応用セラミックス研究所) ○釣本俊輔, 韓奎承, 吉村昌弘

1. 序

近年、マイクロエレクトロニクスデバイスの電源としての全固体リチウムイオンマイクロ電池の研究が盛んになされている。その正極材料となる $LiNiO_2$ の薄膜を、水熱電気化学法により 100-200℃という低温で Ni 電極上に直接作製できることがわかった。本研究ではこれらの膜の特性を調べるとともに、生成機構について考察した。

2. 実験

4M の LiOH 水溶液、洗浄した Ni 基板の陽極と陰極、Ag/AgCl 参照電極[1]からなる電解セルをオートクレーブ内に構築、水熱条件下で電解処理を行い、Ni 陽極上に $LiNiO_2$ 膜をその場作製した。電解は定電流法で行い、電流密度は 0.1-5.0mA/cm^2、温度は 100-200℃、圧力は飽和蒸気圧とした。生成した膜を XRD、XPS、サイクリックボルタンメトリーにより評価した。

3. 結果と考察

作製した膜は、XRD パターン(Fig. 1)から、結晶性の良好な $R\bar{3}m$ 構造の $LiNiO_2$ であること、また XPS スペクトルから Ni^{3+}を含むこと、Li/Ni モル比はおおよそ 1 であることを確認した。

インピーダンス測定より求めたイオン伝導度の値は 3×10^{-5}S/cm(25℃)であった。また作製した膜は電気化学的に活性であることが Fig. 2 のサイクリックボルタモグラムからわかる。Fig. 2 から求めた、試料中の Li イオンの拡散係数は 3.7×10^{-12}cm^2/s となり、これは従来法により高温で作製された $LiCoO_2$ および $LiMn_2O_4$ の膜の拡散係数 10^{-14}-10^{-10}cm^2/s [2]に匹敵する。

$LiNiO_2$ 膜は、作製温度の違いにより異なった電気化学特性を示した。

反応中の電極電位(vs. Ag/AgCl)は時間経過に伴い 0.5V→1.0V→0.7V と推移した。Pourbaix ダイヤグラム[3]により、反応の初期段階では $HNiO_2^-$が安定な種であることも考慮すると、反応機構は次のようになっていると思われる。

$HNiO_2^- + H_2O \leftrightarrow Ni(OH)_2 + OH^-$ E=0.5V
precipitation

$Ni(OH)_2 \leftrightarrow NiOOH + H^+ + e^-$ E=1.0V
oxidation

$NiOOH + Li \leftrightarrow LiNiO_2 + H^+$ E=0.7V
cationic exchange

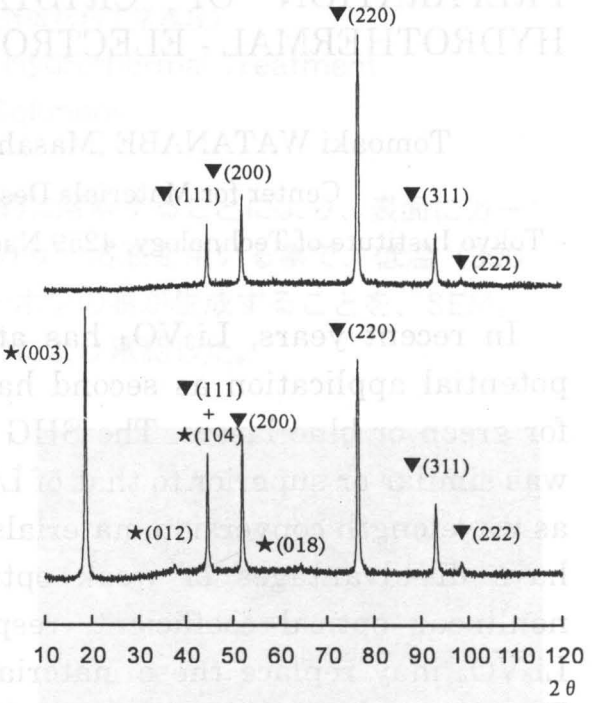

Fig. 1. X-ray diffraction patterns for (A) Ni metal substrate and (B) the prepared film by the electrochemical-hydrothemal treatment in 4M LiOH solution at 150℃ with the current density 1mA/cm^2. Peaks denoted by ★ were assigned to $LiNiO_2$; peaks denoted by ▼ were assigned to Ni substrate.

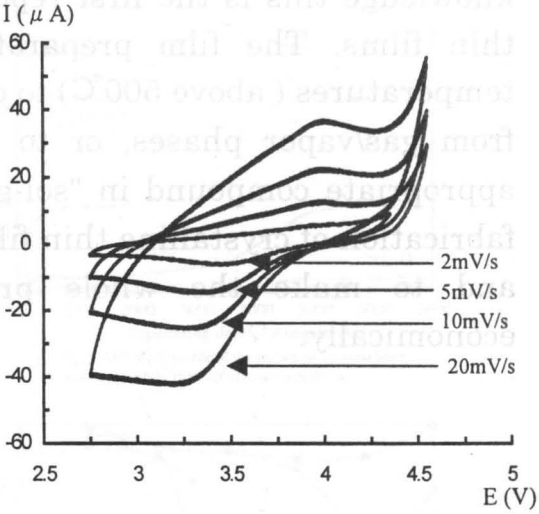

Fig. 2. Cyclic voltammograms of $LiNiO_2$ films prepared at 150℃ taken in 0.1M $LiClO_4$ propylene carbonate (potential is referred to Li/Li$^+$ electrode) with various scan rate.

参考文献

[1] D. D. Macdonalds and D. Owen, *J. Electrochem. Soc.* **120**, 317(1973).
[2] for example, P. Birke, W. F. Chu, W. Weppner, *Solid State Ionics*. **93**, 1(1997).
[3] E. Deltombe, N. de Zoubov, M. Pourbaix, *Atlas of Electrochemical Equilibria in Aqueous Solutions* (National Association of Corrosion Engeneers, Houston, 1974), Nickel, Section 12.3.

炭素、窒化ホウ素ナノチューブの同時合成

（法政大工）○清水禎樹・守吉佑介
（無機材研）小松正二郎・池上隆康・石垣隆正・佐藤忠夫・板東義雄

Concurrent preparation of Carbon- and Boron Nitride- nanotubes/The chemical species evaporated from Porous BC_4N by a dc arc plasma were condensed on a copper disk cooled with water. The nanotubes collected from disk were characterized by TEM and EELS.EELS data indicated these nanotubes prepared by this method were in the mixture of carbon and boron nitride nanotubes.

【目的】

カーボンと窒化ホウ素の積層構造のB-C-N三成分系ナノチューブは、合成の可能性が指摘され、バンドギャップなど物性の理論計算などがされているものの、いまだ合成されていない。我々はB-C-N系原料を強制蒸発させ、それを超急冷することで、超微粒子の合成を試みてきたが、このプロセスでナノチューブが効率よく合成できることを見いだした。本報では、直流アークプラズマを用い、BC_4Nの組成を有する多孔体を蒸発させることで生成した活性な化学種を、超急冷することで、非平衡状態を凍結させ、B-C-N三成分から成るナノチューブの合成を試みた結果について報告する。

【実験】

直流アークプラズマを25V、300Aの条件で発生させた。プラズマガスとして$Ar-N_2-H_2$混合ガスを用い、チャンバー内の雰囲気圧は100Torrを主として行った。被蒸発体として、尿素ーほう酸ーサッカロースの溶融混合物熱分解法により合成したBC_4N多孔体を用いた。この多孔体を水冷式固定装置に固定し、直流アークプラズマの約5000Kと推定される高温部を照射することで蒸発させた。生成した活性な化学種は、固定装置両側に設置した水冷式銅板で超急冷することで凝縮させ、銅板上にナノチューブを析出させた。採集したナノチューブは、TEM、電子線回折（200kV)を用いて構造解析し、同時にEELSを用いて微小領域（約1nm径）の組成分析を行った。

【結果及び考察】

析出したナノチューブは数十本から百数本が凝集した状態で析出していた。ナノチューブの直径は10～30nm、アスペクト比は約200であった。ナノチューブの電子線回折は、ナノチューブのC軸がチューブの軸に対して垂直であることを示した。すなわち、ナノチューブは、炭素の場合と同様に、ab網面のカーペットを巻き上げたような構造をしている。EELSによる合成ナノチューブの分析は、炭素のナノチューブとBNナノチューブの存在を示した。この結果は、被蒸発原料がBC_4N多孔体であり、三成分であることを考慮すると、不思議である。そこで、一本のナノチューブについて、種々の箇所のEELS分析を試みた。その結果、炭素ナノチューブ、BNナノチューブの他に、炭素ナノチューブがBNナノチューブで囲まれたもの（図1）の三種類の存在を明確にした。図から明らかなように、a、b、cから検出されるスペクトルは、主にB、Nであり、Cがわずかに検出された。この炭素がBN中へのCの固溶なのか、電子顕微鏡観察中のコンタミネーションなのかは現在不明であるが、後者でもこの程度の炭素が検出される場合があるので、a、b、cの部分がBNナノチューブであることを示唆しているものと考えられる。それに対し、dの部分からは、B、C、Nがすべて明確に検出された。電子線はナノチューブを十分に通過するので、高い炭素のピークはdの部分の内部に包埋されているナノチューブから由来するものと考えられる。この結果より、このナノチューブは中央にカーボンナノチューブが存在し、その周囲をBNナノチューブが囲んでいる構造をしているものと推測される。ナノチューブの生成機構は、原料であるBC_4N多孔体の微構造と密接に関係する模様であり、現在検討中である。

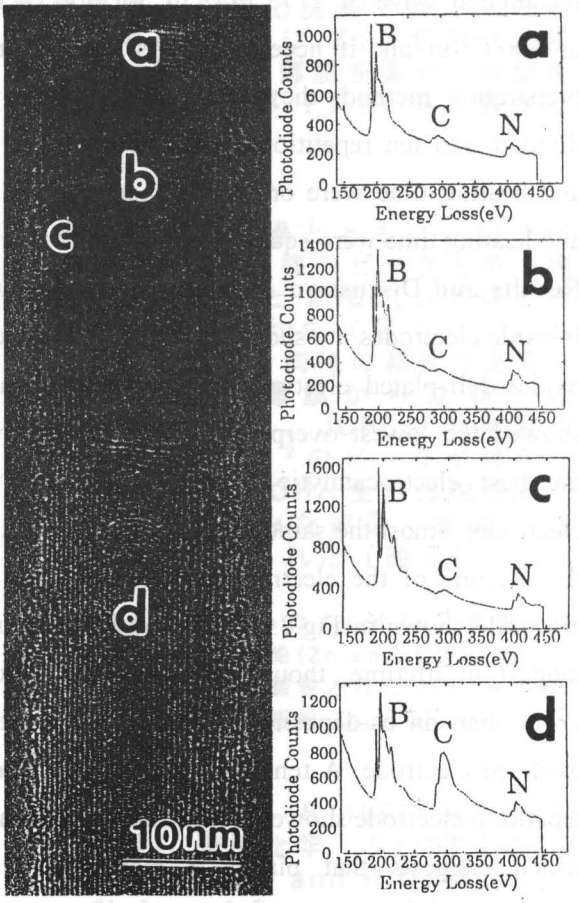

図1　カーボンナノチューブ内包BNナノチューブ

New Preparation Method of Iridium Covered Electrode by Plating for Electrochemical Processes

○Satoshi HONDA, Koichi KOBAYAKAWA, Yuichi SATO,
Ichiro HASHIMOTO*, and Eisaku USHIKU*
Department of Applied Chemistry, Faculty of Engineering, Kanagawa University
3-27-1 Rokkakubashi, Kanagawa-ku, Yokohama 221, Japan
* Tanaka Kikinzoku Kogyo Co., 2-14, Nagatoro, Hiratsuka 254

Introduction: The iridium oxide-coated titanium electrode used as the anode for electrochemical processes is usually prepared by the thermal decomposition method, which is very complicated. In order to simplify this preparation method, we tried to prepare an IrO_2-coated Ti electrode by the electroplating of Ir on Ti followed by an electrochemical or thermal oxidation process. During this study, the electrochemical behavior and the lifetime of the Ir-plated Ti electrode were studied.

Experimental: A 10 × 10 × 0.5 mm Ti substrate was treated by oxalic acid at 90℃ for one hour and then Ir was plated using a bath supplied by the Tanaka Kikinzoku Kogyo Co. at 1.5 mA/cm^2 and 80℃. The Ir-plated electrode was electrolyzed in NaCl solution using a rectangular wave of ±75 mA/cm^2 for 500 cycles or heated at 600℃ in air, if necessary. As another Ir oxide film preparation method, the plating and heating process was divided into ten repetitions. In this case, the plating time and heating time were one-tenth, therefore the total plating and heating time were equal to that of the first process.

Results and Discussion: Polarization curves for the various Ir-oxide electrodes are shown in Fig. 1. The electrolytically oxidized Ir-plated electrode using a rectangular wave (▲) showed the lowest overpotential for oxygen evolution and the best electrocatalytic behavior. As for the chlorine electrode, almost the same results were obtained. However, the lifetime of the electrode is short like the as-deposited electrode shown in Fig.2. The ten times electrode had the longest in lifetime, though the electrocatalytic activity is lower than an as-deposited electrode or an electrolytically oxidized electrode. A ten times plating and heating process repetition electrode showed a significantly increased lifetime, which suggests that plated Ir may not be completely oxidized.

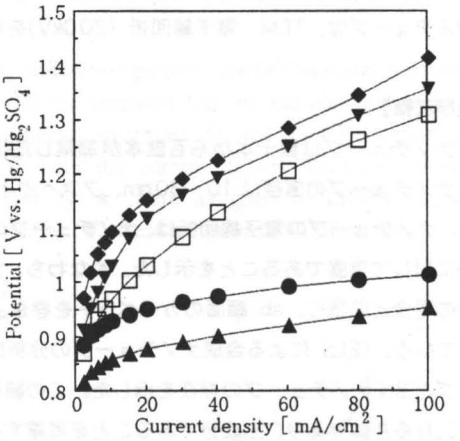

Fig.1 Polarization curves of electrode in 0.5M H_2SO_4 at 30℃.
□ IrO_2 electrode (Commercialized).
● Ir plated Ti electrode.
▲ after 500 cycles electrolysis using a rectangular wave of ±75mA/cm^2 in 0.1M NaCl solution.
◆ after heat teatment at 600℃for 5 hours in air.
▼ 10 times plating and heating process repetition electrode.

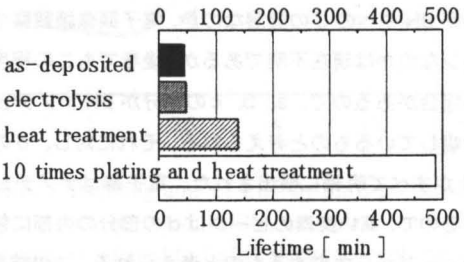

Fig.2 Lifetime of various types of Ir plated Ti electrode.
Electrolyte is a mixed solution of 1.0M H_2SO_4 and 1.0M Na_2SO_4 containing 0.1M Ethylene Chlorohydrin at 40℃.
Applied current density is 1.5A/cm^2.

酸化亜鉛薄膜の炭酸化：二酸化炭素及び水蒸気による反応過程
Carbonation of zinc oxide:reaction process in carbon dioxide and water vapor

○関　成之　　澤田　豊（東京工芸大学大学院工学研究科）
○Shigeyuki SEKI and Yutaka SAWADA(Department of Industrial Chemistry,Graduate School of Engineering,Tokyo Institute of Polytechnics)

【背景と目的】

透明導電膜は、液晶表示素子や太陽電池などの発展に伴い需要が高まっている。ZnO 系透明導電膜は安価で導電性に富むが、化学的耐久性に不安がある。ZnO 粒子を CO_2 と水蒸気の雰囲気中に放置すると塩基性炭酸亜鉛 $Zn_3(CO_3)(OH)_4$ 及び $2ZnCO_3 \cdot 3Zn(OH)_2$ を経由して正炭酸亜鉛 $ZnCO_3$ に変化することが報告[1]されている。

本研究では、粉末状態と薄膜状態の ZnO 微粉末及び薄膜に関する炭酸化の反応過程を追跡する事を目的とする。

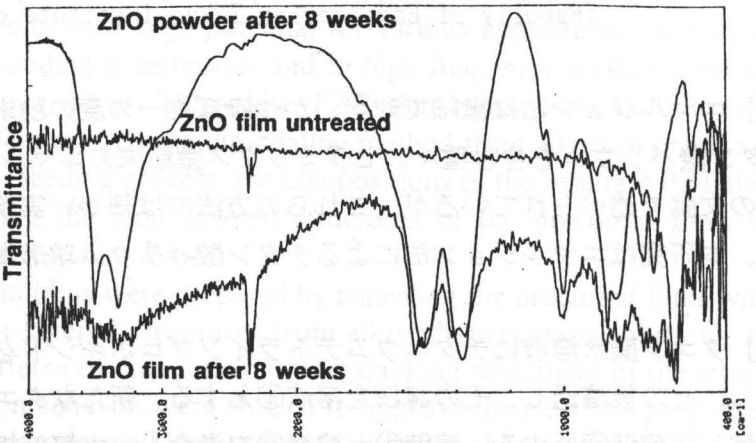

図２．ＺｎＯ粉末と薄膜の水蒸気及び二酸化炭素との反応によるＩＲスペクトルの変化（反応８週間後）

【実験方法】

製膜条件（Ａｒガス，スパッタガス圧 3.0×10^{-3}atm，スパッタ電力 100W）で、ＲＦマグネトロンスパッタリング法により膜厚 400nm の ZnO 薄膜を作製した。飽和水蒸気と二酸化炭素で満たした密閉容器中（20℃）に ZnO 粉末（粒径約１μ，３Ｎ）と薄膜を置き、時間変化をＸ線回折及び FT-IR 等で確認した。

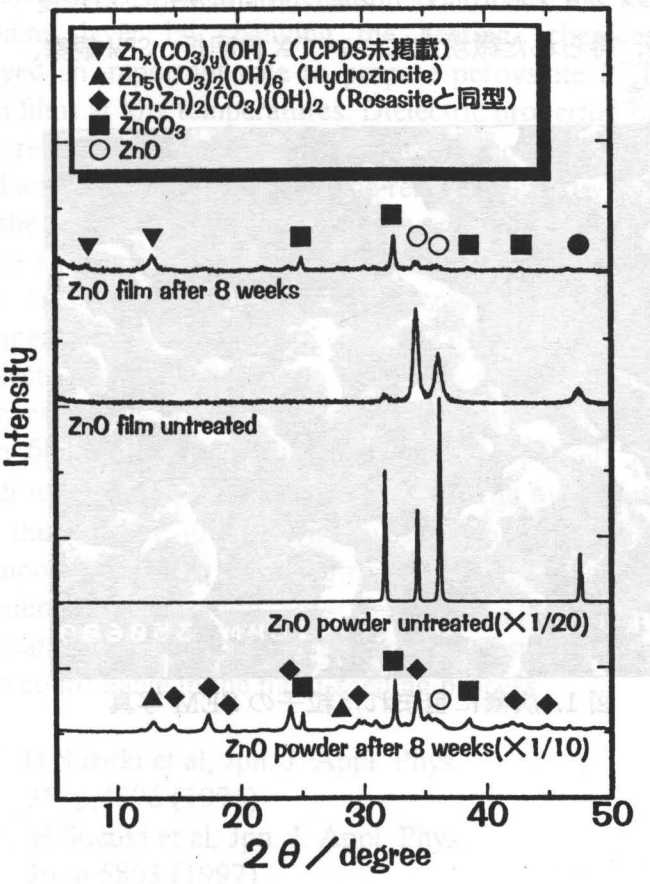

図１．ＺｎＯ粉末と薄膜の水蒸気及び二酸化炭素との反応によるＸ線回折図形の変化（粒径約１μ，膜厚 400nm）

【結果】

反応時間の経過とともに、粉末には Rosasite と同様のピークを持つ塩基性炭酸亜鉛*1と $ZnCO_3$ のＸ線回折ピークが検出された（図１）。これは大隈らの報告と同様の結果である。これに対し、薄膜からは前述の Rosasite に加え、JCPDS 未掲載の塩基性炭酸亜鉛*2のピークが得られた。$ZnCO_3 \cdot 3Zn(OH)_2$ 生成の確認としてＩＲ測定を試みた結果、文献[2]と同様の図形が得られた（図２）。

＊１鉱物名 Rosasite の Cu が Zn に置換された塩基性炭酸亜鉛 $(Zn,Zn)_2(CO3)(OH)_2$

＊２大隈らによって報告された JCPDS 未掲載の塩基性炭酸亜鉛 $Zn_x(CO3)_y(OH)_z$

【文献】

１）大隈ら，日化　５(1987),802 及び
大隈ら，表面化学　９(1988),452
２）R.A.Nyquist and R.O.Kagel, "Infrared Spectra of Inorganic Compounds",pp.84-85, Academic

エマルジョン法による球形チタン酸バリウム微粉末の合成

○江見　森、林　禎之、高島大治、飯泉清賢、久高克也（東京工芸大・工）

Preparation of Spherical Barium Titanate Powders by Emulsion-char Method

○ Shigeru Emi, Sadayuki Hayashi, Daiji Takashima, Kiyokata iizumi, Katuya Kudaka
(Facully of Engineering, Tokyo Institute of polytech.)

【緒言】エマルジョン法は微細で球状、かつほぼ均一の度の粉末を合成するために開発されてきた。チタン酸バリウムを含む種々のセラミックス微粉末のエマルジョン法による合成については、２，３の文献で述べられているが、これらの方法では細かい実験条件が明らかになっていない。従って、本研究はエマルジョン法によるチタン酸バリウム球形微粉末の合成条件の解明を目的とした。

【実験】クエン酸水溶液にチタニウムテトライソプロポキシドを加え、イソプロパノールを完全に除去し、その後濾過し、その濾液を溶液①とする。新たなクエン酸水溶液に炭酸バリウムを加え、溶解し、溶液②とする。溶液①と溶液②を混合し、水溶液相とした。次に低沸点オイルと高沸点オイルを混合し、界面活性剤を加え、有機相とした。有機相に水溶液相を加え、超音波分散機を用いてエマルジョン化し、その後エマルジョン液中の水分を除去し、窒素雰囲気下で表面の界面活性剤を炭化し、その後大気中で加熱し、微粉末の表面の炭素を除去するとともに酸化してチタン酸バリウム球形微粉末の合成をした。エマルジョン液についてレーザー回折法による粒度分布測定、炭素に包まれた粒子についてSEM観察、得られた微粉末についてＸ線回折、SEM観察、およびレーザー回折法による粒度分布測定を行った。

【結果】図１に有機相 600ml に対して溶液相 35ml を加えて窒素雰囲気下で加熱して得られた炭素に包まれた粒子の SEM 写真を示す。2～7μm程度の粒子が見られる。図２にレーザー回折法により求めたエマルジョン液の最頻粒径の関係を示す。溶液量が増加するに従い粒径が減少しているが、35ml を境に増加しているので溶液相／有機相 ＝35ml／600ml の時最小値を示した。

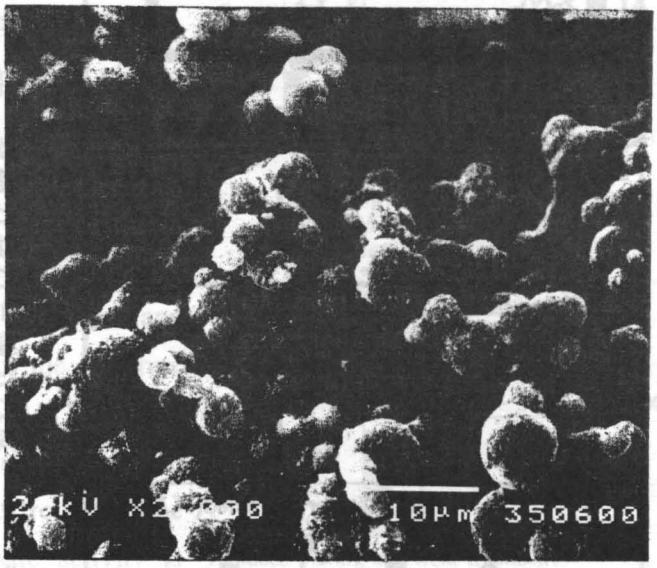

図 1. 炭素に包まれた粒子の SEM 写真

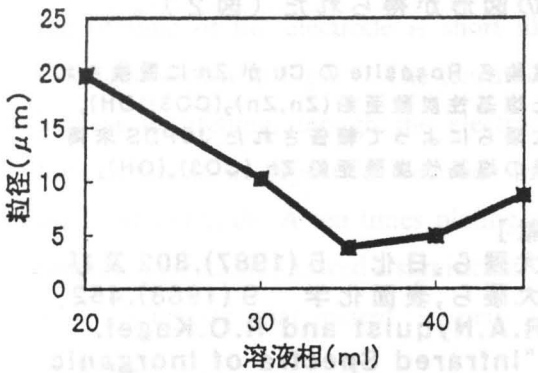

図2，エマルジョン液と最頻粒径の関係

Composition Control of Sol-Gel Derived $Pb(Zr_X Ti_{1-X})O_3$ Thin Films with Multi-Seeding Layers

○Y. KONDO, H. SUZUKI, S. KANEKO (Shizuoka University)

T. HAYASHI (Shonan Institute of Technology)

ABSTRACT

Ferroelectric lead zirconate titanate, $Pb(Zr_X Ti_{1-X})O_3$ (hereafter abbreviated as PZT), thin films have been attracting wide interest due to their high potential for various applications such as in optical modulator, non-volatile semiconductor memories and in high-frequency surface acoustic wave (SAW) devices. In the previous paper, perovskite PZT thin films with multi-layered structures were prepared at low temperatures by the dip-coating method from alkoxide precursor solutions [1, 2]. However in the multi- seeding process, the compositions of the resultant PZT thin film should be modified by controlling the multi-layered structures of the precursor films to improve the electrical properties of the resultant films.

In this study, ferroelectric PZT thin films were prepared by annealing the precursor films with different compositions (X) and multi-layered structures from alkoxide precursor solutions, to lower the processing temperature. Effects of compositions and stacking structures of the multi-layered precursors on the crystallization behavior were studied to improve the electrical properties of the resultant PZT thin films. Alkoxide-derived lead titanate (hereafter abbreviated as PT) thin film with different thickness, of which the crystallization into perovskite phase completed at 450℃, were inserted between every PZT precursor layers with different compositions ranging from X=1 to 0.53 (multi-seeding process). In this process, the compositions of the PZT precursors and/or stackingstructures, as well as the heating schedule, have large effect on the crystallization behavior. As a result, nucleation control of the PT seeding layer by changing the heating schedules played an important role to prepare perovskite PZT thin films at low temperatures. Dielectric properties of the resultant films depended upon the compositions and annealing temperatures. The relative permittivities of the resultant films with thickness of about 500 nm were shown in figure 1. The relative permittivity of the resultant film increased with annealing temperature. Distinct effect of the heating rate on the dielectric property did not observed in this study. However, the nominal composition of the resultant thin film exhibited considerable effect, especially at high temperature annealing of 600 ℃.The maximum of the relative permittivity was obtained at the composition of a morphotropic phase boundary (nominal composition of X=0.53). This result indicated that the composition of the resultant film was controllable in the multi-seeding process.

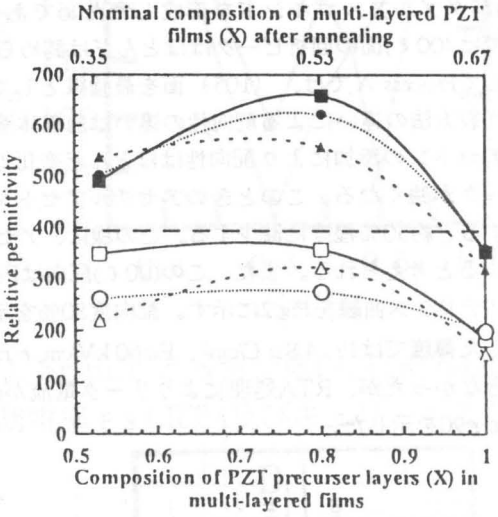

Fig.1 Relative permittivity of the resultant PZT thin films with different compositions.
■:annealed at 600℃ with heating rate of 100℃/h
●:annealed at 600℃ with heating rate of 600℃/h
▲:annealed at 600℃ with heating rate of 3000℃/h
□:annealed at 500℃ with heating rate of 100℃/h
○:annealed at 500℃ with heating rate of 600℃/h
△:annealed at 500℃ with heating rate of 3000℃/h

[1] H.Suzuki et al, Jpn. J. Appl. Phys. 35, p.4896 (1996)
[2] H.Suzuki et al, Jpn. J. Appl. Phys. 36, p.5803 (1997)

ゾル・ゲル法で作製した$SrBi_2Ta_2O_9$薄膜の配向性と強誘電特性

（湘南工科大学）○原　拓也・林　卓

【緒言】

近年、PZTや$SrBi_2Ta_2O_9$,$Bi_4Ti_3O_{12}$などのビスマス層状強誘電体はその自発分極を利用した不揮発性メモリへの応用が盛んに研究されている。特にBLSF薄膜は、繰り返し分極反転による残留分極値の低下、すなわち疲労が殆ど生じないという特徴を持ち様々な方法で作製されてきた。特に$SrBi_2Ta_2O_9$(SBT)は、c軸方向に大きな異方性を持ち、分極方向がa,b軸方向のみに存在するという特徴を有する。しかしながら、これまでに報告されてきた$SrBi_2Ta_2O_9$薄膜の配向性は粉末と類似した回折パターンしか得られていない。本研究では、前駆体溶液の分子設計が可能な金属アルコキシドを用いたゾル・ゲル法によりSBT薄膜を作製し、全駆体溶液作成時におけるアセチルアセトンの添加および混合方法が$SrBi_2Ta_2O_9$薄膜の配向性および強誘電特性に与える影響について調べた。

【実験方法】

SBT前駆体溶液の出発原料には$Sr(O\text{-}n\text{-}Bu)_2$, $Bi(O\text{-}i\text{-}Pr)_3$, $Ta(OEt)_5$、溶媒として2-メトキシエタノールを使用した。前駆体溶液の作製は、以下の2通りの方法で作製した。まずProcess Aは$Sr(O\text{-}n\text{-}Bu)_2$と$Ta(OEt)_5$を混合、溶解した後$Bi(O\text{-}i\text{-}Pr)_3$を混合する方法であり、Process Bは$Sr(O\text{-}n\text{-}Bu)_2$と$Bi(O\text{-}i\text{-}Pr)_3$を混合、溶解した後$Ta(OEt)_5$を混合する方法である。Process A,Bともにアセチルアセトンは、Biアルコキシドおよび Bi-Sr混合アルコキシド溶液に対して所定量添加した。また、Process Bに対してはアセチルアセトンの添加量を変化させた。組成は$Sr_{0.7}Bi_{2.2}Ta_2O_9$とした。

これらの前駆体溶液をPt/Ti/SiO_2/Si基板上にスピンコートし500℃，5分間の仮焼を行い、この行程を繰り返した後800℃,1時間の焼成を行い薄膜を得た。また幾つかの試料に対しては、赤外線加熱炉（RTA）を用いた。得られた薄膜の結晶性，配向性をXRD、微構造をFE-SEMによって調べ、誘電率をインピーダンスアナライザー、ヒステリシス曲線をRT-66Aを用いて測定した。

【実験結果】

一般にBiアルコキシドは難溶性であるがSrアルコキシドと混合することで、容易に溶解した。これは$Sr(O\text{-}n\text{-}Bu)_2$と$Bi(O\text{-}i\text{-}Pr)_3$がダブルアルコキシドを形成したためである。それぞれの前駆体溶液より作製した薄膜のXRD図形は、Process Bでは(00ℓ)面の回折ピークはほとんどは認められず（105）面を最強線とした無配向回折図形から成っている、これに対してProcess Aでは、（105）面を最強線としているが(00ℓ)面の回折ピークも多く確認できる。この様な前駆体溶液の作製方法の違いによる配向性の違いは前駆体溶液中の構造に起因していると考えられる。また、Process Aではアセチルアセトンの添加により配向性はほとんど変化しないが、Process Bではアセチルアセトンを添加すると(00ℓ)面の回折ピークが強くなる。このときのアセチルアセトン添加量と配向度,F,の関係は、AcAc/Bi=0.3で80%を示し、それ以上添加すると約50%程度に減少する。この様に、アセチルアセトンの添加は、Sr-Biダブルアルコキシドの構造に影響を与えていると考えられる。また、この(00ℓ)配向はFig.1に示すようにガラス基板上においても認められた。作製した薄膜のヒステリシス曲線をFig.2に示す。配向度80%を示した薄膜では、Pr : 1.6 μ C/cm^2, Ec : 110kV/cm, ε r : 78、配向度46%を示した薄膜ではPr : 4.8 μ C/cm^2, Ec:60 kV/cm, ε r:220であった。配向度0%を示した試料では、リーク電流が大きく測定できなかったが、RTA処理によりリーク電流が改善された。このとき薄膜の誘電特性は、Pr : 6.5 μ C/cm^2 Ec : 80kV/cm, ε r:90を示した。

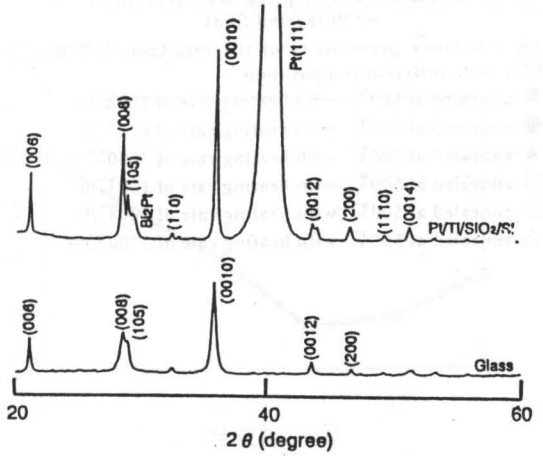

Fig. 1　XRD patterns of SBT thin films prepared on Pt/Ti/SiO_2/Si at 800℃ for 1h and glass at 750℃ for 1h.

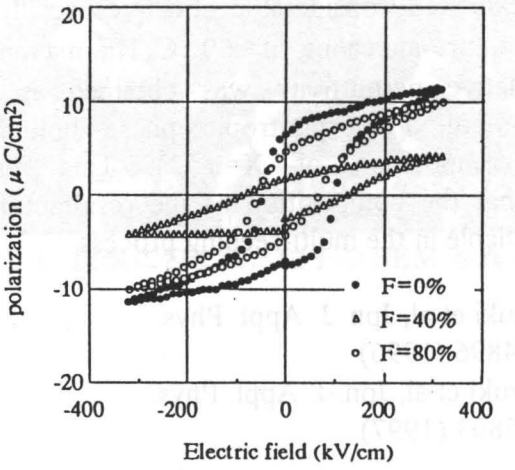

Fig.2　P-E hysteresis loops of SBT thin films prepared by furnace annealing or RTA in process B.
(a) F=43%, Furnace　(b) F=80%, Furnace
(c) F=0 %, RTA

ビスマス層状構造酸化物の強誘電特性

(東理大・理工) ○小村 恭、竹中 正

1. はじめに

近年、一般式 $(Bi_2O_2)^{2+}(A_{m-1}B_mO_{3m+1})^{2-}$ で表されるビスマス層状構造強誘電体薄膜の FRAM 応用が注目されている。その中で、$SrBi_2Ta_2O_9$ (SBT) 薄膜が良い特性を示し、一部実用化されている。しかし、SBT 薄膜は多くの研究者によって様々な特性が報告されているが、統一的な特性、例えばSr/Bi 比による残留分極値 Pr の違いなどは必ずしも明らかではない。

本研究では、SBT セラミックスを用いて、SBT の基本特性を得る目的で、Sr/Bi/Ta 比と、その物理的及び電気的特性との関係を調べた。

2. 実験方法

SBT セラミックス試料は普通焼成法(OF 法)により作製した。出発原料に $SrCO_3$、Bi_2O_3、及び Ta_2O_5 を使用して、$a\,SrCO_3 + b\,Bi_2O_3 + c\,Ta_2O_5 \rightarrow SrBi_2Ta_2O_9 + a\,CO_2$ として、その仕込み量 a、b、c を変化させて秤量し、ボールミルで10h 湿式混合後、800℃で2時間仮焼した。その後、ボールミルで 20h 湿式粉砕後、1250℃で2時間本焼を行ない、セラミックス試料を得た。得られた試料の粉末X線回折を行ない、強誘電的性質を中心とする電気的諸特性を通常の方法により調べた。

3. 結果

図 1 に Sr/Bi と残留分極 Pr、抗電界 Ec、室温での比誘電率 ε_s 及びキュリー温度 Tc との関係を示す。これにより化学量論比 (Sr/Bi = 0.5) において Pr が最も大きく、また Tc は Bi が増加していくにつれて高温側にシフトすることがわかった。また図 2 に Sr/Bi = 0.5 (化学量論比) の D-E ヒステリシスループを示す。今後は、SBT の粒子配向試料を作製し、粒子配向度と電気的諸特性の関係を調べる必要があろう。

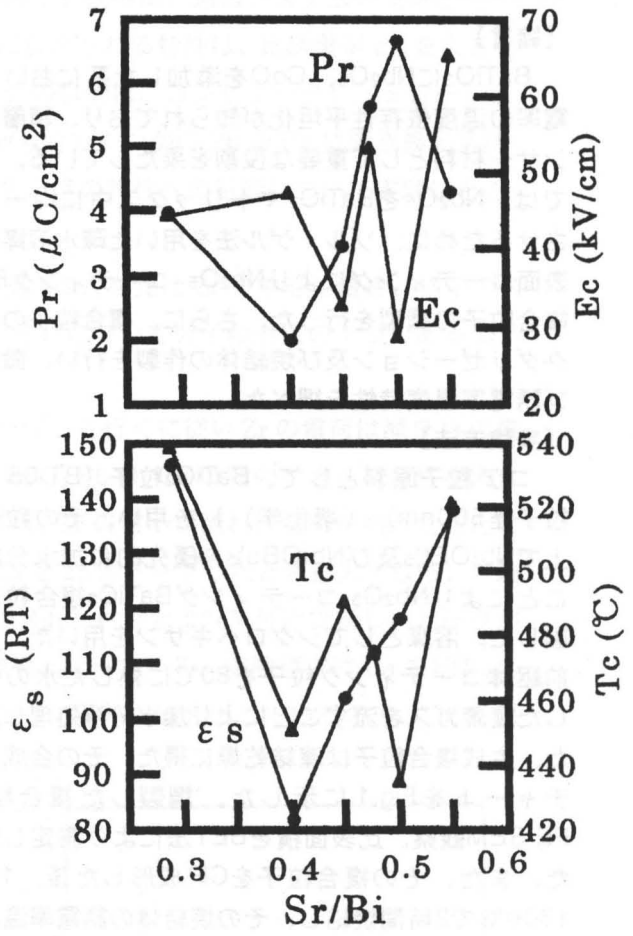

図 1. Sr/Bi比 と残留分極Pr, 抗電界Ec,室温での比誘電率 εs (RT)及びキュリー温度 Tcとの関係

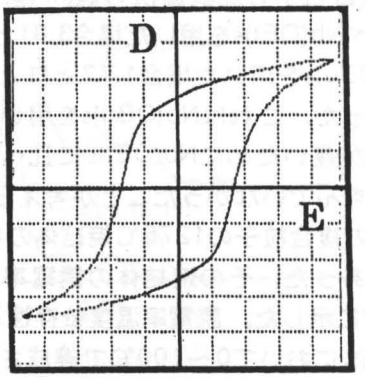

Ec=28.7 (kV/cm)

Pr=6.7 (μC/cm²)

図 2 Sr/Bi =0.5のD-Eヒステリシスループ

疎水性溶媒における金属アルコキシドを用いた Nb_2O_5-コーティング$BaTiO_3$複合粒子の合成と評価

（湘南工科大）○須永孝一・林卓　（元 デュポン）佐々木昌一

Preparation and properties of Nb_2O_5-coated $BaTiO_3$ composite particles using metal alkoxide in hydrophobic solvent.

○K.Sunaga,T.Hayashi (Shonan Institute of Technology), K.Sasaki (former DuPont)

【緒言】

$BaTiO_3$にNb_2O_5，CoOを添加した系において、誘電率の温度依存性平坦化が知られており、積層コンデンサー材料として重要な役割を果たしている。本研究では、Nb_2O_5を$BaTiO_3$マトリックス中に均一に分散させるために、ゾル・ゲル法を用いた疎水溶媒中での表面コーティングによりNb_2O_5-コーティング$BaTiO_3$複合粒子の調製を行った。さらに、複合粒子のキャラクタリゼーション及び焼結体の作製を行い、微構造及び誘電率温度特性を調べた。

【実験方法】

コア粒子原料として、$BaTiO_3$粒子｛BT-05（平均粒子径500nm）（堺化学）｝を用い、その粒子表面上で$Nb(OEt)_5$及び$Nb(OBu)_5$を優先的に加水分解することによりNb_2O_5-コーティング$BaTiO_3$複合粒子を調製した。溶媒としてシクロヘキサンを用いた。また、前駆体コーティング粒子を80℃に熱した水の中を通した窒素ガスを流すことにより加水分解処理した。また、生成複合粒子は凍結乾燥に得た。その合成フローチャートをFig.1に示した。調製した複合粒子をFE-SEM観察，比表面積をBET法により測定し評価した。また、その複合粒子をCIP成形した後、1250～1300℃で2時間焼結し、その焼結体の誘電率温度依存性を調べた。微構造はFE-SEM観察を行った。

【結果】

複合粒子の比表面積の値(m^2/g)は出発原料の1.64に比べ$Nb(OEt)_5$を用いた場合3.01と大きくなったが、$Nb(OBu)_5$を用いた場合1.77とほとんど変化が見られなかった。これは$Nb(OBu)_5$を用いた場合、加水分解速度が遅いために$Nb(OEt)_5$に比べて加水分解が十分にすすんでいなかったことが考えられる。また、それぞれの複合粒子の1275℃焼結体の相対密度は93～95％であった。その焼結体の誘電率温度特性の結果をFig.2に示した。誘電率温度依存性平坦化は、1275℃焼結体において0～100℃で達成されており、焼結体の室温での誘電率は約4600と高い値を示した。また、その焼結体の$BaTiO_3$粒径は約700nmであり、出発原料である$BaTiO_3$焼結体の粒径1.5～2.0μmに比べ、粒界に存在するNb_2O_5により粒成長が著しく抑制された。

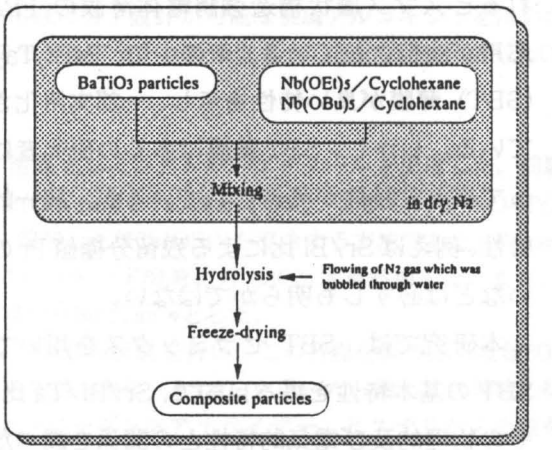

Fig.1 Flow diagram of preparation of Nb_2O_5-coated $BaTiO_3$ composite powders.

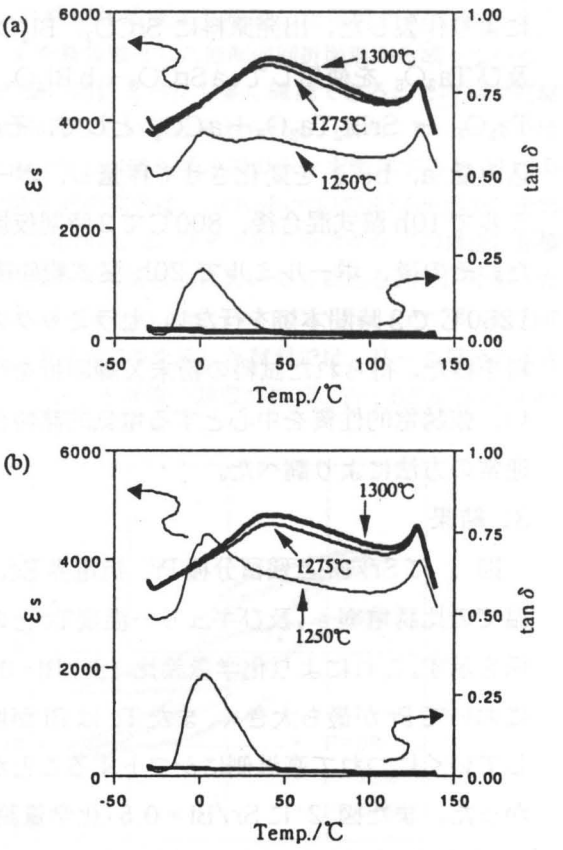

Fig.2 Temperature dependence of dielectric constant of 1wt% Nb_2O_5-doped $BaTiO_3$ bodies sintered at 1250～1300℃ for 2h.
(a) using $Nb(OEt)_5$　(b) using $Nb(OBu)_5$

反強誘電体へのカルシウム添加による電子構造とマイクロ波特性

（湘南工科大）杉原　淳・○藤田昌樹・細谷　朗
（静大）関根理香

【諸言】　誘電体セラミックスをマイクロ波帯に応用する技術は、通信システムの発達とともに活発化している。マイクロ波誘電体セラミックスに要求される特性は、比誘電率 ε_r を大きくすること、またQ値を大きくする必要がある。本研究の目的は、コンピュータシュミレーションであるDV-X α法を用い、反強誘電体である$PbZrO_3$のいくつかのPbをCaに置き換え常誘電体化させた$(Pb_X,Ca_{1-X})ZrO_3$の電子構造を求め、そのときの物性への影響について実験値との関係をを解明することである。

【計算】　クラスター設計は、 $PbZrO_3$の原子間距離 4.2Åを元にZrを中心に置き、格子の角にある8個のPbをCaで置換して行く構造とした。それについて分子軌道法の1つであるDV-X α法を用いて、第一原理計算を行った。

【結果および考察】　有効電荷においてはCaをドープして行くに従いZrの電荷は減りOの電荷が増えて行く。クーロン引力相互作用においてはZr-O, Pb-O, Ca-O間のイオン結合性が大きくなる。これらの原因はCaをドープしたことよりOにZrの電子が流れ、電荷が増えたことによるものと考えられる。Zr-Pb間の共有結合性は、Caを25％ドープしたとき最大となる。理論XPSをFig.1に示す。Caを25％ドープしたときには-14eV付近と-23eV付近で新しいピークが見られる。これは、実験のXPS測定値と一致した結果となっている。実験値ではCaを約25％ドープした試料が、マイクロ波誘電体セラミックスとして優れた値を出しているので、この結果と関連性があるのではないかと考えられる。

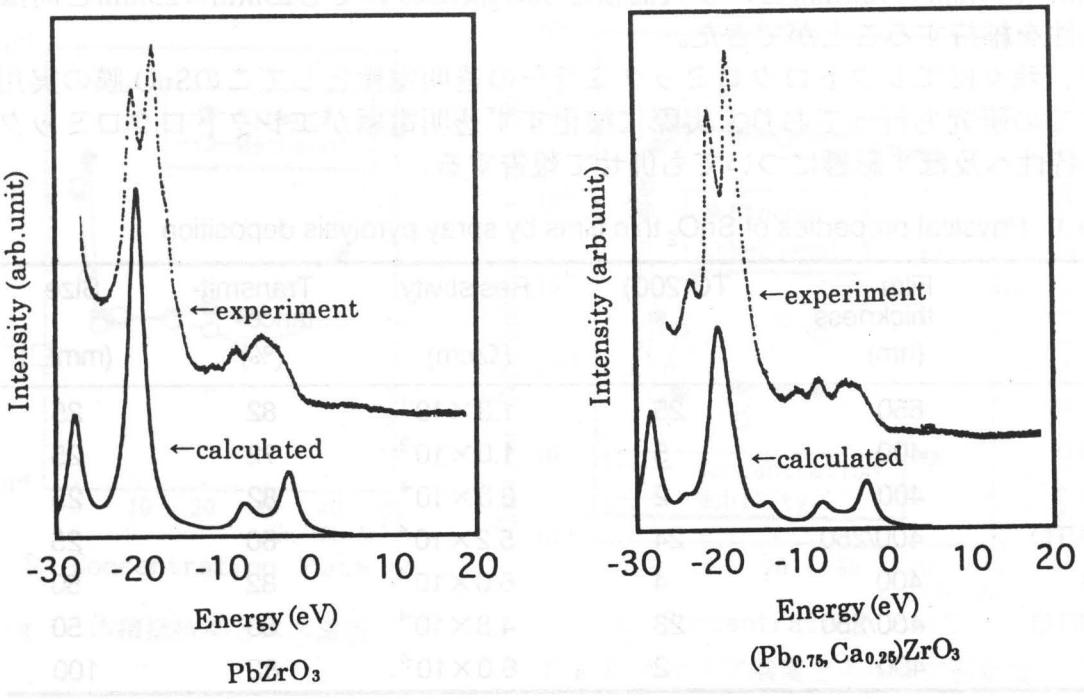

Fig.1　XPS spectra $PbZrO_3$ and $(Pb_{0.75},Ca_{0.25})ZrO_3$.

スプレー熱分解法(SPD)による大面積酸化すず系透明導電膜の作製

○中島清文・小杉津代志・持塚多久男**・深澤彰彦**・村上健司*・金子正治
(静岡大工・*電子研・**村上開明堂)

酸化すずは3eV以上の広いバンドギャップを有するため可視光領域において高い光透明性を示す。また、酸素空孔を持つためにn型の半導体となる。さらに機械的強度が大きく化学的安定性も高い。これらの性質を利用して、SnO_2膜は電子デバイスの透明電極などに用いられている。

SnO_2膜を作製する際に有機金属化合物の$(C_4H_9)_2Sn(OOCCH_3)_2$(di-n-butyltin diacetate : DBTDA)を原料にしてスプレー熱分解法を用いると(200)面に選択配向した酸化すず(TO)薄膜が得られた。このような高配向性の膜を作製することによって薄膜結晶基板としての応用が期待できる。この膜の透過率は82%、抵抗率は$10^{-1}\Omega$cmとなった。そこで、更なる低抵抗化のために、SnO_2膜にSbやFをドープした。その結果、Sbをドープした酸化すず(ATO)膜では抵抗率$1\times10^{-3}\Omega$cm、Fをドープした酸化すず(FTO)膜では$6.8\times10^{-3}\Omega$cmの抵抗率となり、低抵抗を示す膜が作製できた。しかし、同時にSbやFをドープするにつれ(200)面の選択配向性が減少した。このため、あらかじめガラス基板上にドープしていないTO膜を作製し、その上にドープしたATO膜やFTO膜を形成することで、配向性、電気伝導性、光透過性のすべて優れた膜を得ることができた。

電子デバイスの大型化に伴い、大面積基板上への薄膜の作製が要求されている。本研究で作製の際に用いたスプレー熱分解法は比較的簡単な装置で大面積化が可能であるので、次に酸化すず薄膜の大面積化を目指した。具体的にはこれまで作製してきた25mm×25mmの他に50mm×50mm、100mm×100mmのSnO_2膜の作製を試み、配向性、電気特性、透明性について比較、検討を行った(Table 1)。その結果、50mm×50mm、100mm×100mmという大面積なSnO_2膜においても25mm×25mmと同様な高い特性を維持することができた。

最近、我々はエレクトロクロミックミラーの透明電極としてこのSnO_2膜の実用化に向けての研究も行っており、実際に酸化すず透明電極がエレクトロクロミックミラーの特性へ及ぼす影響についても併せて報告する。

Table 1 Physical properties of SnO_2 thin films by spray pyrolysis deposition

Film	Film thickness (nm)	TC(200)	Resistivity (Ωcm)	Transmittance (%)	Size (mm□)
TO	650	25	1.3×10^{-1}	82	25
ATO	400	5	1.0×10^{-3}	72	25
FTO	400	2	6.8×10^{-4}	82	25
FTO/TO	400/250	24	5.2×10^{-4}	80	25
FTO	400	4	6.0×10^{-4}	82	50
FTO/TO	400/250	23	4.8×10^{-4}	83	50
FTO	400	2	6.0×10^{-4}	82	100

TO : Tin Oxide; ATO : Antimony-doped TO; FTO : Fluorine-doped TO; FTO/TO : FTO prepared on TO

酢酸塩を原料としたＩＴＯ薄膜：ディップコート法による作製と評価

ITO thin films prepared by dip-coating with indium and tin acetate

東京工芸大学　　○山口　文親　　澤田　豊

Tokyo Institute of Polytechnics　　YAMAGUCHI Fumichika, Yutaka SAWADA

[背景・目的]

ディップコート法によるＩＴＯ薄膜作製の研究は従来からなされ、良好な薄膜が得られることが確認されおり、原料には酢酸インジウムを主として、アルコキシドなどが用いられていた[1)]。今回、さらなる良好化と低コスト化をはかるため、酢酸インジウム［$In(OH)(CH_3COO)_2$］および、酢酸スズ［$Sn(CH_3COO)_2$］、メタノールまたはエタノール(溶剤)、モノエタノールアミン(安定化剤)を用いて実験を行い、ＩＴＯ薄膜の作製と評価を行った。また、高濃度のスズを添加した場合の薄膜についても実験を行った。

[実験方法]

無アルカリガラス(Corning#7059)を基板とし、酢酸インジウムと酢酸スズを様々な割合で混合し、溶剤と安定化剤を加えディップ溶液とした。この溶液に基板を浸し一定の速度で引き上げ、電気炉を用いて還元雰囲気(窒素ガス中)で約６５０℃、１時間焼成した。(焼成後自然冷却させ、分光透過率、Ｘ線回折、蛍光Ｘ線、ホール測定などを行った。)

[結果]

薄膜の電気的特性を図１，２に示す。薄膜中のスズ濃度は調査中(図中のスズ濃度は添加量)であるが、高スズ濃度(約 30at%)においても体積抵抗率の減少が見られず、ほぼ横ばいとなった。　分光光度計により薄膜は８０%以上の可視光透過率を示した。　薄膜は一様に酸化インジウムのＸ線回折ピークを示した。メタノール溶媒に比べエタノール溶媒の方がスズ添加濃度に比例して膜厚が厚くなることが確認された。

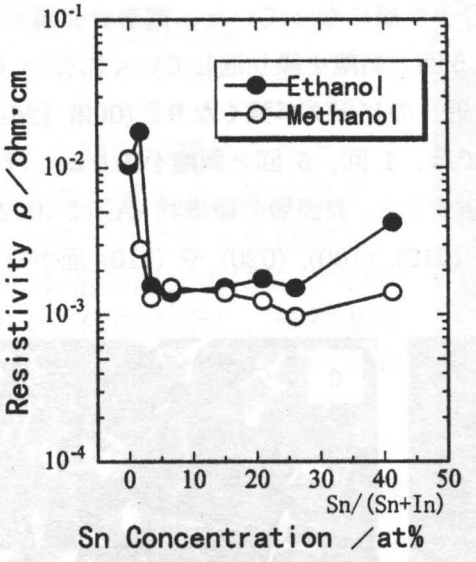

Fig 1: 体積抵抗率とスズ濃度

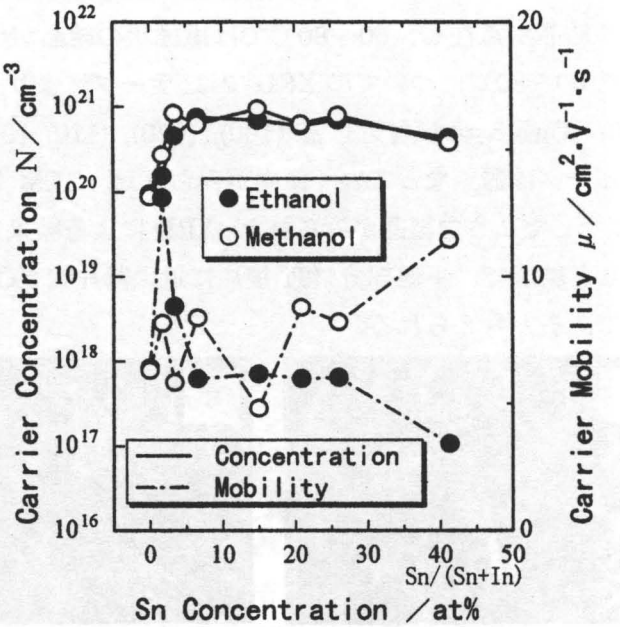

Fig 2: キャリア濃度とキャリア易動度

1)渡邉　智貴　東京工芸大学大学院１９９６年度修士論文

リン酸カルシウム電着層の表面および内部の微細組織

（工学院大・工）○根元央希・門間英毅・高橋　聡・小林偉男

Microstructures of the Surface and Inside of Electrodeposited Calcium Phosphates /

○O.Nemoto, H.Monma, S.Takahashi, H.Kobayashi (Faculty of Eng. Kogakuin Univ.) /

Microstructures of the surface and inside of calcium phosphates electrolytically deposited on a Ti substrate were investigated. Gradual changes in the shape of grains deposited were observed from the surface into the inside. Grains on the surface were fiber-like crystals elongating to the (002) of the OCP structure, whereas the inside grains were thin plate crystals developing the (010), (100), (020) and (110).

1.緒　言　各種リン酸カルシウム系化合物は、生体親和性に優れているために生体材料として期待されているが、高負荷のかかる骨や歯への応用を考慮した場合、これらの単独の焼結体だけでは十分な機械的強度が得られない。そのため金属表面にリン酸カルシウム系化合物をコーティングして、生体親和性と機械的強度を兼ね備えた生体材料を作製する研究が行われており、そのコーティングの方法の中でも比較的温和な条件で実施できる電解電着法が注目されている。本研究では、先述の方法で Ti 板上に電着させたリン酸カルシウム層の表面、および内部の微細組織について検討した。

2.実験方法　電極としてアノードに Pt 板、カソードに Ti 板を使用し、電解液には 0.02mol·dm^{-3} の MCP〔Monocalcium Phosphate : $Ca(H_2PO_4)_2 \cdot H_2O$〕水溶液を使用した。電解の条件は温度：50～80℃、電流密度：0.5mA·cm^{-2}、時間：30min に設定して電着を行った。

各電着物の表面層を Scotch クリアーテープにより 1 回の場合と 5 回の場合で剥離させて、電着表面と内部の微細組織について XRD および SEM を用いてキャラクタリゼーションを行った。

3.結果および考察　電着の表面層は XRD により、50℃で一部ブラッシャイト〔Brushite : $CaHPO_4 \cdot 2H_2O$〕と OCP〔Octacalcium Phosphate : $Ca_8H_2(PO_4)_6 \cdot 5H_2O$〕、60～80℃については OCP であることを確認した。これらの表面層の形態は、50℃では花びら状やフレーク状の結晶が凝集した層に大きな板状の結晶が点在し、60～80℃では繊維状の結晶が絡み合った層になっていた。電着表面層が均一であった 60～80℃についての XRD では、テープにより 1 回、5 回と剥離を繰り返していくに従い、OCP の (010)〔CuKα=4 度付近〕と (100), (020), (110)〔9 度付近〕のピークが強くなり、(002)〔26 度付近〕のピークは弱くなっていく傾向がみられた。SEM 観察では、1 回、5 回と剥離を繰り返し行うと Fig.1 に示したような結晶がみられた。XRD による結果を考慮すると、表面層の繊維状 (A) は (002) 面が成長した結晶で、下地部分（Ti 板）に近い薄片状 (C) は (010), (100), (020) や (110) 面が成長した結晶であると考えられる。

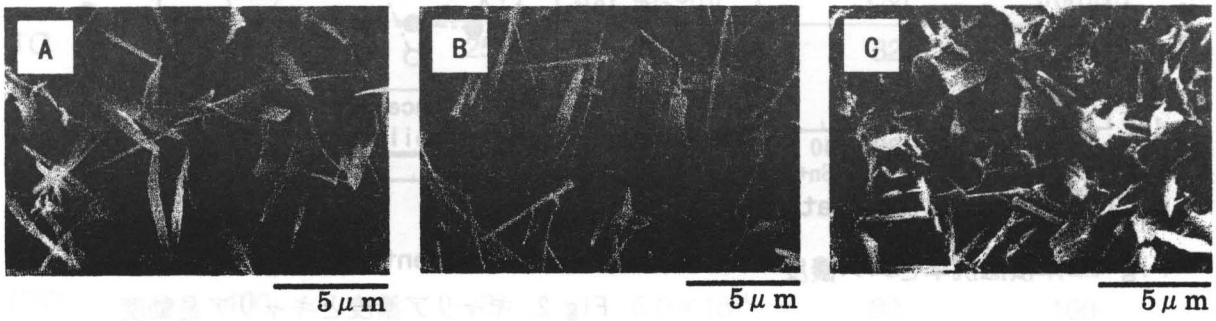

Fig. 1 SEM photographs electrodeposited calcium phosphates at 70℃.(A:Surface, B: Surface layer was torn once with Scotch tape, C: Surface layer was torn five times with Scotch tape)

CrB_2-MoB_2 複合セラミックスの焼結とその性質

（東京工芸大学・工）　○前澤　大輔、村上　真之、飯泉　清賢、久高　克也
（国士舘大学・工）　岡田　繁

Sintering and Properties of CrB_2-MoB_2 composite.

(Faculty of Engineering , Tokyo Institute of Polytechnics and Faculty of Engineering,KokushikanUniversity) Maezawa,Daisuke; Murakami,Masayuki;Iizumi,Kiyokata;Kudaka,Katsuya;Okada,Shigeru.

【緒言】　クロムホウ化物は一般的に高融点、高硬度、電気伝導性を有する化合物であり、高温強度材料の素材として期待される。その中で特に CrB_2 は耐熱性、耐薬品性、耐摩耗性に優れているが、難焼結性の化合物である。一方、MoB_2 もまた高融点、高硬度をもつホウ化物で、CrB_2 と同じ結晶構造（六方晶）をもっている。そこで CrB_2 に MoB_2 を加えることにより、焼結性を促進し、かつ高硬度、高強度の複合セラミックスが得られると期待される。本研究では CrB_2-MoB_2 系複合セラミックスのホットプレスをおこない、焼結体の微細構造、機械的性質、酸化特性等について調べることを目的とした。

【実験】　出発原料は CrB_2 粉末、Mo 粉末、B 粉末を使用し、MoB_2 の量が 20、40、60、80mol%となるように原料を配合した。所定の割合に配合した粉末を遊星型ボールミルを使用して、それぞれ 20 分間混合粉砕した。この粉末を黒鉛製のモールドに入れ、真空（$\times 10^{-3}$Pa）中、プレス圧を約 50MPa にして 1600－1800℃で 1 時間ホットプレスをおこなった。得られた焼結体について硬度、破壊靱性値の測定、水酸化カリウム水溶液で電解エッチングした後、SEM による微細構造の観察をおこない、さらに焼結体を空気中で種々の温度、時間で加熱し酸化挙動について調べた。

【結果】　焼結体の平均粒径は、焼結温度が上昇するに従って増加し、MoB_2 量が増えるにつれ減少する傾向が認められた。焼結体の硬さは、焼結温度が上昇するに従って増加し、MoB_2 量が増えるに従って増加する傾向を示し、焼結温度 1700℃、MoB_2 量が 60%の時に最大 26.4GPa を示した。MoB_2 量 60%までの焼結体の空気中における加熱による重量変化はほとんど差はなかったが、MoB_2 量 80%のとき 900℃の加熱で著しい重量減少が認められた。

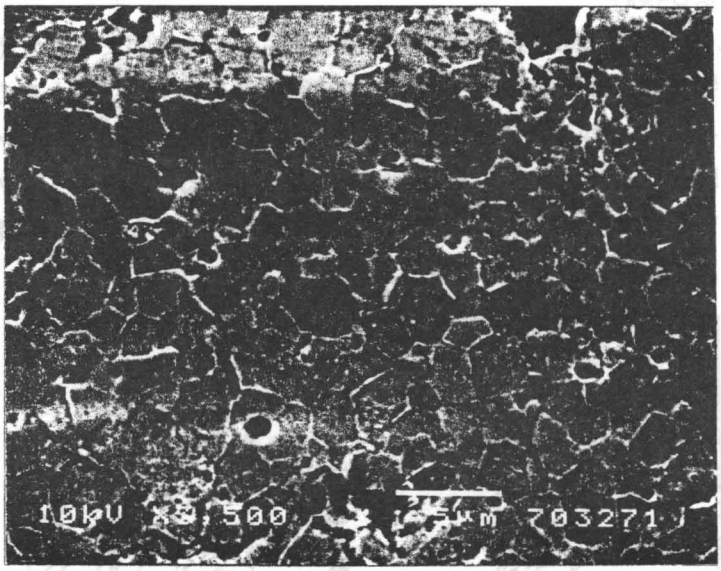

図 1. 1800℃で焼結した CrB_2-MoB_2(60%) セラミックスの微細構造

$PbCrO_4$-BaO 系厚膜素子の感湿特性

Humidity-Sensitive Characteristics of $PbCrO_4$-BaO Thick Film Elements

（関東学院大学）○前田　邦宏　難波　典之　（湘南工科大学）金子　文隆

1.はじめに

セラミックス湿度センサはセラミックス表面への水蒸気の吸着・脱離により電気抵抗が変化することを利用している。従来のセラミックス湿度センサは主に気孔分布を制御し、毛細管凝縮による水蒸気吸着が電気抵抗を変化させる現象を応用した気孔制御型湿度センサである。これに対してクロム酸鉛系湿度センサは、母体となるクロム酸鉛が持つ特性を利用した母体制御型湿度センサ材料である。クロム酸鉛には湿度に対して感度の低いクロムイエロ（$PbCrO_4$）と感度の高いクロムレッド（Pb_2CrO_5）がある（図1）。クロムイエロをクロムレッドに変えるために種々の酸化物が組み合わせされている（図2）。しかし酸化バリウム（BaO）を組み合わせた場合、これまでのものと異なった特性を示した。このことに着目し、酸化バリウムの混合比を変えた場合の感湿特性および生成成分の関係を調べた。

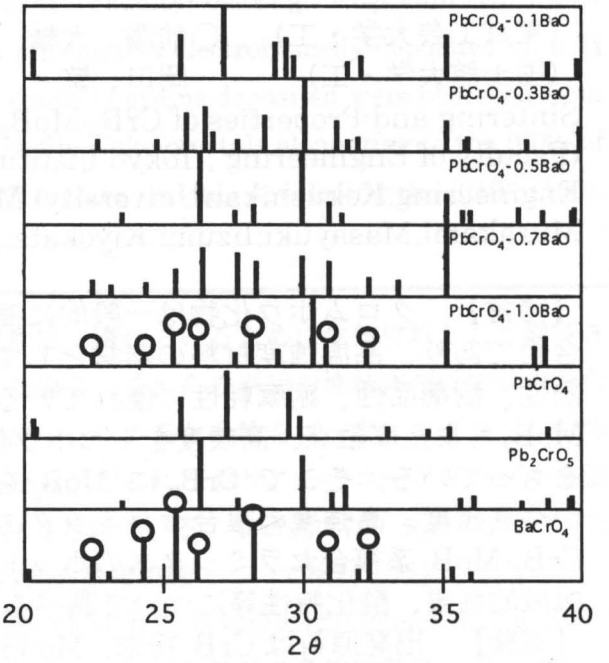

図4　X線回折像

2.実験方法

クロム酸鉛（$PbCrO_4$）に対して酸化バリウム（BaO）が所定のモル比になるように炭酸バリウム（$BaCO_3$）を組み合わせた。今回の混合比は0.1、0.3、0.5、0.7、1.0mol比とした。この粉末を750℃で焼成後、粉砕し印刷原料としペーストを作製した。これらを櫛形電極上に印刷し675℃～750℃で30分熱処理を行い、できあがった素子の感湿特性と生成成分を調べた。

3.結果および検討

図3に$PbCrO_4$-nBaO系厚膜素子の感湿特性を示す。図より混合比による感湿特性への影響は殆ど見られず、感湿特性はほぼ一致した。図4にX線回折像を示す。このときの生成成分を調べると0.1mol比のときはクロムイエロ（$PbCrO_4$）、0.3mol比、0.5mol比のときはクロムレッド（Pb_2CrO_5）、0.7mol比、1.0mol比のときはクロム酸バリウム（$BaCrO_4$）となっている。このようにクロム酸バリウムが主成分となった素子においてもこれまでと同様な感湿特性を得られたことから、クロム酸バリウム（$BaCrO_4$）は新しい母体制御型湿度センサ材料として期待できる。

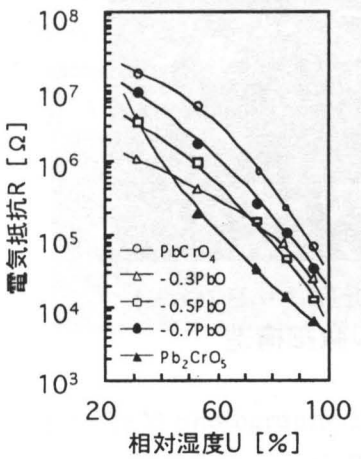

図1　$PbCrO_4$-nPbO系厚膜素子の感湿特性

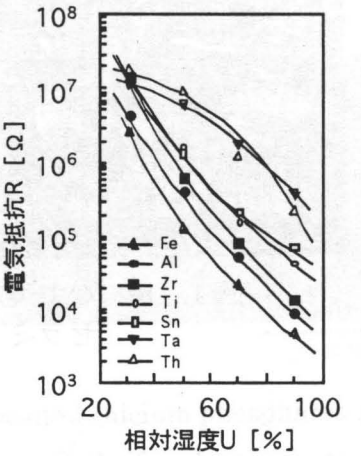

図2　$PbCrO_4$-MO系厚膜素子の感湿特性

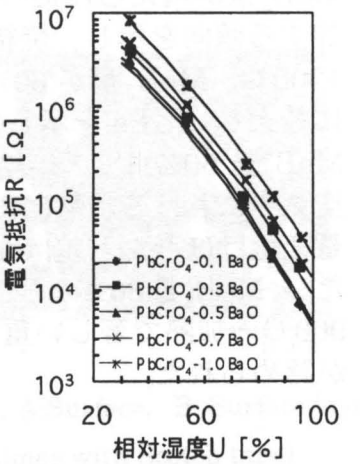

図3　$PbCrO_4$-nBaO系厚膜素子の感湿特性

Study of Carrier-Doping Mechanism in $Sr_{1-x}CuO_2$, $(Sr_{1-y}La_y)CuO_2$ Infinite Layer Films

N. Terada, ○T. Uchida*, Y. Suganuma*, N. Yoshiyama*, H. Yamamoto*, H. Ihara

Electrotechnical Laboratory, 1-1-4 Umezono, Tsukuba, Ibaraki 305, Japan
Nihon University, 7-24-1 Narashinodai, Funabashi, Chiba 274, Japan*

Infinite-layer $SrCuO_2$ is characterized by its crystal structure common to most of high temperature superconducting cuprates (HTSC) and a possibility of both hole- and electron-doping. These features rise importance of preparation of its epitaxial films with various carrier-concentrations and characterization of their intrinsic electronic structure, in order to systematically explicate doping-mechanism of HTSC. In this paper, we report *in-situ* photoemission study of clean surfaces of epitaxial films with the infinite-layer structure prepared by multi-target sputtering and MBE.

Holes and electrons are doped into the $SrCuO_2$ by an introduction of Sr-vacancy and a partial substitution of La for Sr, respectively. For non-doped, that is stoichiometric, specimen, an insulator-like gap-structure was observed. An introduction of either holes or electrons more than 0.06 per unit-cell results in a development of metallic feature. In such regions, photoelectron Fermi edge has been clearly observed. Figure shows a relationship between an electron-energy of Cu 3d signal and a change of electron occupation per unit cell. Origin in this figure is set at the energy of the Cu 3d signal of the stoichiometric sample.

Within each of metallic regions, the Cu 3d peak continuously goes away from Fermi level by a decrease of hole-density and an increase of electron-one. The increase of the electron occupation from -0.2 (hole-doped region) to +0.12 electrons/unit-cell results in a reduction of the energy of the Cu 3d signal by 0.35 eV. An expected shift in rigid-band model based on a band structure calculated by full-potential linearized augmented plane wave method (FLAPW) is about -0.30 eV for the corresponding rise of the electron occupation. This agreements suggests that band-filling should play a certain role in the metallic regions.

On the other hand, the discontinuities of the Cu 3d energy about 0.30 eV was observed around the boundaries between metallic and insulating regions. For the Cu 2p signal, it is observed a similar change to that of the Cu 3d signal, though the shift was about a half of that of the Cu 3d. C 1s and Sr 3d core signals did not exhibit a shift. The latter result means that the discontinuities should not be caused by charging-effect. These results indicate that the observed change of electronic structure around the boundaries should be an intrinsic feature in the infinite layer, and that this phenomenon might relate to a disappearance of anti-ferromagnetism and enhancement of screening effect by the doping.

The above results are obtained on the specimen grown by multi-target sputtering, where hole-density was limited up to +0.2 holes/unit-cell. The MBE growth under a lower temperature enables to obtain the samples with higher oxygen content, which is confirmed by a c-axis length longer than that of the sputtered samples. A study of the systematization of the change of the electronic structure of the $SrCuO_2$ towards a region of higher hole concentration is in progress.

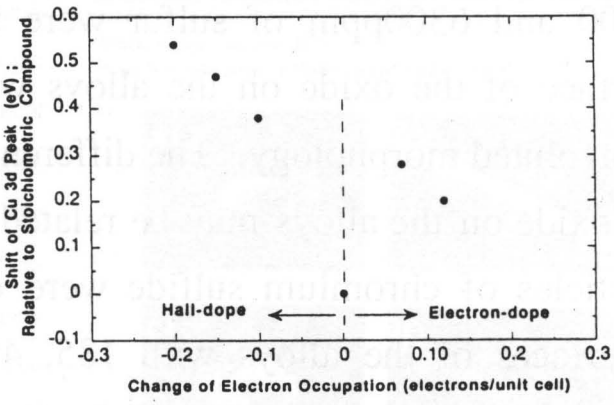

Fig. Energy-shift of Cu 3d signals as a function of change of electron-occupation par unit cell

Behavior of Sulfur of Fe-20Cr-4Al Alloys at 1473K in Oxygen

T. Watanabe, A. Sekiya, T. Amano and K. Sasaki*

Shonan Institute of Technology, 1-1-25, Tsujido-Nishikaigan, Fujisawa 251, Japan

*IMR, Tohoku University, 1-1, Katahira 2-chome, Aoba-ku, Sendai 980-77, Japan

Behavior of sulfur of Fe-20Cr-4Al alloys with 7, 185, 491, 1300 and 6300ppm of sulfur was studied at 1473K for 18.0ks in oxygen. Mass changes of the alloys with 7, 185, 491, 1300 and 6300ppm of sulfur showed positive values. Mass change of the alloys were almost the same values. On the other hand, mass change of the alloy with 7ppm of sulfur showed a negative value. This result suggested that oxide scales on the alloy spalled markedly during cooling after high temperature oxidation. Surface morphology of the oxides on the alloys with 185, 491, 1300 and 6300ppm of sulfur were almost smooth. However, surface of the oxide on the alloys with 7ppm of sulfur showed convoluted morphology. The differences to surface morphologies of oxide on the alloys may be related to oxide adherence. Many particles of chromium sulfide were observed at the oxide/alloy interfaces of the alloys with 185, 491, 1300 and 6300ppm of sulfur after oxidation at 1473K for 18.0ks. The existence of many particles of chromium sulfide play probably a role in improvement of the oxide adherence. The plasticity of oxide on the alloys was studied using a micro-vickers tip. The plasticity of oxide on the alloy with 6300ppm of sulfur was larger than that of oxide on the alloy with 171ppm of sulfur.

Laser Enhanced Electroless Plating of Gold

○ Satoshi NAGAMINE, Koichi KOBAYAKAWA, Yuichi SATO

Department of Applied Chemistry, Faculty of Engineering, Kanagawa University,

3-27-1 Rokkakubashi, Kanagawa-ku, Yokohama 221

Introduction : Laser-enhanced Au electroless plating on Ni plated iron-nickel alloy, brass and copper was conducted in a cyanide-free bath developed by us. The plating bath consists of chlorauric acid, sodium hypophosphite, succinimide, and potassium thiocyanate at pH 8.0 [1]. The thermal conductivity of the substrate is an important factor. Using the nickel-plated Ni-Fe alloy, which had the lowest heat-conductivity of the three materials, the gold deposit height is the heighest for the same laser power and irradiation time. It was found that the gold deposit height and its diameter can be controlled by the laser power, irradiation time and the flow velocity of the plating solution.

Experimental : As a substrate, Cu, brass, and the Ni-Fe (42:58) alloy with a 5μm Ni plating were used. Using the bath shown in Table 1 , laser enhanced electroless gold plating was carried out at various laser powers, irradiation times and plating solution flow rates. The shape of the deposits was observed by SEM.

Results and Discussion : The deposit obtained by laser irradiation has a slight hilly sharp at 0.5 W of laser power and 60 s of irradiation time (Fig.1, a). The diameter of the deposit was nearly equal to that of the laser beam (25μm), but changed to some degree due to the irradiation conditions. The deposit were found to be Au based on an EDX analysis. Increasing the laser power, the shape of the deposit collapsed. For 3 watts of laser power, the shape became ring-like, which might be caused by the fact that the Au ion could not be supplied because the solution at the center of the laser focus boiled . In the case of the Cu or brass substrate with higher thermal conductivies, the diameter of the deposit was smaller than that obtained on the Ni-Fe alloy substrate. There may be a tendency that the higher the thermal conductivity of the substrate, a larger laser power is required to obtain the same size of deposit. Line drawing was attempted using the laser enhanced electroless Au plating. Upon changing the scan rate of the laser beam between 2.5 μm/s and 10 μm/s at 0.5 W～2.0 W of laser power, the best results were obtained at a 5 μm/s scan speed and 0.5 W laser power.

Table 1 Bath composition and condition of laser enhanced electroless plating of gold.

Chemcals	Concentration
$HAuCl_4$	0.01M
$NaPH_2O_2$	0.10M
Na_2SO_3	0.10M
Succinimide	0.10M
KSCN	0.05M
$(CH_3COO)_2Pb$	6ppb
NBS*	4.7×10^{-3}M

pH 8.0 (adjusted with NaOH)
Bath temperature :R.T.
* m-Nitrobenzensulfonic acid sodium salt

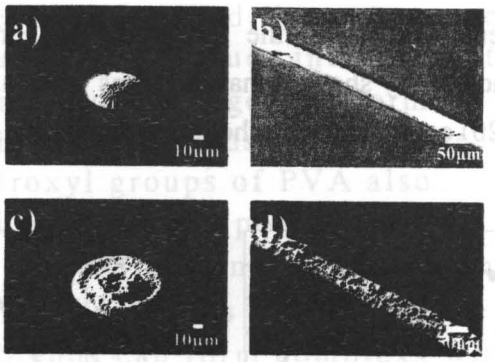

Fig.1 SEM phograph of laser enhanced Au spot deposit and Au line pattern on 5μm Ni plated Ni-Fe alloy substrate.
Flow rate : 175cm/s.
Laser power : a) ,b) 0.5W c) , d) 2.0W
Irradiation time (a, c): 60s.
Scan speed (b, d) : 5μm/s

Reference

1) Satoshi Nagamine, Koichi Kobayakawa, Yuichi Sato, JIPC .,**12** .,497(1997).

Magnetic Properties of Co Ferrite Thin Films for Perpendicular Magnetic Recording Media

S. Kantake, S. Takaya, Y. Kitamoto, and M. Abe
Tokyo Institute of Technology

Introduction

Ferrite thin film recording media have a good potential because of their low noise characteristics and good mechanical durability. But physical vapor deposition methods need high temperature over 300℃ and ferrite films have lower Ms than metalic thin film such as Co-Cr alloy films. The "ferrite-plating" method that it was developed in our laboratory facilitates to deposit polycrystalline spinel type of ferrite films at low temperature below 100℃ in aqueous solutions. The purpose of this study is to prepare Co ferrite thin films for perpendicular magnetic recording media by "ferrite-plating" method. We investigated their magnetic characteristics of it.

Experimental and Results

$(Co,Fe)_3O_4$ films were prepared by the spin-spray ferrite-plating on glass substrates at 90℃ using a reaction solution of $FeCl_2$+$CoCl_2$ and an oxidizing solution of $NaNO_2$+CH_3COONH_4 (pH=5～7). The crystallographic characteristics were estimated using a X-ray diffractometer. The magnetic characteristics were investigated using a vibrating sample magnetometer (VSM).

Figure 1 shows dependence of coercivity on $NaNO_2$ concentration in the oxidizing solution. High ratio of the perpendicular coercivity to in-plane one, Hcp/Hci suggests the films have perpendicular magnetic anisotropy in the case of low $NaNO_2$ concentration below 2.9×10^{-2} mol/l. Ms was 80～500emu/cc.

Figures 2 and 3 show the dependences of the coercivity on Co/Fe ratio at the $NaNO_2$ concentration of 3.6×10^{-3} and 2.5×10^{-2} mol/l. Hci decreased by the increase of the $NaNO_2$ concentration, and the perpendicular anisotropy was improved. The results of X-ray diffractometry showed that the films with maximum Hcp/Hci ratio have a preferential orientation in (220) compared with the other films.

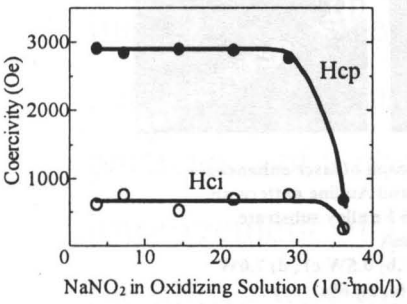

Fig.1 Dependence of coercivity on $NaNO_2$ concentration in the oxidizing solution

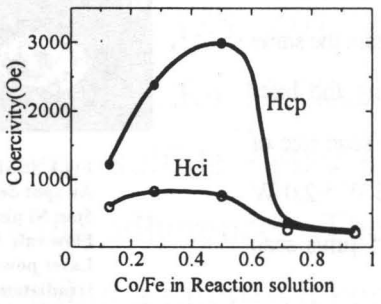

Fig.2 Dependence of coercivity on Co/Fe ratio in reaction solution at the $NaNO_2$ concentration 3.6×10^{-3} mol/l

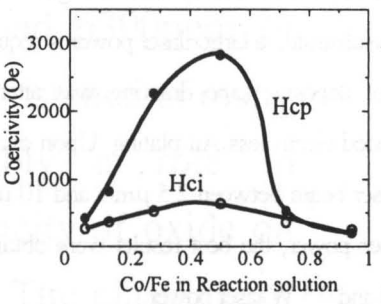

Fig.3 Dependence of coercivity on Co/Fe ratio in reaction solution at the $NaNO_2$ concentration 2.5×10^{-2} mol/l

Preparation of Functional Materials by Blending Poly(vinyl Alcohol) with Copolyesters Having Amine Salt Groups and Their Metal Complex Formation

○Daisuke Iwami, Chonghui Wang, and Shigeo Nakamura
Department of Applied Chemistry, Faculty of Engineering
Kanagawa University, Kanagawa-Ku, Yokohama 221, Japan

Introduction

We have previously reported the preparation of polymer blends of PVA with polyesters having pendant quaternary ammonium groups and aminosulfonic acid moieties.[1] Now, we intend to describe the preparation of blends of PVA with copolyesters having secondary and tertiary amine salt groups and their complex formation with metal ions.

Experimental

Copolyester **P 1** and **P 2** was obtained from maletic anhydride and diols **S1 2** having secondary and tertiary amine salt groups and from phthalic anhydri-de and **S1 2**, resprctively.[2] Blend films of **P 1** and **P 2** with PVA were prepared by dissolving the copolyesters in an aqueous 10% PVA solution and casting on a glass plates. Metal complex films were obtained by adding $CuCl_2$ and $CoCl_2$ to the solution before casting.

Results and Discussion

The IR spectra of the **S1 2**, **P 1** and **P 2** all show absorption bands at 2750-2800 cm^{-1} ($>NH_2^+$, $>NH^+-$) and 1620-1600 cm^{-1} ($>NH_2^+$) assigned to secondary and tertiary amine salts. For all of the blend films and their metal complexes, an IR absorption band appears at 1720 cm^{-1} corresponding to the -CO(O)- stretching vibrations. For blend films, the absorption bands due to $>NH^+$- vibration does not appear at 2800 cm^{-1}. Therefore, these tertiary amine salt groups are easily dissociated to amino groups in blends due to the proton exchange. **P 1** and **P 2** are amorphous and has a softening point at 52 and 43 °C, respectively. Dry blend films show each one T_g which is higher than that of PVA, and the T_g values increase with the increasing **S1 2** content. Therefore, ionic crosslinkages are formed between PVA and the copolyesters. The hydrogen bonds between the ester groups of the copolyester and the hydroxyl groups of PVA also contribute to the rise of T_g. These blend films are ionic polymer blends and possess higher σ values (10^{-6} Scm^{-1}) when these blends contain about 5 wt% of water. The σ value of blend metal complexes is lowered as compared with the that of blends. These blends can form complexs with $CuCl_2$ and $CoCl_2$. The coordination structure with two chelate rings is suggested between the tertiary amino groups of copolyester and hydroxyl groups of PVA.

REFERENCES

1) C.Wang and S. Nakamura, *J. Polym. Sci., Polym. Chem. Ed.*, **3 2**, 1255 (1994).
2) S. Nakamura and C. Wang, *Seni Gakkai, Preprints ,G* 131, (1997).

Gas Permiability and Stability of Poly[1-(trimethylsilyl)-1-propyne] Blend Membranes

Tsutomu Nakagawa, Shingo Tabei and Tetsuya Watanabe

(Department of Industrial Chemistry, Meiji University Kawasaki 214-71, Japan)

Tel: 044-934-7211 Fax: 044-934-7906

E-mail address: ce77620@isc.meiji.ac.jp

Poly[1-(trimethylsilyl)-1-propyne] (PMSP) membrane has the highest gas permeability of all polymeric membranes. However, the PMSP membrane exhibits a significant deterioration of the gas permeability with time. In previous study, the permeability of PMSP may be stabilized against physical aging by blending PMSP with small amounts of poly(1-phenyl-1-propyne) (PPP)[1]. In this study, we investigated the effect of blending PMSP with poly(*tert*-buthylacetylene) (PTBA) or polyvinyltrimethylsilane(PVTMS) which expected higher affinity with PMSP than PPP on the stability of their gas permeability.

The membranes were prepared by casting a polymer solution from toluene. The gas permeation properties and gas sorption isotherms were determined by the vacuum-pressure method and the gravimetric method, respectively.

As the PTBA or PVTMS content was increased, the gas permeability was decreased and approached that of PTBA or PVTMS, whereas selectivity of O_2/N_2 was increased.The decrease of permeability was due to the decrease in the unrelaxed volume. During storge under vacuum, the gas permeability and C_H' value of the PMSP was dramatically reduced. Most stable gas permeability was obtained when the PMSP membranes contained 20 vol% PTBA or 5 vol% PVTMS. And these blend membranes had their stable C_H' values for aging. In these volume fractions of blend polymers, the polymers were highly miscible compared with those of other blend polymers from results of permeability coefficients and density values on blend composition. These results suggest that higher miscibility of polymers with PMSP might be required to stabilize the gas permeability of the PMSP membrane. In particular, the addition of a small amount of the PTBA or PVTMS provived excellent stability with high gas permeability.

Reference

1. K. Nagai. et. al., *J. Polym. Sci., Polym. Phys. Ed.*, **35**, 119(1997).

Separation of Olefin/Paraffin by Facilitated Transport through Polymeric Membranes containing Ag^+

Tsutomu Nakagawa and Yasuko Ogihara

(Department of Industrial Chemistry, Meiji University Kawasaki 214-71, Japan)
Tel: 044-934-7211 Fax: 044-934-7906
E-mail address: ce66612@isc.meiji.ac.jp

Facilitated transport through liquid membranes has been investigated for more than 30 years as a potential technology for separation for hydrocarbon separations. Although the liquid membranes have many promising attributes, there are few successful industrial applications. Recently, on behalf of the membrane such as liquid membranes involving the mobile carrier, the charged membranes in which a carrier is fixed have been investigated.

In this study, we synthesized copolymers by copolymerization of methacrylate (MAA) and n-buthylacrylate (nBA). These membranes were soaked in an aqueous silver nitrate ($AgNO_3$) with an adequate concentration. Separation property of propane/propylene gaseous mixtures through the membranes was determined using an updated apparatus including a permeation cell saturated with water vapor.

The propylene flux monotonically increased with increasing MAA content of copolymer membranes. This result indicate that Ag^+ ion in membranes acted as a carrier. The propylene transport was facilitated by this carrier. The propane/propylene selectivity of these membranes increased linearly with the increase of total Ag^+ content. Consequently, the separation factor of propane/propylene was controled by the MAA content in copolymer membranes.

The propylene flux decreased with the concentration of $AgNO_3$ solution to 1.0M. More than 1.0M in concentration, the propylene flux increased. Increasing the $AgNO_3$ concentration, the amount of Ag^+ ion in copolymer membranes increased although their water content significantly declined. Generally, the concentration of sorbed propylene gas in membranes increases with the increase in Ag^+ ion. In these membranes the higher the concentration of $AgNO_3$ solution, the more effective mobile Ag^+ ion acted as a carrier. On the other hand, decreasing in water content caused the reduction in diffusion of Ag^+ ion. For these interaction, the minimum of propylene flux was observed in the 1.0M $AgNO_3$ solution. The propane/propylene selectivity of copoly(MAA:nBA=9:1) membrane increased until 370, as increase the $AgNO_3$ concentration.

Effect of Ion Irradiation for Dissolved-Oxygen Permeability of Methacrylate Copolymer Membranes Containing Hydrophilic Group

Tsutomu Nakagawa and Shuuichi Takahashi

Department of Industrial Chemistry, Meiji University
1-1-1 Higashi-mita, Tama-ku, Kawasaki 214-71, Japan

Tel: 044-934-7211 Fax: 044-934-7906
e-mail: ce66619@isc.meiji.ac.jp

In a medical field, the polymeric membranes exhibiting high permeability for oxygen and dissolved oxygen have been required for materials such as contact lens or artificial lung, which must be swelled with the water to fit the human body. In this study, we investigated the effect of the composition of hydrophilic group in copolymer membranes on the water content, dissolved- oxygen permeability, and their handling under wet condition. Furthermore we also investigated the effect of ion beam irradiation on dissolved-oxygen permeability.

The copolymer membranes were synthesized by the radical bulk copolymerization of monomers having hydrophobic group, trimethylsilylmethylmethacrylate(TMSMMA) or methylmethacrylate(MMA), with phydrophilic group, N,N-dimethylacrylamide(DMAA). The copolymer membranes were prepared by casting methods. The relationship between the DMAA content and the permeability coefficient for oxygen in the gaseous state in the poly(MMA-*co*-DMAA) and poly(TMSMMA-*co*-DMAA) membranes were accorded to the typical representative equations for random structures:
$\log P = \phi_1 \log P_1 + \phi_2 \log P_2$ Therefore, the DMAA units would be randomly dispersed in the copolymer. The dissolved-oxygen permeability coefficients of the copoly(MMA-*co*-DMAA) membranes increased with the increase of DMAA contents. Those of the copoly(TMSMMA-*co*-DMAA) membranes decreased initially as the increase of DMAA contents. When the DMAA content is more than 40 mol%, the value were increased as the increase of DMAA contents. This observation indicates that dissolved-oxygen permeability coefficients initially decreases as the silicon content in the copolymers decreases. Then, the rise of the dissolved-oxygen permeability coefficients indicate that the water took in these membranes, most of which was the freezing water, largely affected the oxygen permeability. Furthermore, we attempted to ion beam irradiation for the copoly(TMSMMA-*co*-DMAA) membranes. For ion beam irradiation, ^{129}Xe ion and ^{84}Kr ion were supplied from the cyclotron. The dissolved-oxygen permeability of the irradiated copolymer membranes were higher than that of nonirradiation membranes. The ion irradiation would be useful for application to medical field, especially contact lens.

Synthesis and Microstructure of Lithium Titanium Niobium Oxides

○H.Hayashi, T.Sekino, Y.H.Choa, *K.Urabe and K.Niihara
ISIR, Osaka University, 8-1 Mihogaoka, Ibarki, Osaka, Japan,
*Ryukoku University, 1-5 Oetyouyokotani, Seta, Otsu, Siga, Japan

Introduction

The $Li_{1+x-y}Nb_{1-x-3y}Ti_{x+4y}O_3$ solid solutions show superstructure along the c-axis of the $LiNbO_3$-like subcell. The X-ray powder diffraction patterns of $Li_{1+x-y}Nb_{1-x-3y}Ti_{x+4y}O_3$ solid solutions are similar to that of $LiNbO_3$ except for the presence of satellite reflections. The superstructure is observed as layer-like domains by HREM. The period of the superstructure decresed with TiO_2 content. The superstructure is attributed to insert stacking faults into oxygen layer sequence. However, the powder processing and sintering condition to obtain a stable superstructure of $Li_{1+x-y}Nb_{1-x-3y}Ti_{x+4y}O_3$ solid solutions are not clear. In this study, therefore, the purpose is to investigate the powder preparation with sol-gel processing and The sintering condition for highly densed samples.

Experimental Procedure

Lithium ethoxide(99.9%), niobium ethoxide(99.9%) and titanium ethoxide(99.9%) were dissolved in ethanol. The mixed alkoxide solution was stirred at 74℃ for 2 days. Then, distilled water added slowly to the mixed alkoxide solution for partial hydrosis. After the solution was stirred for 2 days, the wet gel is dried by vaporizing. These powders were calcined at 400 to 700℃ for 1 hour. Samples were sintered at 900, 1000 and 1100℃ at 2 to 6 hours. To determine the condition of calcination, TG/DTA analysis was conducted. The density was measured by Archimedes method, and the phase analysis was done by X-ray diffraction from room to high temperatures. The superstructure of $Li_{1+x-y}Nb_{1-x-3y}Ti_{x+4y}O_3$ solid solutions was observed by High-Resolution TEM.

Results and Discussion

TG/DTA analysis for the gel powder showed that H_2O and OH radical was evaporated from 400℃ to 700℃ and weight loss did not occur at above 700℃. Therefore, the 700℃ may be suitable to calcinate the wet-gel powder and the characteristic of solid solutions was detected by XRD measurement for the powder calcined at 700℃. Also, at above 700℃, the peak sprits which show the superstructure are slightly observed for the calcinated powders. Figure 1 shows X-ray diffraction patterns of $Li_{1+x-y}Nb_{1-x-3y}Ti_{x+4y}O_3$ solid solutions at (a) 700℃, (b) 800℃ and (c) 900℃ for powders calcinated at 700℃. The peak sprit which contains the satellite lines on (012) and (202) planes is clearly seperated at 900℃. This result show that the $Li_{1+x-y}Nb_{1-x-3y}Ti_{x+4y}O_3$ solid solutions with complete superstructure are formed at above 900℃. Therefore, to obtain the densed sintered material with superstructure, the samples calcinated at 700℃ were sintered at 900℃, 1000℃ and 1100℃ for various duration time. The density was measured with sintering temperature and reached up to 3.9 g/cm^2. The density value for $Li_{1+x-y}Nb_{1-x-3y}Ti_{x+4y}O_3$ solid solutions was much higher than those for $Li_{1+x-y}Nb_{1-x-3y}Ti_{x+4y}O_3$ solid solutions prepared by conventional powder mixing methods.

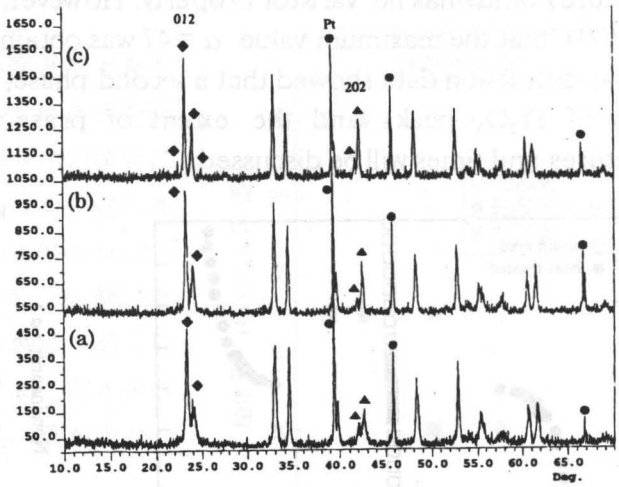

Fig. X-ray diffraction patterns solid solution at (a) 700℃, (b) 800℃ and (c) 900℃ for $Li_{1+x-y}Nb_{1-x-3y}Ti_{x+4y}O_3$ powder calcinated at 700℃

ZnO Varistor by Grain Boundary Diffusion of $ZnO-PrO_x$ liquid

(Tokyo Inst. of Tech.) ○ S. Y. Chun, N. Wakiya, O. Sakurai, K. Shinozaki and N. Mizutani

Diffusion of liquid ($ZnO-PrO_x$) into the grain boundaries of sintered Co-doped ZnO ceramics resulted in varistors with breakdown voltages per grain boundary in the 1-3 V range and nonlinearity coefficient (α) of 15-58. Further higher heat-treatment (1200° -1400℃) and times (0-60 min) resulted in progressively higher breakdown voltages. Eventually the devices became varistor, which was attributed to the formation of liquid ($ZnO-PrO_x$) layer between the ZnO grains.

1. Introduction

Grain boundary controlled electronic ceramics, such as ZnO varistors are polycrystalline semiconducting ceramics whose remarkable properties arise from the presence of electrically "active" grain boundaries. Thus, grain boundaries are an essential feature to obtain the desired electrical behavior. However, the mere presence of grain boundaries does not result in useful components. Careful processing before and during firing is required to obtain the proper condition that yields electrically active grain boundaries.

The purpose of this study is to investigate the role of $ZnO-PrO_x$ liquid on varistor properties such as, I-V characteristics and C-V characteristics. Thus, the possible technique of varistor-formation via diffusion of molten ZnO-PrOx liquid into the grain boundaries of pre-sintered ZnO ceramics and their influence on the resulting properties were studied.

2. Results and discussion

Figure 1 compares the I-V response of the as-sintered 7 mol% Co-doped ZnO disks with those were heat-treated with Pr_6O_{11}-paste at 1300℃ for 30 min. The marked nonlinear I-V response of the Pr_6O_{11} heat-treated sample is obvious. The braekdown voltage at a current density of 0.1 mA/cm^2 is determined to be 220 V/cm which is about the lower than that of the conventionally fabricated low voltage varistors.

The change of nonlinearity (α) vs. heat-treatment temperature is shown in Figure 2. From this figure nonlinearity was 1 for the sample heat-heated at 1250℃ (below liquid-phase formation temperature) which has no varistor property. However, the value of nonlinearity begins to increase above 1300℃ that the maximum value α =47 was obtained at 1350℃.

X-ray diffraction data showed that a second phase, namely Pr_2O_3, was present in all samples. The intensity of Pr_2O_3 peaks and the extent of praseodymium penetration with heat-treatment temperatures and times will be discussed.

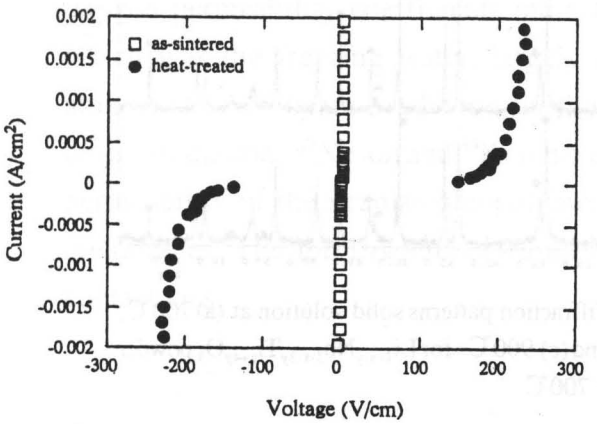

Fig. 1. I-V characteristics of Co-doped ZnO sample before and after heat-treated at 1300℃ for 30 min.

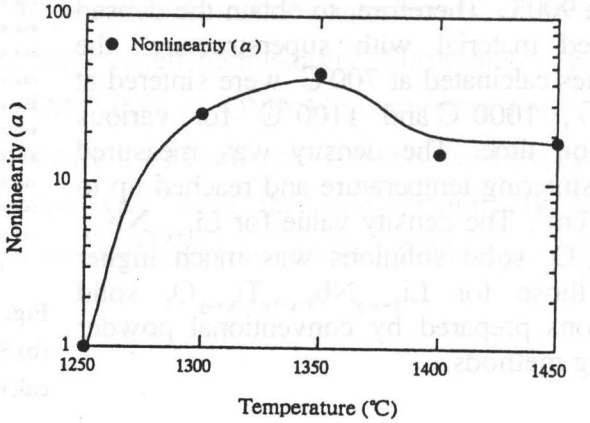

Fig. 2. Log nonlinearity vs. heat-treatment temperature of 7 mol% Co-doped ZnO samples after heat-treated at elevated temperatures for 30 min.

ゾルゲル法による$(Ba,Sr)TiO_3$結晶性モノリシックゲルの室温合成

(東大工) 椎橋 博之、松田 弘文、桑原 誠

Synthesis of $(Ba,Sr)TiO_3$ crystalline monolithic gels by sol-gel method at low temperature

(University of Tokyo) H. Shiibashi, H.Matsuda and M. Kuwabara

[緒言]

$(Ba,Sr)TiO_3$ は高誘電率材料として利用されている。本研究では金属アルコキシドを原料としたゾルゲル法により$(Ba,Sr)TiO_3$ の結晶性モノリシックゲルを低温合成することを目的とした。また、作製条件による結晶性の変化についても調べた。

[実験]

$Ti(OC^iC_3H_7)_4$, $Ba(OC_2H_5)_2$, $Sr(OC_2H_5)_2$ を所定量秤量し、2-メトキシエタノールに溶解させたものを前駆体溶液として用いた。0℃で前駆体に脱気水を噴霧して加水分解させ 30℃ 5 日間＋50℃ 5 日間という条件でエージングした後、90℃で 1 日間乾燥して乾燥ゲルを得た。

$Ba_{1-x}Sr_xTiO_3$ の組成は x=0, 0.2, 0.4, 0.6, 0.8, 1.0 の 6 種類とした。前駆体溶液濃度は 0.2mol/l、加水量は H_2O/Ti=50mol 倍とし、各試料の作製条件を一定とした。また組成 $Ba_{0.4}Sr_{0.6}TiO_3$(x=0.6)の試料に対して前駆体溶液濃度を 0.05～0.5 mol/l、加水量を 10～100 mol 倍と変化させてゲルの結晶性の変化を調べた。

得られたモノリシックゲルを粉末にして、XRD,DTA-TG,TEM 等でキャラクタリゼーションを行った。

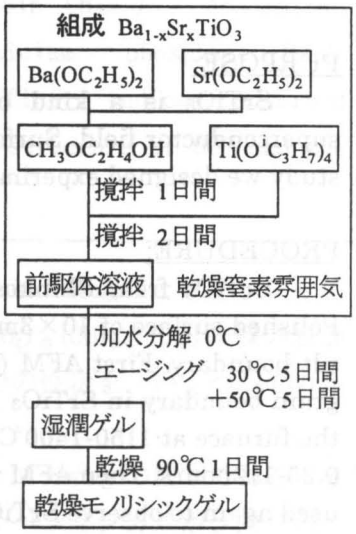

図1 試料作製手順

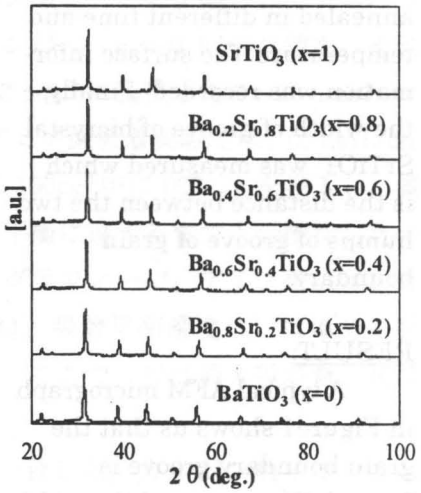

図2 各組成の乾燥ゲルの X線回折パターン

[実験結果]

$Ba_{1-x}Sr_xTiO_3$ の 90℃乾燥ゲルの XRD パターンを図 2 に示す。全試料で単一のペロブスカイト構造の回折ピークが得られていることから、Ba と Sr が一様に固溶した結晶性のゲルが生じていることがわかる。DTA-TG の結果からゲル内には未反応のアルキル基や水酸基が残留していて、Sr が多いほどその残留量が多いことがわかった。

$Ba_{0.4}Sr_{0.6}TiO_3$(x=0.6)の 90℃乾燥ゲルを前駆体濃度と加水量を変化させて作製し、XRD 測定を行った結果観測された相を図 3 に示す。この図から前駆体濃度が低く加水量が少ない場合に非晶質相となり、ペロブスカイト結晶相になるのはその逆の条件が必要であることがわかる。前駆体濃度が高い試料(0.5mol/l)は 30℃エージングの段階ですでに結晶化していた。X 線回折ピークの面積強度から求めた結晶化度は、前駆体濃度が高く加水量が多い場合に高くなる。同様に前駆体濃度が高く加水量が多い方が、ゲル内に残留するアルキル基や水酸基の量が少なくなる。

結晶化度の高いゲルを焼成した場合、今までよりも低い温度で$(Ba,Sr)TiO_3$セラミックスの緻密化が可能であると考えている。

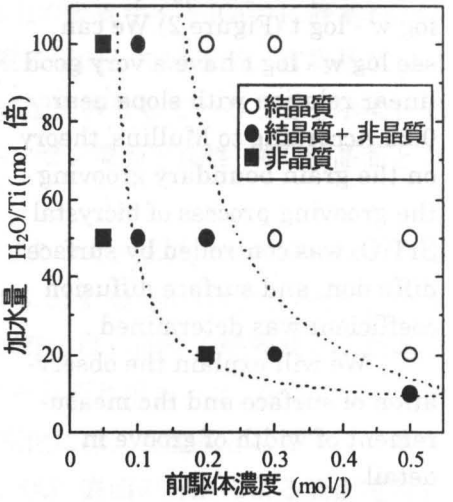

図3 前駆体濃度と加水量の変化に対する BST乾燥ゲルの結晶性の変化

GRAIN BOUNDARY GROOVING IN BICRYSTAL $SrTiO_3$

Minxian Jin , Eriko Shimada , Yasuro Ikuma
Kanagawa Institute of Technology, Atsugi ,Kanagawa, 243-02

PURPOSE:

$SrTiO_3$ is a kind of important material which is used in semiconductor and superconductor field. Surface phenomenon in this material is not well understood. In this study we designed experiment to measure the surface diffusion coefficient of $SrTiO_3$.

PROCEDURE:

$SrTiO_3$ from Shinkosha company was cut into pieces with size $10 \times 3 \times 0.5$ mm. Polished surface of 10×3mm is (100) plane in both crystals and the grain boundary is 24° tilt boundary. First AFM (SPA300) was used to confirm that there are no any observable grain boundary in $SrTiO_3$. Bicrystal $SrTiO_3$ sample put into Pt-crucible was annealed in the furnace at 1150-1400℃ for 0.25-112hours. Then AFM was used again to observe $SrTiO_3$ grain boundary grooving annealed in different time and temperature.The surface information was recorded. Finally, the width of groove of bicrystal $SrTiO_3$ was measured which is the distance between the two humps of groove of grain boundary.

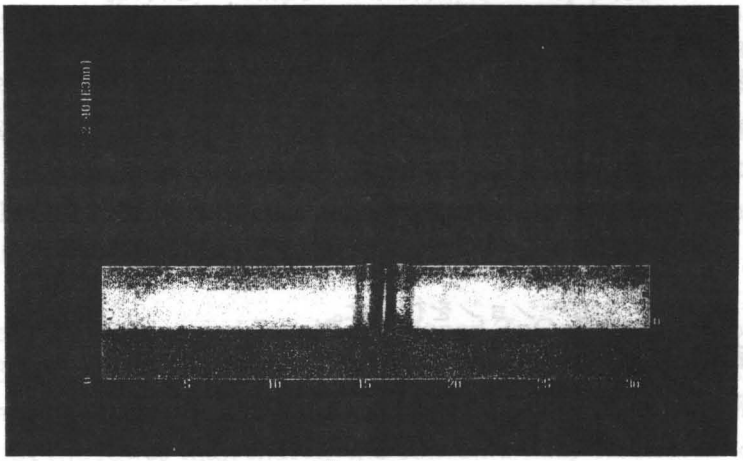

Figure1

RESULT:

A typical AFM micrograph in Figure1 shows us that the grain boundary groove is formed. We measured the width of groove to make a graph of log w - log t (Figure 2).We can see log w - log t have a very good linear relation with slope near 0.25.According to Mullins' theory on the grain boundary grooving the grooving process of bicrystal $SrTiO_3$ was controlled by surface diffusion, and surface diffusion coefficient was determined .

We will explain the observation of surface and the measurement of width of groove in detail.

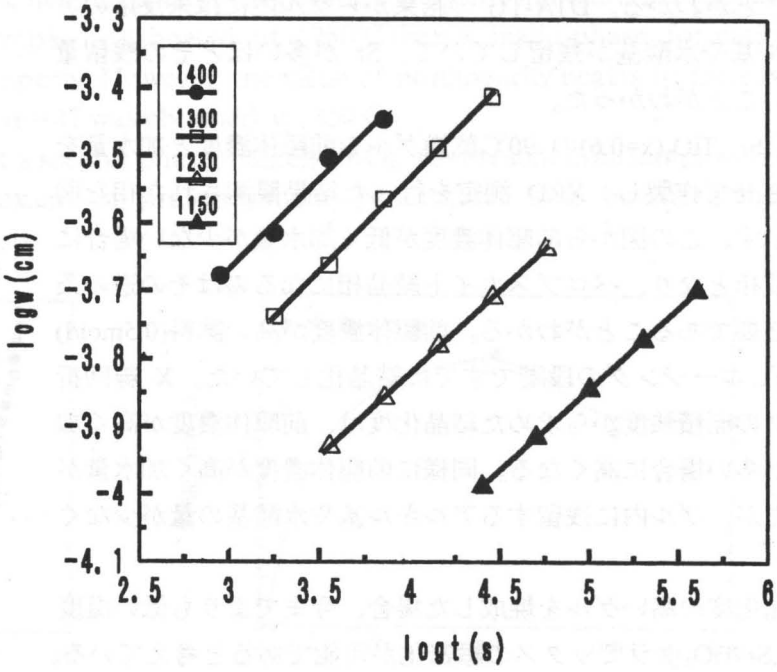

Figure 2

リン酸八カルシウム結晶面上でのカルボン酸およびアミノ酸の吸着

(工学院大・工)○太田一史、門間英毅、高橋聡、小林偉男、大勝靖一

Adsorption Models of Carboxylic Acids and Amino Acids on Octacalcium Phosphate Crystals / ○K. Ohta, H. Monma, S. Takahashi, H. Kobayashi, and Y. Ohkatsu (Kogakuin Univ.) / Adsorption characteristics of carboxylic acids and amino acids on octacalcium phosphate (OCP) microcrystals were investigated by using adsorption amounts and affinity indices, adsorbed configurational models, and certain dynamic changes of the surface structure of OCP and the dissolution of absorbates depending on pH.

[緒言] リン酸八カルシウム($Ca_8(HPO_4)_2(PO_4)_4\cdot 5H_2O$、以下 OCP)は、アパタイト構造相とブラッシャイト組成相($CaHPO_4\cdot 2H_2O$)の層状構造を持つことから、水酸アパタイト($Ca_{10}(PO_4)_6(OH)_2$、HAp)同様の表面機能材料としての展開が考えられる。本研究では、OCP 結晶表面の液相中での性状を、いくつかのカルボン酸とアミノ酸の液相吸着データから検討した。

[実験] OCP 試料はα-$Ca_3(PO_4)_2$の加水分解によって合成した板状微結晶で 12.8m^2/g の粉末である。吸着質には、安息香酸(MonoA)，o-ジベンゼンカルボン酸 (DiA) ，2,4,6-トリベンゼンカルボン酸(TriA)および 1,2,4,5-テトラベンゼンカルボン酸(TetraA)の 4 種のカルボン酸を、アミノ酸としてアスパラギン酸(Asp, 等電点 pI=2.8)、 セリン(Ser, pI=5.7)およびアルギニン(Arg, pI=10.8)の３種を、それぞれ使用した。カルボン酸吸着実験では、0.1mol/dm^3 Tris-HCl 緩衝液で pH10 に調整した 2～20μmol/dm^3 のカルボン酸水溶液 100cm^3 中に OCP 2g を投入し、37℃で攪拌した。アミノ酸吸着実験では、0.1mol/dm^3 Tris-HCl 緩衝液中に所定量の吸着質を溶解し(1～15μmol/dm^3)、これ 100cm^3 中に OCP 3g を投入し、素早く pH を 6.5～11 の間に調整して、37℃で攪拌した。それぞれ吸着平衡に達するまで十分攪拌したのち(2 時間)、液相中の吸着質の濃度を、カルボン酸はイオンクロマトグラフィーで、アミノ酸はニンヒドリン－吸光光度法によってそれぞれ求めた。吸着データ（吸着量Q、吸着平衡濃度C）は単分子吸着様式のラングミュア式[C／Q＝C/N＋１／(K・N)]で整理した。ここで、Nは最大吸着量、Kは固体表面上の吸着サイトと吸着質との親和力に対応する。

[結果と考察] 各カルボン酸の等温吸着線はラングミュア型にほぼ一致した。カルボン酸イオンのQおよびNは、MonoA＞DiA≫ TriA≫ TetraA の順であった。すなわち、単分子状で吸着している MonoA や DiA では、その吸着官能基のカルボシキル基($-COO^-$)一つが OCP 表面上の吸着サイト(Ca^{2+})に静電的に結合できるので、そのベンゼン環は OCP 表面に対して斜めあるいは縦に配向しているが、官能基が 3,4 個になる TriA や TetraA ではベンゼン環面を OCP 表面に対して横に配向吸着していることを示唆している。Kは、MonaA＞DiA＞TriA、となった。このことは疎水性のベンゼン環面と極性 OCP 結晶面との反発が大きくなるためと推察される。

各アミノ酸の液相 pH を変えて得た吸着等温線もラングミュア型であった。また pH の違いによるQは、Asp(等電点、pI=2.8)：Q(pH=7)≪ Q(pH=10)、Ser(pI=5.7)：Q(pH=6.5)≪ Q(pH=11)、Arg(pI=10.8)：Q(pH=6.5) ≫ Q(pH=11)、であった。一方、OCP 表面の電荷ゼロ点(ZPC)は、pH6 の懸濁液の流動電位法からは pH6.3、pH10.5 の懸濁液の塩酸滴定法では pH8.6、のようにそれぞれ求まった。後者の値は HAp の文献値とほぼ同じ値であった。結局、アミノ酸吸着の pH による変化には、官能基としてアミノ基($-NH_2 \rightarrow -NH_3^+$)とカルボキシル基($-COOH \rightarrow -COO^-$)のイオン化の程度、OCP 表面の pH による表面電荷あるいは組成・構造(アパタイト層→水和層) の変動が絡み合っているものと推察される。

SYNTHESIS OF THE HIGH-T_c SUPERCONDUCTORS BY USING A DOMESTIC MICROWAVE OVEN

Masatsune KATO, Kenji SAKAKIBARA and Yoji KOIKE

Department of Applied Physics, Graduate School of Engineering, Tohoku University, Aramaki Aoba, Aoba-ku, Sendai 980-77, Japan

We have synthesized the High-T_c superconductors of Y-123[1] and Bi-based systems, using a domestic microwave oven operated at 2.45 GHz for several ten minutes.

$YBa_2Cu_3O_x$ was prepared from powders of the relevant metal-oxides, Y_2O_3, BaO_2 and CuO in the stoichiometric ratio. As shown in Fig.1, a pellet of mixed powders of starting materials was surrounded by mixed powders of starting materials and subsequently wrapped in glass wool, in order to suppress rapid dissipation of heat from the surface of the pellet. Then the sample was put in an alumina crucible. This crucible was placed on the center of the turntable in an oven. At 200 W, the pellet did not react at all for up to 24 min, while it partially melted beyond 26 min. The single phase of $YBa_2Cu_3O_x$ was obtained through the radiation for 25 min. Without annealing in flowing oxygen gas, the as-prepared pellet showed superconductivity with $T_c \sim 90$ K, as shown in Fig. 2. The oxygen content x was estimated to be 6.8 from the lattice parameters.

$Bi_{2.2}Sr_{1.8}Cu_{1.05}O_x$ of the Bi-2201 phase was also prepared from Bi_2O_3, SrO and CuO in the same way as in the Y-123 system. The single phase pellet with $T_c \sim 9$ K was obtained through the radiation at 350 W for 14 min 50 sec as shown in Fig. 3. In addition, we have attempted to prepare Bi-2212 and Bi-2223 phases. A sample whose major phase was Bi-2212 was obtained. However, no sample with the Bi-2223 phase could be obtained.

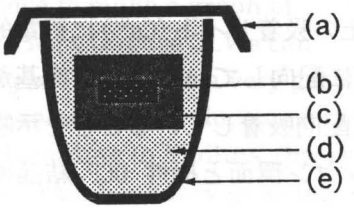

Fig. 1. Schematic of the sample enviornment: (a) almina cover,(b) pellet, (c) mixed powder, (d) glass wool and (e) alumina crucible.

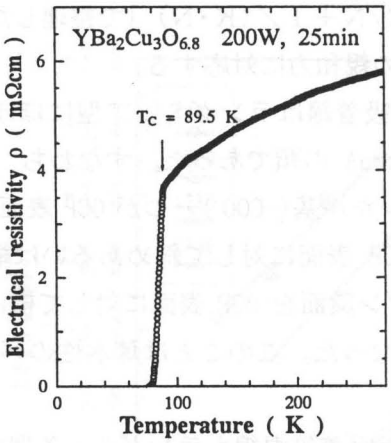

Fig. 2. Temperature dependence of electrical resistivity ρ for $YBa_2Cu_3O_{6.8}$ obtained by radiation at 200W for 25min.

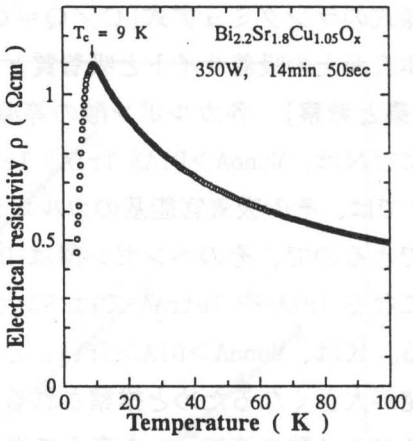

Fig. 3. Temperature dependence of the electrical resistivity ρ for Bi2201 phase obtained by radiation at 350W 14min 50sec

Reference

1) M. Kato, K. Sakakibara and Y. Koike: Jpn. J. Appl. Phys. 36 (1988) L1291.

Preparation of SiGe/Si sintered alloys and their thermoelectric properties

K. Kishimoto, M. Tsukamoto, and T. Koyanagi
Faculty of Engineering, Yamaguchi University

Introduction

The microstructure control at grain boundaries for SiGe thermoelectric sintered alloys has been made to improve their thermoelectric figure-of-merit $Z = S^2\sigma/\kappa$ (S: Seebeck coefficient, σ: electrical conductivity, κ: thermal conductivity). The potential barrier scattering is expected to enhance the Seebeck coefficient, leading to an increase in the figure-of-merit[1]. The scattering may occur in the SiGe/Si composite alloy schematically shown in Fig.1, where the Si grain boundary may act as a barrier for holes. We tried to prepare the SiGe/Si composite alloys and investigated their thermoelectric properties.

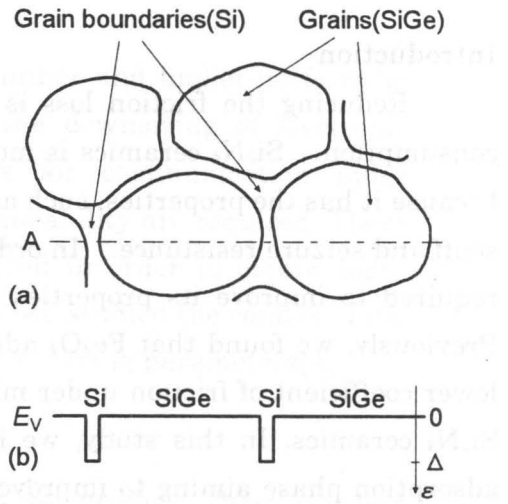

Fig.1. Schematic diagrams of (a)the microstructure and (b)the valence band edge for SiGe/Si composite alloy.

Experimental

The raw $Si_{80}Ge_{20}$:0.2 at%B powder was treated in an rf plasma of SiH_4/Ar for 60~180 min to be coated with Si thin layers. The Si-coated powder was sintered by the spark plasma sintering, resulting in preparation of SiGe/Si composite alloys. Untreated SiGe powder was also sintered for comparison. The Seebeck coefficient was measured at 300~800 K.

Results

The SiH_4-plasma-treated SiGe alloys had larger Seebeck coefficients than untreated ones. The longer plasma treatment time brought a larger increase in the Seebeck coefficient. Figure 2 shows the temperature dependence of the Seebeck coefficient for 180 min-treated and untreated SiGe alloys. An increase of about 20 μV K^{-1} is observed in the whole temperature region. This result suggests that the potential barrier scattering occurs in the plasma-treated alloys.

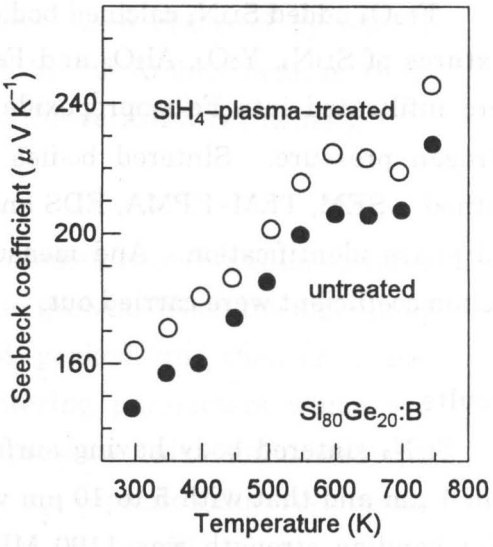

Fig.2. The temperature dependence of the Seebeck coefficient.

[1] Y. I. Ravich, CRC handbook of thermoelectrics, edited by D. M. Rowe, (CRC Press, 1995), chap.7, p.67.

MICROSTRUCTURE AND PROPERTIES OF Si_3N_4 CERAMICS INCORPORATING NANO-MICRON ORDER Fe COMPOUNDS

*Takene Hirai and Hideki Kita
Isuzu Ceramics Research Institute Co. Ltd., Fujisawa, Japan.
Toshihiro Murao
Synergy Ceramics Research Laboratory, Fine Ceramics Research Association, Nagoya, Japan.

Introduction

Reducing the friction loss is one of the key issue to improve the engine's fuel consumption. Si_3N_4 ceramics is most promising material for reducing the friction loss because it has the properties, such as high strength, high Young's modulus and favorable scuff and seizure resistance. In order to put Si_3N_4 ceramics to practical use, it has been required to improve its properties by adding function, such as oil adsorption ability. Previously, we found that Fe_3O_4 added Si_3N_4 provided better oil adsorption ability and lower coefficient of friction under mixed lubricating condition compared to conventional Si_3N_4 ceramics. In this study, we have tried to control the shape and the size of oil adsorption phase aiming to improve the strength and the frictional properties of Fe_3O_4 added Si_3N_4 mentioned above.

Experimental Procedures

Fe_3O_4 added Si_3N_4 calcined bodies were prepared by heating green body of powder mixtures of Si_3N_4, Y_2O_3, Al_2O_3 and Fe_3O_4 at 1300℃ under a nitrogen pressure. They were infiltrated into Fe isopropoxide solution, dried and sintered at 1850℃ under a nitrogen pressure. Sintered bodies were ground, polished and evaluated following method. SEM, TEM, EPMA, EDS and XRD were used for morphology characterization and phase identification. And measurement of the 4-point bending strength and the friction coefficient were carried out.

Results

Si_3N_4 sintered body having surface layer where iron compounds phase with less than 1 μm and that with 5 to 10 μm were coexisted was successfully obtained. The 4-point bending strength was 1190 MPa for the Si_3N_4 applied the infiltration process. This result shows a increase in strength to that of the conventional Si_3N_4, which has the strength of 900 MPa. And the friction coefficient of the Si_3N_4 applied the infiltration process was lower than that of conventional Si_3N_4 in the mixture lubrication region to boundary lubrication region.

Research promoted by AIST, MITI, Japan under the Synergy Ceramics Project of ISTF program. Under this program, part of the work has been supported by NEDO.

Control of the microstructure of Mn-Zn Ferrite

K.Ono, Y.Matsuo, and M.Ishikura
FDK CORPORATION, 2281 Washizu, Kosai, Shizuoka 431-04, Japan

Introduction

Recently, the demand for more compact, lighter, thinner and higher-performing electronic components has increased in line with the downsizing of electronic equipment. In order to miniaturize ferrite cores for communication pulse transformers, Mn-Zn ferrites with a higher initial permeability are required. There are some important factors that need to be considered in order to obtain high-permeability ferrite[1]-[3]. In the present experiments, we studied the control of the microstructure of Mn-Zn ferrite by MoO_3 addition and sintering parameters[4].

Experimental procedure

The ferrite powders were prepared by the regular wet process. These powders were mixed with a prescribed amount of MoO_3 powder. The mixtures were formed into toroidal-shaped samples. These samples were sintered under set conditions at 1,380℃. The permeability of the sintered samples was measured, using an HP4194A impedance analyzer. Their microstructures were observed by optical microscope and SEM. Their density was determined by the Archimedean method, and porosity was determined by comparison with the theoretical X-ray density.

Results

It was found that MoO_3 addition could expand the diameters of crystalline grains, it could also promote porosity, thereby impeding grain growth. When the amount of MoO_3 was increased, the grain diameter expanded, peaked, and then gradually declined under the influence of porosity. The sintering parameters which are sintering time, heating rate and oxygen partial pressure, also influenced the microstructure of ferrite. We set each parameter to an appropriate value. As a result, we obtained high-initial-permeability Mn-Zn ferrite, $\mu_{iac} = 24{,}400$.

References

[1] R.Morineau: Phys. Stat. Sol., (a)38, 559(1976)
[2] I.Lin, R.K.Mishra, G.Thomas: IEEE Trans. Magn., 22, 175(1986)
[3] K.Yasuhara, K.Horino, T.Nomura, T.Sano: J.Magn. Soc. Jpn., 19, 417(1995)
[4] Y.Matsuo, K.Ono, M.Ishikura: IEEE Trans. Magn., 33, 3751(1997)

Effects of Particle Size of MoO_3 Additives on Manganese Zinc Ferrites

Y. Matsuo, K. Ono, M. Ishikura, I. Sasaki
FDK CORPORATION, 2281, Washizu, Kosai-shi, Shizuoka 431-04, Japan

Introduction

We examined the effect of added MoO_3 on initial permeability and other material characteristics in order to develop Mn-Zn ferrites with a high permeability[1]. As a result, Mn-Zn ferrites with high initial permeabilities of more than 24000 have been developed in recent years[2]. Ferrites with these high initial permeabilities are used to miniaturize ferrite cores for communication pulse transformers.

In this study we have studied the effect of added MoO_3 on initial permeability and simultaneously, have investigated the relationship between the particle size of MoO_3 addition and physical properties.

Experimental procedure and Results

Mn-Zn ferrite sintered ceramics were prepared by the usual ceramic process[1]. The starting raw materials of Fe_2O_3, MnO, ZnO were weighed and mixed in a ball mill for 5 hours. After drying, the mixture was calcined at 750℃ in the atmosphere for 2 hours and then pulverized in a ball mill for 7 hours. This dried powder was mixed with a prescribed amount of MoO_3 powder 〔(a):commercial grade/ particle size is under 10 μ m, (b):wet pulverization in a planetary mill, (c):ultra fine powder/ particle size is about 10～20nm〕. Then this mixture was granulated using PVA and formed into a toroidal shape under a uniaxial pressure of 3 ton/cm^2. The samples were sintered at 1380℃. Afterwards the sintered samples were wound with 10 turns of Cu wire and the permeability of the samples was measured using an HP4194A impedance analyzer. Their microstructures were observed microscopically by SEM. Their density was determined by the Archimedean method, and porosity was determined by comparison with the theoretical X-ray density.

Fig.1 shows the initial permeability of each sample in relation to the amount of MoO_3. Initially, we predicted that the initial permeability would increase by decreasing the particle size of MoO_3, however the initial permeability of sample(c) was lower than samples(a) and (b) in each quantity of MoO_3. It is thus guessed that the MoO_3 volatilization from the core surface is more active below the maximum temperature due to fine particle size.

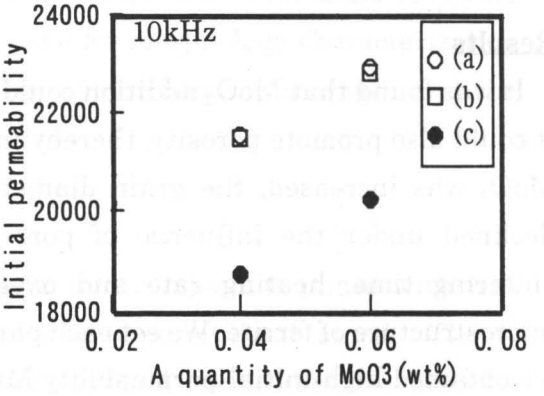

Fig.1 Dependence of μ i on MoO_3.

[1] Y.Matsuo, K.Ono, M.Ishikura: IEEE Trans. Magn., 33, 3751(1997)
[2] K.Ono, Y.Matsuo, M.Ishikura: Digests of the 21st Annual Conference on Magnetics in Japan 2pG12(1997)

Evaluation of Ferrite Plated Thin Films by Mössbauer Spectroscopy

F. Shirasaki, Y. Kitamoto, S. Kantake, S. Takaya, and M. Abe
Tokyo Institute of Technology

Mössbauer spectroscopy gives us magnetic and microstructural information, such as magnetic anisotropy, existence of non-magnetic phase, and etc.

We investigated the magnetic properties of spinel ferrite films prepared by the ferrite-plating method. The ferrite-plating can facilitate to deposit the ferrite films at low temperature below 100℃ in aqueous solutions. Ni-, NiZn-, Co-ferrite films were prepared by the spin-spray ferrite-plating method on glass substrates. The Mössbauer spectra of them were obtained by Conversion Electron Mössbauer Spectroscopy using Co^{57} source at room temperature.

Ni-, NiZn-, and Co-ferrite films have two resolved spectra, which are generally identified as one due to the Fe^{3+}in Asite, and the other due to the $Fe^{2.5+}$in B site; beside, both sites is splitted six-line spectrum by Zeeman effect. The ratio of the peaks for a randomly oriented films is 3:2:1:1:2:3. In the case of perpendicular anisotropic films, the ratio of the peaks should be 3:0:1:1:0:3, and it should be 3:4:1:1:4:3 in the case of parallel anisotropy ones. The spectrum of Ni-, and NiZn-ferrite films is very similar to the parallel anisotropic films as shown in Fig.1. The spectra of Co-ferrite films are very similar to the perpendicular anisotropic films as shown in Fig.2. We calculated Mössbauer parameters of measured spectrum by Mössbauer fitting program. In the case of Ni-ferrite films, the quadrupole splitting of A site was –0.0116 mm/s, and B site was 0.0565 mm/s. The isomer shift of A site was 0.1722 mm/s, and B site was 0.5436 mm/s. The magnetic hyperfine field of A site was 49.29 Tesla and B site was 46.19 Tesla.

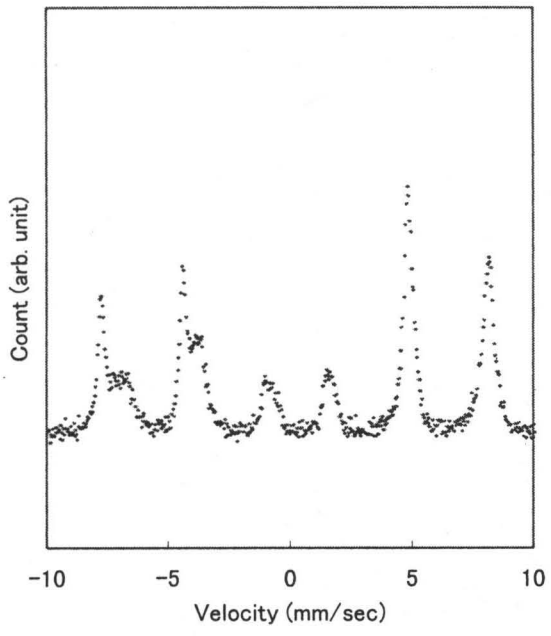

Fig.1 Mössbauer spectrum of Ni-ferrite films.

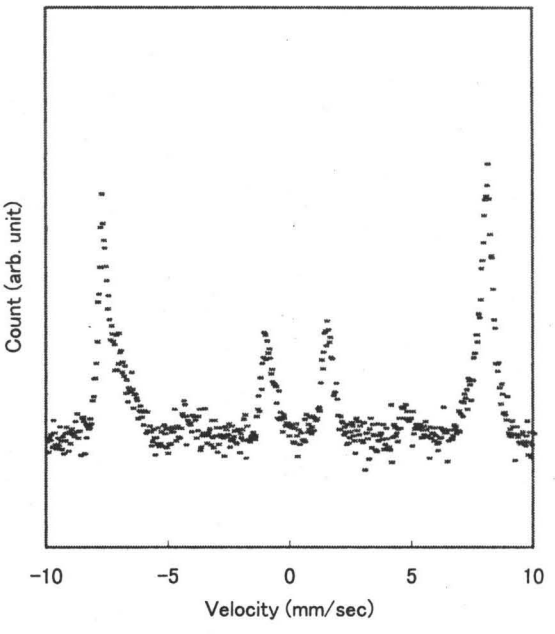

Fig.2 Mössbauer spectrum of Co-ferrite films.